



Pinces moléculaires photo-isomérisables pour l'étude des changements allostériques des récepteurs pentamériques canaux

Thi Hong Long Nguyen

► To cite this version:

Thi Hong Long Nguyen. Pinces moléculaires photo-isomérisables pour l'étude des changements allostériques des récepteurs pentamériques canaux. Chimie thérapeutique. Université Paris-Saclay, 2017. Français. NNT : 2017SACL395 . tel-02435593

HAL Id: tel-02435593

<https://theses.hal.science/tel-02435593>

Submitted on 11 Jan 2020

HAL is a multi-disciplinary open access archive for the deposit and dissemination of scientific research documents, whether they are published or not. The documents may come from teaching and research institutions in France or abroad, or from public or private research centers.

L'archive ouverte pluridisciplinaire **HAL**, est destinée au dépôt et à la diffusion de documents scientifiques de niveau recherche, publiés ou non, émanant des établissements d'enseignement et de recherche français ou étrangers, des laboratoires publics ou privés.

Pinces moléculaires photo-isomérisables pour l'étude des changements allostériques des récepteurs pentamériques canaux

Thèse de doctorat de l'Université Paris-Saclay
préparée à l'Université Paris Sud

École doctorale n°569 Innovation thérapeutique :
du fondamental à l'appliqué
Spécialité de doctorat: Chimie pharmaceutique

Thèse présentée et soutenue à Châtenay-Malabry, le 27 novembre 2017, par

Thi Hong Long Nguyen

Composition du Jury :

Mme. Joanne Xie Professeure, ENS de Cachan	Présidente du jury
Mme. Sabine Berteina-Raboin Professeure, Université d'Orléans	Rapporteur
M. Alexandre Specht DR CNRS, Université de Strasbourg	Rapporteur
M. Philippe Belmont Professeur, Université Paris Descartes	Examinateur
Mme. Delphine Joseph Professeure, Université Paris Sud	Directrice de thèse
Mme. Sandrine Delarue-Cochin Maître de conférences, Université Paris Sud	Co-Directrice de thèse

REMERCIEMENTS

En premier lieu, je suis honorée de la présence des membres du jury et je tiens à remercier: Professeure Joanne Xie, Professeur Sabine Berteina-Raboin, Docteur Alexandre Specht et Professeur Philippe Belmont d'avoir accepté de juger ma thèse et d'assister à la présentation de ce travail.

Je souhaite adresser mes sincères remerciements au Professeure Delphine Joseph pour m'avoir acceptée dans son équipe, m'avoir permise de travailler sur un sujet passionnant, pour la vision perfectionniste et la compréhension qu'elle a fourni à mon égard tout au long de ma thèse.

Je voudrais remercier ma codirectrice de thèse, Docteure Sandrine Delarue-Cochin, pour son écoute, sa disponibilité, sa gentillesse et la confiance qu'elle m'a accordée en dirigeant cette thèse.

J'exprime mes remerciements particuliers au Docteur Nicolas Gigant pour ses nombreux conseils de chimie et son aide au laboratoire qui m'ont permis d'avancer rapidement le projet.

Je tiens à remercier les membres de l'équipe avec laquelle j'ai pu travailler : Dr. Emmanuelle Drège, Dr. Laurent Evanno, Dr. Laurent Ferrier, Blandine Méniel-Séon, Dr. Sylvain Petit, Dr. Pierre-Etienne Venot, Dr. Noémie Scornet et Marco Lepron pour leur aide et leur bonne humeur.

Je souhaite également remercier le Professeur Pierre-Jean Corringer pour son aide précieuse dans la collaboration sur ce sujet. Je souhaiterais aussi adresser ma gratitude au Professeure Joanne Xie et au Docteur Nicolas Bogliotti pour m'avoir accueillie dans leur équipe lors des mesures de photoisomérisation. Je tiens également à remercier la Docteur Athéna Kasselouri pour m'avoir donné un accès aux appareils lors les tests de détection d'ions

Je voudrais aussi remercier Karine Leblanc, Camille Dejean et Jean-Christophe Jullian pour leurs aides analytiques.

Je remercie également tous mes amis du laboratoire pour la bonne ambiance et les déjeuners au restaurant universitaire, je remercie plus particulièrement Thuy Linh Nguyen et Siguara Bastos De Lemos E Silva.

Enfin les remerciements venant du plus profond de mon cœur... Je remercie mes parents et ma sœur vivant au Vietnam pour le soutien tout au long de mon séjour en France. Je remercie mon ami et sa famille pour les encouragements, la patience et la bienveillance au quotidien.

SOMMAIRE

ABBREVIATION.....	4
INTRODUCTION.....	6
1. Les récepteurs nicotiques à l'acétylcholine (nAChRs) : une cible thérapeutique	7
1.1. Structure et allostéries des nAChRs.....	7
1.2. Vers une meilleure compréhension des transitions allostériques : mécanisme d'ouverture-fermeture du canal ionique.....	9
2. Optogénétique	11
2.1. Optogénétique : comment contrôler le mouvement des protéines avec la lumière dans des systèmes vivants ?.....	11
2.2. Optogénétique chimique	14
2.3. nAChRs et l'optogénétique chimique.....	17
3. Molécules photo-isomérisables : introduction	21
4. Projet de thèse	23
CHAPITRE 1 : SYNTHESE DES AZOBENZENES TETRASUBSTITUÉS	26
1. Introduction sur les azobenzènes tétrasubstitués	27
1.1. Généralités sur les azobenzènes	27
1.2. Caractéristiques des azobenzènes <i>o,o'</i> -tétrasubstitués.....	29
1.2.1. Spectre UV	29
1.2.2. Demi-vie de l'isomère (<i>Z</i>)	31
1.2.3. Stabilité.....	31
1.3. Synthèse d'azobenzènes <i>o,o'</i> -tétrasubstitués.....	35
1.3.1. Synthèse par construction directe la fonction azobenzène	36
1.3.2. Synthèse impliquant une fonctionnalisation tardive	41
2. Article 1 : Efficient access to symmetrical tetra- <i>ortho</i> -substituted azobenzenes.....	43
3. Conclusion	52
CHAPITRE 2 : AZOPHENOLS : DE LA SYNTHESE VIA C-H ACTIVATION A L'APPLICATION	55
1. Revue sur la fonctionnalisation des azobenzènes par C-H activation.....	56
2. Article 2 : Palladium-Catalyzed Direct Oxidative Synthesis of Unsymmetrical Azophenols	104
3. Article 3 : Azophenol <i>via</i> C-H activation: regioselectivity, mechanistic understanding and potential ion sensor	114
CONCLUSION.....	132

ABBREVIATION

Comme il s'agit d'une thèse sur publication, le choix a été fait de rédiger les abréviations en langue anglaise.

5-HT3	5-hydroxytryptamine type 3 receptor
acac	acetylacetone
AChBP	acetylcholine binding protein
AMPA	α -amino-3-hydroxy-5-methyl-4-isoxazolepropionic acid receptor
anh.	anhydrous
AE	ethyl acetate
ChR2	channelrhodopsine
CLS	caged ligands
COD	1,5-cyclooctadiene
Cp*	pentamethylcyclopentadienyl
DABCO	1,4-diazabicyclo-[2.2.2]-octane
DCE	1,2-dichloroethane
DCM	dichloromethane
DEAD	diethyl azodicarboxylate
DMF	dimethylformamide
EC	extracellular domain
ELIC	<i>Erwinia chrysanthemi</i> ligand ion-gated channel
equiv	equivalent
GABA	gamma-aminobutyric acid receptor
GFP	green fluorescent protein
GLIC	<i>Gloebacter violaceus</i> ligand ion-gated channel
GluCl	Glutamate-gated chloride channel
GSH	glutathione
IC	intracellular domain
IR	infra-red
KIE	kinetic isotope exchange
LG	leaving group
LiGluR	light-gated ionotropic glutamate receptor
m-CPBA	<i>meta</i> -chloroperoxybenzoic acid
Mp	melting point
nAChR	nicotinic acetylcholine receptor
NCS	N-chlorosuccinimide
NHPI	N-hydroxypthalimide
NMR/RMN	nuclear magnetic resonance
	δ chemical shift
	s singulet
	d doublet
	t triplet
	m multiplet
	J coupling constant
NpHR	halorhodopsine
PCL	photochromic ligand
pH	potential of hydrogen
PIFA	[bis(trifluoroacetoxy)iodo]benzene
PIDA	[(diacetoxy)iodo]benzene

PINO	phthalimide N-oxyl radical
pGLICs	pentameric ligand-gated ion channels
PSS	photostationary state
PTL	photoswitch tethered ligand
Rf	retardation factor
RT	room temperature
SDS	sodium dodecylsulfate
TBHP	tert-butyl hydroperoxide
TEMPO	2,2,6,6-tetramethyl-1-piperidinyloxy
TFA	trifluoroacetic acid
THF	tetrahydrofuran
TLC	thin-layer chromatography
TM	transmembrane domain
TMA	trimethylammonium
TRPV1	transient receptor potential vanilloid 1

Introduction

1. Les récepteurs nicotiques à l'acétylcholine (nAChRs) : une cible thérapeutique

Les récepteurs nicotiniques à l'acétylcholine ont été les premiers récepteurs transmembranaires activés par les neurotransmetteurs à avoir été isolés et identifiés. Il s'agit de l'un des récepteurs ionotropiques les mieux connus en matière de transduction du signal.¹ Les nAChRs font l'objet de nombreux programmes de recherche du fait de leur implication dans un grand nombre de processus physiologiques liés aux fonctions cognitives : ces récepteurs constituent des cibles thérapeutiques majeures, notamment pour les anxiolytiques, les sédatifs, les anesthésiques généraux, les facilitateurs cognitifs, les neuroprotecteurs (maladies d'Alzheimer et de Parkinson) et les composés anti-tabac (addictions). De récentes avancées sur la connaissance de la structure et des transitions allostériques des nAChRs induites par la fixation du ligand endogène, l'acétylcholine, ont été rapportées récemment dans la littérature.^{1, 2} Cependant la maîtrise de la pharmacologie et la modulation de l'activité de cette cible thérapeutique requiert une meilleure compréhension de la dynamique de ses changements conformationnels à l'échelle atomique.³ En effet, bien que les informations biochimiques et électrophysiologiques sur les nAChRs soient abondantes, un manque de données structurales sur ce récepteur persiste encore. Cette carence de données provient de la difficulté à cristalliser ces protéines transmembranaires et d'obtenir des clichés radiocristallographiques nécessaires à l'acquisition d'informations à l'échelle atomique.

1.1. Structure et allostéries des nAChRs

Les nAChRs appartiennent à la superfamille des récepteurs canaux pentamériques activés par des ligands p(LGICs). Ils sont considérés comme les prototypes des protéines allostériques, c'est-à-dire qu'ils sont capables d'assurer la transduction du signal *via* des activations topographiques distinctes induisant ainsi un changement conformationnel du récepteur au travers de la membrane plasmique.²

D'une masse moléculaire d'environ 290 kDa, les nAChRs s'organisent en 5 sous-unités identiques ou homologues arrangées pseudo-symétriquement autour d'un canal ionique. Chez les mammifères, il existe différents sous-types de nAChRs qui diffèrent par leur composition en sous-unités (α , β , γ , δ et ϵ) et dont l'expression est elle-même fonction de leur localisation tissulaire : ainsi, 9 sous-unités α et 3 sous-unités β sont exprimées dans le système nerveux central (Figure 1). Ces sous-unités protéiques sont codées par 17 gènes. Il existe une multitude de combinaisons pentamériques possibles découlant de l'association de ces sous-unités. Toutefois, seules certaines d'entre elles sont fonctionnelles et leur fonction biologique est directement liée à leur localisation tissulaire.

¹ Changeux, J.-P.; Taly, A., Nicotinic receptors, allosteric proteins and medicine, *Trends. Mol. Med.* **2008**, 14, 93-102.

² Gotti, C.; Zoli, M.; Clementi, F., Brain nicotinic acetylcholine receptors: native subtypes and their relevance, *Trends Pharmacol. Sci.* **2006**, 27, 482-491.

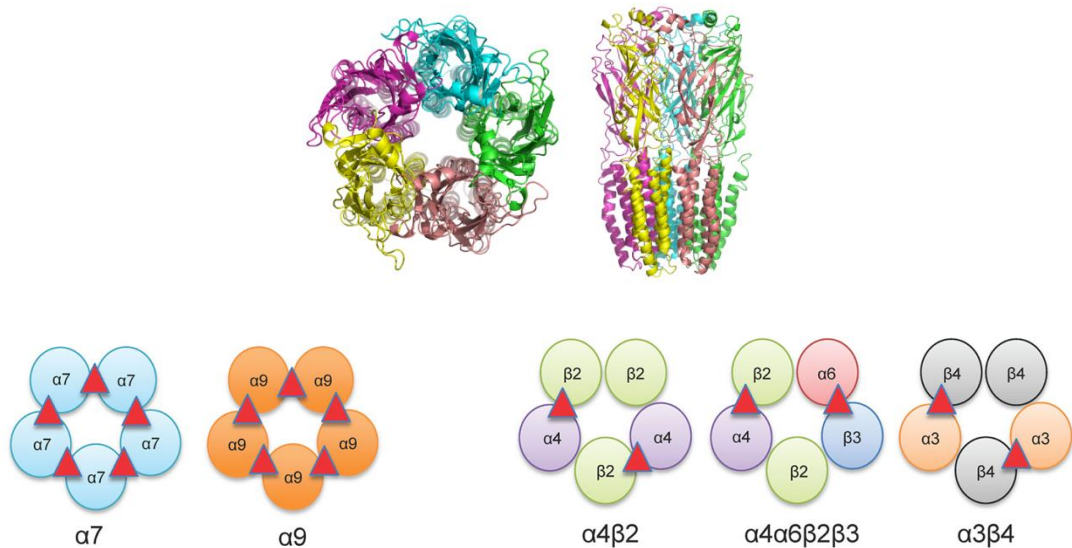


Figure 1. Structure et exemples de sous-types de nAChRs

Les structures tridimensionnelles (3D) des nAChRs et de leurs homologues sont relativement bien caractérisées. La structure primaire de chaque sous-unité se compose d'un domaine extracellulaire (EC) hydrophile amino-terminal, d'un domaine transmembranaire (TM) comprenant quatre segments hydrophobes (M1-M4), et d'un domaine hydrophile variable cytoplasmique ou intracellulaire (IC), absent dans les pLGICs procaryotes (Figure 2). Il y a entre 2 et 5 sites actifs liant ACh dans le domaine EC, qui sont éloignés (d'environ 60 Å") mais fonctionnellement liés à un canal cationique unique, situé sur l'axe symétrique du domaine TM. La structure atomique du domaine EC a été d'abord résolue pour l'ACh binding Protein (AChBP), un homologue pentamérique soluble du domaine EC du nAChR, initialement cloné à partir d'escargots invertébrés.³ Les structures complètes de pLGICs en résolution atomique ont ensuite été obtenues avec deux homologues procaryotes des nAChRs issus de *Gloeobacter violaceus* (GLIC)^{4, 5} et d'*Erwinia chrysanthemi* (ELIC)⁶ et plus récemment avec trois récepteurs eucaryotes: GluCl de *Caenorhabditis elegans*⁷, le récepteur 5-HT3 de la souris⁸ et le récepteur GABA chez l'Homme.⁹ En général, les structures cristallographiques disponibles des procaryotes et des eucaryotes des pLGICs révèlent une similitude frappante de la structure 3D des nAChRs avec ses homologues.^{10, 11}

³ Smit, A. B.; Syed, N. I.; Schaap, D.; van Minnen, J.; Klumperman, J.; Kits, K. S.; Lodder, H.; van der Schors, R. C.; van Elk, R.; Sorgedrager, B., A glia-derived acetylcholine-binding protein that modulates synaptic transmission, *Nature* **2001**, 411, 261-268.

⁴ Hilf, R. J.; Dutzler, R., Structure of a potentially open state of a proton-activated pentameric ligand-gated ion channel, *Nature* **2009**, 457, 115-118.

⁵ Bocquet, N.; Nury, H.; Baaden, M.; Le Poupon, C.; Changeux, J.-P.; Delarue, M.; Corringer, P.-J., X-ray structure of a pentameric ligand-gated ion channel in an apparently open conformation, *Nature* **2009**, 457, 111-114.

⁶ Hilf, R. J.; Dutzler, R., X-ray structure of a prokaryotic pentameric ligand-gated ion channel, *Nature* **2008**, 452, 375-379.

⁷ Hibbs, R. E.; Gouaux, E., Principles of activation and permeation in an anion-selective Cys-loop receptor, *Nature* **2011**, 474, 54-60.

⁸ Hassaine, G.; Deluz, C.; Grasso, L.; Wyss, R.; Tol, M. B.; Hovius, R.; Graff, A.; Stahlberg, H.; Tomizaki, T.; Desmyter, A., X-ray structure of the mouse serotonin 5-HT3 receptor, *Nature* **2014**, 512, 276-281.

⁹ Miller, P. S.; Aricescu, A. R., Crystal structure of a human GABAA receptor, *Nature* **2014**, 512, 270-275.

¹⁰ Corringer, P.-J.; Poitevin, F.; Prevost, M. S.; Sauguet, L.; Delarue, M.; Changeux, J.-P., Structure and pharmacology of pentameric receptor channels: from bacteria to brain, *Structure* **2012**, 20, 941-956.

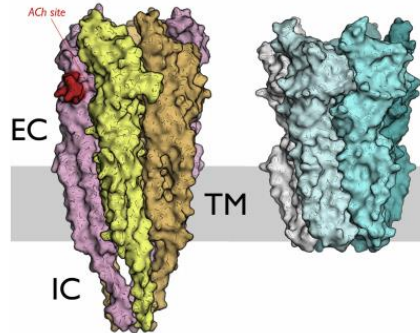


Figure 2. Topologie générale des pLGICs

Les structures cristallographiques des AChBP (AcetylCholine Binding Protein) qui représentent la partie extracellulaire de la protéine donnent une image partielle, figée des nAChRs, compliquant de fait le développement rationnel de molécules bioactives. Si les récepteurs ELIC et GluCl ont été obtenus dans un seul état, respectivement fermé et ouvert, le récepteur GLIC a lui pu être obtenu dans un état ouvert actif, puis dans deux états complémentaires, localement fermé et fermé par les équipes des Dr Pierre Jean Corringer et Marc Delarue.^{12, 13} Ceci fait de GLIC un modèle de choix pour la compréhension des transitions allostériques de la famille des récepteurs canaux pentamériques, car ces trois structures cristallographiques de GLIC ont permis de donner un regard nouveau sur les mouvements de transitions entre ces différents états.

1.2. Vers une meilleure compréhension des transitions allostériques : mécanisme d'ouverture-fermeture du canal ionique.

La combinaison des structures de haute résolution des pLGICs avec des études de simulations de dynamique moléculaire a fourni une nouvelle dimension temporelle et a mis en lumière la séquence d'événements reliant la liaison du neurotransmetteur à l'ouverture du canal ionique, distant de 60 Å. Ce processus d'ouverture et fermeture procède par une isomérisation progressive qui commence à partir du site de liaison orthostérique (boucles A, B et C), se propage aux domaines d'interface EC/TM (boucle β 1- β 2 et boucle Cys) via un réarrangement de la partie extracellulaire en sandwich β et se déplace vers le bas aux hélices transmembranaires (d'abord M2, puis M4 et M3) pour finalement ouvrir le pore^{12, 14} (Figure 3). Dans ce contexte, le caractère quaternaire d'isomérisation d'ouverture-fermeture du canal, qui a lieu même en l'absence de l'agoniste, assure le lien entre la fixation de l'agoniste et les modifications structurelles fonctionnelles du récepteur, et est l'élément clé pour élucider la nature de la régulation allostérique dans les pLGICs.

¹¹ Taly, A.; Hénin, J.; Changeux, J.-P.; Cecchini, M., Allosteric regulation of pentameric ligand-gated ion channels: an emerging mechanistic perspective, *Channels* **2014**, 8, 350-360.

¹² Sauguet, L.; Shahsavar, A.; Poitevin, F.; Huon, C.; Menny, A.; Nemecz, Á.; Haouz, A.; Changeux, J.-P.; Corringer, P.-J.; Delarue, M., Crystal structures of a pentameric ligand-gated ion channel provide a mechanism for activation, *Proc. Natl. Acad. Sci. USA* **2014**, 111, 966-971.

¹³ Prevost, M. S.; Sauguet, L.; Nury, H.; Van Renterghem, C.; Huon, C.; Poitevin, F.; Baaden, M.; Delarue, M.; Corringer, P.-J., A locally closed conformation of a bacterial pentameric proton-gated ion channel, *Nat. Struct. Mol. Biol.* **2012**, 19, 642-649.

¹⁴ Calimet, N.; Simoes, M.; Changeux, J.-P.; Karplus, M.; Taly, A.; Cecchini, M., A gating mechanism of pentameric ligand-gated ion channels, *Proc. Natl. Acad. Sci. USA* **2013**, 110, E3987-E3996.

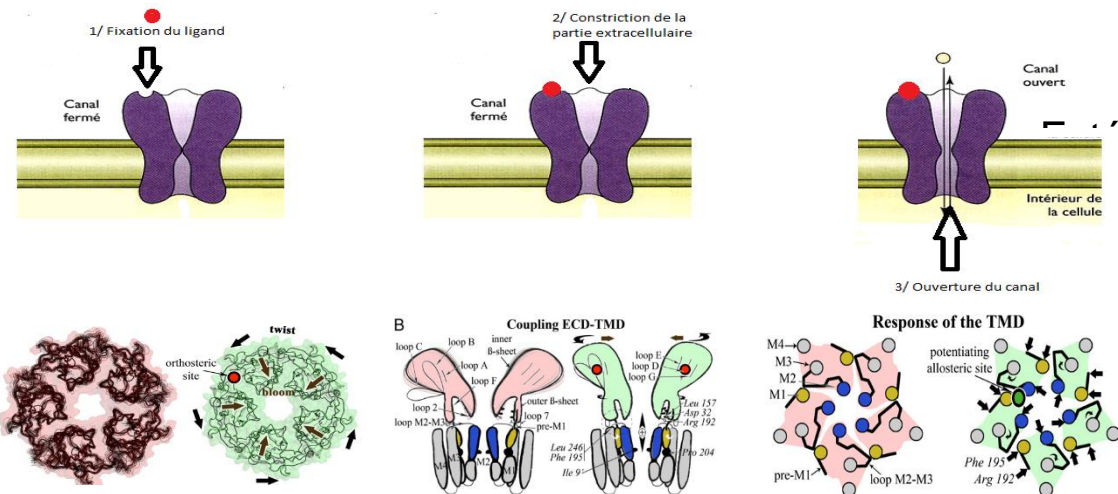


Figure 3. Mécanisme d'ouverture et de fermeture du canal.

Les structures cristallographiques des homologues procaryotiques GLIC pH4 (canal ouvert) et ELIC ou GLIC pH7 (canal fermé) ont montré sans ambiguïté une torsion globale lors de l'activation du récepteur.⁷ La structure localement fermée (LC) de GLIC, qui présente un pore ionique fermé en préservant la plupart des caractéristiques de la forme ouverte, remet sérieusement en question le couplage direct entre la torsion globale et le basculement de M2.

L'isomérisation en deux étapes, "blooming" puis "torsion", suggère que l'étape de "blooming" est déterminante pour l'activation alors que l'étape de "torsion" l'est pour la fermeture du pore. La fixation de l'agoniste sur le site orthostérique favoriserait l'activation en régulant principalement l'étape de "blooming" (en favorisant la contraction du domaine extracellulaire), alors que la fixation du ligand sur le site allostérique transmembranaire activerait le récepteur en empêchant la torsion globale du récepteur¹⁵ (Figure 4).

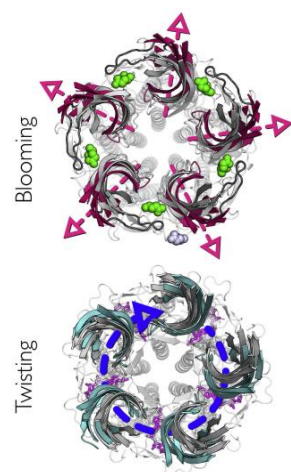


Figure 4. Mécanisme d'ouverture et de fermeture du canal.

¹⁵ Cecchini, M.; Changeux, J. P., The nicotinic acetylcholine receptor and its prokaryotic homologues: Structure, conformational transitions & allosteric modulation, *Neuropharmacology* 2015, 96, 137-149.

Les zones d'ombre concernant la compréhension des transitions allostériques du récepteur GLIC pourraient être franchies par une méthode bien développée ces dernières décennies. L'utilisation de la lumière pour contrôler l'isomérisation des outils structuraux et donc de la structure de la protéine est inspirée des récents développements de l'optogénétique chimique.

2. Optogénétique

2.1. Optogénétique : comment contrôler le mouvement des protéines avec la lumière dans des systèmes vivants ?

Pour déchiffrer un processus biologique complexe, il est nécessaire de disposer d'outils capables de perturber les différents acteurs concernés afin d'obtenir des informations sur les paramètres importants de ce processus. Dans ce contexte, la lumière semble un élément idéal pour perturber un système, car elle offre un haut niveau de résolution spatio-temporelle; elle est généralement non invasive dans une large gamme de longueurs d'onde; elle est orthogonale vis-à-vis de la plupart des éléments des systèmes vivants; et, elle ne provoque pas de contamination de l'échantillon.¹⁶ De plus, sa longueur d'onde et son intensité peuvent être précisément contrôlées. Ces propriétés uniques ont conduit à l'utilisation de la lumière dans l'étude par fluorescence de petites molécules marquées et de protéines dans les cellules. Elles ont inspiré récemment des développements pour le marquage bioorthogonal de biomolécules par de composés photoactifs.¹⁷

La perturbation spécifique d'un processus biologique *via* la lumière implique la capacité à photo-contrôler ses acteurs, généralement des protéines. Pour atteindre cet objectif, on peut agir directement au niveau des protéines et photo-induire un changement de leur activité. Cela nécessite la présence d'un module sensible à la lumière, qui peut déjà exister au sein de la protéine (comme dans les photorécepteurs) ou être attaché, génétiquement ou chimiquement, à la protéine d'intérêt.¹⁸ Cette approche crée des dispositifs hybrides qui peuvent être contrôlés avec des signaux d'entrée non naturels et peuvent être facilement intégrés dans des systèmes biologiques complexes. En tant que tel, ce dispositif fonctionne non seulement *in vitro* ou dans des cellules individuelles (*in cellulo*), mais également dans des réseaux cellulaires complexes, dans des tissus neuronaux (*ex vivo*) et des animaux vivants (*in vivo*). Cette technique s'appelle "l'optogénétique".

L'optogénétique correspond ainsi à un nouveau domaine de recherche et d'application, associant l'optique à la génétique. Elue méthode de l'année d'après *Nature Methods* en 2010, elle permet de rendre des neurones sensibles à la lumière en combinant le génie génétique à l'optique.¹⁹ Elle permet ainsi de stimuler spécifiquement un type cellulaire en laissant les cellules voisines intactes, cela dans le but de pouvoir un jour cartographier l'ensemble des réseaux neuronaux.

¹⁶ Mayer, G.; Heckel, A., Biologically active molecules with a "light switch", *Angew. Chem. Int. Ed.* **2006**, *45*, 4900-4921.

¹⁷ Szymanski, W.; Beierle, J. M.; Kistemaker, H. A.; Velema, W. A.; Feringa, B. L., Reversible photocontrol of biological systems by the incorporation of molecular photoswitches, *Chem. Rev.* **2013**, *113*, 6114-6178.

¹⁸ Gautier, A.; Gauron, C.; Volovitch, M.; Bensimon, D.; Jullien, L.; Vriz, S., How to control proteins with light in living systems, *Nat. Chem. Biol.* **2014**, *10*, 533-541.

¹⁹ Deisseroth, K., Optogenetics, *Nat. Methods* **2011**, *8*, 26-29.

Le fonctionnement de l'optogénétique repose principalement sur l'insertion au niveau cérébral de gènes codant pour une protéine «photo-activable» le plus souvent d'origine bactérienne, appelée opsine. Une fois les opsines produites par l'individu hôte, elles sont activées par la lumière, à une longueur d'onde spécifique, à l'aide d'une fibre optique directement implantée dans le cerveau de l'animal (Figure 5).



Figure 5. L'implantation d'une fibre optique dans le cerveau de la souris.

Les canaux que forme l'opsine s'ouvrent et, en fonction de leur nature, peuvent provoquer la dépolarisation ou l'hyperpolarisation du neurone. Cela conduit à l'observation de résultats comportementaux et à des enregistrements électrophysiologiques. La technique a recours à une grande diversité d'opsines dont les deux principales sont²⁰:

- La channelrhodopsine 2 (ChR2), dont le gène est issu d'algues unicellulaires, s'ouvre par action de la lumière bleue, laissant entrer les ions sodium dans les neurones, ce qui les dépolarise, et les rend excitables. Elle utilise le rétinal comme molécule photo-activable, mais contrairement aux pigments visuels des mammifères, le rétinal n'est pas excisé après photo-activation. Par conséquent, ChR2 peut être utilisée de façon répétée. Un avantage supplémentaire est que le rétinal est produit de manière endogène dans de nombreux tissus et n'a pas besoin d'être administré en supplément.
- L'halorhodopsine (NpHR), dont le gène est tiré d'archéobactéries, s'ouvre par action de la lumière jaune, laissant entrer les ions chlorure dans les neurones, ce qui les hyperpolarise, et les rend, à l'inverse, inexcitables.

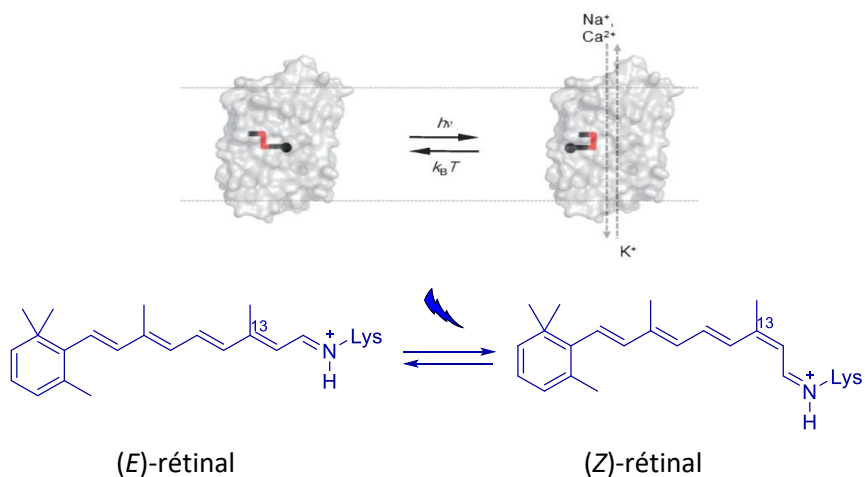


Figure 6. La ChR2 et le rétinal

²⁰ Fehrentz, T.; Schönberger, M.; Trauner, D., Optochemical genetics, *Angew. Chem. Int. Ed.* **2011**, *50*, 12156-12182.

Depuis sa création au début du nouveau millénaire, l'optogénétique a été utilisée dans de nombreuses applications dans les systèmes de circuits neuronaux et a aidé à répondre à diverses questions fondamentales en neurosciences. Cette approche a été notamment utilisée pour photoréguler une multitude de processus biologiques, comme la transcription de l'ADN et la traduction de l'ARN, le repliement des protéines, l'activité enzymatique, les interactions protéine-ligand, la structure et la fonction de peptides, le transport membranaire, et la modulation de récepteurs.¹⁹ L'optogénétique a également trouvé, ces dernières années, ses premières applications en recherche thérapeutique. Par exemple, ChR2 et NpHR ont été utilisées pour étudier le mécanisme de stimulation cérébrale profonde afin d'améliorer les symptômes de la maladie de Parkinson.²¹ Une deuxième étude a visé la rétinite pigmentaire, maladie qui implique la perte de cellules photoréceptrices. Dans ce cas, la sensibilité à la lumière du rétinal peut être restaurée par l'expression de NpHR, qui est mis en évidence dans le comportement visuel guidé chez les souris aveugles.²² Dans une autre application de ChR2 et NpHR, le fonctionnement des cellules cardiaques du poisson zèbre peut être inhibé ou stimulé optiquement, permettant ainsi le contrôle du battement du cœur.²³

Une autre famille de protéines largement utilisée avec l'optogénétique est la protéine fluorescente verte (GFP). La GFP est depuis quelques décennies "le microscope" des biochimistes, biologistes et autres chercheurs dans le domaine médical, la forte couleur verte de la GFP apparaissant sous lumière bleue ou UV. Ainsi dans les applications directes, la GFP permet de visualiser la croissance des tumeurs cancéreuses, le développement de la maladie d'Alzheimer ou l'évolution de bactéries pathogènes.²⁴ Les chercheurs ont réussi à attacher le gène codant pour la GFP à ceux codant pour d'autres protéines. Quand la cellule a besoin d'une protéine pour son fonctionnement, elle envoie un signal au gène correspondant qui active alors la production de la dite protéine. Ainsi lorsqu'un gène, attaché à celui codant pour la GFP, est activé, on sera capable de voir les cellules pour lesquelles ce gène est activé ainsi que les lieux de production de la protéine correspondante. La lumière verte de la GFP sert de balise de ces différents événements. Deux américains, Roger Tsien et Martin Chalfie, et un japonais, Osamu Shimomura, ont été récompensés par le prix Nobel de chimie en 2008 pour la découverte de la protéine fluorescente GFP et la mise au point de son utilisation comme marqueur.

²¹ Gradinaru, V.; Mogri, M.; Thompson, K. R.; Henderson, J. M.; Deisseroth, K., Optical deconstruction of parkinsonian neural circuitry, *Science* **2009**, 324, 354-359.

²² Busskamp, V.; Duebel, J.; Balya, D.; Fradot, M.; Viney, T. J.; Siegert, S.; Groner, A. C.; Cabuy, E.; Forster, V.; Seeliger, M.; Biel, M.; Humphries, P.; Paques, M.; Mohand-Said, S.; Trono, D.; Deisseroth, K.; Sahel, J. A.; Picaud, S.; Roska, B., Genetic reactivation of cone photoreceptors restores visual responses in retinitis pigmentosa, *Science* **2010**, 329, 413-417.

²³ Arrenberg, A. B.; Stainier, D. Y.; Baier, H.; Huisken, J., Optogenetic control of cardiac function, *Science* **2010**, 330, 971-974.

²⁴ Chalfie, M.; Tu, Y.; Euskirchen, G.; Ward, W. W.; Prasher, D. C., Green fluorescent protein as a marker for gene expression, *Science* **1994**, 263, 802-805.

2.2. Optogénétique chimique

Actuellement, une extension de l'optogénétique est de remplacer les protéines photoactivables qui nécessitent des techniques complexes de biologie par de petites molécules synthétiques photoactivables qui se lient sélectivement au récepteur cible.

Trois stratégies générales ont émergé dans ce domaine. La plus simple et plus ancienne approche utilise des ligands "cagés" (CLS). Le ligand y est doté d'un groupement protecteur qui le rend pharmacologiquement inefficace. Ce groupement est rarement une véritable cage moléculaire, mais en général, un groupement photolabile qui masque un groupement fonctionnel essentiel pour l'interaction ligand-récepteur. Le clivage photochimique du groupement protecteur conduit alors à la fixation du ligand actif libre au récepteur et déclenche l'effet biologique souhaité (Figure 7).

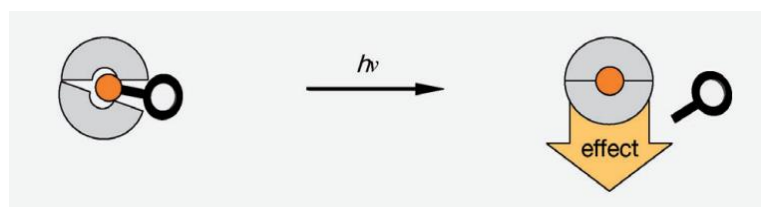
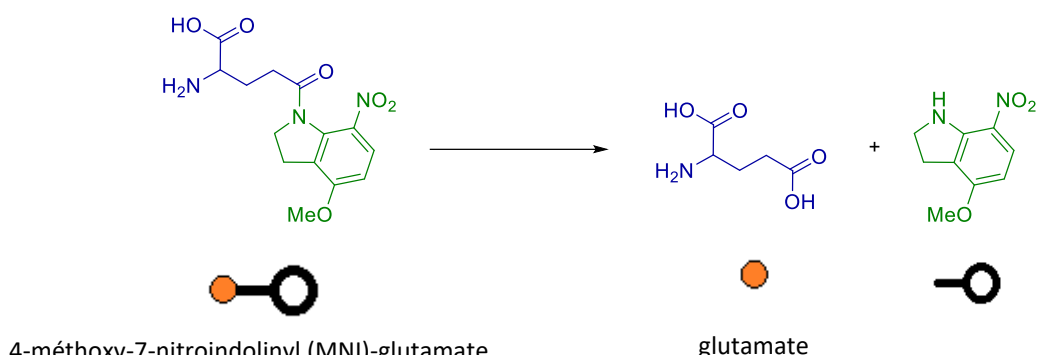


Figure 7. Principe des ligands cagés.

Les ligands "cagés" ont ainsi été largement utilisés en neuroscience. Matsuzaki et ses collaborateurs ont mis au point une molécule "cagée" dérivée du glutamate pour étudier systématiquement les fonctions du récepteur glutamate AMPA au niveau des synapses individuelles. La photolyse du glutamate "cagé" par deux photons déclenche la libération locale de glutamate libre, ce qui entraîne la génération de potentiels d'action dans les neurones au niveau du site de libération (Figure 8).²⁵

La photosensibilisation du récepteur TRPV1 avec un dérivé capsaïcine "cagé" a par la suite été la première approche fonctionnant sur des animaux vivants (l'hippocampe) (Figure 8).²⁶



²⁵ Matsuzaki, M.; Ellis-Davies, G. C.; Nemoto, T.; Miyashita, Y.; Iino, M.; Kasai, H., Dendritic spine geometry is critical for AMPA receptor expression in hippocampal CA1 pyramidal neurons. *Nat Neurosci*. 2001. 4: 1086-1092.

²⁶ Zemelman, B. V.; Nesnas, N.; Lee, G. A.; Miesenbock, G., Photochemical gating of heterologous ion channels: remote control over genetically designated populations of neurons. *Proc. Natl. Acad. Sci. USA* **2003**, *100*, 1352-1357.

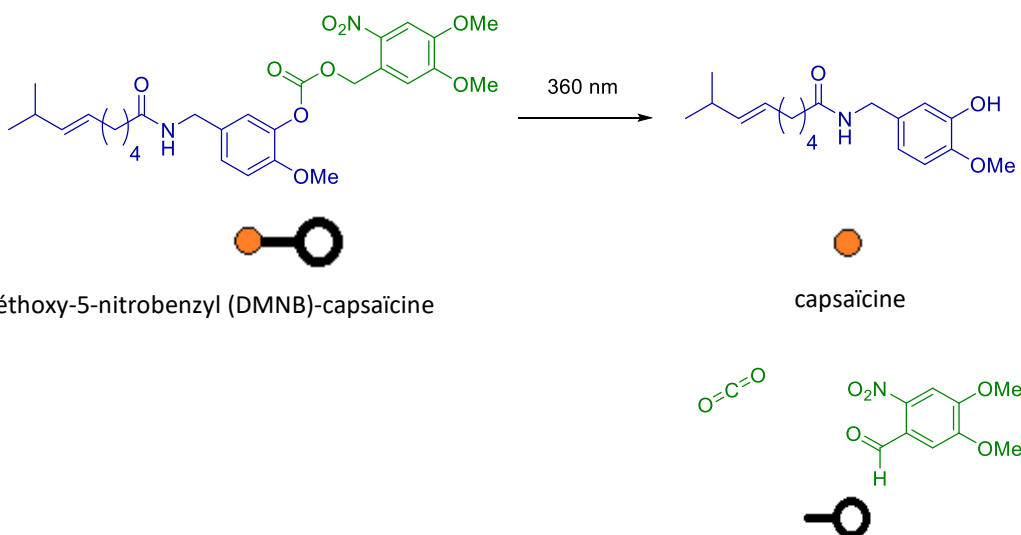


Figure 8. Exemples de molécules "cagés" : la capsaïcine et le glutamate

Il existe, cependant, certains inconvénients fonctionnels associés à ces ligands "cagés". La déprotection est un processus irréversible et il est difficile, voire impossible, de revenir à la molécule protégée. De plus, la déprotection conduit à la formation de sous-produits qui peuvent être toxiques.

Certains de ces problèmes peuvent être surmontés par une deuxième approche utilisant des ligands photochromiques (PCL). Ici, le ligand porte d'un côté une chaîne photo-isomérisable. La molécule photoisomérisable peut basculer entre deux géométries dont l'une déclenche l'effet biologique souhaité, et ce, de manière réversible. Le ligand peut changer son efficacité selon sa structure tridimensionnelle et pourrait même être un agoniste sous une forme et un antagoniste sous l'autre forme (Figure 9). Ainsi, le composé 4-GluAzo s'est avéré être un agoniste photochromique très efficace de certains récepteurs kainate qui sont impliqués dans l'épileptogénèse, la transduction sensorielle, et la plasticité synaptique.²⁷ Son application aux canaux GluK1 et GluK2 a démontré le contrôle réversible par la lumière des courants entrants. Dans ce cas, les récepteurs sont préférentiellement activés par l'état *trans* du 4-GluAzo, ce dernier ayant montré par ailleurs une sélectivité légèrement plus élevée pour GluK1 que pour GluK2. Lorsqu'il est appliqué à des neurones dans l'hippocampe de souris, le 4-GluAzo a ainsi fonctionné comme un glutamate "réversiblement cagé". La réponse biologique peut en effet être déclenchée par le changement de la lumière de 380 à 500 nm, et peut être arrêtée en revenant à la longueur d'onde inférieure.

²⁷ Volgraf, M.; Gorostiza, P.; Szobota, S.; Helix, M. R.; Isacoff, E. Y.; Trauner, D., Reversibly caged glutamate: a photochromic agonist of ionotropic glutamate receptors, *J. Am. Chem. Soc.* **2007**, 129, 260-261.

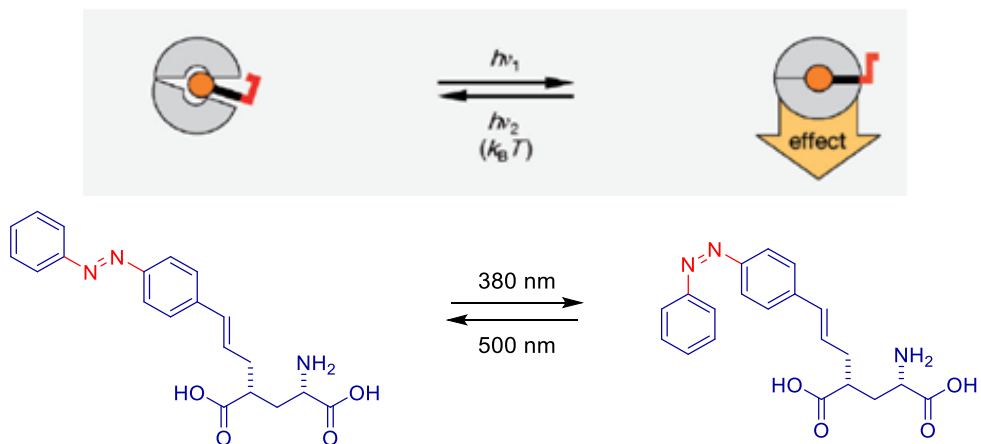


Figure 9. Exemple d'approche par PCL : le 4-GluAzo

Les PCLs répondent aux critères associés aux petites molécules médicaments, y compris leur facilité d'administration et la distribution rapide dans les tissus. Mais comme pour les médicaments, la sélectivité entre les sous-types de récepteurs peut être une limitation. De plus, les deux isomères ont parfois peu de différences d'activité vis-à-vis de la cible.

Bien sûr, il y a des situations où la sélectivité envers un sous-type du récepteur est une donnée essentielle. Dans ce cas, une troisième approche, que nous appelons l'approche "ligand photoisomérisable fixé" (approche PTL), peut être utilisée. Ici, le ligand est lié de manière covalente à son récepteur par un bras espaceur qui contient une molécule photo-isomérisable. Comme la molécule photoisomérisable alterne entre ses deux formes, elle peut être amenée au site de la protéine d'une manière réversible, ce qui conduit à une réponse biologique. Comme le PTL est attaché de manière covalente, sa concentration locale au niveau du site de fixation est très élevée lorsqu'il est sous la forme dite active, ce qui signifie que l'affinité du ligand n'est pas un souci important. En effet, les ligands de moyenne d'affinité sont généralement préférés pour s'assurer que la molécule photoisomérisable puisse quitter le site de fixation si nécessaire (Figure 10). Par exemple, la molécule photoisomérisable du dérivé glutamate MAG-1 est attachée à chacun des quatre sites allostériques du récepteur ionotropique de glutamate LiGluR. Le récepteur est désactivé quand le ligand isomérisable, azobenzène, est sous forme *trans* et il est activé avec la forme *cis* de la molécule (Figure 10).

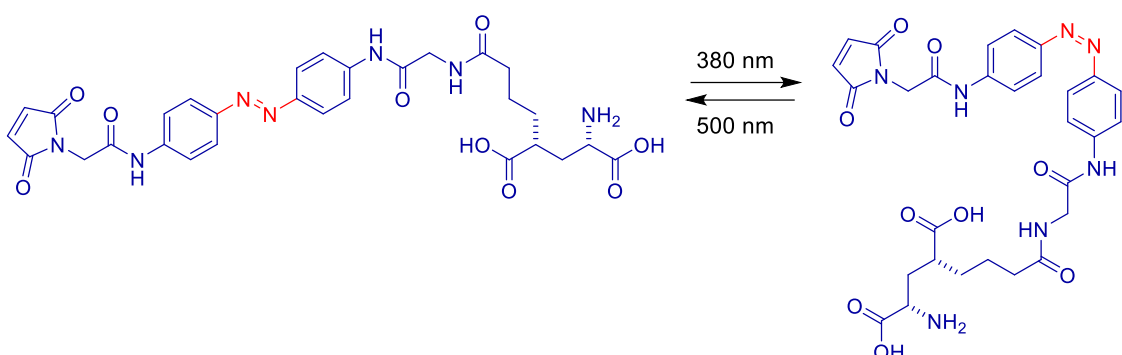
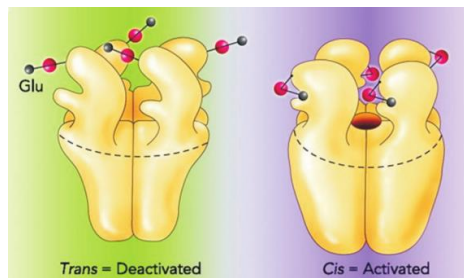
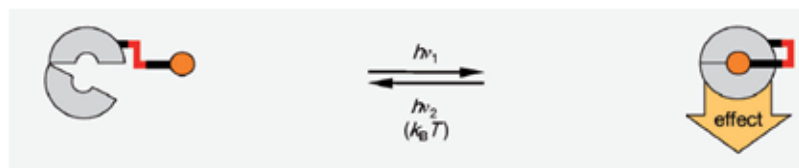
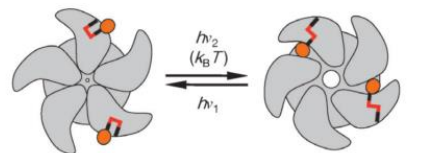


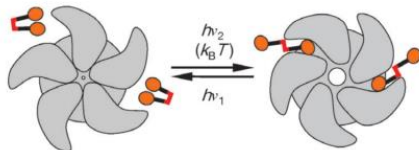
Figure 10. Exemple d'approche par PTL : le MAG-1.

2.3. nAChRs et l'optogénétique chimique

Le nAChR a été le premier récepteur à être photosensibilisé, à la fois avec des PCLs et des PTLs (Figure 11).²⁸ Étonnamment, cela a été réalisé au début des années 1970, bien avant l'avènement du clonage moléculaire, de l'expression hétérologue, de la biologie structurale moderne et de l'électrophysiologie.



L'action réversible du PTL sur le nAChR



Le contrôle d'un PCL sur le nAChR

Figure 11. Mécanisme de contrôle du nAChR par PTL et PCL.

²⁸ Bartels, E.; Wassermann, N. H.; Erlanger, B. F., Photochromic activators of the acetylcholine receptor, *Proc. Natl. Acad. Sci. USA* **1971**, 68, 1820-1823.

Les études de Karlin et *al.* ont montré que les liaisons disulfures du nAChR sont facilement réduites en groupes sulphydryles qui peuvent réagir sélectivement avec des partenaires électrophiles. (Figure 12)^{29, 30} Ces composés contiennent un fragment avec une affinité connue pour le site de liaison des nAChRs et une ancre électrophile, ce qui permet de lier le ligand de manière irréversible au récepteur à proximité du site de liaison. Dans le même temps, Erlanger et *al.* ont élaboré deux inhibiteurs photoisomérisables (Figure 13) de nAChR.³¹ Ces inhibiteurs dérivent d'agonistes connus du nAChR, la carbamylcholine et l'ion phényltriméthylammonium, et portent un fragment azobenzène photoisomérisable.

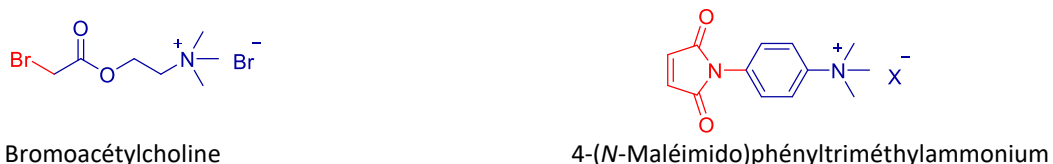


Figure 12. Les molécules avec des partenaires électrophiles.



Figure 13. Les deux inhibiteurs de nAChR.

L'activité biologique des composés **1** et **2** a été testée sur *Electrophorus electricus*.^{32, 33} Les isomères *trans*-**1** et *trans*-**2** sont plus fortement inhibiteurs des nAChRs que les isomères *cis*. En commutant les états *trans* et *cis* de ces inhibiteurs, il a ainsi été possible de réguler la dépolarisation de la membrane cellulaire avec la lumière.

Le composé QBr (Figure 14) est constitué d'un azobenzène photoisomérisable, fonctionnalisé avec un atome de brome à une des extrémités et un groupement triméthylammonium (TMA), à l'autre.²⁸ Le groupe TMA est un ligand connu pour la poche de liaison du nAChR. L'isomère *trans* de QBr (5×10^{-7} M) provoque une dépolarisation de 3 mV. QBr peut être lié de manière covalente au récepteur et il cause alors une dépolarisation plus importante de 5 mV. De plus, l'effet de la carbamylcholine³⁴ est complètement annulé lorsque QBr est fixé de manière covalente. L'effet observé de QBr conjugué est

²⁹ Karlin, A.; Winnik, M., Reduction and specific alkylation of the receptor for acetylcholine, *Proc. Natl. Acad. Sci. USA* **1968**, 60, 668-674.

³⁰ Silman, I.; Karlin, A., Acetylcholine receptor: covalent attachment of depolarizing groups at the active site, *Science* **1969**, 164, 1420-1421.

³¹Deal, W. J.; Erlanger, B. F.; Nachmansohn, D., Photoregulation of Biological Activity by Photochromic Reagents, III. Photoregulation of Bioelectricity by Acetylcholine Receptor Inhibitors. *Proc. Natl. Acad. Sci. USA* **1969**, *64*, 1230-1234.

³² Schoffeniels, E.; Nachmansohn, D., An isolated single electroplax preparation I. New data on the effect of acetylcholine and related compounds. *Biochim. Biophys. Acta* **1957**, *26*, 1-15.

³³ Higman, H. B.; Podleski, T. R.; Bartels, E., Correlation of membrane potential and potassium flux in the electroplax of Electrophorus. *Biochim. Biophys. Acta* **1964**, *79*, 138-150.

³⁴ Devillers-Thiéry, A.; Galzi, J.; Eisele, J.; Bertrand, S.; Bertrand, D.; Changeux, J., Functional architecture of the nicotinic acetylcholine receptor: a prototype of ligand-gated ion channels. *J. membrane biol.* **1993**, *136*, 97-112.

expliqué par le groupe TMA, qui dans l'isomère *trans* peut interagir avec le site de liaison, provoquant l'ouverture du canal, suivie par la dépolarisation de la membrane. Quand le ligand est isomérisé sous fome *cis* par la lumière UV, le groupe TMA n'est plus capable de se lier au site actif. Par conséquent, aucune dépolarisation n'est détectée. Le QBr fonctionne alors comme un PTL (Figure 15).



Figure 14. Le composé QBr.

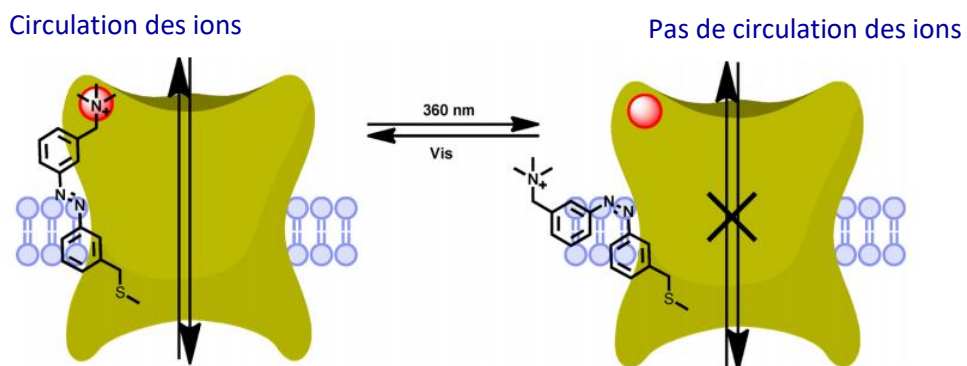


Figure 15 : nAChR modifié par la molécule QBr

Ce fût la première fois qu'une molécule photoisomérisable, liée à un récepteur était rapportée. L'utilité de cette technique pour l'étude de la fonction du récepteur a été démontrée au cours de la décennie suivante.^{35, 36} Comme le ligand est lié au récepteur, l'interaction entre le ligand et le récepteur devient indépendante de la probabilité de rencontre entre le ligand et la poche active. Cela permet de mener une étude pharmacodynamique d'une manière unique. Ainsi, Lester et al. ont étudié la transition entre les formes ouverte et fermée du récepteur nACh.³⁶ Deux hypothèses pour l'étape limitante ont été initialement suggérées : (i) la fixation et la dissociation de l'agoniste au niveau du site actif du récepteur, et (ii) un changement conformationnel du récepteur lorsque l'agoniste est lié. La conductance induite par l'agoniste QBr conjugué au récepteur étant comparable à celle induite par des agonistes liés de façon réversible, il a été supposé que l'étape cinétiquement limitante n'était pas la rencontre de l'agoniste avec le site de liaison du récepteur, car cette étape aurait dû être plus rapide pour l'agoniste lié de façon covalente. Cependant, les auteurs n'ont pas pu établir clairement l'étape cinétiquement limitante dans le processus d'activation.

³⁵ Lester, H. A.; Krouse, M. E.; Nass, M. M.; Wassermann, N. H.; Erlanger, B. F., A covalently bound photoisomerizable agonist. Comparison with reversibly bound agonists at Electrophorus electroplaques, *J. Gen. Physiol.* **1980**, 75, 207.

³⁶ Chabala, L.; Lester, H. A., Activation of acetylcholine receptor channels by covalently bound agonists in cultured rat myoballs, *J. Physiol.* **1986**, 379, 83-108.

Bien sûr, dans les années 1970 et 1980, les nAChRs photo-activés ne pouvaient pas être exprimés de manière hétérologue et génétiquement ciblée. Par conséquent, il n'a jamais été utilisé pour contrôler une fonction. De même, les PCLs ont été la plupart du temps considérés comme un outil pour étudier la fonction innée des nAChRs et non pas comme un moyen pratique pour contrôler optiquement le système nerveux ou le comportement des animaux. Toutefois, avec les structures détaillées et les outils modernes de la biologie moléculaire actuellement disponibles, il est très probable que les nAChRs photo-contrôlés seront bientôt réutilisés dans l'optogénétique chimique. En outre, des PCLs et PTLs pour les autres pLGICs continueront à être développés.³⁸

En conclusion, les approches CLS, PCL et PTL fournissent la base pour ce que nous appelons "l'optogénétique chimique" qui a pour but de contrôler l'activité des neurones (ou toute l'activité du réseau) par la lumière *via* des molécules synthétiques sensibles à la lumière, avec ou sans un composant génétiquement déterminé, la méthode utilisée dépendant de l'application envisagée. Pour des applications thérapeutiques, où un certain manque de sélectivité peut être toléré ou même souhaitable, l'approche PCL est la plus appropriée. D'autre part, dans l'analyse de voies fonctionnelles, par exemple, dans la cartographie de circuits neuronaux, la transfection génétiquement ciblée d'une cellule spécifique est clairement avantageuse. Par ailleurs, les PTLs pourraient être extrêmement utiles dans la dissection fonctionnelle de types de récepteurs étroitement liés : la sélectivité peut être obtenue par une liaison covalente sur un isoforme d'un récepteur génétiquement modifié (Figure 16). Dans tous les cas, des protéines modifiées et des ligands non naturels sont nécessaires. L'approche par PTL, cependant, ne fournit pas seulement une réponse précise à la question «qui», mais aussi aux questions «quand» et «où» .

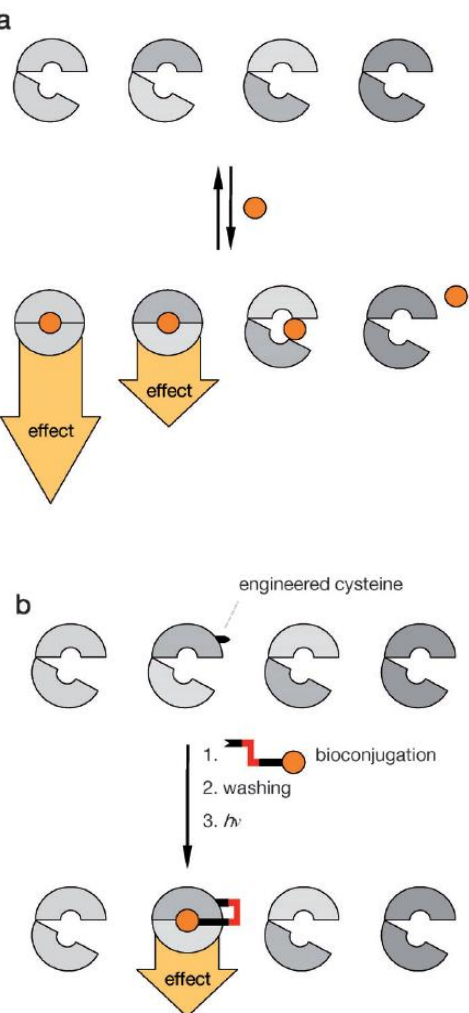


Figure 16. L'approche par PTL pour la pharmacologie sélective. a) La génétique chimique et la ciblage individuel de récepteur et ses isoformes : les ligands doivent lier avec une haute affinité et sélectivité. b) Optogénétique chimique : la sélectivité est obtenue en modifiant génétiquement un site de conjugaison. Remettant la fixation d'un ligand de faible affinité pour le récepteur sous-type.

Ces développements de l'optogénétique chimique ont conduit à l'intérêt croissant pour les petites molécules synthétiques photoisomérisables.

3. Molécules photo-isomérisables : introduction

Plusieurs familles de molécules photo-isomérisables, pouvant subir un changement réversible dans leur structure par action de la lumière, ont été conçues (Tableau 1). Elles sont communément caractérisées par les maxima d'absorption de leurs isomères, ainsi que par leur état photostationnaire (PSS), défini comme la composition en isomères à l'équilibre au cours de l'irradiation. Pour les applications biologiques, ces composés nécessitent un processus d'isomérisation rapide et un grand coefficient d'extinction avec un haut rendement quantique à des longueurs d'onde qui sont non destructives pour les cellules vivantes.

Entrée	Molécules photoisomérisable	Structure
1	Azobenzènes	
2	Stilbènes	
3	Spiropyranes	
4	Diaryléthènes	
5	Thiophènefulgides	
6	Hémithioindigos	

Tableau 1. Familles de molécules synthétiques photoisomérisable.

Les azobenzènes sont ainsi les molécules photoisomérisable les plus largement utilisées dans des applications biologiques,³⁷ en raison de³⁸ leur synthèse facile, de leurs états photostationnaires et de leurs rendements quantiques relativement élevés, de leur photo-isomérisation rapide, et de leur forte photostabilité. Tandis que le milieu a une influence plutôt faible sur la photochimie, il a été démontré que la cinétique de l'étape thermique est fortement influencée par des interactions secondaires avec les protéines.³⁹ Les rapports récents suggèrent que la différence d'énergie des

³⁷ Beharry, A. A.; Woolley, G. A., Azobenzene photoswitches for biomolecules, *Chem. Soc. Rev.* **2011**, *40*, 4422-4437.

³⁸ Renner, C.; Moroder, L., Azobenzene as conformational switch in model peptides, *ChemBioChem* **2006**, *7*, 868-878.

³⁹ Gorostiza, P.; Volgraf, M.; Numano, R.; Szobota, S.; Trauner, D.; Isacoff, E. Y., Mechanisms of photoswitch conjugation and light activation of an ionotropic glutamate receptor, *Proc. Natl. Acad. Sci. U. S. A.* **2007**, *104*, 10865-10870.

isomères et la hauteur de la barrière thermique pour l'isomérisation *cis-trans* (~18 kcal/mol) sont suffisantes pour entraîner des changements de conformation des protéines, permettant le contrôle photochimique du repliement et du dépliement des protéines.⁴⁰ Une des limitations à l'utilisation des azobenzènes est néanmoins la nécessité d'une utilisation de la lumière UV qui pénètre difficilement dans les tissus et qui peut causer de graves dommages pour les cellules vivantes. Cependant, une nouvelle classe d'azobenzènes a été développée récemment par les groupes de Temps⁴¹ et Woolley⁴². La forme *trans* peut être commutée en la forme *cis* par la lumière visible (Figure 17).



Figure 17. Azobenzènes tétrasubstitués.

4. Projet de thèse

Comme vu dans la première partie concernant les nAChRs, les structures cristallographiques de GLIC nous ont permis de proposer un modèle de transitions allostériques. Afin de comprendre le déroulement du processus d'ouverture jusqu'à la fermeture des pLGICs, c'est à dire d'avoir une image complète des déterminants moléculaires impliqués dans la liaison du ligand induisant le réarrangement conformationnel, il est maintenant indispensable d'accéder à des structures des états intermédiaires de GLIC et de comprendre leur rôle fonctionnel dans la transmission du signal. L'accès à des structures de conformations intermédiaires des nAChRs par nature fugaces, ne peut se faire qu'en introduisant au niveau de la protéine des éléments structuraux permettant de figer cette protéine dans cet état intermédiaire.

Il est ici proposé d'induire les changements de conformations de la protéine au travers d'un couplage avec des pinces moléculaires photoisomérables de type azobenzène (diphényldiazène),⁴³ ces structures ayant déjà été utilisées dans le cadre de la modulation conformationnelle de peptides.⁴⁴ Il est ainsi possible de faire réagir sélectivement des composés adéquatement fonctionnalisés avec des résidus cystéine judicieusement positionnés par mutagénèse dirigée.⁴⁵ L'accès aux structures cristallographiques fermée, localement fermée et ouverte de GLIC permet par ailleurs de connaître *a priori* les zones les plus sensibles à la transition allostérique et ainsi de proposer les sites de positionnement des cystéines les plus stratégiques.

⁴⁰ Zhang, F.; Zarrine-Afsar, A.; Al-Abdul-Wahid, M. S.; Prosser, R. S.; Davidson, A. R.; Woolley, G. A., Structure-based approach to the photocontrol of protein folding, *J. Am. Chem. Soc* **2009**, 131, 2283-2289.

⁴¹ Siewertsen, R.; Neumann, H.; Buchheim-Stehn, B.; Herges, R.; Näther, C.; Renth, F.; Temps, F., Highly efficient reversible Z-E photoisomerization of a bridged azobenzene with visible light through resolved S1 ($\pi\pi^*$) absorption bands, *J. Am. Chem. Soc* **2009**, 131, 15594-15595.

⁴² Beharry, A. A.; Sadovski, O.; Woolley, G. A., Azobenzene photoswitching without ultraviolet light, *J. Am. Chem. Soc* **2011**, 133, 19684-19687.

⁴³ Beharry, A. A.; Woolley, G. A., Azobenzene photoswitches for biomolecules, *Chem. Soc. Rev.* **2011**, 40, 4422-4437.

⁴⁴ Zatsepin, T. S.; Abrosimova, L. A.; Monakhova, M. V.; Pingoud, A.; Kubareva, E. A.; Oretskaya, T. y. S., Design of photocontrolled biomolecules based on azobenzene derivatives, *Russ. Chem. Rev.* **2013**, 82, 942-963.

⁴⁵ Zhang, F.; Zarrine-Afsar, A.; Al-Abdul-Wahid, M. S.; Prosser, R. S.; Davidson, A. R.; Woolley, G. A., Structure-based approach to the photocontrol of protein folding, *J. Am. Chem. Soc* **2009**, 131, 2283-2289.

Des résultats préliminaires encourageants ont été obtenus récemment par l'équipe du Dr Pierre-Jean Corringer dans la construction de ces mutants, deux sont d'ores et déjà fonctionnels, l'un modifié en position D136 et G101 (rouge/rose), l'autre en position D136 et S46 (rouge/bleu) (Figure 18). L'élément clé du projet est ici de viser la fixation de ces pinces à des cystéines positionnées sur deux sous-unités différentes du récepteur.

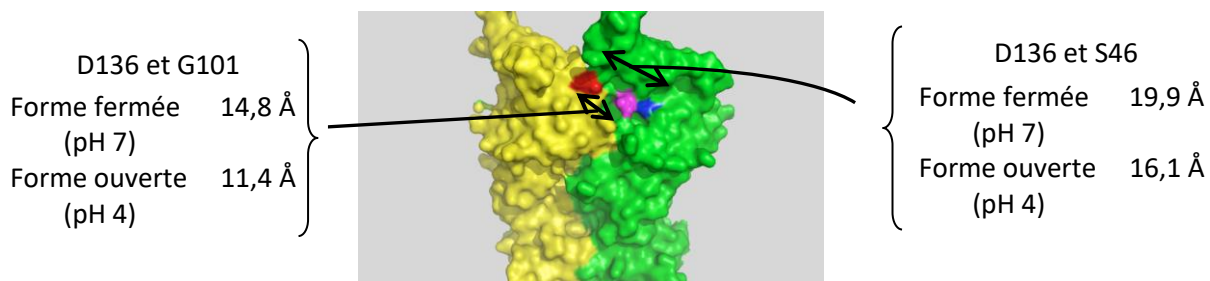


Figure 18. Deux mutants cystéines disponibles sur GLIC.

Le projet repose donc sur la synthèse de structures azobenzènes bifonctionnelles originales (Figure 19) répondant à différents critères. Des variations structurales au niveau des fonctions d'ancrage et des "linkers" permettront :

- d'adapter la pince en fonction du récepteur mutant sélectionné, par l'utilisation de linkers de taille variable,
- de moduler l'amplitude des changements conformationnels par l'utilisation de pinces plus ou moins flexibles.

Par ailleurs, une étude sera menée sur la fonctionnalisation du noyau azobenzène afin :

- d'adapter les propriétés de photoisomérisation, notamment en accédant à des composés photoisomérisables dans le visible pour ne pas altérer le matériel vivant, et de demi-vies compatibles avec les expériences réalisées.
- et d'accéder à des structures solubles dans les conditions biologiques,

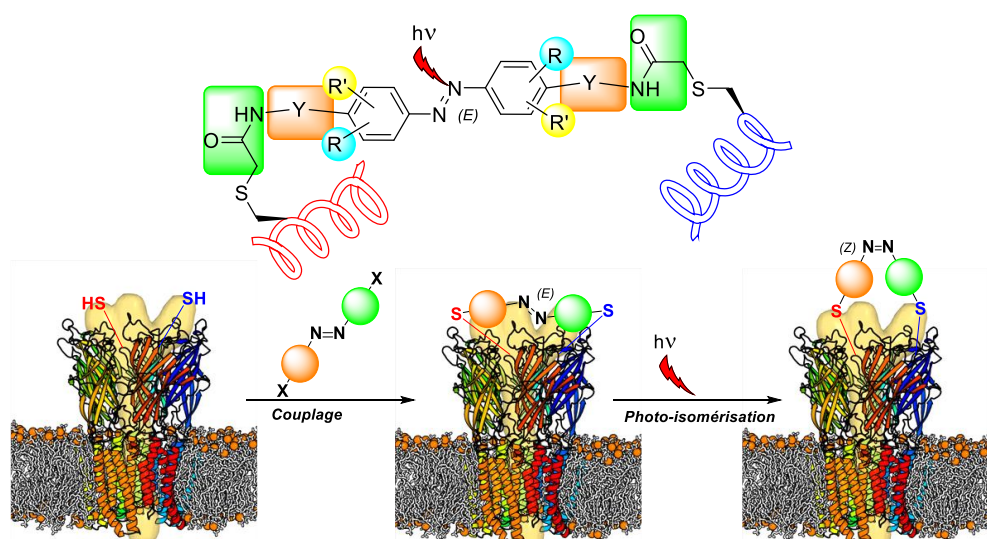


Figure 19. Modèle d'azobenzène et le fonctionnement sur la protéine.

Lors de nos résultats préliminaires de modélisation moléculaire avec le logiciel Openbabel, quelques modèles d'azobenzènes ont été conçus, afin de proposer des structures dont la configuration *E* est compatible avec la fixation sur les deux mutants de cystéine en terme de distance (Tableau 2). La distance entre les deux atomes de carbone S-méthylés (C_a - C_b) a été déterminée. La taille de la première molécule (Tableau 2, entrée 1) est en accord avec la distance pour le mutant D136 et G101 (14,8 Å). L'introduction de la chaîne alcyne (Tableau 2, entrée 2) permet d'augmenter la taille de la pince moléculaire tout en maintenant sa rigidité, la rendant donc compatible avec le mutant D136 et S46 (19,9 Å). Une pince dissymétrique (Tableau 2, entrée 3) a aussi été conçue. En effet, cette pince possède d'un côté un maléimide et de l'autre côté une chaîne latérale éthérée issue d'une fonction allyle flexible. Cette pince possède ici deux fonctions orthogonales permettant d'envisager la fixation en deux temps sur la protéine. La taille des molécules n'a été calculée qu'en forme *E*, forme thermodynamiquement plus stable, car nous avons d'abord privilégié la fixation de la pince avec les cystéines.

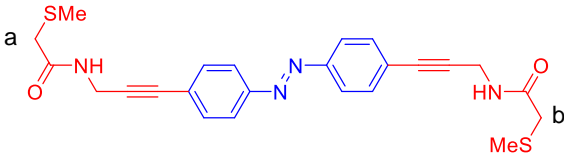
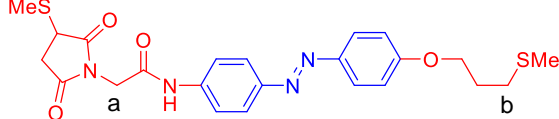
Entrée	Structures	Distance théorique C_a - C_b
1		16,6 Å
2		19,9 Å
3		17,5 Å

Tableau 2. Exemples de pinces azobenzène ayant des tailles théoriquement compatibles

Chapitre 1

Synthèse des azobenzènes tétrasubstitués

1. Introduction sur les azobenzènes tétrasubstitués

1.1. Généralités sur les azobenzènes

La famille des azobenzènes est l'une des plus grandes classes de molécules photosensibles développées actuellement. Les azobenzènes existent sous forme de 2 isomères *E* et *Z* : l'isomère *E* est plus stable thermodynamiquement que la forme *Z*, avec une différence de 50 KJ/mol dans le cas de l'azobenzène non-substitué **1** (Figure 20). La photo-isomérisation de *E* en *Z* induit de nombreuses modifications des propriétés physico-chimiques associées.⁴⁶ On peut citer par exemple le changement de moment dipolaire (μ) de 0.5 D pour l'isomère (*E*)-**1** contre 3.1 D pour l'isomère (*Z*)-**1**, qui détermine le caractère hydrophobe ou hydrophile.

Les structures des isomères (*E*)-**1** et (*Z*)-**1** ne sont pas planes : l'angle dièdre C, N=N, C est de 17,5° pour l'isomère (*E*)-**1**, et il est de 56° dans le cas de l'isomère (*Z*)-**1**. La distance entre les 2 atomes de carbone en position 4 et 4' est également fortement modifiée avec respectivement 9.0 Å et 5.0 Å pour les isomères *E* et *Z* (Figure 20).

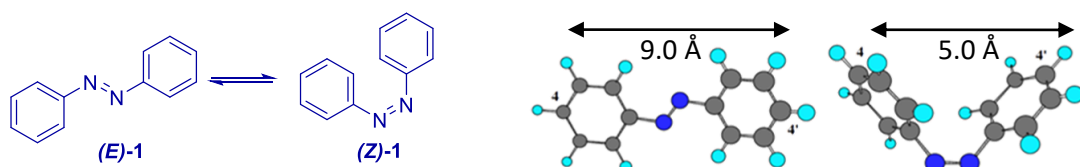


Figure 20. Structures planes et tridimensionnelles des 2 isomères de l'azobenzène **1**.

Le spectre d'absorption UV-visible du dérivé (*E*)-**1** montre trois maxima d'absorbance : une bande à 230 nm venant de la transition $\pi-\pi^*$ localisée sur le groupement phényle, une bande forte à 320 nm résultant de la transition symétrique $\pi-\pi^*$ et une absorbance faible à 430 nm venant de la transition symétrique défendue $n-\pi^*$. Le spectre de l'isomère (*Z*)-**1** est totalement différent, la transition $\pi-\pi^*$ est déplacée à 260 nm, la transition $n-\pi^*$ autorisée est à la même longueur d'onde mais avec une plus forte intensité (Figure 21).

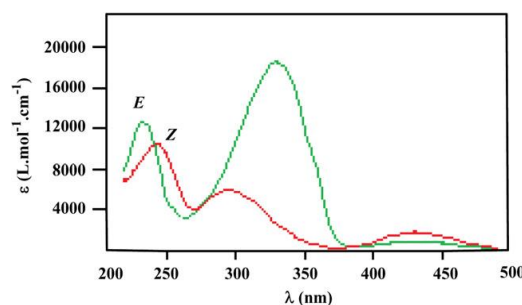


Figure 21. Spectre UV-visible de l'azobenzène **1**.

⁴⁶ Hamon, F.; Djedaini-Pilard, F.; Barbot, F.; Len, C., Azobenzenes-synthesis and carbohydrate applications, *Tetrahedron* **2009**, 65, 10105-10123.

Le mécanisme de la photo-isomérisation des azobenzènes peut être décrit selon deux voies: (i) la rotation autour de la liaison N=N par analogie avec le stilbène et (ii) l'inversion du doublet non liant de l'un des atomes d'azote (Schéma 1).

L'existence de ces deux mécanismes et la présence de 2 transitions électroniques de faible énergie $\pi-\pi^*$ et $n-\pi^*$ impliquent que l'isomérisation suit un processus complexe non encore totalement élucidé. Il est accepté que l'isomérisation thermique (*Z*) \rightarrow (*E*) passe par un mécanisme d'inversion.⁴⁷ En revanche, le mécanisme de l'isomérisation (*E*) \rightarrow (*Z*) est encore discuté. Pour Cattaneo, les 2 mécanismes coexistent avec l'inversion par excitation $n-\pi^*$ et la rotation par excitation $\pi-\pi^*$.⁴⁸ Fujino propose un seul processus d'inversion.^{49, 50} D'autres émettent l'hypothèse d'un unique mécanisme par rotation.⁵¹

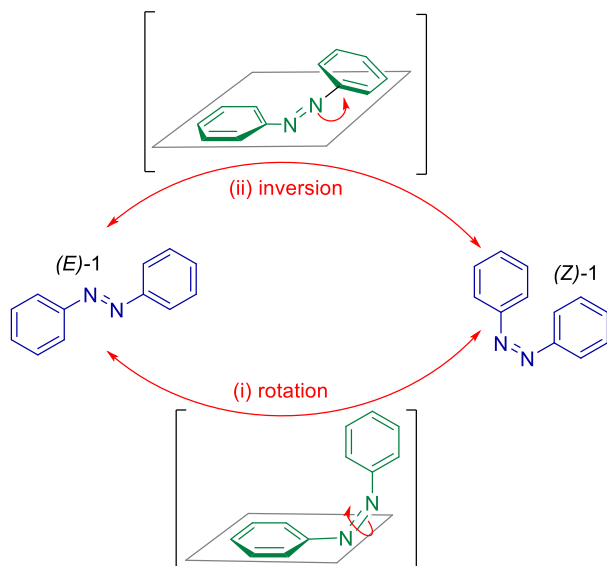


Schéma 1. Mécanismes proposés de la photo-isomérisation.

La plupart des azobenzènes non substitués liés à des biomolécules requiert la lumière UV pour leur photo-isomérisation. C'est une limitation pour leur application *in vivo*. En effet, la lumière UV pénètre difficilement dans les cellules et tissus et peut causer des réponses non-voulues comme l'apoptose cellulaire.^{52,53} Cependant, l'incorporation de groupements en position *ortho* ou *para* des azobenzènes conduit au déplacement des bandes $n-\pi^*$ vers la zone du visible.^{54, 55} Aussi, nous nous sommes intéressés aux propriétés des azobenzènes *o,o'*-tétrasubstitués.

⁴⁷ Delaire, J. A.; Nakatani, K., Linear and nonlinear optical properties of photochromic molecules and materials, *Chem. Rev.* **2000**, *100*, 1817-1846.

⁴⁸ Sánchez, C.; Alcalá, R.; Hvilsted, S.; Ramanujam, P. S., Biphotonic holographic gratings in azobenzene polyesters: Surface relief phenomena and polarization effects, *Appl. Phys. Lett.* **2000**, *77*, 1440.

⁴⁹ Fujino, T.; Tahara, T., Picosecond time-resolved Raman study of *trans*-azobenzene, *J. Phys. Chem. A* **2000**, *104*, 4203-4210.

⁵⁰ Fujino, T.; Arzhantsev, S. Y.; Tahara, T., Femtosecond time-resolved fluorescence study of photoisomerization of *trans*-azobenzene, *J. Phys. Chem. A* **2001**, *105*, 8123-8129.

⁵¹ Möller, G.; Harke, M.; Motschmann, H.; Prescher, D., Controlling microdroplet formation by light, *Langmuir* **1998**, *14*, 4955-4957.

⁵² Banerjee, G.; Gupta, N.; Kapoor, A.; Raman, G., UV induced bystander signaling leading to apoptosis, *Cancer lett.* **2005**, *223*, 275-284.

⁵³ Cheong, W.; Prahl, S.; Welch, A., A review of the optical properties of biological, *IEEE J. Quantum Electron.* **1990**, *26*, 2166-2185.

1.2. Caractéristiques des azobenzènes *o,o'*-tétrasubstitués

1.2.1. Spectre UV

La séparation des bandes $n-\pi^*$ des isomères *o,o'*-tétrasubstitués est la clé pour l'isomérisation par la lumière visible.^{54, 55} Les recherches de Woolley et Hecht tendent à prouver que le spectre UV-visible des azobenzènes *o,o'*-tétrasubstitués par différents groupements possède toujours une séparation des bandes $n-\pi^*$ dans la zone des 500 nm permettant la photo-isomérisation par la lumière visible. Par contre, les bandes séparées des azobenzènes non-substitués sont dans la zone UV et correspondent à la transition $\pi-\pi^*$ (Figure 22).^{56,57} En particulier, les dérivés *o,o'*-tétrachlorés **5** et *o,o'*-tétraéthylsulfanylés **6** (Tableau 3) s'isomérisent avec la lumière rouge, gamme de longueur d'ondes moins dégradante et pénétrant mieux dans les tissus par rapport aux autres parties de spectre visible (Tableau 3).

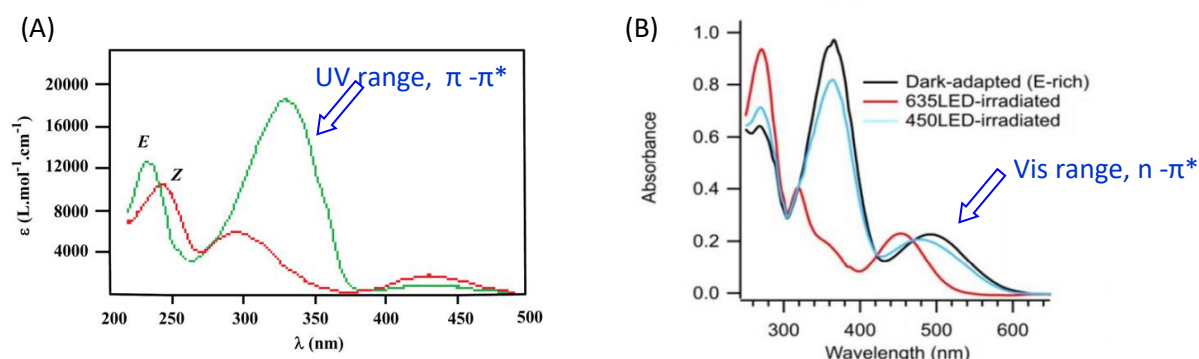


Figure 22. Spectres UV-visible d'azobenzènes non-substitué (A) et *o,o'*-tétrasubstitués (B).

Selon les études de Hecht, l'introduction d'atomes en *ortho* induit la séparation des bandes $n \rightarrow \pi^*$ des deux isomères, permettant une excitation sélective des deux isomères dans le visible. Contrairement aux groupements *ortho*-méthoxy, qui déstabilisent l'orbitale n du (Z)-azobenzène par des interactions répulsives entre les doublets non liants des atomes d'O (OMe) et de N (N=N), les atomes de fluor en position *ortho* réduisent la densité électronique aux environs de la liaison N=N, réduisant ainsi l'énergie de l'orbitale n (Figure 23).^{54, 55} De plus, comme les fluors ont un rayon relativement petit, ils induisent une faible distortion de la géométrie de l'isomère (E).

⁵⁴ Beharry, A. A.; Sadovski, O.; Woolley, G. A., Azobenzene photoswitching without ultraviolet light, *J. Am. Chem. Soc.* **2011**, 133, 19684-19687.

⁵⁵ Bleger, D.; Schwarz, J.; Brouwer, A. M.; Hecht, S., *o*-Fluoroazobenzenes as readily synthesized photoswitches offering nearly quantitative two-way isomerization with visible light, *J. Am. Chem. Soc.* **2012**, 134, 20597-20600.

⁵⁶ Samanta, S.; Beharry, A. A.; Sadovski, O.; McCormick, T. M.; Babalhavaeji, A.; Tropepe, V.; Woolley, G. A., Photoswitching azo compounds *in vivo* with red light, *J. Am. Chem. Soc.* **2013**, 135, 9777-9784.

⁵⁷ Samanta, S.; McCormick, T. M.; Schmidt, S. K.; Seferos, D. S.; Woolley, G. A., Robust visible light photoswitching with *ortho*-thiol substituted azobenzenes, *Chem. Commun.* **2013**, 49, 10314-10316.



Figure 23. Deux exemples d'azobenzènes tétrasubstitués : *ortho*-méthoxylés **3** et *ortho*-fluororés **4**.

Il a été montré par des calculs d'orbitales moléculaires que l'isomère *E* est différent de l'isomère *Z* : concernant la forme des orbitales, les orbitales moléculaires de l'isomère *E* sont symétriques, tandis que celles de l'isomère *Z* sont sous forme d'hélice (Figure 24).

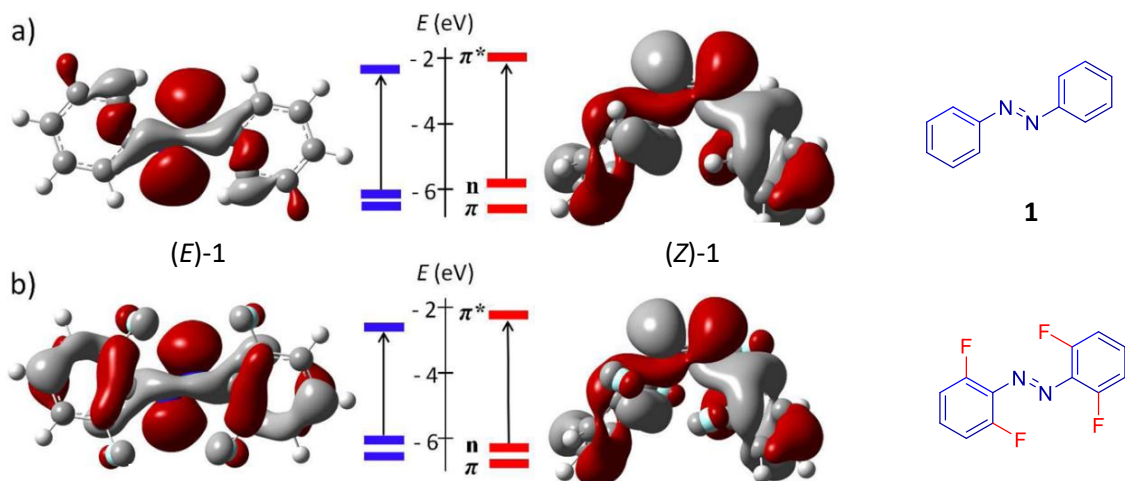


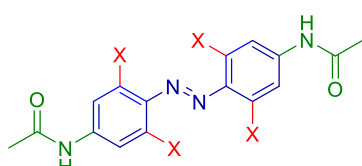
Figure 24. Diagramme énergétique des orbitales π , n et π^* de (a) l'azobenzène **1** et (b) azobenzène *ortho*-tétrafluorés, et la représentation des orbitales n (HOMO) (les flèches mettent en évidence les transitions $n \rightarrow \pi^*$).

Pour l'isomère *Z*-(**1**), la délocalisation des électrons π est réduite en raison des grands angles dièdres autour des liaisons simples N-C. Il en résulte que le niveau énergétique de l'orbitale π^* est beaucoup plus élevé que celui de l'isomère *E*-(**1**). Cependant, le niveau d'énergie de l'orbitale n de l'isomère *Z*-(**1**) est également beaucoup plus élevé que celui de l'isomère *E*. Il en résulte que les énergies d'excitation $n \rightarrow \pi^*$ sont très similaires pour les isomères *E* et *Z*. Les niveaux relativement élevés de l'orbitale moléculaire n dans l'azobenzène s'expliquent par l'interaction répulsive des doublets non liants des atomes d'azotes. Ainsi, une diminution de l'énergie de l'orbitale n est obtenue en réduisant la densité électronique des orbitales n par des groupements électro-attracteurs σ , tels que des substituants fluor en positions *ortho* (Figure 24b). En effet les atomes de fluor ont un effet inductif très fortement attracteur, tandis que son effet mésomère est plutôt négligeable (constante de Hammett $\sigma_{para} = 0,062$). Ceci conduit à une séparation des bandes $n \rightarrow \pi^*$ permettant une isomérisation dans le visible.

En conclusion, il faut donc privilégier les groupements électro-attracteurs afin de concevoir des pinces photoisomérisables dans le visible.

1.2.2. Demi-vie de l'isomère (Z)

La durée de vie courte de l'isomère (Z)-**1**, de 12 minutes, implique une source intense de lumière pour maintenir la fraction de cet isomère, ce qui limite l'utilisation *in vivo*. L'introduction de groupements en position *ortho* permet en général de prolonger cette demi-vie. Le Tableau 3 résume l'effet de la nature des substituants sur la demi-vie et sur la longueur d'onde d'irradiation. On voit que les demi-vies vont de 2 minutes pour le dérivé tétraéthylsulfanylé (Z)-**6** à 700 jours pour le dérivé *o,o'*-tétrafluoré (Z)-**3**. L'isomère (Z)-**3** *o,o'*-tétrafluoré devient ainsi la forme thermodynamiquement stable.^{53, 54, 55}



Composé	X	(Z)-T _{1/2}	λ irradiation (nm)
2	H	12 min	< 400
3	OMe	14 jours	450 – 560
4	F	700 jours	400 – 500
5	Cl	3.5 h	560 – 636
6	SEt	2-25 min	606 - 660

Tableau 3. Demi-vies des isomères (Z) et longueur d'onde d'irradiation d'isomérisation d'azobenzènes *o,o'*-tétrasubstitués.

1.2.3. Stabilité

Outre les propriétés de photo-isomérisation, la stabilité *in vivo* des isomères constitue un point important pour le développement d'outils pharmacologiques. *In vivo*, les composés azobenzènes peuvent être altérés soit par photoblanchiment, soit par métabolisation. Le mécanisme de réduction des composés azoïques par les thiols a été étudié par Kosower et ses collègues.⁵⁸ Le thiol du glutathion (GSH) attaque un des azotes de l'azobenzène pour donner un intermédiaire sulfényl-hydrazide. L'attaque d'un second équivalent GSH conduit à la forme oxydée GSSG ainsi qu'au dérivé hydrazinobenzène (Schéma 2).

⁵⁸ Kosower, E. M.; Kanety-Londner, H., Glutathione. 13. Mechanism of thiol oxidation by diazenedicarboxylic acid derivatives, *J. Am. Chem. Soc.* **1976**, 98, 3001-3007.

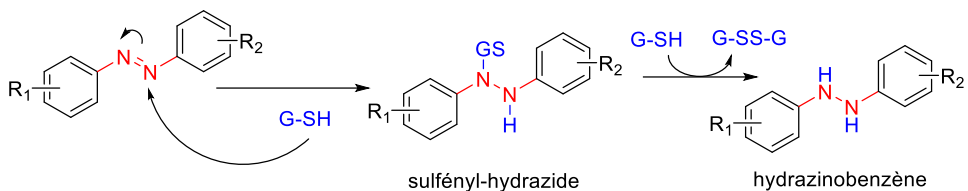


Schéma 2. Mécanisme de réduction des azobenzènes par le glutathion.

Le composé *o,o'*-tétraméthoxylé **3** est stable au photoblanchiment mais est facilement réduit en présence de glutathion.⁵⁴ Les composés *o,o'*-tétrachloré **7** et *o,o'*-tétraéthylsulfanylé **8** ont prouvé être résistants à cette réduction et sont également stables au photoblanchiment (Tableau 4).⁵⁵

Composé	X	R	T-réduction
3	OMe		1 h
7	Cl		>16 h
8	SEt		>14 h

Tableau 4. Stabilité d'azobenzènes *o,o'*-tétrasubstitués à la réduction par le glutathion.

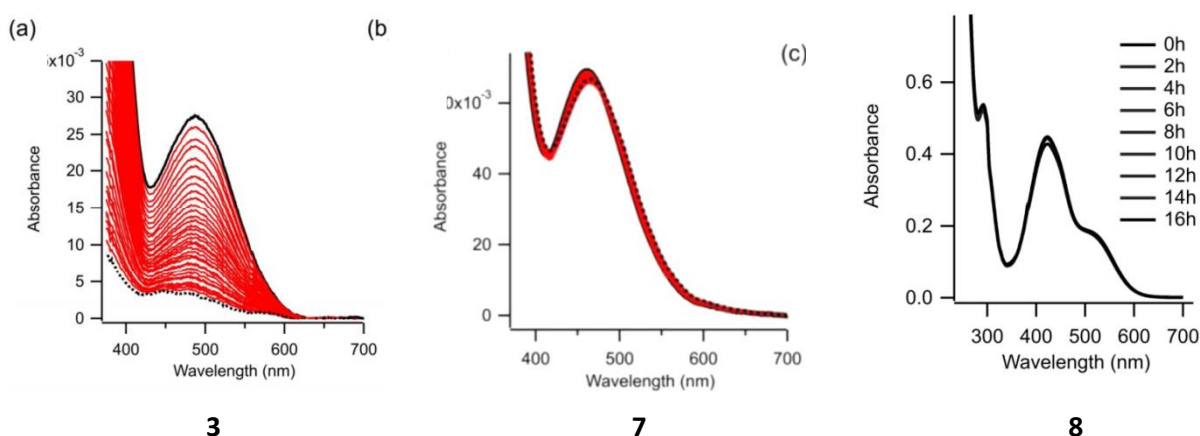


Figure 25. Réduction en présence de glutathion en 16 h des composés **3**, **7**, **8**.

Ce résultat est inattendu puisque les substituants chlorés, plus électroattracteurs par effet inductif que les substituants méthoxy, devraient augmenter la sensibilité à la réduction du composé azobenzène correspondant. La conformation non plane de l'isomère *E* diminue la capacité électrodonneur des groupements méthoxy par résonance, rendant ce dérivé plus sensible à la réduction.

Wooley et ses collègues ont supposé que l'attaque de la fonction thiol du glutathion serait facilitée, préalablement ou simultanément, par protonation du groupement azo pour augmenter son électrophilie. Le taux accru de réduction du composé tétra-*ortho*-méthoxylé **3** pourrait alors être dû à un pKa effectivement supérieur du groupement azo. Ainsi, la protonation du tétra-*ortho*-méthoxy azobenzène **3** et du tétra-*ortho*-chloro azobenzène **7** a été évaluée en mesurant les spectres UV-visible en fonction du pH (Figure 26). Ces données confirment que l'espèce tétra-*ortho*-méthoxylée **3** est protonée plus facilement que le tétra-*ortho*-chloré **7**. Les conformations de ces composés protonés ont été élucidées par modélisation moléculaire et sont représentées dans la figure 26. Dans le cas des dérivés protonés, l'isomère protoné *E* tétra-*ortho*-méthoxylé est planaire cette fois, tandis que l'analogue protoné tétra-*ortho*-chloré reste angulaire (Figure 26c, d). La conformation plane du substrat *E*-(**3**) protoné est assuré pour une liaison hydrogène au groupement méthoxy, jouant un rôle important dans le comportement de ce composé. La protonation d'un azote azoïque facilite ainsi l'attaque des thiols comme le montre la figure 26e. Cela peut se produire avant ou en même temps qu'une attaque nucléophile.

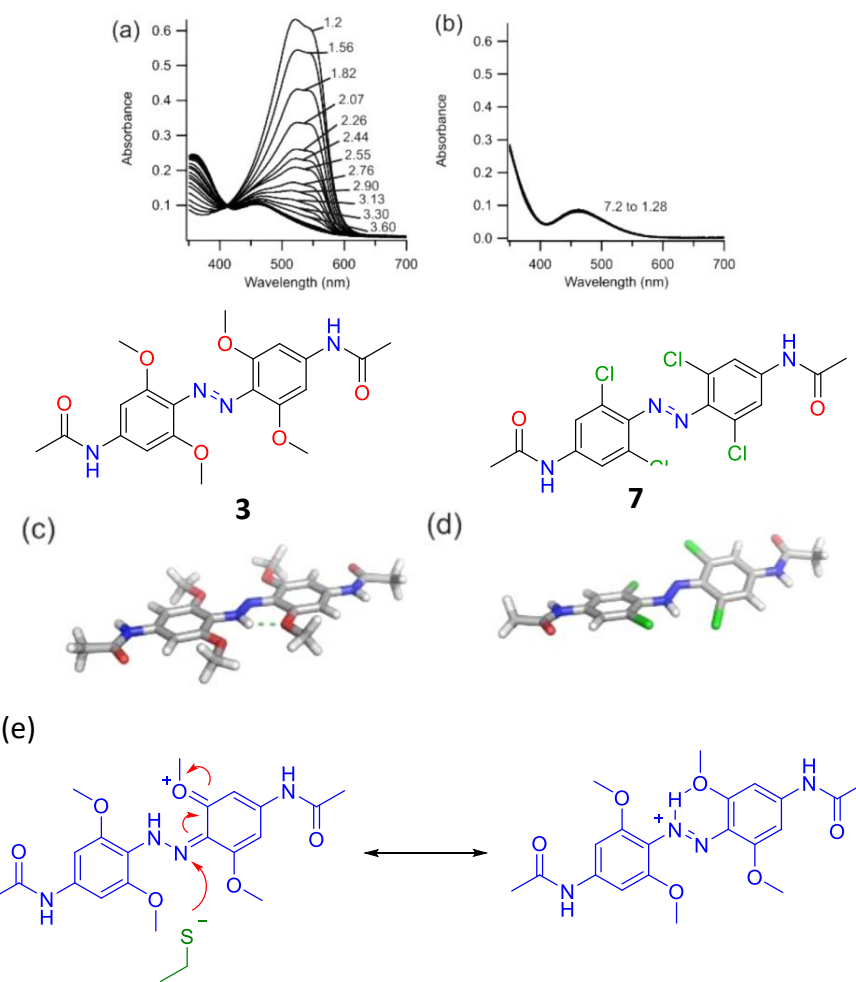


Figure 26. (a), (b) La protonation du groupement azo du composé tétra-méthoxy devient significative en dessous de pH 4, tandis qu'il n'y a pas de protonation évidente pour le composé tétra-chloré même à pH 1,3. (c), (d) Structures calculées au minimum d'énergie du **3** et du **7**. (e) Le composé **3** protoné est attaqué plus facilement par les thiols que lorsqu'il est sous sa forme non-protonée.

Le remplacement du groupement méthoxylé par le groupement éthylsulfanyle devrait diminuer la stabilisation de l'ion azonium par résonance. Les constantes de Hammett pour les groupements -OMe et -SEt sont en effet respectivement de -0,27 et 0,00. Par ailleurs, la liaison hydrogène au soufre moins forte devrait induire des préférences géométriques différentes à celles observées pour le dérivé méthoxylé. Par conséquence, l'azobenzène éthylsulfanyl devrait être moins sensible à la réduction par le glutathion que l'azobenzène méthoxylé. Ceci est confirmé expérimentalement (Figure 25).

Le photoblanchiment, ou la photodégradation est la perte d'intensité d'absorption et donc la perte d'activité du chromophore lorsque l'azobenzène est exposée à la lumière. Cet inconvénient est pour applications des azobenzènes comme photocommutaté.⁵⁹ Le mécanisme de cette photodégradation passe soit par une oxydation soit par une réduction, ce qui conduit à la décomposition de la molécule d'azobenzène (Schéma 3).^{60, 61} Lors de l'oxydation, il peut s'agir d'une réaction avec l'oxygène singulet actif. Ce dernier a été détecté et piégé par l'ajout du DABCO (1,4-diazabicyclo-[2,2,2]-octane), ce qui diminue donc le photoblanchiment. En passant par la réduction, l'hydrazine et les anilines correspondantes sont formés. La photostabilité des azobenzènes dépend de la nature de la molécule, de l'environnement du système (température, humidité, solvant) et de l'intensité de la source de lumière.⁶² Jusqu'à maintenant, les azobenzènes tétrasubstitués ont montré une grande stabilité face au photodégradation (Figure 27).

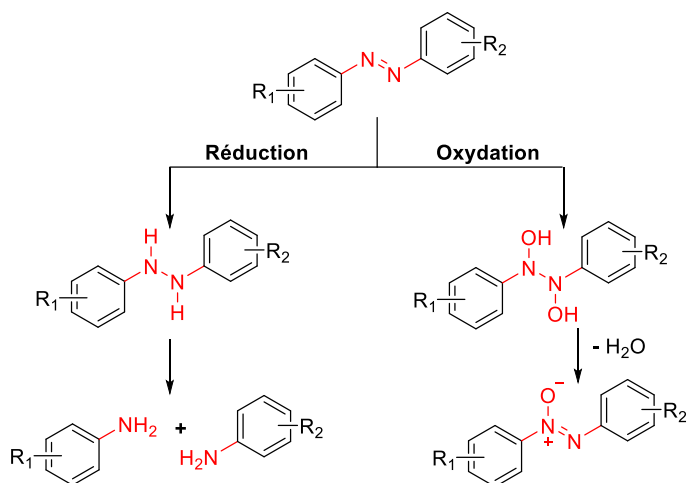


Schéma 3. Mécanisme de la photodégradation

⁵⁹ Costanzo, G. D.; Goyanes, S.; Ledesma, S., Photobleaching effect in azo-dye containing epoxy resin films: the potentiality of carbon nanotubes as azo-dye dispensers, *J. Phys.: Conf. Ser.* **2015**, *605*, 012024.

⁶⁰ Kuramoto, N.; Kitao, T., Contribution of singlet oxygen to the photofading of some dyes, *Color. Technol.* **1982**, *98*, 334-340.

⁶¹ Allen, N., Photofading and light stability of dyed and pigmented polymers, *Polym. Degrad. Stab.* **1994**, *44*, 357-374.

⁶² Galvan-Gonzalez, A.; Canva, M.; Stegeman, G. I.; Sukhomlinova, L.; Twieg, R. J.; Chan, K. P.; Kowalczyk, T. C.; Lackritz, H. S., Photodegradation of azobenzene nonlinear optical chromophores: the influence of structure and environment, *J. Opt. Soc. Am. B* **2000**, *17*, 1992-2000.

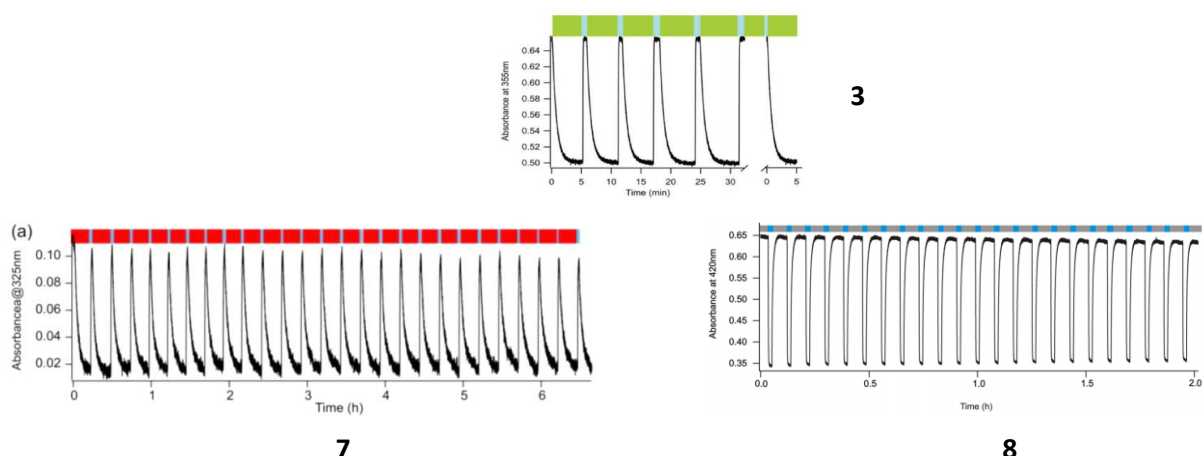


Figure 27. Test de photostabilité des composés **3**, **7**, **8** en les irradiant pendant plusieurs cycles avec une forte intensité lumineuse $70\text{-}90 \text{ mW/cm}^2$.

En tenant compte de ces différents paramètres, il nous apparaît que les azobenzènes tétrachlorés/tétrafluorés sont les plus intéressants pour le développement d'outils pharmacologiques utilisables sur du matériel biologique vivant.

1.3. Synthèse d'azobenzènes *o,o'*-tétrasubstitués

Si la construction du lien azo portant des benzènes non substitués est largement décrite dans la littérature, la synthèse d'azobenzènes *o,o'*-tétrasubstitués, plus délicate, est peu étudiée et conduit, en général, à des rendements faibles. Trois voies d'accès à la fonction azo sont décrites dans la littérature et passent respectivement par un intermédiaire nitrosobenzène, un sel de diazonium ou une diiodoaniline (Schéma 4-voies **1**, **2**, **3**). Par opposition à la construction directe du lien diazène N=N, une fonctionnalisation tardive par C-H activation permettant d'introduire des atomes de chlore sur des azobenzènes non-substitués a également été décrite (Schéma 4-voie **4**).

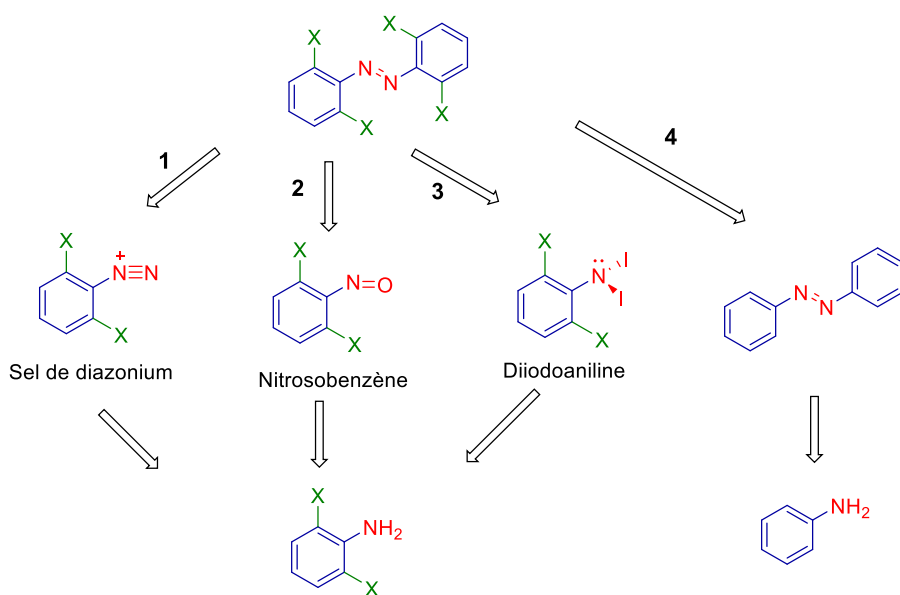


Schéma 4. Rétrosynthèse des azobenzènes tétrasubstitués.

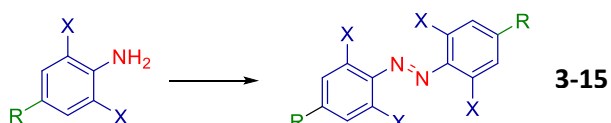
1.3.1. Synthèse par construction directe la fonction azobenzène

a) Synthèse impliquant un intermédiaire nitrosobenzène

La synthèse d'azobenzènes symétriques par oxydation d'amines primaires aromatiques en nitrosobenzènes est une méthode classique et largement utilisée.⁶³ De nombreux réactifs oxydants sont utilisés comme l'oxyde de manganèse, le permanganate de potassium ou d'argent, l'acide boronique, l'oxyde d'argent (I) ou encore l'oxone. La formation de l'azobenzène se fait selon une réaction monotope ou selon un processus en deux étapes impliquant l'isolement de l'intermédiaire nitroso suivi du couplage avec un second équivalent d'aniline.

Cette méthode a été largement exploitée pour la synthèse des azobenzènes *o,o'*-tétrasubstitués avec différents oxydants (Tableau 5).

L'équipe de Woolley a synthétisé les dérivés tétraméthoxylés **3** et **9**, tétraéthylsulfanylés **15** et tétrabromés **10** selon cette méthode oxydante en utilisant soit l'oxyde d'argent soit le permanganate de potassium avec des rendements ne dépassant pas 20 %.^{54, 56, 57} En 2012, Hecht et al. ont aussi utilisé cette méthode pour synthétiser des dérivés tétrafluorés toujours avec des rendements faibles.⁵⁵



Composé	X	R	Conditions	Rdt
3		NHCOMe	AgO/acétone, 6 h	10%
9	OMe	C ₆ H ₄ -NHCOMe	KMnO ₄ -CuSO ₄ .5H ₂ O, DCM, reflux, 48 h	20%
10	Br	NHCOMe	AgO/acétone, t. amb., 72 h	10%
11		H	KMnO ₄ -FeSO ₄ .7H ₂ O, DCM, reflux, 12 h	24%
12		Br	KMnO ₄ -FeSO ₄ .7H ₂ O, DCM, reflux, 12 h	22%
13	F	I	KMnO ₄ -FeSO ₄ .7H ₂ O, DCM, t. amb., 2 j	10%
14		COOEt	KMnO ₄ -FeSO ₄ .7H ₂ O, DCM, reflux, 12 h	23%
15	SEt	NO ₂	KMnO ₄ -FeSO ₄ .7H ₂ O, DCM, t. amb., 72 h	2%

Tableau 5. Synthèse des dérivés tétrasubstitués via l'oxydation en nitrosobenzène.

⁶³ Beharry, A. A.; Woolley, G. A., Azobenzene photoswitches for biomolecules, *Chem. Soc. Rev.* **2011**, *40*, 4422-4437.

Un azobenzène *ortho*-tétrasubstitué dissymétrique a aussi été préparé via la formation d'un intermédiaire de type nitroso.⁶⁴ Le rendement global des deux étapes reste très moyen (Schéma 5).

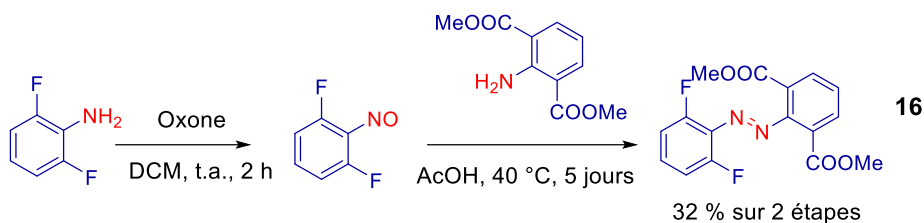


Schéma 5. Synthèse d'une molécule azobenzène tétrasubstitués dissymétrique impliquant un intermédiaire nitrosobenzène.

Le mécanisme de la réaction est bien décrit : oxydation de l'aniline en phénylhydroxylamine, puis en nitrosobenzène, suivie de l'attaque nucléophile d'un second équivalent d'aniline sur cet intermédiaire nitroso pour former, après déshydratation, l'azobenzène (Schéma 6).

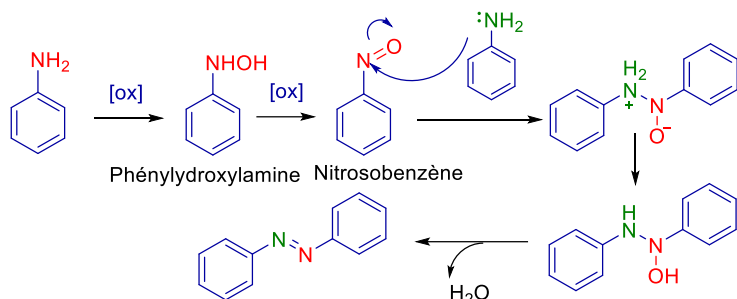


Schéma 6. Mécanisme de synthèse des azobenzènes par oxydation impliquant un intermédiaire nitrosobenzène.

b) Synthèse impliquant un intermédiaire diazonium

Cette méthode est également assez générale pour la synthèse des azobenzènes. La méthodologie est basée sur la diazotation initiale d'une amine primaire aromatique à basse température, qui réagit ensuite avec un nucléophile aromatique enrichi en électrons. La réaction est souvent rapide et conduit aux dérivés azo avec de bons rendements. Cette réaction est cependant dépendante du pH. En accord avec le mécanisme décrit sur le Schéma 7, la présence d'un acide est nécessaire pour libérer *in situ* l'acide nitreux. Une séquence protonation-déshydratation permet la formation de l'électrophile nitrosonium, qui réagit ensuite avec l'amine pour donner le dérivé *N*-nitroso, tautomère du diazohydroxyde. Une seconde séquence protonation-déshydratation conduit finalement au sel de diazonium stabilisé par résonance.

La deuxième étape du mécanisme repose sur une substitution électrophile régiosélective en position *para* par rapport au groupe électrodonneur -NH₂ du cycle aromatique activé, jouant le rôle d'un

⁶⁴ Castellanos, S.; Goulet-Hanssens, A.; Zhao, F.; Dikhtierenko, A.; Pustovarenko, A.; Hecht, S.; Gascon, J.; Kapteijn, F.; Bleger, D., Structural effects in visible-light-responsive metal-organic frameworks incorporating *ortho*-fluoroazobzenes, *Chem. Eur. J.* **2016**, 22, 746-752.

nucléophile. Le pH de la deuxième réaction doit être légèrement basique dans le cas du couplage avec un phénol, alors qu'avec une amine aromatique, il doit être légèrement acide ou neutre.

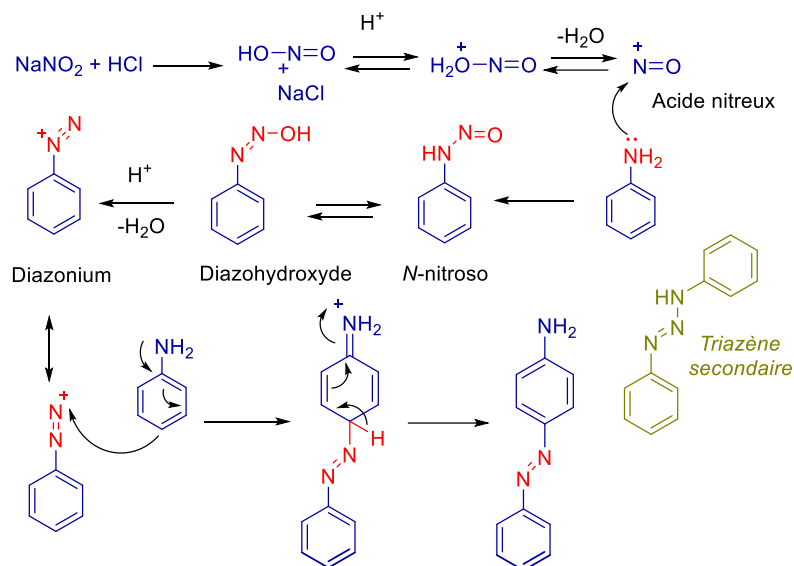


Schéma 7. Mécanisme de synthèse des azobenzènes par couplage avec un sel de diazonium.

Utilisant cette méthode, Woolley a synthétisé le dérivé tétraméthoxylé **17** avec un rendement de 31% (Schéma 8).

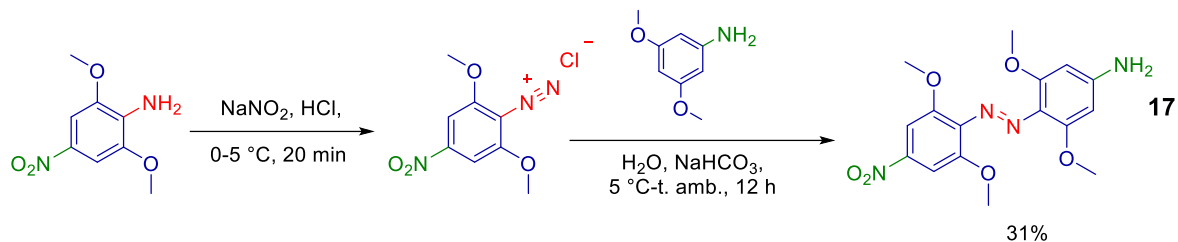


Schéma 8. Synthèse du dérivé tétra-méthoxylé **17** par couplage du sel de diazonium.

Le couplage avec une amine aromatique peut parfois former un produit secondaire de type triazène (Schéma 7). L'utilisation d'un dérivé méthanesulfonate de sodium permet d'éviter cette réaction secondaire et conduit au dérivé tétrachloré **18** avec un rendement de 26% (Schéma 9).⁵⁶

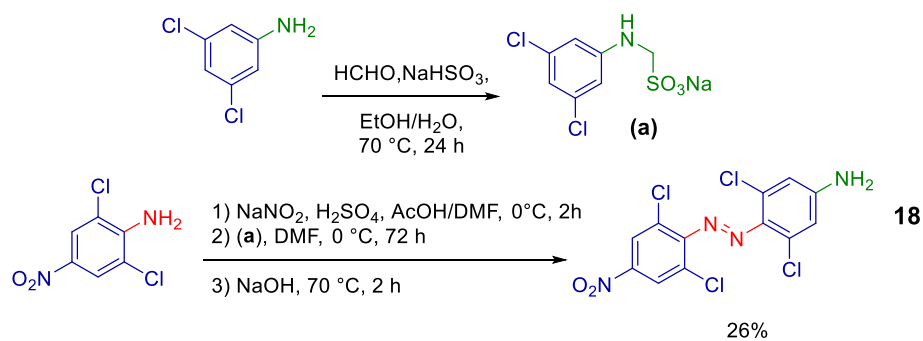


Schéma 9. Synthèse du dérivé tétrachloré **18** par couplage avec un sel diazonium.

Quels que soient les substituants en position *ortho* et *para* de l'amine aromatique et, quelle que soit la méthode utilisée, on obtient néanmoins toujours des rendements faibles. De plus, aucune étude rationnelle ne permet d'expliquer ces rendements.

Récemment, un accès assez rapide et efficace pour synthétiser des azobenzènes tétrabustitués symétriques ainsi que dissymétriques a été développé par l'équipe de Feringa à l'université de Groningen.⁶⁵ Les chercheurs ont utilisé une réaction d'*ortho*-lithiation sélective suivie d'une réaction avec un sel de diazonium formé au préalable (Tableau 6).

Composé	Ar ¹ -Li	Ar ² -N ₂	Produits	Rendement
19				81 %
20				82 %
21				77 %
22				91 %
23				89 %

Tableau 6. Exemples de synthèse d'azobenzènes tétrasubstitués via *ortho*-lithiation et couplage à un sel de diazonium.

⁶⁵ Hansen, M. J.; Lerch, M. M.; Szymanski, W.; Feringa, B. L., Direct and versatile synthesis of red-shifted azobenzenes, *Angew. Chem. Int. Ed.* **2016**, 55, 13514-13518.

Néanmoins, la méthode a seulement été étudiée avec des dérivés non-substitués en position *para* ou avec un substituant identique à ceux en *ortho*.

c) Synthèse impliquant un intermédiaire diiodoaniline

Une nouvelle méthode efficace pour la synthèse des composés azobenzènes symétriques et dissymétriques a été publiée récemment par l'équipe de Minakata.⁶⁶ En utilisant le *tert*-butylate d'iodonium dans des conditions douces, un large panel d'azobenzènes non-substitués, disubstitués et même tétrasubstitués en position *ortho* a été préparé avec des bons rendements. Deux exemples de synthèse de dérivés tétra-fluorés sont donnés avec de bien meilleurs rendements, de 62 et 82%, par rapport aux méthodes vues précédemment (Tableau 7).

Composé	R	Solvant, temps	Rdt
24	Br	<i>t</i> -BuOH, 3 h	62%
25	NHCOMe	Et ₂ O, 12 h	82%

Tableau 7. Synthèse des dérivés tétra-fluorés par oxydation avec *t*-BuOI.

Un avantage majeur de cette étude est également la possibilité de construire des azobenzènes substitués différemment sur les 2 noyaux en une seule étape (Figure 28).

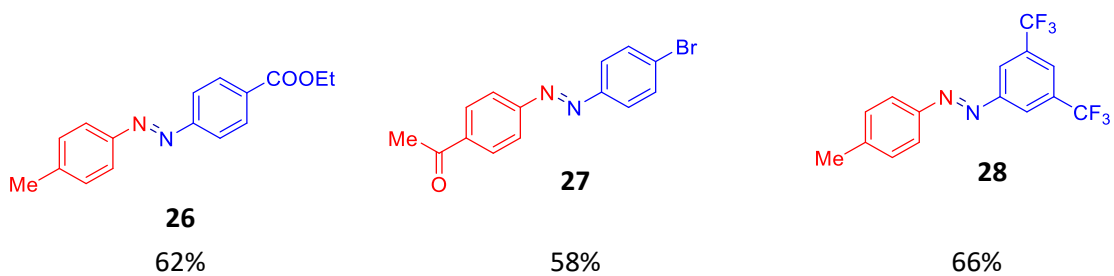


Figure 28. Exemples des azobenzènes dissymétriques obtenus par oxydation avec du *t*-BuOI.

Le mécanisme plausible de cette réaction commence par une *N*-iodation de l'aniline enrichie en électrons grâce à un échange H/I donnant l'aniline *N*-monoiodée **A**. Une deuxième iodation de **A** conduit à l'intermédiaire clé *N,N*-diiodoaniline **B**. L'aniline diiodée **B** réagit alors avec le second équivalent d'aniline appauvrie en électrons pour former la simple liaison N-N, conduisant à **C** et qui s'accompagne de la libération d'acide iodhydrique. Finalement, l'élimination d'un autre équivalent

⁶⁶ Okumura, S.; Lin, C. H.; Takeda, Y.; Minakata, S., Oxidative dimerization of (hetero)aromatic amines utilizing *t*-BuOI leading to (hetero)aromatic azo compounds: scope and mechanistic studies, *J. Org. Chem.* **2013**, *78*, 12090-12105.

d'acide iodhydrique donne le produit azobenzène. L'acide iodhydrique libéré est piégé par le *tert*-butylate d'iodonium, formant ainsi du iodure et du *tert*-butanol (Schéma 10).

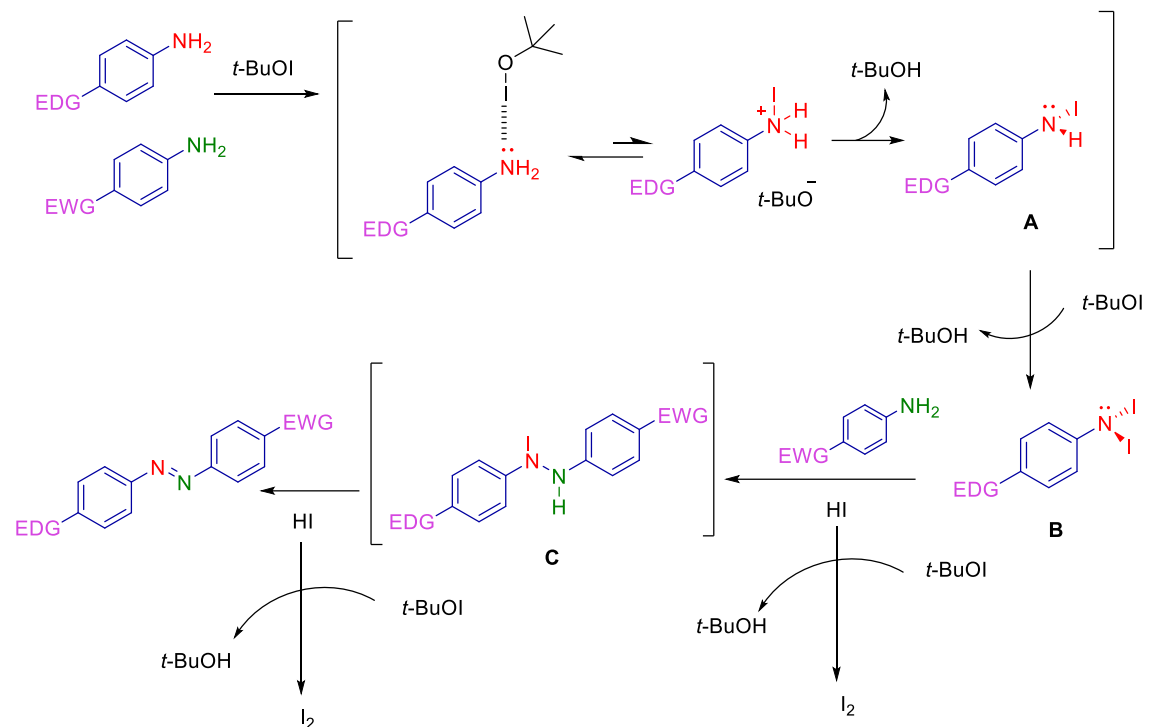


Schéma 10. Mécanisme de synthèse des azobenzènes par oxydation avec du *t*-BuOI.

Cette méthode récente semble prometteuse. Cependant, elle n'a été réalisée que sur deux exemples de molécules *o,o'*-tétrafluorées (Tableau 7).

1.3.2. Synthèse impliquant une fonctionnalisation tardive

Comme nous l'avons vu lors des trois méthodes précédentes, l'oxydation directe des anilines pour accéder aux azobenzènes tétrasubstitués reste très ardue et toutes les études ont conduit à des rendements assez faibles. Afin d'éviter le couplage délicat à partir de dérivés anilines encombrés, il serait envisageable de synthétiser des azobenzènes non-substitués et ensuite d'introduire des substituants en position *ortho*.

Dans ce contexte, l'équipe de Trauner a développé en 2016 une nouvelle méthode de tétra-*ortho*-chloration *via* une réaction de C-H activation sur des azobenzènes simples.⁶⁷ En utilisant une quantité catalytique de Pd(OAc)₂, du *N*-chlorosuccinimide (NCS) dans l'acide acétique et en chauffant le milieu réactionnel à 140 °C, de nombreux azobenzènes symétriques ainsi que dissymétriques ont été synthétisés. Des dérivés contenant deux groupements fonctionnels utiles en *para*, comme le 4-iodo-4'-nitroazobenzène (**31**) et le 4,4'-dibromoazobenzène (**32**) ont été obtenus avec de bons rendements (Schéma 11).

⁶⁷ Konrad, D. B.; Frank, J. A.; Trauner, D., Synthesis of redshifted azobenzene photoswitches by late-stage functionalization, *Chem. Eur. J.* **2016**, 22, 4364-4368.

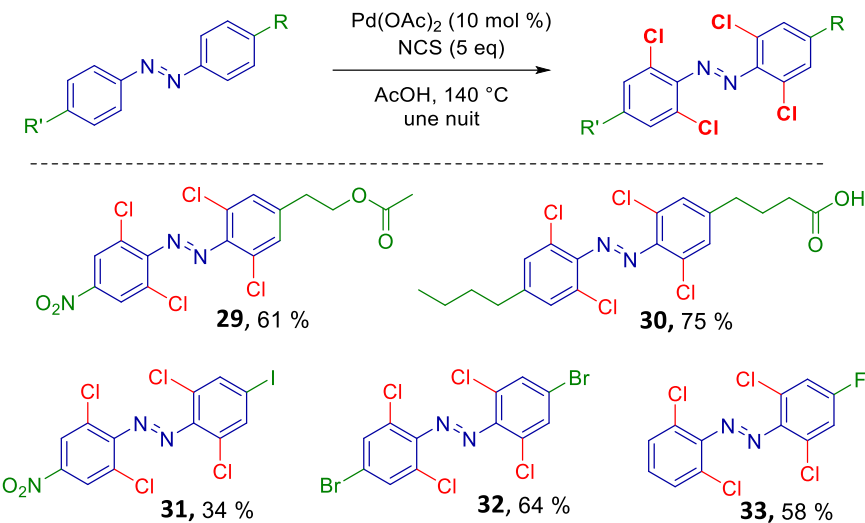


Schéma 11. Tétrachloration par C-H activation.

Le mécanisme de la réaction repose sur un cycle catalytique commençant par l'insertion du Pd dans la liaison C-H de l'azobenzène. Le Pd(II) est alors oxydé en Pd(IV) par addition oxydante du NCS. L'élimination réductrice permet de former la liaison C-Cl et de régénérer le Pd(II) sous sa forme active (Schéma 12).^{68, 69}

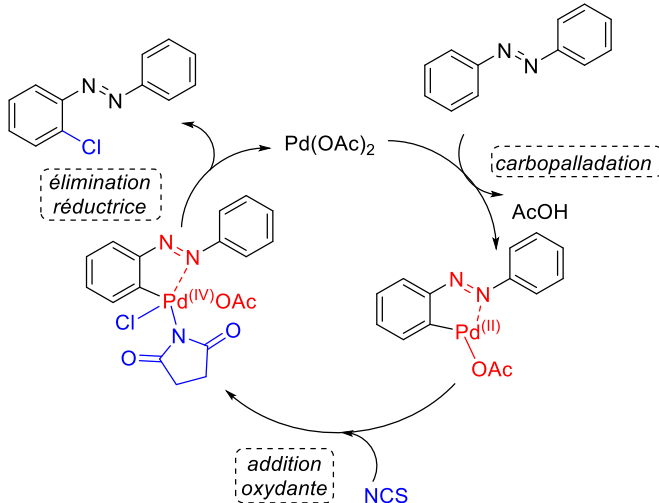


Schéma 12. Mécanisme de C-H activation.

Cette étude est la seule méthode d'*ortho*-tétra fonctionnalisation des azobenzènes décrite à ce jour. Les questions relatives à la fluoruration, à la méthoxylation ou à d'autres fonctionnalisations pour accéder aux azobenzènes tétrasubstitués restent ouvertes.

⁶⁸ Lyons, T. W.; Sanford, M. S., Palladium-catalyzed ligand-directed C–H functionalization reactions, *Chem. Rev.* **2010**, *110*, 1147–1169.

⁶⁹ Fahey, D. R., The homogeneous palladium-catalysed *ortho*-chlorination of azobenzene, *J. Chem. Soc. D.* **1970**, 417a–417a.

2. Article 1 : Efficient access to symmetrical tetra-*ortho*-substituted azobenzenes

Efficient access to symmetrical tetra-*ortho*-substituted azobenzenes

Thi Hong Long Nguyen,^a Nicolas Gigant,^a Sandrine Delarue-Cochin,^a Delphine Joseph.*^a

In this article, we described the methodological study we carried out to synthesize, in good to excellent yields, sterically hindered tetra-*ortho* substituted azobenzenes. This method allowed us to prepare efficiently a redshifted photoswitch in 6 steps with an overall 30% yield.

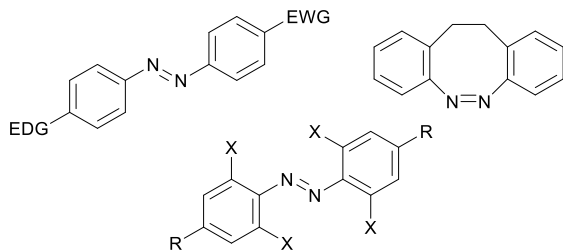
Introduction

The possibility offered by the photocontrol of biomolecules *in vivo* is opening tremendous opportunities for the study of biological processes at the single-cell level in living organisms¹ and incited the prestigious Nature Method review to choose optogenetics as Method of the Year 2010.² While the first optogenetic tools exploited natural light sensitive proteins, in particular rhodopsins, a subdiscipline called optochemical genetics has rapidly emerged, combining genetic modifications of the target proteins and use of exogenous photoactive synthetic molecules.³⁻⁵ Among the numerous molecular classes undergoing photoisomerization, azobenzenes form one of the largest and most studied photoswitch classes considering their numerous advantages: easy synthesis, high photostationary states and quantum yields, fast photoisomerization and low rate of photobleaching.⁶⁻⁸ The main limitation is that the majority of photochromic compounds are hydrophobic and requires UV light for at least one photoswitching direction while *in vivo* optical applications need visible light, in particular red light, to achieve significant penetration through tissue and to limit damage to living cells.

Nevertheless three classes of azobenzenes were reported where the *trans/cis* switch could be controlled using visible light: the push-pull,⁹ the bridged¹⁰ and the tetra-*ortho*-substituted azobenzenes¹¹ (Figure 1). This last family was largely studied over the last five years in order to improve the different photochemical properties, mainly by varying the *ortho*-substituents.¹²⁻¹⁶ Examples of *in vivo* applications showed the high potency of such compounds.¹³⁻¹⁴

However, if the synthesis of non-substituted azobenzenes is well established, access to tetra-*ortho*-substituted azobenzenes is scarcely described, using either a nitrosoarene or a diazonium salt intermediate and leading to low yields, not exceeding 30% yield.¹¹⁻¹⁶ Only two tetra-*ortho*-fluoroazobenzenes were synthesized efficiently by employing *tBuO*I as oxidant.¹⁷ Two recent alternatives were proposed, one consisting in a late-stage functionalization of existing azobenzenes, but only with chlorine atoms,¹⁸ the other employing an *ortho*-lithiated aromatic substrate condensed with a diazonium salt.¹⁹ The scope of this last method was however limited to *para*-substituent identical to the *ortho*-ones. So, widespread use of these promising pharmacological tools was limited by their laborious syntheses.

Figure 1. Structure of push-pull, bridged and tetra-*ortho*-substituted azobenzenes.



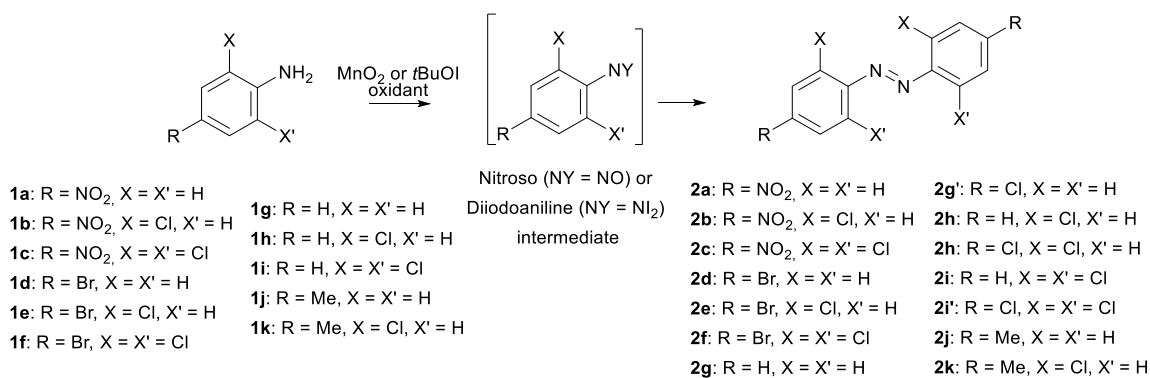
Here, we report the study we carried out in order to access efficiently tetra-*ortho*-substituted azobenzenes and its application to prepare a new redshifted photoswitch.

Results and Discussion

In order to better understand the reasons of such low yields in the case of *ortho*-disubstituted anilines, we decided first to compare some of the classical methods to access azobenzenes,^{14,17,20} on *para*-substituted anilines presenting or not chlorine atom(s) at the *ortho* positions (Scheme 1, Table 1).

Methodology implying a diazonium salt was found to be ineffective in our case, leading either to degradation or to the triazene by-product, C-alkylation being disadvantaged with regard to the direct *N*-alkylation of the aniline. This phenomenon was already observed in the literature data making necessary the use of a protected aniline.¹⁴ The two other representative methods using MnO₂²⁰ or *t*BuO¹⁷ as oxidant were effective for non-substituted aniline **1a**, but efficiency decreased drastically even with only a chlorine atom on the *ortho* position, with increasing reaction time and yield loss for **1b** (Table 1, Assay 1 *versus* Assay 2). With di *ortho*-substituted aniline **1c**, the desired azobenzene **2c** was only obtained as traces in the case of MnO₂ oxidant even after 3 days in refluxing toluene (Table 1, Assay 3). *t*BuO¹ appeared to be more efficient allowing access to **2c** in 18% yield after 4 days at room temperature, and was selected to study the combined impact of *ortho* and *para*-substitution. If steric hindrance caused by *ortho*-substitution is responsible for most of yield loss (Table 1, Assays 1,2 and 3, Assays 4,5 and 6 and Assays 10 and 11) electronic effect of *para*-substitution had also a sizeable impact on the reaction, electron withdrawing group leading to a reduced yield compared to electron donating group (Table 1, Assays 2, 5 and 11, Assays 3 and 6).

It is noteworthy that in the case of **1g-1i** presenting no substituent at the *para*-position, a mixture of expected azobenzenes **2g-2i** and *para*-chlorinated azobenzenes **2g'-2i'** was obtained. This was in contradiction with the results of Okumura *et al* who did not mention any chlorination.¹⁷ In our hand, this reaction proved to be highly dependent of the *t*BuOCl quality and origin, this compound was not commercially available in Europa and its preparation proved to be non reproducible in our hand.



Scheme 1.

Assay	Starting material	Isolated Compound	Yield (%) with MnO ₂ as oxidant ^(a)	Yield (%) with tBuOI as oxidant ^(b)
1	1a	2a	60	78
2	1b	2b	30 ^(c)	40 ^(c)
3	1c	2c	6	18
4	1d	2d	nd	84
5	1e	2e	nd	50
6	1f	2f	nd	30
7	1g	2g / 2g' ^(d)	nd	20 / 50
8	1h	2h / 2h' ^(d)	nd	15 / 38
9	1i	2i / 2i' ^(d)	nd	0 / 10
10	1j	2j	nd	87
11	1k	2k	nd	60

(a) Conditions: MnO₂ (10 eq.), refluxing toluene, 24 h (for non *ortho*-substituted anilines), 72 h (for mono *ortho*-substituted anilines) or 6 days (for di *ortho*-substituted anilines); (b) Conditions: tBuOCl/NaI (2 eq.), Et₂O or THF, room temperature, 1 h (for non *ortho*-substituted anilines), 12 h (for mono *ortho*-substituted anilines) or 4 days (for di *ortho*-substituted anilines); (c) Estimated conversion into compound **2b** by means of ¹H NMR (d) *para*-chlorinated azobenzenes were obtained as major products

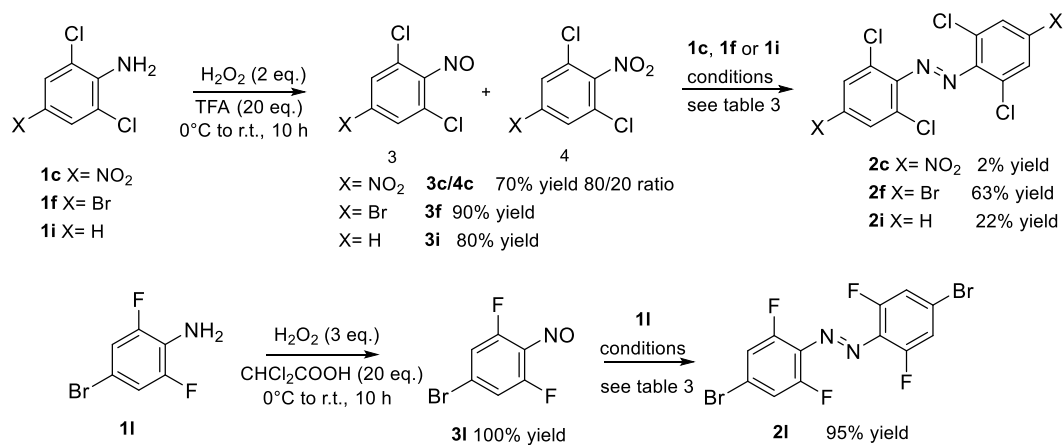
Table 1. Effect of *ortho*-and *para*-substitution of aniline on azobenzene synthesis.

Thus satisfying results obtained in the literature for tetra-*ortho*-fluoroazobenzenes (62% with bromine as *para*-substituent)¹⁷ were not reproduced with tetra-*ortho*-chloroazobenzenes **2c**, **2f** and **2h**. Attempts to improve yield (Use of 4 eq. of tBuOI instead of 2 eq. as well as addition of tBuOK or increase of the reaction temperature) remained unsuccessful.

In conclusion, the limitation appeared to be the rough access to the oxidized intermediate, *ortho*-substituted anilines being in general majority recovered and was caused by steric hindrance of *ortho*-susbtitution and, to a lesser extent, by electronic effects of *para*-substitution.

A way to circumvent this limitation was to find conditions to prepare efficiently the *ortho*-disubstituted nitroso intermediates and to make it react with a second equivalent of aniline in a Mills reaction allowing access to the desired azobenzenes. Oxone, *m*-CPBA as well as hydrogen peroxide were described as suitable methods to access hindered nitrosoarenes.²¹⁻²³ So, we carried out a study of oxidation with oxone in biphasic conditions, *m*-CPBA in DCM or H₂O₂ in various acidic media in the case of the hindered aniline **1c**. Unfortunatly, oxidation with oxone in biphasic conditions²¹ was unsuccessfull for aniline **1c**, completely insoluble in water which prevented it from oxone oxidation. With *m*-CPBA as oxidant,²² we failed to obtain the desired nitrosoarene **3c**, reaction stopping to the hydroxylamine intermediate.

With hydrogen peroxide as oxidant and use of acetic acid as solvent, only starting material **1c** was recovered, which was in contradiction with literature data.²³ Use of more acidic solvent such as formic acid and TFA and optimization of the reaction conditions allowed to access nitrosoarene **3c** as the major compound, with nitroarene **4c** as the byproduct (Scheme 3). The best compromise was the use of 2 eq. of hydrogen peroxide in 20 eq. of TFA, at 0°C to room temperature for 10h with access to a mixture of nitrosoarene **3c** and nitroarene **4c** in a 80/20 ratio. These conditions in hand, we applied them to different hindered anilines. The nitrosoarenes **3c**, **3f** and **3i** were thus obtained efficienlty (Scheme 3). For difluorinated aniline **1l**, less acidic medium was required, and with dicholoroacetic acid as solvent, nitrosoarene **3l** was obtained quantitatively (Scheme 3).



Scheme 3.

Crude nitrosoarenes were used for condensation with anilines. Nitrosoarene **3f** was condensed to aniline **1f** (Table 2). The solvent acidity was crucial in the Mills reaction, yields of azobenzene **3f** starting from 0% for acetic acid to 48% for trichloroacetic acid (Table 2, Assays 1 to 6). Furthermore,

a portionwise addition and an excess of nitrosoarene allowed us to improve yield to 63% (Table 2, Assay 7). However the conditions were highly dependent on the nitrosoarene used. For nitrosoarenes **2c** and **2i**, azobenzenes **3c** and **3i** were obtained in modest yields (Table 2, Assays 8 to 10).

Nitrosoarene **3l** proved to be highly reactive, and stoichiometric proportion in chloroacetic acid was sufficient to access azobenzene **2l** in excellent yield (95%).

Assay	Nitroso/Aniline proportion	Solvent	Temp.	Time	Azobenzene	Isolated Yield (%)
1	3f/1f: 1/1	AcOH	40°C	6 days	2f	0
2	3f/1f: 1/1	TFA	60°C	4 days	2f	18
3	3f/1f: 1/1	TFA/H ₂ O	50°C	4 days	2f	10%
4	3f/1f: 1/1	Chloroacetic acid/H ₂ O	50°C	4 days	2f	5%
5	3f/1f: 1/1	Dichloroacetic acid/H ₂ O	50°C	4 days	2f	20%
6	3f/1f: 1/1 or 2/1	Trichloroacetic acid/H ₂ O	50°C	4 days	2f	48%
7	3f/1f: 2.5/1 ^a	Trichloroacetic acid/H ₂ O	50°C	5 days	2f	63%
8	3c/1c: 1/1	Trichloroacetic acid/H ₂ O	50°C	4 days	2c	2%
9	3c/1c: 1/1	TFA/H ₂ O	50°C	4 days	2c	3%
10	3i/1i: 2.5/1 ^a	Trichloroacetic acid/H ₂ O	50°C	5 days	2i	22%
11	3l/1l: 1/1	Chloroacetic acid/H ₂ O	35°C	1 day	2l	95%

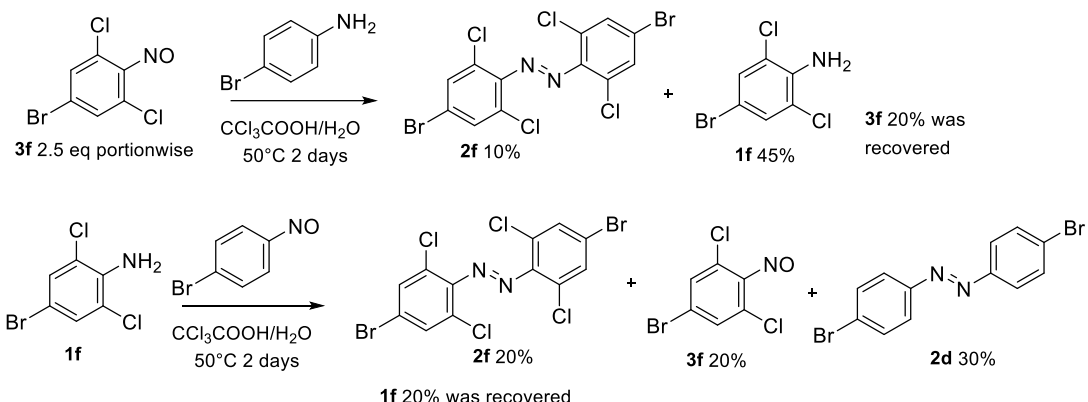
(a): portionwise addition of nitrosoarene **2** (0.5 eq. *per day*).

Table 2. Condition screening of tetracholoazobenzene synthesis

This methodology being fairly efficient in the case of symmetrical *ortho*-chloro- and fluoro-azobenzenes, we would like to know if this allowed us to access unsymmetrical *ortho* substituted azobenzenes.

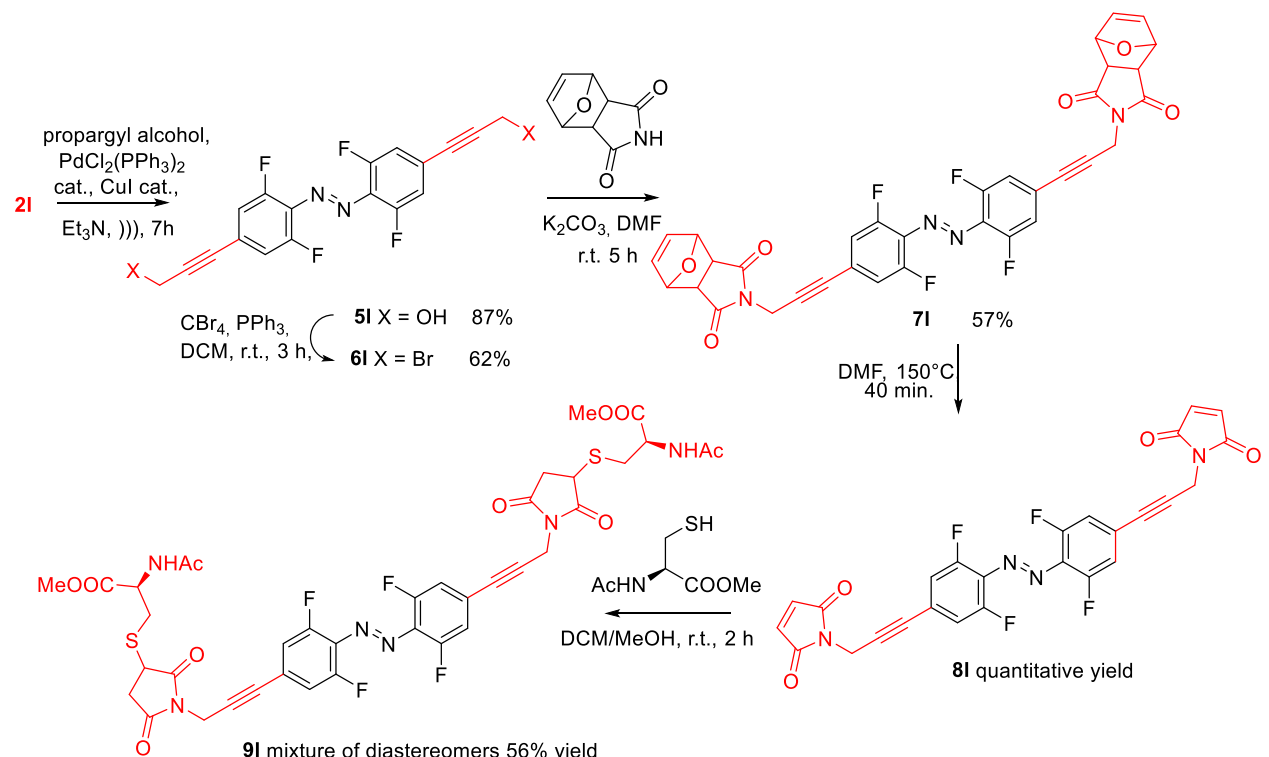
Different attempts were carried out (Scheme 4). However, we only obtained the symmetrical azobenzenes **2f** and **2d**. Azobenzene coupling seemed to be in competition with redox reactions

between aniline and nitroso starting materials. This hypothesis was supported by isolation of byproducts **1f** (case 1) or **3f** (case 2) which were not present initially.



Scheme 4.

Finally, possessing an efficient method to access tetra-*ortho*-fluoro- and tetra-*ortho*-chloroazobenzenes, we developed an efficient synthesis of a redshifted azobenzene photoswitch (Scheme 5). We focused our attention on the tetrafluoroazobenzenes because of their promising photochemical properties as reported in the literature.¹² We first optimized a Sonogashira coupling with propargyl alcohol by using ultrasonic irradiation to obtain the diol **5I**.²⁴ An Appel reaction²⁵ gave us the dibrominated derivative **6I**. Finally, we introduced the maleimide groups by a two-step procedure.²⁶ The desired photoswitch linker **8I** was thus synthesized in 6 steps starting from aniline **1I** in a 30% global yield.



Scheme 5.

Our photoswitch **8I** was easily condensed with a cysteine derivative (Scheme 5) to afford a diastereomeric mixture of bis-adduct **9I**, mimicking the bioconjugation of **8I** with peptides.

The photochemical behavior of the compound **9I** was then evaluated. The UV-Vis absorption spectrum of **9I**, which was in a *E/Z* 65/35 equilibrium, was measured in MeOH and shows a $\pi-\pi^*$ maxima band at 337 nm and a $n-\pi^*$ slight band at 463 nm (Figure 2). Irradiation with UV light at 370 nm induced *E*→*Z* isomerization in only 10 secondes, causing the intense decrease of $\pi-\pi^*$ band. A photostationary state (PSS) containing 80% *Z* was observed, accompanied by the effective 42 nm separation of the $n-\pi^*$ bands. Indeed, as reported by Hecht and coworkers¹², the significant bathochromic shift of $n-\pi^*$ band proved that azobenzene **9I** can be selectively excited with the visible light. As expected, irradiation with green light at 543 nm also induced *trans* to *cis* isomerization in a slower way, around 8 minutes. Use of visible light is essential for *in vivo* application, avoiding the danger for the living cells and tissues relative to UV light. Noteworthy, *E* isomer can be regenerated to 90% in 15 secondes with blue light (433 nm).

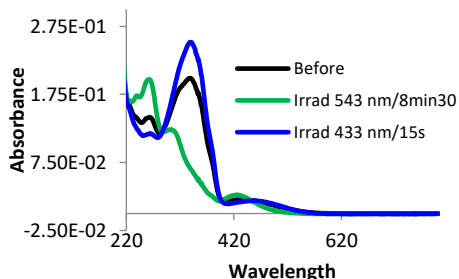


Figure 2. UV-Vis absorption spectra of **9I** in MeOH: before irradiation, after irradiation by green light at 543 nm and by blue light at 433 nm.

Compound **9I** has also been demonstrated photostable, since multiple cycles of photosisomerization by alternating UV and blue light in solution gave no evidence of degradation (Figure 3).

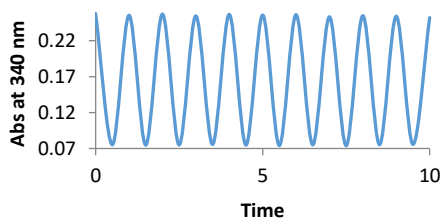


Figure 3. Photobleaching test of **9I**

The thermal *cis* to *trans* isomerization was remarkably slow in the dark with a half-life for the *cis* isomer of 72 days at 25 °C (Figure 4). Interestingly, *E* isomer can be regenerated up to nearly 100% in the perfect dark. This particularly long half life was not usual in the literature and was hugely interesting for the biological application in which a spatiotemporal measure to control a long process

was desired. A tetrafluoroazobenzene derivative reported by the team of Hecht had an impressive half-life of 700 days at 25 °C, obtained from theoretical calculation to an activation barrier energy. Other tetrafluoroazobenzenes were declared from 30 h up to 96 h at 60 °C,²⁷ while an *o*-tetramethoxyazobenzene derivative with a significant half life of 14 days in DMSO at 25 °C was disclosed.¹¹ So, our compound **9I** presented one of the highest thermal stability measured and reported.

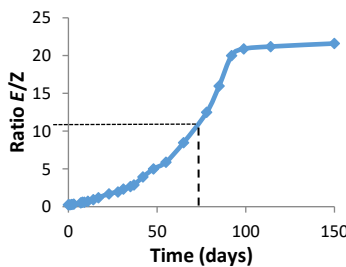


Figure 4. Half-life of compound *cis*-**9I**

Conclusions

In summary, we have realized a methodological study of the synthesis of *ortho*-tetrasubstituted azobenzenes. An efficient strategy for the construction of a tetrachloro and a tetrafluoro azobenzene has also been reported. The bioconjugated *o*-tetrafluorophotoswitch with the cysteine showed excellent photochemical properties with a redshifted *E/Z* isomerisation and an exceptional half-life of 72 days. These results are actually hopeful for a wide range of biological applications.

Notes and references

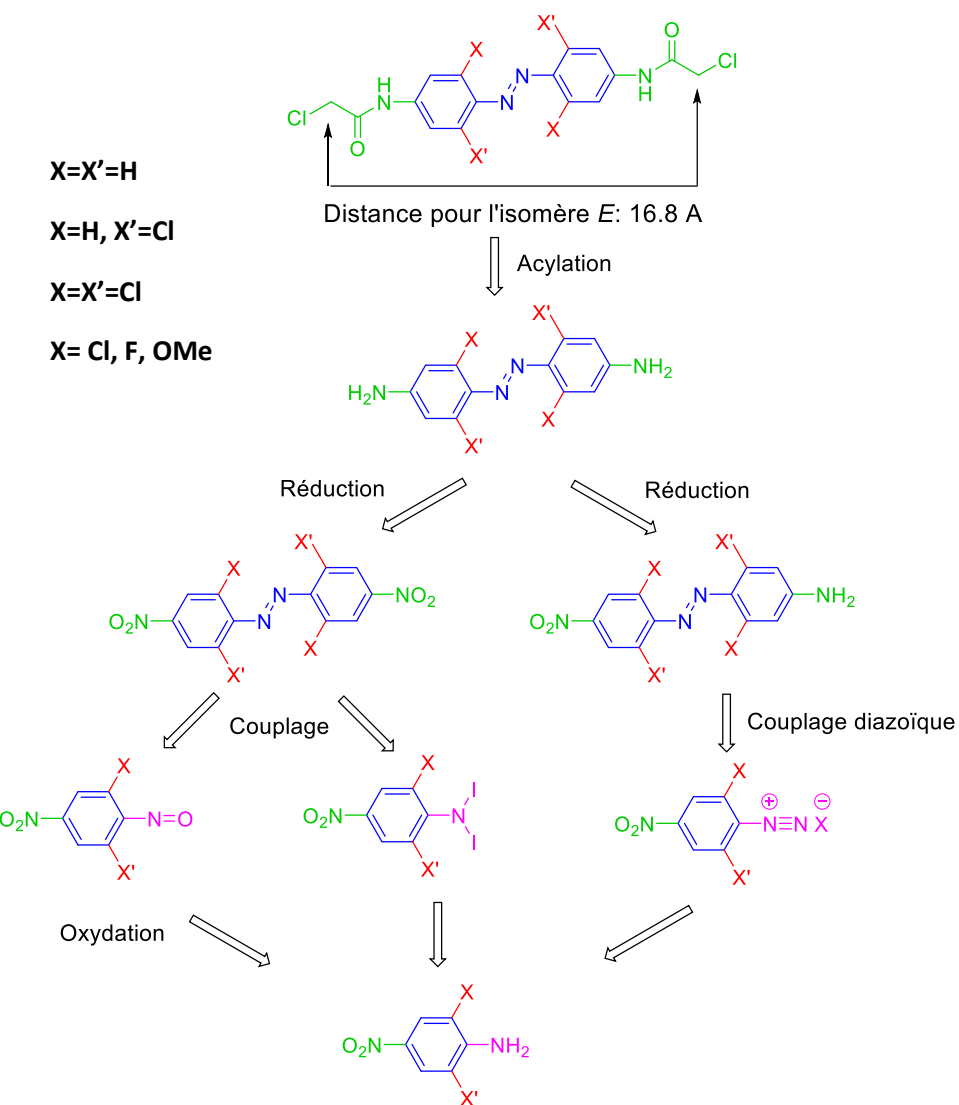
- 1 A. Gautier, C. Gauron, M. Volovitch, D. Bensimon, L. Jullien, S. Vriz, *Nature Chem. Biol.*, 2014, **10**, 533.
- 2 "Method of the Year: Optogenetics", *Nature Methods*, 20th of december 2010.
- 3 T. Fehrentz, M. Schönberger, D. Trauner, *Angew. Chem. Int. Ed.*, 2011, **50**, 12156.
- 4 J. Broichhagen, D. Trauner, *Curr. Opinion Chem. Biol.*, 2014, **21**, 121.
- 5 M. M Lerch, M. J. Hansen, G. M. van Dam, W. Szymanski, B. L. Feringa, *Angew. Chem. Int. Ed.* 2016, **55**, 2.
- 6 F. Hamon, F. Djedaini-Pilard, F. Barbot, C. Len, *Tetrahedron* 2009, **65**, 10105.
- 7 W. Szymanski, J. M. Beierle, H. A. V. Kistemaker, W. A. Velema, B. L. Feringa, *Chem. Rev.* 2013, **113**, 6114.
- 8 A. A. Beharry, G. A. Wooley, *Chem. Soc. Rev.* 2011, **40**, 4422.
- 9 C. Poloni, W. Szymanski, L. Hou, W. R. Browne, B. L. Feringa, *Chem. Eur. J.* 2014, **20**, 946.
- 10 R. Siewertsen, H. Neumann, B. Buchheim-Stehn, R. Herges, C. Näther, F. Renth, F. Temps, *J. Am. Chem. Soc.* 2009, **131**, 15594.
- 11 A. A. Beharry, O. Sadovski, G. A. Wooley, *J. Am. Chem. Soc.* 2011, **133**, 19684.

- 12 D. Bléger, J. Schwarz, A. M. Brouwer, S. Hecht, *J. Am. Chem. Soc.* 2012, **134**, 20597.
- 13 H. A. Wegner, *Angew. Chem. Int. Ed.* 2012, **51**, 4787.
- 14 S. Samanta, A. A. Beharry, O. Sadovski, T. M. McCormick, A. Babalhavaeji, V. Tropepe, G. A. Wooley, *J. Am. Chem. Soc.* 2013, **135**, 9777.
- 15 S. Samanta, T. M. McCormick, S. K. Schmidt, D. S. Seferos, G. A. Wooley, *Chem. Commun.* 2013, **49**, 10314.
- 16 S. Samanta, A. Babalhavaeji, M.-X. Dong, G. A. Wooley, *Angew. Chem. Int. Ed.* 2013, **52**, 14127.
- 17 S. Okumura, C. H. Lin, T. Takeda, S. Minakata, *J. Org. Chem.* 2013, **78**, 12090.
- 18 D. B. Konrad, J. A. Frank, D. Trauner, *Chem. Eur. J.* 2016, **22**, 4364.
- 19 M. J. Hansen, M. M. Lerch, W. Szymanski, B. L. Feringa, *Angew. Chem. Int. Ed.* 2016, **55**, 13712.
- 20 M. Hirano, S. Yakabe, H. Chikamori, J. H. Clark, J. H. Morimoto, *J. Chem. Soc.* 1998, **12**, 770.
- 21 B.-C. Yu, Y. Shirai, J. M. Tour, *Tetrahedron* 2006, **62**, 10303.
- 22 S. J. Wratten, H. Fujiwara, R. T. Solsten, *J. Agric. Food Chem.* 1987, **35**, 484.
- 23 R. R. Holmes, R. P. Bayer, *J. Am. Chem. Soc.* 1960, **82**, 3454.
- 24 O. Lavastre, I. Illitchev, G. Jegou, P. H. Dixneuf, *J. Am. Chem. Soc.* 2002, **124**, 5278.
- 25 K. S. Woodin, T. F. Jamison, *J. Org. Chem.* 2007, **72**, 7451.
- 26 R. C. Clevenger, K. D. Turnbull, *Synthetic Communications* 2000, **30**, 1379.
27. C. Knie, M. Utecht, F. Zhao, H. Kulla, S. Kovalenko, A. M. Brouwer, P. Saalfrank, S. Hecht, D. Bléger, *Chem. Eur. J.* 2014, **20**, 16492.

Pour plus d'informations sur la partie expérimentale, veuillez contacter delphine.joseph@u-psud.fr

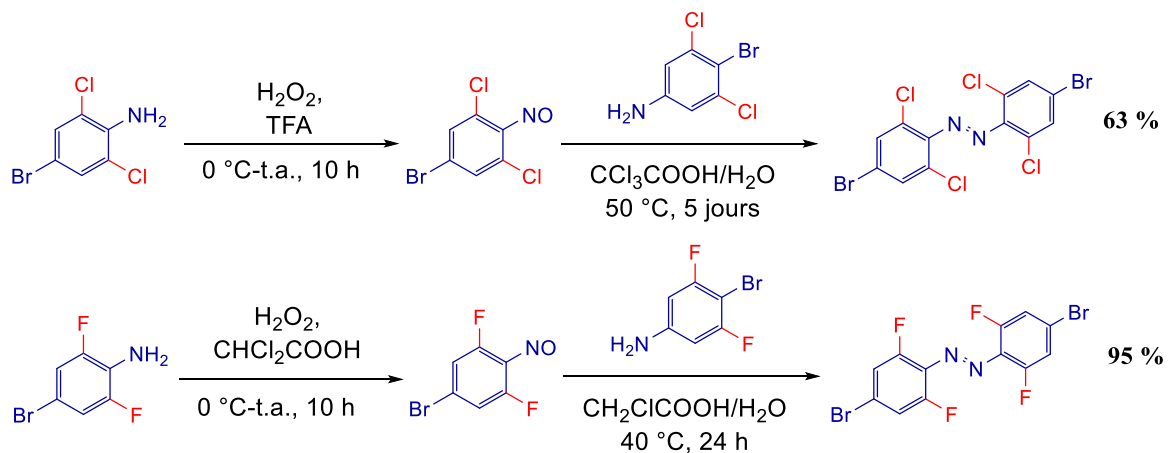
3. Conclusion

Dans ce chapitre, nous avons effectué une étude méthodologique pour mieux comprendre les éléments affectant les synthèses des azobenzènes tétrasubstitués et afin d'en améliorer les rendements. Avec la modélisation moléculaire, nous avons choisi le modèle de pince suivant ayant une distance compatible avec celle des cystéines sur la protéine GLIC.

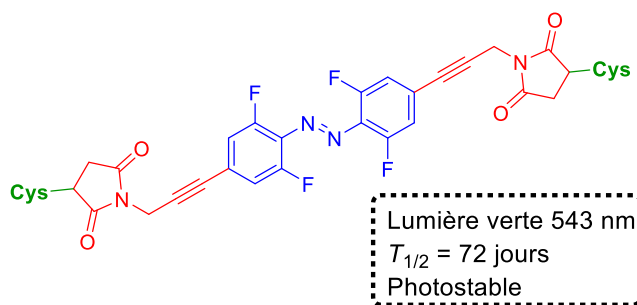


Les méthodes passant par l'intermédiaire diazonium n'ont pas fonctionné. Elles conduisent uniquement majoritairement à de la dégradation. Avec le produit de départ non-substitué, le seul composé parfois isolé est le dérivé secondaire triazène. Les résultats des deux autres méthodes (intermédiaires nitrosobenzène et diiodoaniline) mettent en évidence que quel que soit le substituant en position *para*, la synthèse de l'azobenzène est forcément affectée par l'encombrement stérique des atomes de chlore en position *ortho*. Comme vu dans la littérature, la synthèse des azobenzènes tétra-substitués est un grand défi pour la chimie. L'effet stérique en position *ortho* et l'effet électronique en position *para* bloquent l'efficacité de la réaction, quel que soit la méthode utilisée.

Nous sommes retournés vers la méthode d'oxydation par le peroxyde d'hydrogène H_2O_2 qui implique l'isolement de l'intermédiaire nitroso suivi de son couplage avec un second équivalent d'aniline afin de pouvoir améliorer les conditions de chaque étape. Pour la première étape, en baissant la température jusqu'à $0\text{ }^\circ\text{C}$, l'intermédiaire nitroso a été isolé. Après plusieurs essais en jouant sur les différents acides de la famille acide acétique et en chauffant légèrement le milieu réactionnel, nous avons réussi à synthétiser un azobenzène tétrafluoré et un azobenzène tétrachloré avec 95% et 63%, respectivement.



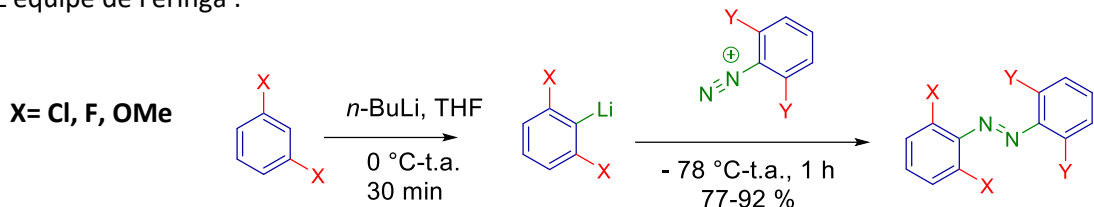
Face aux difficultés de préparer le dérivé *para*-dinitro, fonctions chimiques trop désactivantes, nous avons décidé d'exploiter le dérivé *para*-dibromo. En particulier, le dérivé *ortho*-tétrafluoré, a été obtenu avec un excellent rendement. En plus, selon la littérature, ce dernier présente une grande stabilité métabolique et une longue demi-vie intéressante pour nos applications biologiques. Nous avons donc conçu une seconde pince ciblant les cystéines plus éloignées sur la protéine GLIC. Cette pince est mise en réaction avec la cystéine avec l'intention de mimer le bioconjugé. Ce composé s'est montré isomérisable par la lumière verte, photostable et possède une demi-vie très longue de 72 jours à $25\text{ }^\circ\text{C}$.



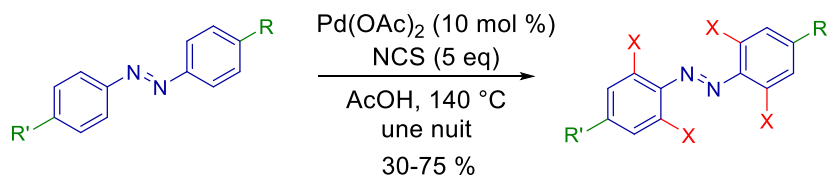
Les voies de synthèse classiques se sont montrées inefficaces pour la synthèse des azobenzènes tétrasubstitués. Comme présenté dans la première partie de ce chapitre, deux nouvelles voies de synthèse ont été développées récemment. L'équipe de Feringa a publié en 2016 une méthode

d'*ortho*-lithiation suivie de son couplage avec un dérivé diazonium préparé au préalable. Cette voie de synthèse présente des difficultés telles que l'absence de groupements en *para* permettant une fonctionnalisation ou une pauvre diversité chimique des groupements en position *ortho*. Pour dépasser ces limitations, une voie alternative a été développée en synthétisant l'azobenzène non-substitué et ensuite en introduisant des groupements en *ortho*. Nous avons choisi d'exploiter cette méthode, s'appelant C-H activation et les expériences seront abordées dans le second chapitre.

L'équipe de Feringa :



L'équipe de Trauner :



Chapitre 2

**Azophenols : de la synthèse *via*
C-H activation à l'application**

1. Revue sur la fonctionnalisation des azobenzènes par C-H activation



DOI: 10.1021/acscatal.7b03583

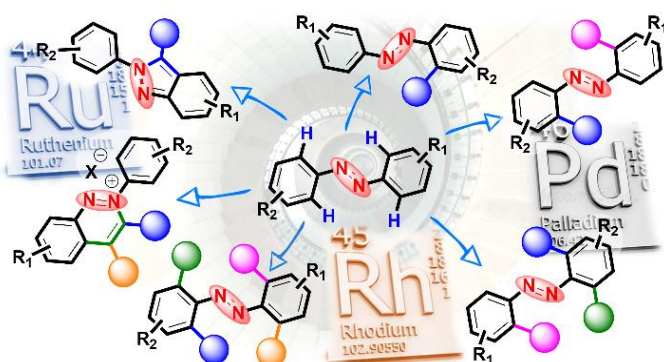
Advances in Direct Metal-Catalyzed Functionalization of Azobenzenes

T. H. Long NGUYEN, Nicolas GIGANT and Delphine JOSEPH*

BioCIS, Université Paris-Sud, CNRS, Université Paris-Saclay, F-92296 Châtenay-Malabry, France.

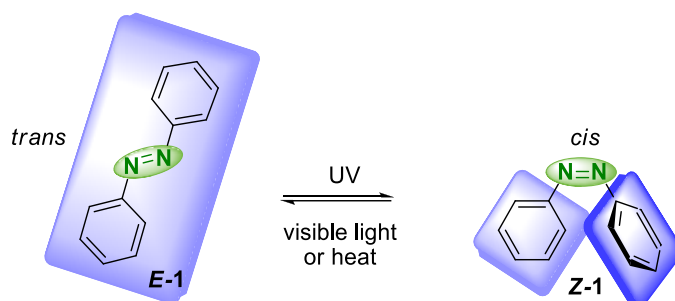
KEYWORDS: azobenzenes, C-H activation, catalysis, metal, mechanism.

ABSTRACT: Azobenzenes are a unique class of compounds that originally aroused interest due to their exceptional photochromic properties. Selective reactions allowing the preparation of complex poly-substituted azo-based photoswitches, in a direct and efficient manner, have received considerable attention over the past few years. Among them, regio- and chemoselective C–H bond activation in the presence of transition-metal catalyst has emerged as the most attractive and challenging strategy in the synthesis of sterically-constrained azo compounds. This synthetic approach is currently an intensive research field for introducing functional and structural diversity from azobenzenes. This short review summarizes the recent advances in both *ortho*-functionalization of azobenzenes and the synthesis of azo-derived heterocycles based on transition metal-catalyzed direct C–H bond activation. The substrate scope, limitation, reaction mechanism as well as additional applications are discussed.



1. INTRODUCTION

The design and the synthesis of molecular switches which can adopt two or more geometries by external stimuli such as light, electric field, temperature, electrons or chemical modifications, is undeniably a topic of high interest for the entire scientific community.¹ Among them, azobenzenes, also called diphenyldiazenes were discovered by Mitscherlich in 1834,² and have recently gained considerable attention for their unique photochromic properties that make them excellent candidates to build dynamic molecular devices with wide applications, e.g. molecular machines, materials, biosensors, pharmaceuticals, FD&C dyes and additives, indicators, nonlinear optics...³ The *trans-cis* isomerization of the azo moiety is usually accomplished with UV-light irradiation, while the reverse *cis-trans* isomerization can be released by either visible-light irradiation or thermal relaxation (Scheme 1).

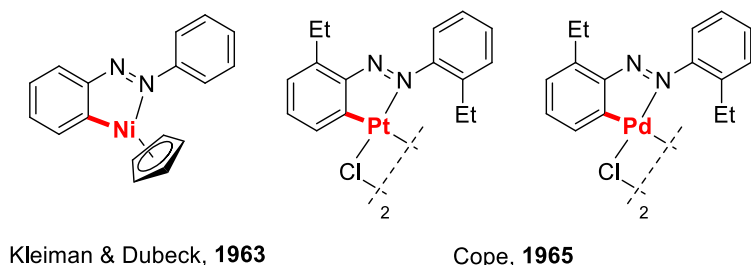


Scheme 1. *Trans-cis* Isomerization of Azobenzenes

In this context, the development of synthetic methods that could improve their highly tunable light-responsive properties, has recently emerged as one of the most important challenge for organic chemists. More especially, tetra-*ortho*-substituted azobenzenes are well known to bathochromically shift their photoswitch wavelengths towards the red-light and visible range authorizing new opportunities for *in vivo* nondestructive experiments. Regarding the synthesis of azo compounds, three classical methods are mainly reported in the literature: i) the azo coupling reaction between a diazonium salt and an activated arene, ii) the Mills reaction consisting in the condensation of a nitroso compound with a primary arylamine, and iii) the Wallach transformation implying the rearrangement of an azoxybenzene into a hydroxylated azobenzene.⁴ If recent developments in the synthesis of azobenzenes have solved some restrictions, the specific preparation of sterically encumbered azo compounds is hampered by the absence of general and efficient synthetic methods. The commonly used strategies for their synthesis required laborious procedures and remained unselective generating byproducts, challenging purification and low to moderate yields.

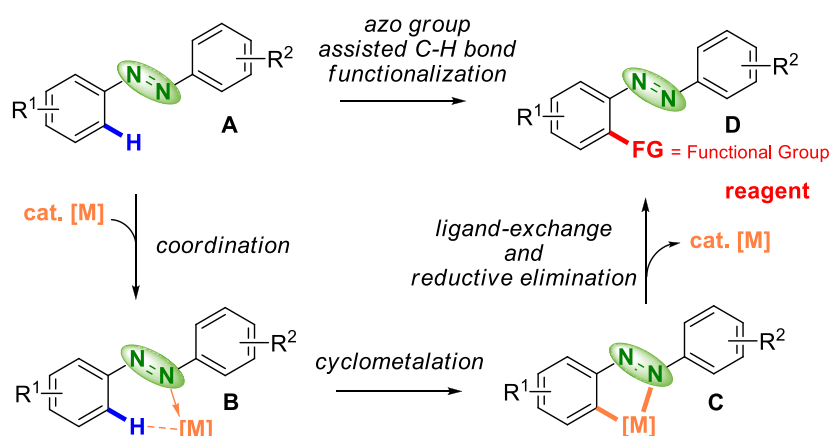
Knowing that the direct functionalization of inert C_{sp2} -H bonds has recently shown an extraordinary potential,⁵ several limitations can be addressed by elegantly using this strategy for the straightforward preparation of diversely-functionalized azo compounds, not only from a synthetic point of view but also from an eco-friendly and sustainable approach. Indeed, by selectively directing a transition-metal catalyzed reaction by the N=N (azo) group, a high diversity of *ortho*-substituted

azobenzenes could be reached. If this approach was historically explored by Kleiman and Dubeck,⁶ and Cope⁷ more than 50 years ago for the synthesis of metallacycles, it has attracted extensive attention during the past decade (Scheme 2).



Scheme 2. Early Examples of Azo-Based Metallacycles

Indeed, the azo moiety has the dual ability of both electronically increasing the reactivity of the inert C_{sp^2} -H bond and controlling the site selectivity of the reaction (Scheme 3). The procedure relies on a sequence of well-established mechanistic steps in the field of catalysis, including metal coordination, cyclometalation with intramolecular C_{sp^2} -H cleavage, ligand-exchange, and final reductive elimination.



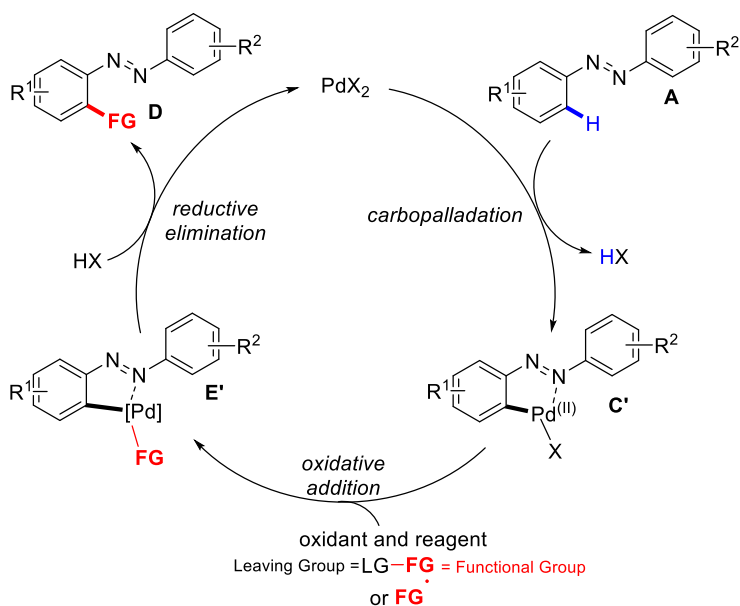
Scheme 3. General Reaction Pathway of N=N Directing C–H Bond Functionalization

This perspective focuses on the advances in transition-metal catalyzed C_{sp^2} -H functionalization of azobenzenes. It will cover not only the recent progresses in mono- and poly-functionalization but also the diversity-oriented synthesis of relevant heterocycles. The choice of mainly illustrating this Perspective with examples of poly-*ortho*-functionalization of azo scaffolds was made in respect to the advantageous potential applications of these photoresponsive molecules.

2. MONO-FUNCTIONALIZATION OF AZOBENZENES

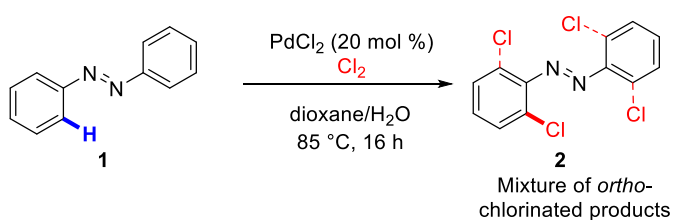
2.1. Palladium-Catalyzed C_{sp^2} -H Bond Functionalization

Palladium (II) catalysts occupy a unique and prominent place in the activation of C_{sp^2} -H bond and are the most common metal catalysts used for the direct functionalization of azo-compounds. Pallado-catalyzed C-H activation reactions are based on a general mechanism depicted in Scheme 4. The initial step proceeds through a C_{sp^2} -H directing-group assisted carbopalladation affording a five-membered palladacycle complex **C'** by coordination of the starting diazene **A** to the Pd(II)-catalyst. The complex formation is then followed by the oxidative addition of the coupling partner (LG-FG or FG^\bullet), generating a palladium(III or IV) intermediate **E'**. Finally, subsequent reductive elimination yields the functionalized azobenzene **D**. Regenerated in its Pd(II) active form, the catalyst pursues its catalytic cycle. An alternative catalytic cycle implying the formation of a bimetallic Pd(III) complex intermediate has also been proposed.



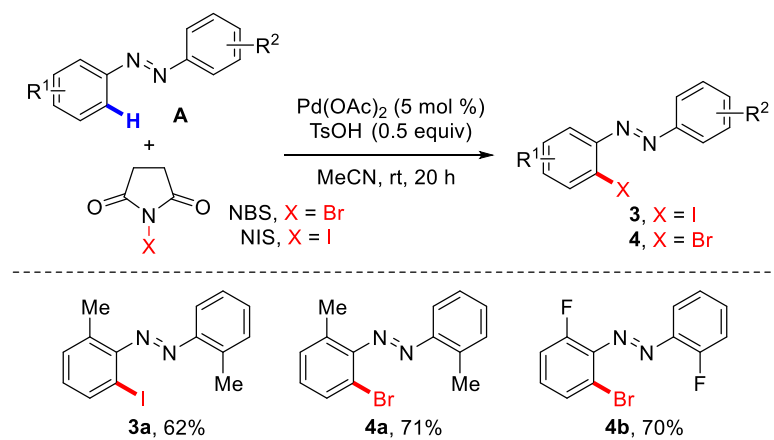
Scheme 4. The Most Common Mechanism for Pallado-Catalyzed Functionalization of Azobenzenes

An early report of Pd-catalyzed *ortho*-chlorination of the symmetrical azobenzene **1** with gaseous chlorine was disclosed by Fahey in 1970 (Scheme 5).⁸ Nevertheless, this elegant study presents severe drawbacks with the uncontrolled formation of a mixture of mono-, di-, tri-, and tetra-*ortho*-chlorinated products **2** and the use of the poisonous chlorine gas as both the oxidant and the chlorinating agent. Consequently, more practical, and more selective catalytic reactions have been developed with the aim of preparing halogenated azo compounds under milder reaction conditions.



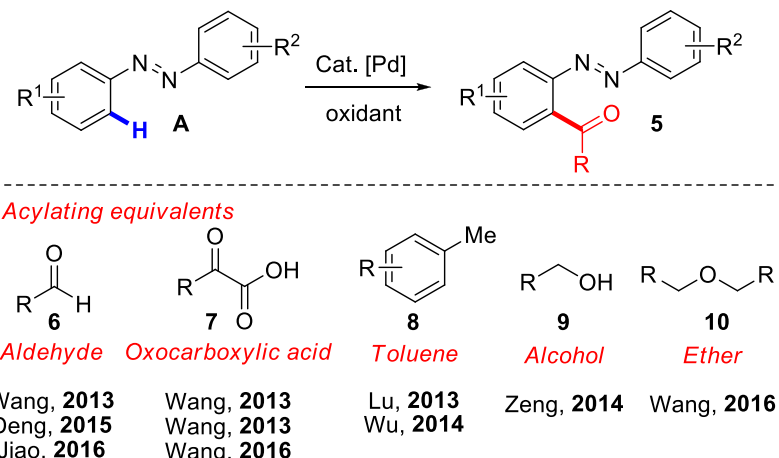
Scheme 5. Seminal Work by Fahey⁸

Following this proof of concept, a single example of mono-iodination had been reported in 2006 by Sanford and coworkers starting from the di(*m*-tolyl)diazene.⁹ The use of a combination of Pd(OAc)₂ and *N*-iodosuccinimide (NIS) as oxidant in acetic acid at 100 °C afforded the corresponding *ortho*-iodinated product in a 41% yield. Based on this original example, the Tian's group developed, seven years later, an efficient and general method of monohalogenation of symmetrical and unsymmetrical azo compounds at room temperature or at 50 °C for the most reluctant examples (Scheme 6).¹⁰ The reaction required the combined presence of 5 mol% Pd(OAc)₂ and a half-equivalent of *p*-toluenesulfonic acid in acetonitrile. This Brønsted acid was proved to promote the reaction both by enhancing the electrophilicity of the Pd(II) catalyst *via* the probable generation of Pd(OTs)₂ and by rendering the *N*-halosuccinimide (NBS or NIS) a more effective source of X⁺ (Br⁺ or I⁺ respectively) *via* protonation of the carbonyl moiety. In the case of symmetric azos, the reaction tolerated a large diversity of functional groups such as halogen, ester or alkyl. With unsymmetrical azobenzenes, the monohalogenation occurred preferentially on the electron-enriched aromatic ring. In both cases of symmetrical and unsymmetrical azobenzenes, the monohalogenation was highly *ortho*-selective.



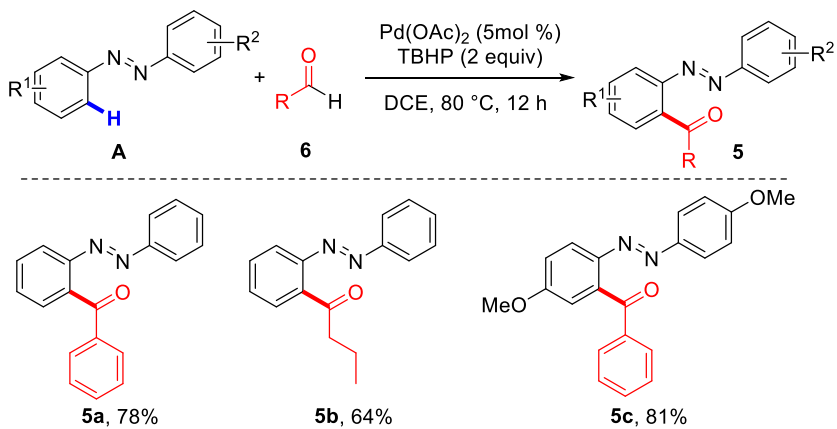
Scheme 6. Pd-Catalyzed Direct *ortho*-Monohalogenation of Azobenzenes

Undoubtedly, in the past decades, much more efforts in Pd-catalyzed C_{sp²}-H activation were devoted to the development of efficient processes permitting the formation of C-C bonds and remarkable progresses have been obtained for regioselective transformation involving substrates containing a directing group, in particular azo compounds. In this context, the direct acylation of azobenzenes has been explored using the reactivity of wide range of acylating agents including aldehydes **6**, α-oxocarboxylic acids **7**, toluene derivatives **8**, alcohols **9** and ethers **10** (Scheme 7).



Scheme 7. Pd-Catalyzed Direct *ortho*-Acylation of Azobenzenes

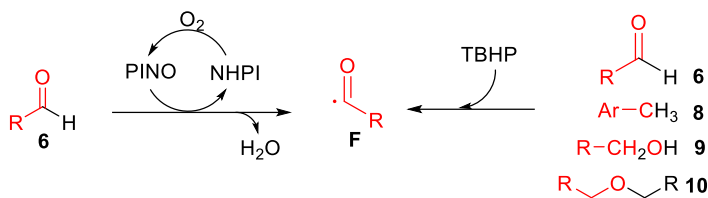
The first synthesis of *ortho*-acylated azobenzenes **5** through a Pd-catalyzed C_{sp²}-H activation approach has been reported in 2013 by the Wang's group (Scheme 8).¹¹ The reaction was carried out in the presence of 5 mol% of Pd(OAc)₂ and 2 equivalents of tert-butyl hydroperoxide (TBHP) as oxidant using aromatic or aliphatic aldehydes **6** as acylating reagent. A wide range of substituted benzaldehydes was investigated and both electron-donating and electron-withdrawing groups (with exception of fluorine) were well tolerated. A slight steric effect was observed starting from *meta*- or *ortho*-substituted benzaldehydes, conferring lower yields. If the reactivity of several *para*-disubstituted azobenzenes was surveyed and proven effective, the scope was not explored with *meta* or *ortho*-substituted azo derivatives.



Scheme 8. Pd-Catalyzed Direct Acylation of Azobenzenes in the Presence of Aldehydes

On a mechanistic point of view, the presence of a radical scavenger such as 2,2,6,6-tetramethyl-1-piperidinyloxy (TEMPO) inhibited the reaction, indicating the involvement of a reactive acyl radical (RCO[•]) in the reaction pathway (Scheme 4). This radical species reacted with the five-membered palladacycle complex **C'** to undergo the oxidation of Pd(II) to Pd(IV) (or dimeric Pd(III)). Finally, the active Pd(II) catalyst was regenerated through reductive elimination concomitantly with the release of the acylated azo compounds **5**.

In 2015, Deng and coworkers developed an eco-friendlier protocol by using water as inexpensive and non-toxic solvent.¹² The acylating catalytic system required the addition of 5 mol% of the ionic surfactant sodium dodecylsulfate (SDS), used as phase-transfer catalyst, to enhance the reactants solubility in water. In the same context of green chemistry, Jiao *et al.* recently described an aerobic oxidative C-H acylation of arenes by initiating the formation of the active benzoyl radical **F** from benzaldehyde using a *N*-hydroxyphthalimide (NHPI)/O₂ oxidant system (Scheme 9).¹³ Indeed, as O₂ is easily available, natural, inexpensive and environmentally friendly, the direct oxidation by using molecular oxygen as oxidant is a very appealing research area. In this aerobic version of the acylation reaction, NHPI could be used in a 20 mol% catalytic amount. The latter is oxidized *in situ* by molecular oxygen into PINO (phthalimido-*N*-oxyl) and regenerated with the formation of the reactive benzoyl radical and H₂O as byproduct.

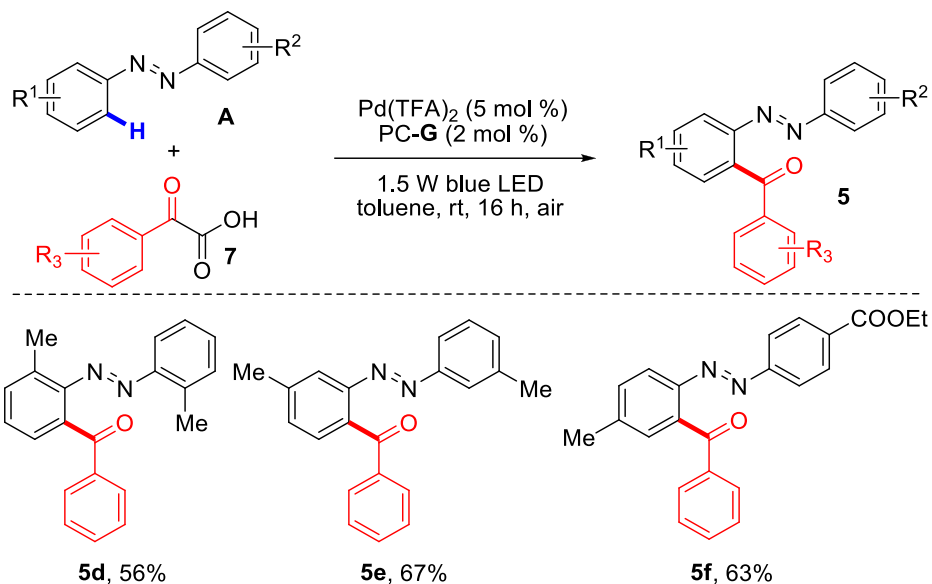


Scheme 9. Generation of Active Acyl Radical Species

If the reaction was very efficient under one atmosphere of O₂ for a wide range of arenes bearing diverse *ortho*-directing groups, the process furnished a disappointing 27% yield with a simple azobenzene. Following the same leading idea of *in situ* generation of active radical species **F**, the Pd(OAc)₂/TBHP catalytic system was proved more efficient to catalyze the cascade oxidation/C_{sp²}-H bond acylation reactions. It also allows the use of a more diversified source of acylating agents such as α -oxocarboxylic acids **7**, aryl methanes **8** and benzyl alcohols **9** as well as dibenzyl ethers **10** (Scheme 9).¹⁴ In general, electronic effects of azobenzene substituents in *para*-position have no significant influence on the reaction outcomes whereas the steric congestion induced by *ortho*-substituents has detrimental consequences. Moreover, starting from unsymmetrical azobzenes, the direct *ortho*-acylation mainly took place on the more electron-rich aromatic rings.

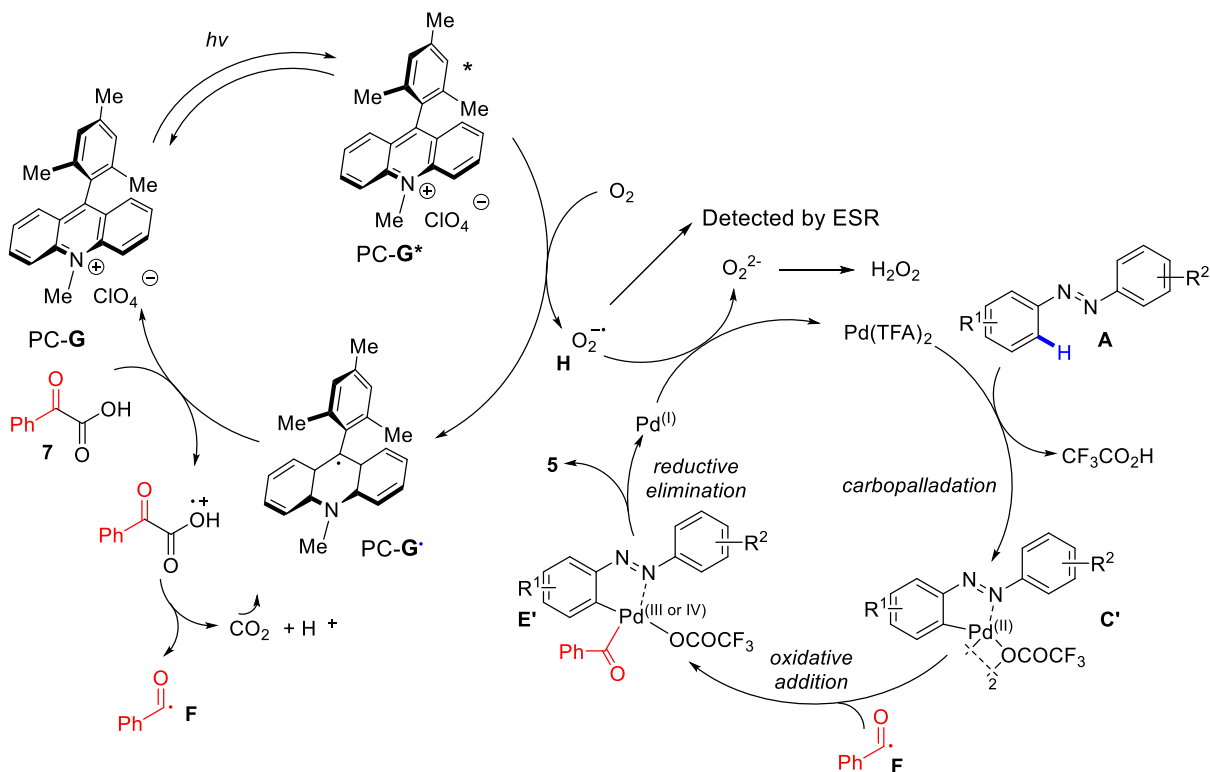
The same year, Wang described the first example of acylation promoted by visible-light by merging palladium catalysis with organic photoredox catalysis in the presence of phenyl-2-oxoacetic acid as acyl source (Scheme 10).¹⁵ Milder conditions based on the use of the photoredox catalyst 9-mesityl-10-methylacridinium perchlorate (PC-**G**) under blue LED irradiation at room temperature, allow to avoid some drawbacks commonly associated to C_{sp²}-H activation such as the presence of a strong external oxidant and the use of high reaction temperature. Azo substrates scope evaluation showed the same electronic and steric effects as already observed. Albeit tolerant of substituents diversity, the coupling reaction offered better yields for azobenzenes activated by electron-donating groups. Unsymmetrical azobenzenes led to compounds **5** selectively acylated on the more electron-enriched aromatic ring. Due to slight effect of steric hindrance, *ortho*-substituted azobenzenes generally gave

lower yields than *meta*- and *para*-substituted ones and the acylation of *meta*-substituted azo derivatives occurred at the less hindered *ortho*-position.



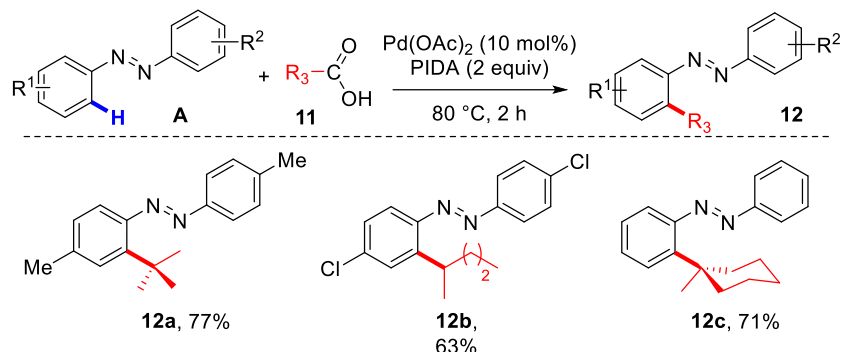
Scheme 10. Pd-Catalyzed Direct *ortho*-Acylation of Azobenzenes with Visible-Light Photocatalysis

The proposed mechanism is based on two concomitant catalytic cycles as depicted in Scheme 11. The first cycle involves the following steps: (i) the photo-excitation of PC-G by visible light; (ii) the oxidation of PC-G^* by O_2 into the radical PC-G^\bullet with the concomitant generation of superoxide anion $\text{H}\cdot$; (iii) the single-electron oxidation of phenyl-2-oxoacetic acid 7 by PC-G^\bullet to regenerate ground-state photocatalyst PC-G for the following cycle and to form the active benzoyl radical species F by CO_2 extrusion. In the second cycle, after a traditional sequence of carbopalladation, oxidative addition of the acyl radical F and reductive elimination, the desired acylated product 5 is liberated with the concurrent formation of Pd(I) which is immediately reoxidized by the superoxide anion $\text{H}\cdot$ to regenerate the active Pd(II) catalyst. These detailed mechanistic investigations were corroborated by the capture of the active O_2^\bullet species H by 5,5-dimethyl-1-pyrroline-N-oxide.



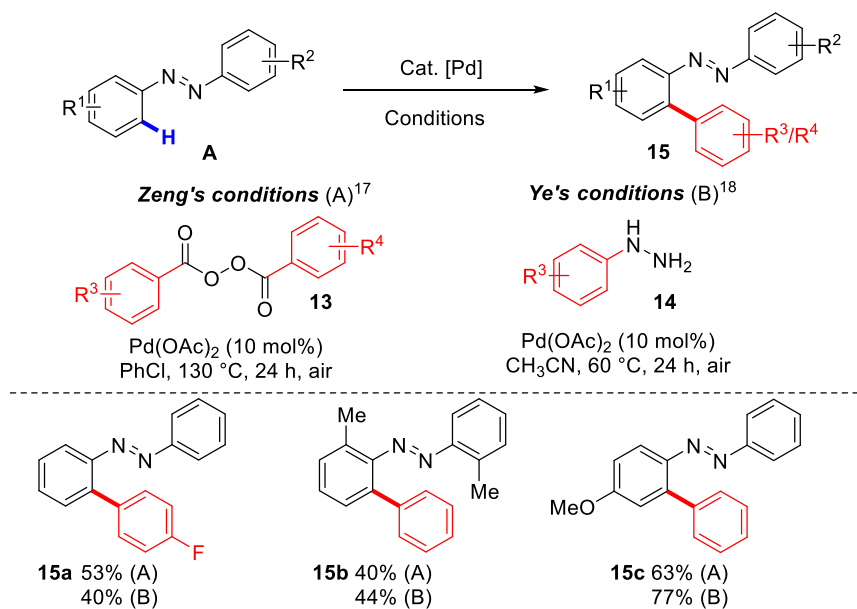
Scheme 11. Catalytic Cycle Proposed for Photocatalyzed Direct Acylation of Azobenzenes

A decarboxylative cross-coupling reaction was also exploited by Premi *et al.* for the only one example reported to date of Pd-catalyzed direct alkylation of azobenzenes (Scheme 12).¹⁶ This directing group assisted $\text{C}_{sp^2}\text{-C}_{sp^3}$ bond formation has been developed for a range of secondary or tertiary α -substituted, cyclic, and acyclic aliphatic carboxylic acids **11** as alkyl source under mild solvent-free conditions. The authors highlighted the reaction robustness with a couple of symmetric azobenzenes. Monoalkylated products **12** were obtained in good yields along with a weak amount of dialkylated products. It is also interesting to note that, despite the steric hindrance induced by the introduction of the first alkyl group, the second *ortho*-alkylation occurred on the same aromatic ring. The reaction pathway involved an alkyl radical whose formation was facilitated by thermal decomposition of PhI(OAc)_2 (PIDA) followed by abstraction of hydrogen radical and then release of CO_2 . This plausible free-radical path was strongly supported by the trapping of a pivalyl radical when the cross-coupling reaction was performed under optimized reaction conditions in the presence of pivaloic acid and styrene used as model substrate instead of azo.



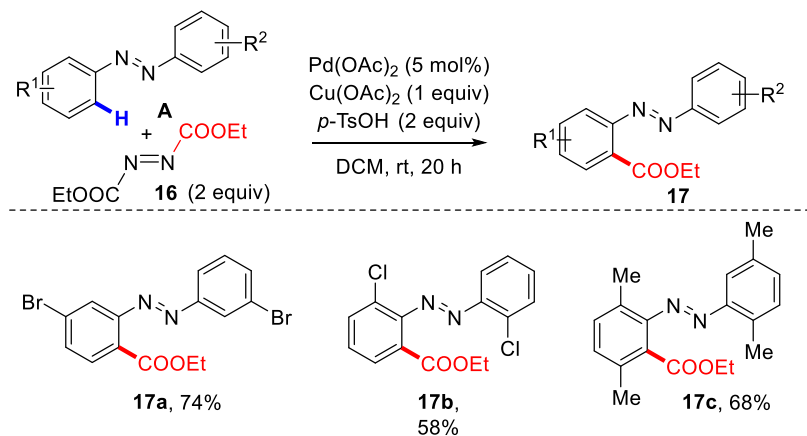
Scheme 12. Decarboxylative Pd-Catalyzed *ortho*-Alkylation of Azobenzenes

In regard to the $C_{sp^2}-C_{sp^2}$ bonds formation, Pd(II) complexes are also effective to catalyze direct *ortho*-selective arylation of azoarenes using either aryl acylperoxides¹⁷ **13** or arylhydrazines¹⁸ **14** as coupling partners (Scheme 13). The optimal reaction conditions combined 10 mol% of Pd(OAc)₂ with atmospheric oxygen as oxidant. The substrates scope showed significant electronic and steric effects: electron-donating substituents on azobenzene resulted in better yields and *ortho*-substitution of the aryl sources totally inhibited the coupling reaction. Moreover, due to the steric encumbrance induced by the introduced arene, the arylated azobenzenes **15** were mostly isolated as a mixture of *trans*-*cis* diastereomers. Mechanistically, a radical pathway is postulated. Starting from aryl acylperoxides **13**, homolysis followed by decarboxylation explained the radical species formation. With arylhydrazines **14**, the authors observed the total inhibition of the arylation processus when the reaction was placed under argon atmosphere. They thus proposed that the radical formation could result from the initial transformation of arylhydrazine into the corresponding diazene which would undergo oxidation by air affording the active phenyl radical species by release of molecular nitrogen.



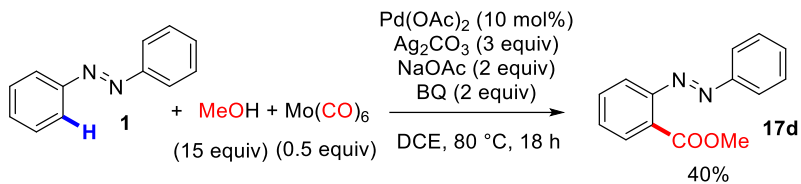
Scheme 13. Pd(II)-Catalyzed *ortho*-Arylation of Azobenzenes

In the same way as arylhydrazines **14** are efficient sources of reactive aryl species, the readily available azodicarboxylates are also good precursors for the direct alkoxy carbonylation of aromatic C-H bond. Usually, Pd-catalyzed oxidative alkoxy carbonylation of C_{sp^2} -H bond requires a combination of CO and alcohols as sources of ester groups. The necessity to handle the toxic and odorless CO gas under high pressure restrict its use in standard laboratories. Used as alkoxy carbonyl surrogates, azodicarboxylates offered new opportunities to develop safer and more environmentally friendly CO-free strategies. Applied to the azobenzene substrates, the Wang's group reported a Pd-catalyzed process of direct *ortho*-ethoxycarbonylation by using diethyl azodicarboxylate (DEAD) **16** as the source of ester group, Cu(OAc)₂ as the oxidant and *p*-toluenesulfonic acid (*p*-TsOH) as the additive (Scheme 14).¹⁹ The reaction was carried out at room temperature under air for 20 h giving the desired ethoxycarbonyl azobenzenes **17** in good yields. Substrate scope studies indicated that the reaction tolerated a wide range of functional groups and was obviously not affected by any electronic effect. The reaction proceeded selectively in *ortho* position even with *meta*-substituted azobenzenes. Steric hindrance effect was noticed for *ortho*-substituted azobenzenes causing slightly lower product yields but tetra-substituted azobenzenes were shown reactive enough to provide the corresponding products in relatively satisfying yields (Scheme 14). No regioselectivity was detected with unsymmetrical azobenzene. Mechanistic studies revealed that the reaction may involve a reactive ethoxyacyl radical resulting from the decomposition of diethyl azodicarboxylate **16** induced by the copper salt.



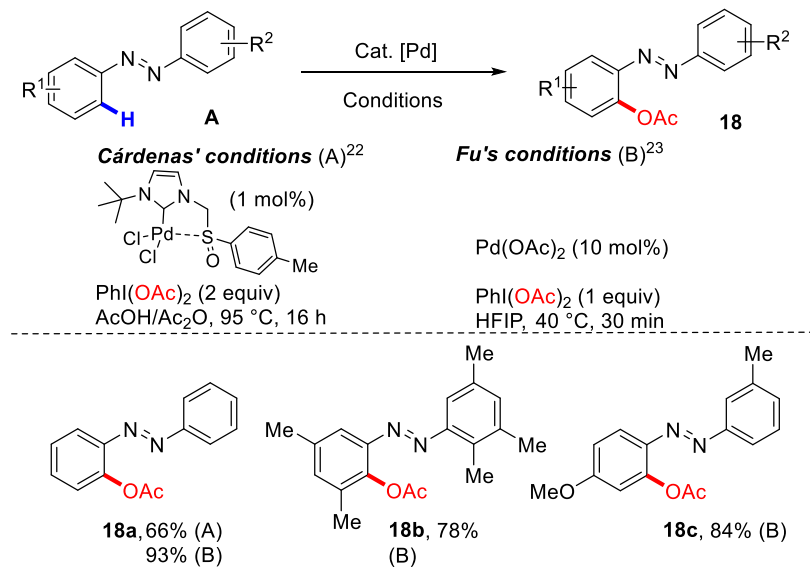
Scheme 14. Pd-Catalyzed Direct *ortho*-Alkoxy carbonylation of Azobenzenes

Albeit the process was first limited to the synthesis of ethyl esters, Wu and collaborators reported in 2016 one example of *ortho*-methoxycarbonylation of the simple azobenzene **1** using Mo(CO)₆ as the nontoxic source of carbon monoxide (Scheme 15).²⁰



Scheme 15. Pd-Catalyzed Direct *ortho*-Methoxycarbonylation of a Simple Azobenzene with $\text{Mo}(\text{CO})_6$

If the formation of the C-C bonds by Pd-catalyzed C_{sp^2} -H activation has been by far the most studied reaction, challenging methods of C_{sp^2} -X bond formation with the chelation assistance of directing group have attracted increasing attention, particularly the formation of C_{sp^2} -O bonds. In 2004, the Stanford's group reported a major gap forward the field of regio- and chemoselective oxidative functionalization of arenes through a Pd-catalyzed C-H activation/oxidation sequence.²¹ In this seminal paper, the authors demonstrated that $\text{Pd}(\text{OAc})_2$ could catalyze the oxidation of simple azobenzene with the hypervalent iodine $\text{PhI}(\text{OAc})_2$ (PIDA) to furnish the *ortho*-monoacetylated compound **18** in 62% yield. A decade later, inspired by this Sanford's work, Cárdenas applied a similar oxidant system for catalyzing the acetoxylation of arenes in the presence of sulfinyl *N*-heterocyclic carbene (NHC) palladium complexes (Scheme 16).²² The electron-enrichment of these NHC-Pd(II) complexes primed the oxidation of Pd(II) into Pd(IV) prior to the C-H activation (Scheme 16). In the case of simple azobenzene, the catalyst loading can be reduced to 1 mol% without significant loss of yield.

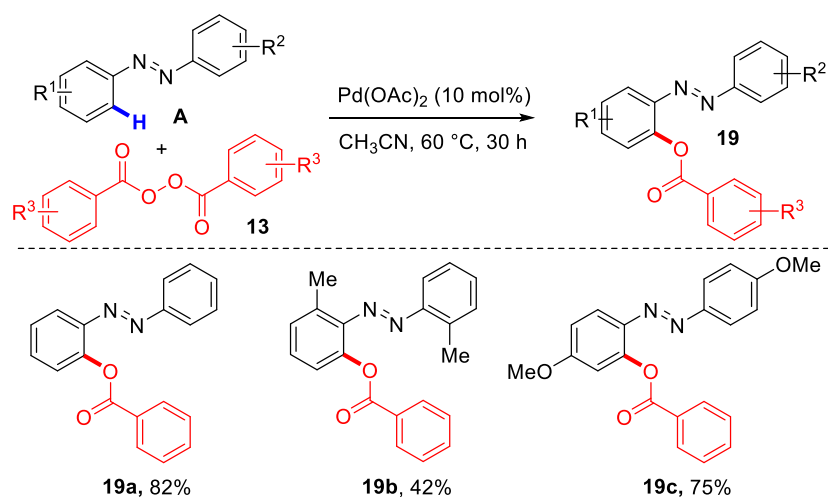


Scheme 16. Pd-Catalyzed Direct Azobenzene C-H Bond Acetoxylation

Very recently, Fu *et al.* proposed more standard and mild reaction conditions for *ortho*-acetoxylation of azobenzenes by using $\text{Pd}(\text{OAc})_2$ and a stoichiometric amount of PIDA in HFIP under air at 40 °C (Scheme 16).²³ The authors highlighted the important role played by the solvent hexafluoroisopropanol (HFIP). The latter contributed to shorten reaction time and to enhance reaction efficacy. The process was more efficient starting from azobenzenes substituted by electron-donating substituents and it was little impeded by steric hindrance of bulky substituents in *meta*- or

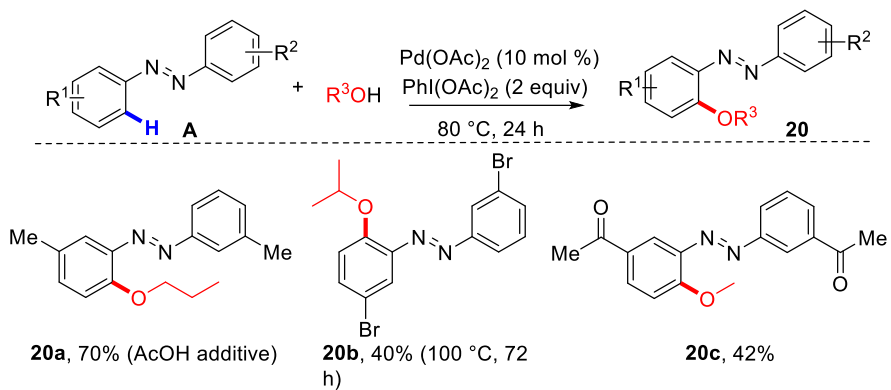
para-positions. However, it should be noted that *ortho*-substituted azobenzenes have not been investigated. Starting from unsymmetrical azobenzenes, the acetoxylation reaction proceeded on the more electron-enriched aromatic core. Noticeably, by using two equivalents of PIDA and doubling the reaction time, diacetylated azobenzenes could be prepared. The double acetylation proceeds in moderate yields on the same aromatic ring.

Earlier, Zeng and co-workers reported the Pd-catalyzed *ortho*-acyloxylation of azobenzenes in the presence of aryl acylperoxides **13** (Scheme 17).¹⁷ A set of *ortho*-phenacyloxylated azos **19** were selectively prepared in moderate to good yields. Carrying out the process in acetonitrile and controlling the reaction temperature at 60 °C permitted to avoid the side reaction of arylation. Steric hindrance or electro-deficient substituents on azobenzene or aryl acyl peroxide **13** are detrimental to the reaction efficiency.



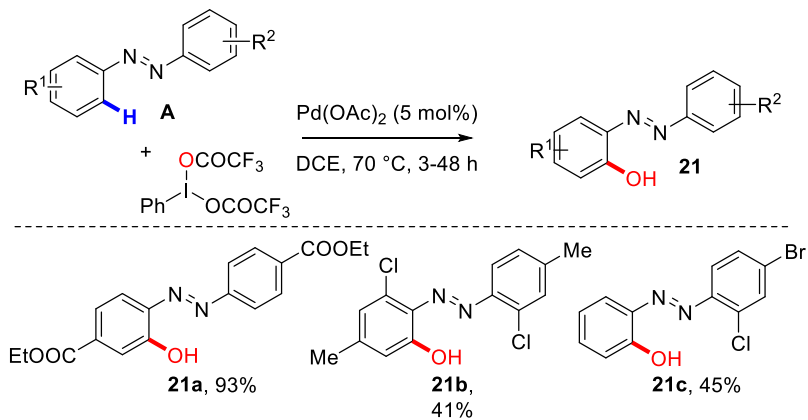
Scheme 17. Pd-Catalyzed Acyloxylation of Azobenzenes with Aryl Acyl Peroxides

The strategy based on the reactivity of hypervalent iodine was also elegantly exploited by Sun and collaborators for the regioselective synthesis of *ortho*-alkoxylated azos **20** using alcohols as both the solvent and the alkoxylation reagents and PIDA as the oxidant under air atmosphere (Scheme 18).²⁴ The reaction was optimal when performed at 80 °C in the presence of $\text{Pd}(\text{OAc})_2$ as catalyst. The method was efficiently applicable to primary alcohols whereas secondary alcohols required the addition of AcOH (20 equiv) and gave moderate yields. The reaction did not proceed with tertiary alcohols. Although the reaction was highly selective giving the sole monoalkoxylated product **20**, the azobenzene substitution significantly influences the reaction outcomes. *Meta*-substituted azobenzenes were clearly better coupling partners than both *ortho*- and *para*-substituted derivatives and the reaction was favored with the presence of electron-donating groups. The study covered only symmetrical azobenzenes.



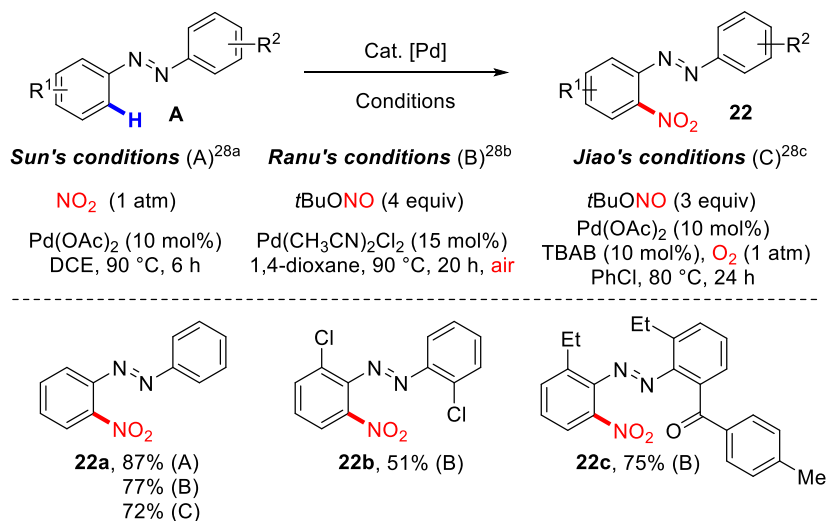
Scheme 18. Pd-Catalyzed Direct *ortho*-Alkoxylation of Azobenzenes

In 2015, Chakraborti shaped a practical Pd-catalyzed hydroxylation of arenes using 1,4-dioxane as solvent in combination with sodium persulfate.²⁵ This study highlights the unprecedented role of 1,4-dioxane as a source of hydroxyl radical. While this direct hydroxylation method was efficient in the presence cyclic directing groups such as benzoxazoles and benzothiazoles, this latter appears unselective starting from azo compounds affording the corresponding azoxybenzenes as byproducts. In the same year, the group of Joseph depicted an efficient synthesis of azophenols **21** through the selective *ortho*-hydroxylation of azobenzenes under mild reaction conditions using the hypervalent iodine [bis(trifluoroacetoxy) iodo]benzene (PIFA) (Scheme 19).²⁶ Substrates scope of this reaction was investigated at the expense of symmetrical and unsymmetrical azobenzenes showing a very good functional group tolerance and a major control of the regioselectivity by the steric hindrance. Interestingly, a catalytic process was developed by generating PIFA *in situ* from a catalytic amount of iodobenzene in the presence of Oxone® as oxidant and TFA as cosolvent. Mechanistic investigations were also conducted and both intra- and inter-molecular isotope effects were measured, indicating that the aromatic C–H bond cleavage could be involved in the rate-determining step of the reaction. If some alternative procedures of direct C–H *ortho*-hydroxylation were recently described, the substrate scope was relatively limited.²⁷



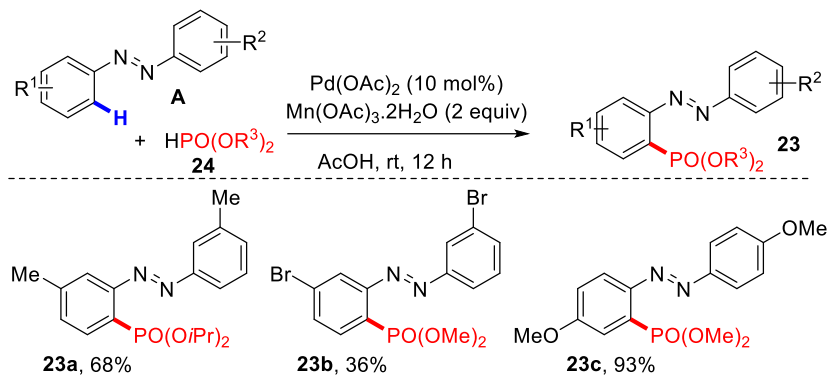
Scheme 19. Pd-Catalyzed Direct *ortho*-Hydroxylation of Azobenzenes

In contrast to the extensively studied Pd-catalyzed formation of C-C and C-O bonds, reactions involving the construction of C-N, C-P and C-S bonds have been much less explored. In this context, transition-metal-catalyzed chelation-assisted functionalization of C_{sp^2} -H bonds offers new opportunities for the development of milder and greener conditions to nitrate an aromatic scaffold. In this way, the direct *ortho*-nitration of azoarenes was achieved by using NO_2 or *t*-BuONO as “clean” nitro sources in the presence of a Pd(II) catalyst (Scheme 20).²⁸ The Sun’s group reported, for the first time, the use of one atmosphere of NO_2 as both nitro source and oxidant. If other groups have developed analogous catalytic systems, Ranu’s and Jiao’s groups reported the regioselective synthesis of densely substituted nitro-azoarenes **22** using *tert*-butyl nitrite as nitrating agent under atmospheric or molecular oxygen as oxidant. Generally, the reactions exhibited good functional groups compatibility and in case of unsymmetrical substrates, the reaction took place exclusively on the electron-enriched benzene rings. In addition, lower yields were obtained for the nitration of *ortho*-substituted azobenzenes because of the steric effect.



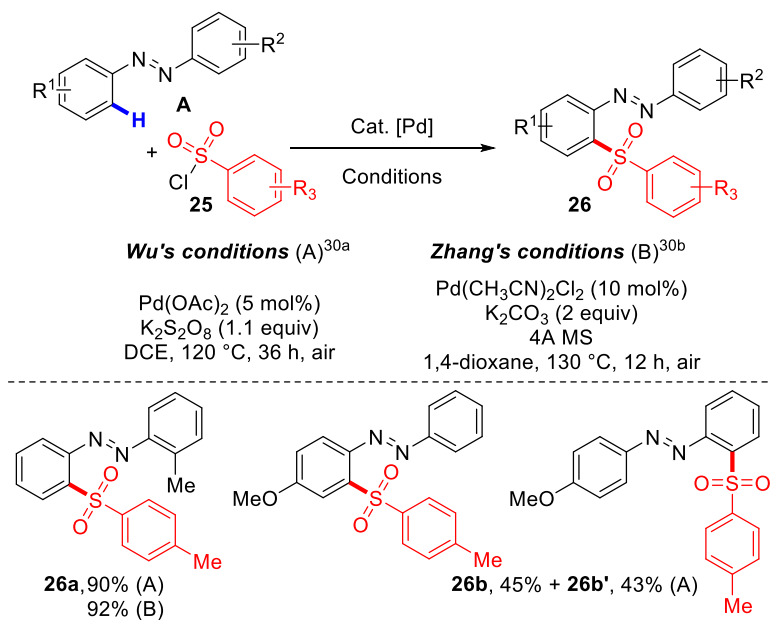
Scheme 20. Pd-Catalyzed Direct *ortho*-Nitration of Azobenzenes

Among catalytic systems elaborated to construct C_{sp^2} -P bonds, the combination of $\text{Pd}(\text{OAc})_2$ with $\text{Mn}(\text{OAc})_3 \cdot 2\text{H}_2\text{O}$ as oxidant in acetic acid has permitted the regioselective preparation of various phosphorylated azobenzenes **23** by using dialkyl phosphites **24** as phosphorus source (Scheme 21).²⁹ This C-H *ortho*-phosphonation reaction respected the rules of selectivities commonly observed: the reaction was disfavored for azobenzenes substituted by electron-withdrawing or bulky groups justifying that monophosphonation only occurred. Better yields were recorded for azobenzenes bearing electron-donating groups positioned in *meta* or *para* rather than in *ortho*. Mechanistical studies suggested that C-H *ortho*-phosphonation reaction proceeded through the formation of key phosphoryl radicals.



Scheme 21. Direct Pd-Catalyzed *ortho*-Phosphonation of Azobenzenes

The success of the C-H activation strategy prompted the groups of Zhang and Wu to explore the C_{sp^2} -S bond formation starting from azobenzene derivatives (Scheme 22).³⁰ They reported two different Pd-catalyzed systems using similarly arylsulfonyl chlorides **25** as sulfonylation agents for the selective synthesis of sulfonylated azos **26**. If the scope studies of the both approaches revealed similar trends such as a good substituents tolerance for the arylsulfonyl derivatives, a better reactivity of electron-enriched azobenzenes and a lack of site-selectivity for unsymmetrical azos, the main difference lied in the speculated mechanism. The oxidant $K_2S_2O_8$ necessary to the Wu's catalytic system favored the formation of a *p*-tolylsulfonyl radical proved by the reaction inhibition in the presence of a radical scavenger whereas this pathway was ruled out in the Zhang's work. For the latter, the sulfonylation could proceed through a direct displacement-type reaction.

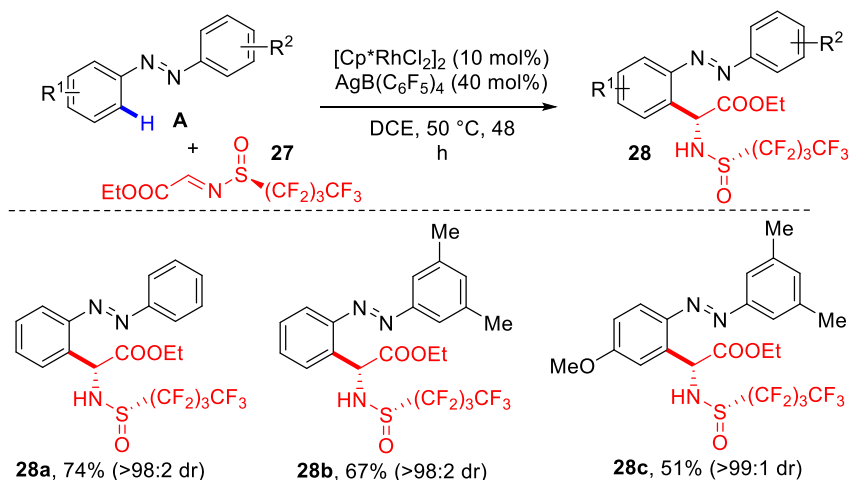


Scheme 22. Direct Pd-Catalyzed *ortho*-Sulfonylation of Azobenzenes

2.2. Rhodium-Catalyzed C_{sp}²-H Bond Functionalization

Rhodium(III) complexes were proved to be effective alternative catalysts in complement of palladium transition metal for C-H bond activation and subsequent construction of diversified carbon-carbon and carbon-heteroatom bonds. In this context, rhodium(III)-mediated coupling reactions have also been developed for the efficient *ortho*-oriented C-H functionalization of azo compounds.

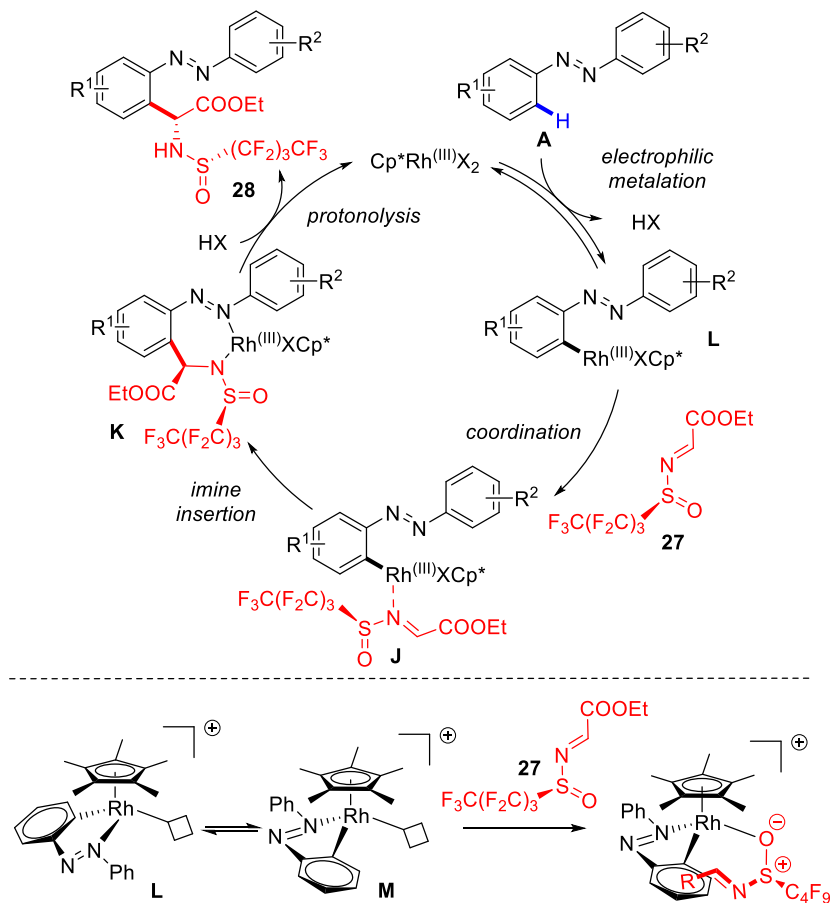
Considering the great interest to prepare chiral α -branched amines through C-C bond formation, Ellman and collaborators explored for the first time the asymmetric intermolecular addition of a non-acidic C-H bond to chiral sulfinyl imines **27** catalyzed by the commercially available complex [Cp*RhCl₂]₂ (Scheme 23).³¹ If the use of traditional *N*-*tert*-butanesulfinyl imines resulted in a lack of reactivity, imines **27** derived from the more activating *N*-perfluorobutanesulfinyl group enabled the formation of the corresponding chiral branched amines **28**. Good conversions and outstanding diastereoselectivities (dr > 98:2) were obtained when the rhodium(III) catalyst is used in combination with the completely non-coordinating halide abstractor AgB(C₆F₅)₄ in a non-coordinating solvent (Scheme 23). Various protected aryl glycines **28** were regioselectively prepared by addition of azobenzenes to *N*-perfluorobutanesulfinyl imino ester **27**. Starting from unsymmetrical azobenzenes, the coupling occurred at the less crowded ring.



Scheme 23. Rh-catalyzed Functionalization of Azobenzenes with Chiral Sulfinyl Imine

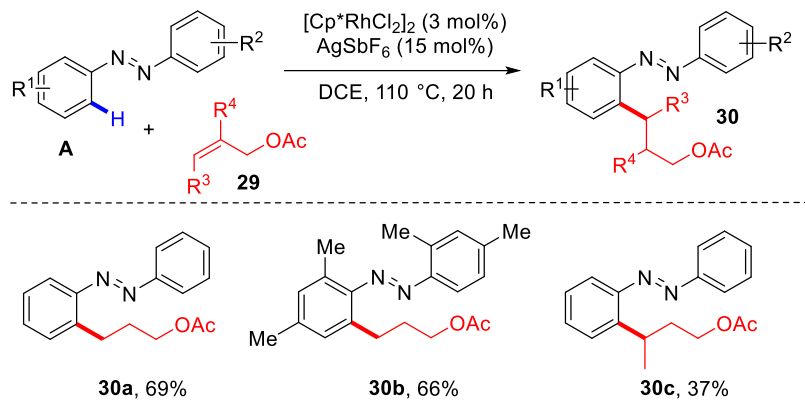
The mechanism of this transformation is proposed in Scheme 24. The catalytic cycle is initiated by an electrophilic substitution generating the azo-Rh complexes **I**, releasing one equivalent of proton. After coordination of the nitrogen atom of sulfinylimine **27** to the metal and imine insertion, a seven-membered rhodacycle **K** is formed. This latter is then reprotonated, producing the targeted α -branched amino scaffold **28** accompanied by the regeneration of the catalyst in its active form. The authors explained the asymmetric induction using stereochemical models built from X-ray structures of cationic rhodacycle analogs derived from 2-phenylpyridine. The high diastereoselectivity requires equilibration between enantiomeric rhodacycles **L** and **M** either before or after coordination of *N*-

sulfinylimino ester **27** whose the perfluorinated substituent pointed away from the reaction center (Scheme 24).³²



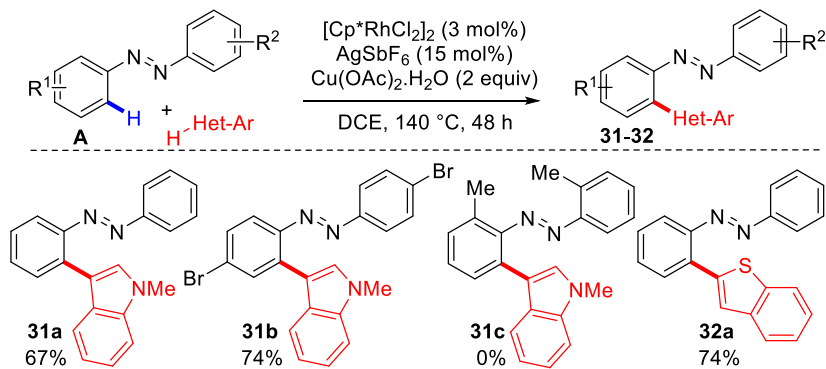
Scheme 24. Proposed Mechanism and Stereochemical Model

Later, Wang *et al.* reported an innovative method of Rh(III)-catalyzed direct *ortho*-alkylation of azobenzenes using allyl acetates **29** as source of alkyl electrophiles (Scheme 25).³³ Surprisingly, in the presence of [Cp^{*}RhCl₂]₂ as catalyst and AgSbF₆ as additive, no olefination products were detected, and only alkylation occurred. Moreover, this direct C-H alkylation protocol allowed a widely-diversified substrate scope: azobenzenes bearing both electron-rich and electron-deficient groups, as well as methylated allyl acetates such as crotonate or 2-methyl derivatives, led to the alkylated compounds **30** in satisfying yields and excellent regioselectivity. Preliminary mechanism investigations were carried out by evaluating the D/H exchange (96%) and the kinetic isotope effect ($K_H/K_D = 4:1$). These experiments revealed that the C-H cleavage is irreversible and may be involved in the rate-determining step. In addition, an anion exchange between [Cp^{*}RhCl₂]₂ and AgSbF₆ was postulated. By reaction with azobenzene, the resulting active species [Cp^{*}Rh][SbF₆] induced the formation of a five-membered cyclorhodium intermediate which evolved to the formation of standard seven-membered rhodacycle through alkene insertion.



Scheme 25. Rh(III)-Catalyzed Direct Alkylation of Azobenzenes with Allyl Acetates

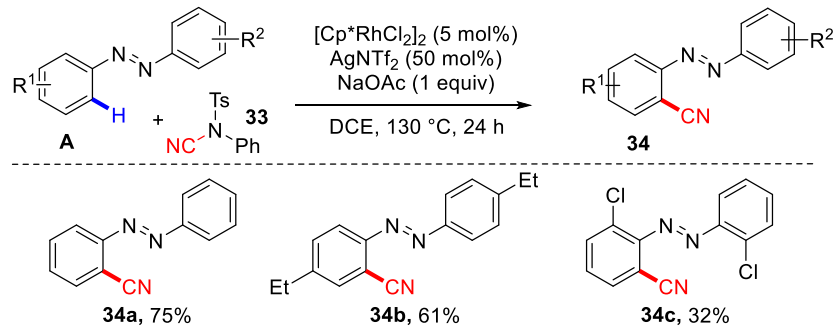
Having demonstrated the efficiency of Rh-catalysis in the C-C bond formation with azobenzenes, the same group developed in 2016 an elegant cross-dehydrogenative coupling of azo compounds with heteroarenes using the same catalytic system combining $[\text{Cp}^*\text{RhCl}_2]_2$ to AgSbF_6 (Scheme 26).³⁴ Assisted by the *ortho*-directing azo group, this C-H/C-H coupling reaction using $\text{Cu}(\text{OAc})_2 \cdot \text{H}_2\text{O}$ as oxidant provides an original alternative approach to synthesize steric π -conjugated biaryls **31-32** without observing heterocycle decomposition or oxidative homocoupling. Interestingly, the coordinated anion SbF_6^- was proved to be crucial for the *ortho*-heteroarylation reaction since attempts to accelerate the reaction by using other additives such as carboxylic acids or other silver salts remained unsuccessful. Regarding the azo substrate, the process tolerated electron-withdrawing and electron-donating groups in *meta* and *para* positions, whereas *ortho*-substituted azobenzenes were unreactive. About heteroarenes, *N*-methyl indole, benzothiophene and benzothiazole coupled regioselectively. Large kinetic isotope effects ($K_{\text{H}}/K_{\text{D}}$ ranges from 3.6 to 4.1) were measured from intermolecular competing experiments, indicating that the coupling reaction is initiated by the Rh(III)-mediated *ortho* C-H activation of azobenzene. As aforementioned for palladium catalysis (Scheme 4), the plausible mechanism is based on the initial formation of an active rhodium species through anion exchange, followed by *ortho*-C-H activation of the azobenzene. The latter undergoes an insertion into the heterocycle C-H bond providing a five-membered rhodacycle which, through a reductive elimination, gives the expected coupling product and the formation of Rh(I). A final reoxidation of Rh(I) in active Rh(III) by the copper salt allows to initiate the next catalytic cycle.



Scheme 26. Rh(III)-Catalyzed Synthesis of Azo-Based π -Conjugated Biaryls

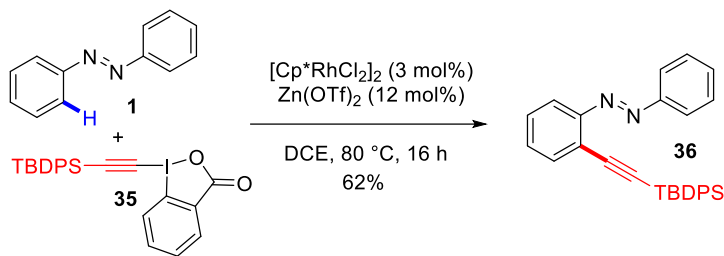
In parallel, using the same rhodium complex derived from $[\text{Cp}^*\text{RhCl}_2]_2$ and AgSbF_6 , Kim and co-authors described the construction of C2-alkylated azobenzenes by coupling α -diazo compounds. If the alkylation reaction tolerated a wide range of symmetrical and unsymmetrical α -diazo esters, moderate yields were obtained starting from *ortho*- or *meta*-substituted azobenzenes. Conversely, when applied to *para*-substituted azobenzene in the presence of a large excess of α -diazo esters, the catalytic system induced a subsequent intramolecular cyclization affording an efficient method of synthesis of cinnolin-3-(2*H*)-ones (see infra - Scheme 53).³⁵

Considering nitrile moiety as a valuable source of functional diversity, synthetic methods allowing the direct cyanation of C-H bonds are arousing considerable interest. Recently, a particular attention has been paid to develop step-economical and environmentally sustainable process, especially by using a source of “non-metallic” cyanide. In this way, the groups of Jia and Zhu developed a rhodium-catalyzed *ortho*-cyanation reaction of symmetrical azobenzenes employing *N*-cyano-*N*-phenyl-*p*-toluenesulfonamide **33** as electrophilic cyanating reagent (Scheme 27).³⁶ The optimal reaction conditions were reached by combining $[\text{Cp}^*\text{RhCl}_2]_2$ to AgNTf_2 as additive in the presence of NaOAc as base. A reactive cationic rhodium(III) species, $[\text{Cp}^*\text{RhOAc}]^+\text{Tf}_2\text{N}^-$, was formed by ligand exchanges between $[\text{Cp}^*\text{RhCl}_2]_2$, AgNTf_2 and NaOAc . If this cyanation reaction tolerates diversely-substituted azobenzenes to proceed in satisfying yields, electron-withdrawing groups and steric hindrance have negative effects on the reaction efficiency. H/D exchange experiments demonstrated that this cyanation reaction was typical of a Rh-catalyzed $\text{C}_{\text{sp}}^2\text{-H}$ bond activation process.



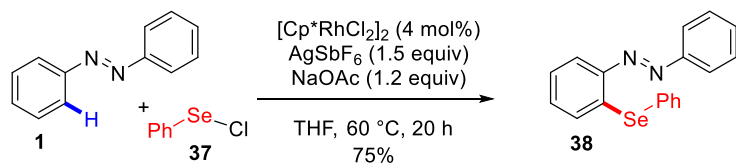
Scheme 27. Rh-Catalyzed Direct Cyanation of Azobenzenes

In this context of C-C bond formation, direct alkynylation of an aryl C-H bond is also very attractive and has been intensively explored using haloalkynes or alkynylated hypervalent iodine. Concerning the azobenzene substrate, the sole example of C-H alkynylation was described in 2014 by Li *et al.* using the hypervalent iodine-alkyne oxidant, 1-[(triisopropylsilyl)-ethynyl]-1,2-benziodoxol-3(1*H*)-one **35** (Scheme 28).³⁷ After intensive screening of reaction conditions, it was found that the reaction efficacy was dramatically improved when the commercially available $[\text{Cp}^*\text{RhCl}_2]_2$ catalyst was employed in the presence of an additive such as AgSbF_6 , $\text{Zn}(\text{NTf}_2)_2$ or $\text{Zn}(\text{OTf})_2$. The latter was preferred due to its cost-effectiveness. Although the activation role of AgSbF_6 through chloride abstraction is relatively clear, the role played by $\text{Zn}(\text{OTf})_2$ may be dual by both activating the catalyst with a reversible chloride abstraction and electrophilically activating the alkyne substrate.



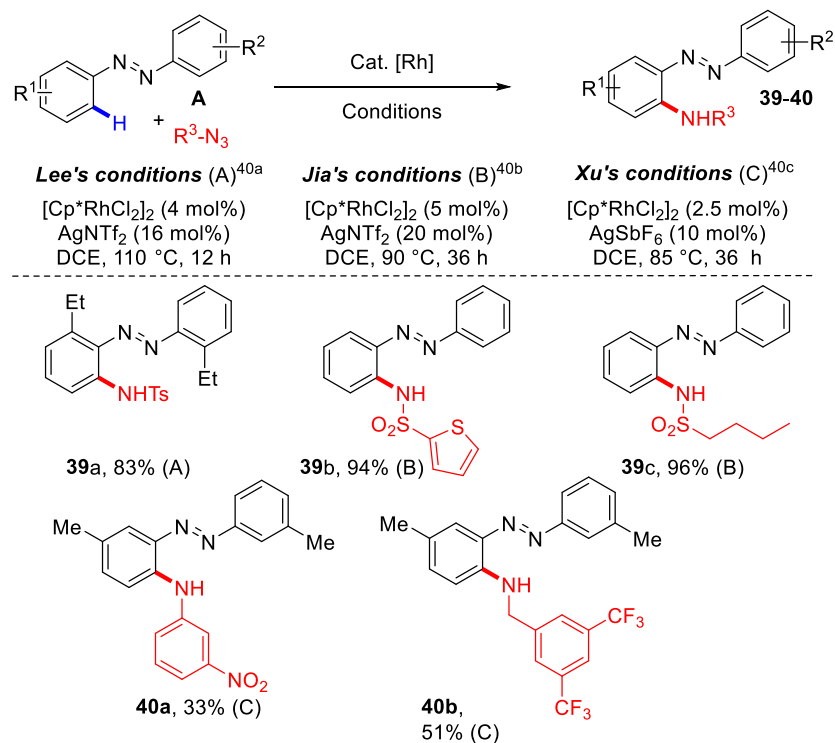
Scheme 28. Rh-Catalyzed Direct Alkynylation of Azobenzene

Beside their efficacy of C_{sp²}-H bond activation for the construction of alkylated, arylated and alkynylated azobenzenes, Rh(III) complexes also enable the formation of carbon-heteroatom bonds. Inspired by the Rh(III)-catalyzed arene amination with electrophilic N-chloramines, independently described by Glorius and Yu;³⁸ Wan, Li *et al.* reported an efficient C_{sp²}-Se bond formation with phenylselenenyl chloride **37** under relatively mild conditions.³⁹ The selenated azo **38** was generated in a 62% yield using [Cp*RhCl₂]₂ catalyst in the presence of a superstoichiometric amount of the additive AgSbF₆ and the base NaOAc (Scheme 29). Mechanistic studies agree with an electrophilic selenation pathway implying the formation of a six-membered cyclometalated rhodium complex. In this mechanism, silver salt may play a double role in activation of both catalyst and substrate by assisting the nucleophilic chloride displacement.



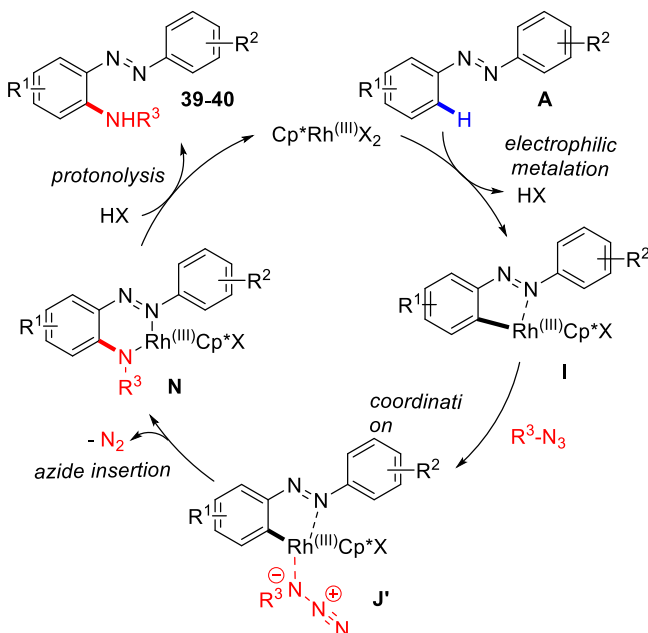
Scheme 29. Rh-Catalyzed Synthesis of *ortho*-Seleno-Azobenzene

However, the most studied Rh(III)-catalyzed direct functionalization of azobenzenes concerns the formation C_{sp²}-N bond. Several research groups have independently disclosed rhodium-catalyzed direct intermolecular amination or amidation of azobenzenes using azides as nitrogen sources (Scheme 30). Their works differ by the choice of the additive employed which is AgNTf₂ for the Lee's and Jia's groups, and AgSbF₆ for the Xu's group.⁴⁰ In the Lee's study, it is important to note that the azo scaffold is often used in excess (1.5 to 2 equiv.) in order to avoid the formation of the diamidated azobenzene as by-product. Interestingly, when diamidation occurred, the two newly coupled nitrogen-atoms are regioselectively on the same arene. A large choice of diversely *ortho*-, *meta*- and *para*-substituted azobenzenes as well as aromatic and aliphatic sulfonyl azides were well tolerated in the amidation reaction giving the corresponding amidated compounds **39** in acceptable to good yields (Scheme 30). From unsymmetrical azobenzenes, the amidation reaction mainly took place on the electron-enriched aromatic ring. The Xu's group extended the scope of this transformation to aryl and alkyl azides affording the aminated azobenzenes **40** in moderate yields (Scheme 30).



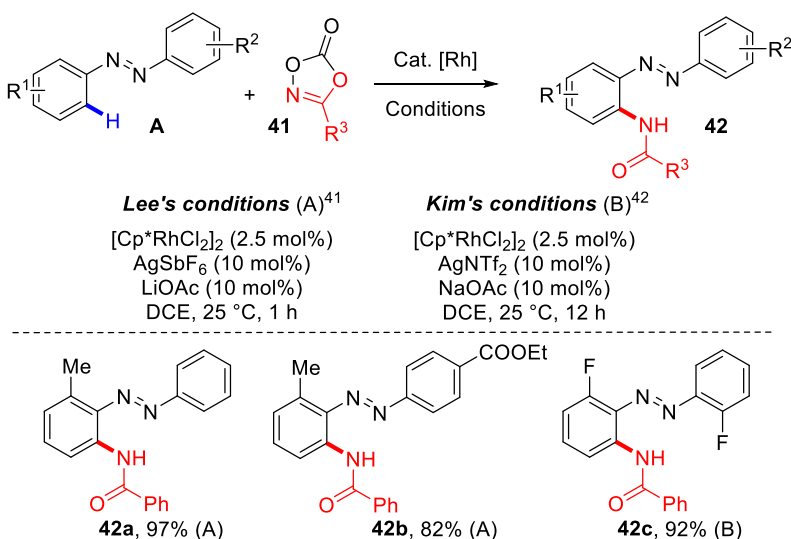
Scheme 30. Rh-Catalyzed Direct *ortho*-Sulfamidation and *ortho*-Amination of Azobenzenes

The reaction is believed to begin *via* the generation of a cationic Rh(III) active species, which assists the C–H bond activation to give a five-membered rhodacycle **I** (Scheme 31). Azide coordination followed by extrusion of molecular N₂ concerted to migratory insertion leads to the intermediate **N**. Finally, protonolysis of this latter releases the targeted *ortho*-functionalized azo **39–40** and regenerates the active Rh(III) catalyst.



Scheme 31. Proposed Catalytic Cycle for Direct *ortho*-Amination of Azobenzenes

One year later, as a logical extension of these studies, two conceptually related methodologies based on decarboxylative process were simultaneously disclosed by the groups of Lee⁴¹ and Kim⁴² (Scheme 32). The reaction proceeds smoothly using dioxazolones **41** as amidating agents in the presence of cocatalytic amounts of additive (silver salt) and base (acetate salt) to generate the cationic Rh(III) active catalyst. Unsymmetrical azobenzenes **42** bearing either aliphatic or aromatic amides groups in *ortho* position have been prepared in good to high yields. Similarly to the case of azides, the reaction tolerates a wide range of both azobenzenes **A** and dioxazolones **41** but the amount of dioxazolones **41** has to be adjusted and increased in order to counterbalance the lower reactivity of electron-deficient azobenzenes. Starting from unsymmetrical azobenzenes, the C-H amidation mainly took place on the electron-rich aromatic ring. For azobenzenes composed by sterically different aromatic cores, the reaction occurred on the less hindered ring underlining that the reaction regioselectivity is also controlled by steric effects. Moreover, no KIE was observed, suggesting that the metal insertion in the C-H bond is not involved in the rate determining step of the reaction.



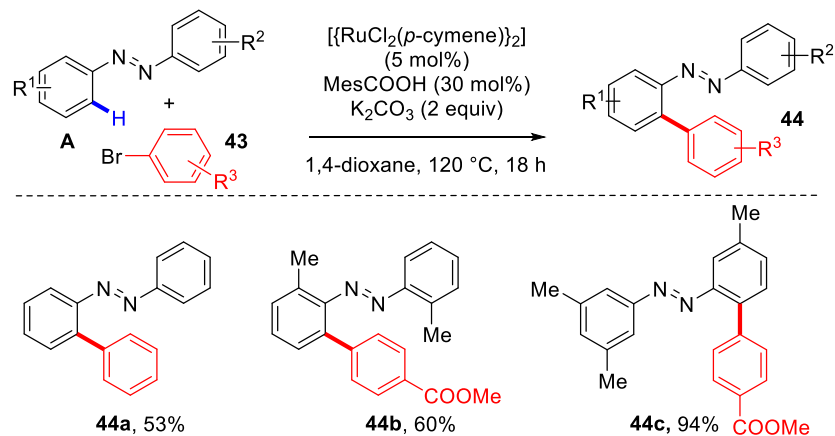
Scheme 32. Rh-Catalyzed Direct Amidation of Azobenzenes

In another example, Kim and co-workers reported the formation of *N*-sulfonylamidated and amidated azobenzenes under a similar catalytic system using arylsulfonyl, alkyl and aryl isocyanates as sources of nitrogen.⁴³ In this case, KIE ($K_H/K_D = 4.5$) indicates that C-H bond cleavage may be involved in the rate-limiting step.

2.3. Ruthenium-Catalyzed C_{sp^2} -H Bond Functionalization

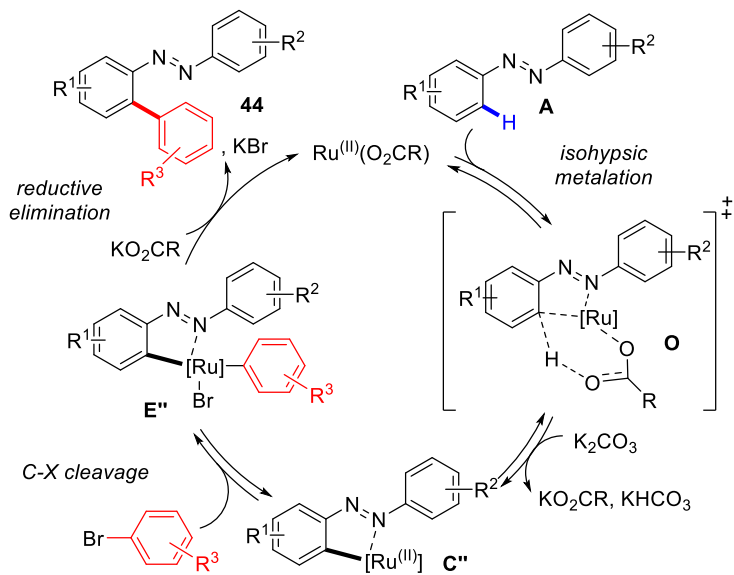
Among several conceivable transition metal-based catalytic systems for more efficient C-H functionalization, ruthenium complexes also play a key role in terms of regioselectivity in nitrogen-metal chelation-assisted reaction. If an early example of direct *ortho*-silylation of azobenzene was explored with a modest yield by Kakiuchi and co-workers in 2003,⁴⁴ the group of Ackermann proved that ruthenium(II) carboxylate complexes could efficiently catalyze azobenzene *ortho*-arylation (Scheme 33).⁴⁵ The choice of the carboxylic acid turned out to be crucial for reaching high conversion

and MesCOOH was found to be the most active. Even if the scope of azobenzenes is limited to electron-enriched substrates, diverse aromatic and heteroaromatic bromides were effective electrophilic coupling partners, with a range of electron-deficient to more challenging electron-rich derivatives.



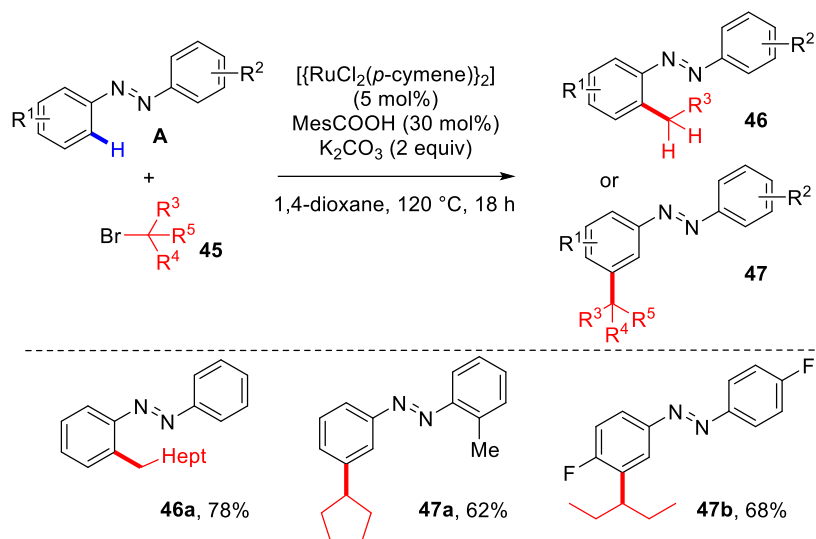
Scheme 33. Ru(II)-Catalyzed Direct *ortho*-Arylation of Azobenzenes with Ru(II) Complex

The authors evaluated the possible H/D scrambling in the presence of D₂O as cosolvent. The H/D exchange was total in the *ortho* position, demonstrating the reversibility of the C–H ruthenation step. Interestingly, they also noticed a variation in initial rates depending on the electronic properties of aryl bromides **43**. The Hammett plotting between the initial rates and the σ_p values revealed a linear correlation with a negative slope showing that the C–H arylation is facilitated in the presence of electron-donating groups. These mechanistic studies reflect a possible rate-determining reductive elimination. The postulated mechanism is based on the formation of a five-membered ruthena(II)cycle **C'** via a reversible isohypsic cyclometalation with a Ru(II) complex **O** (Scheme 34). The subsequent C–H activation by arylbromide through probable SET-type elementary steps allows the formation of a standard intermediate **E'**. The latter undergoes reductive elimination to forge the targeted product **44** and regenerate catalytically active Ru(II).



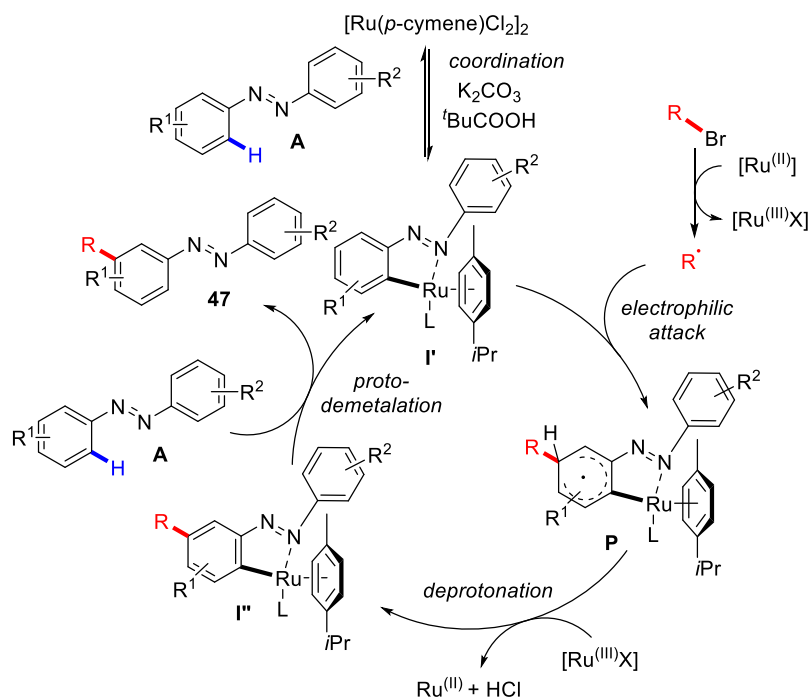
Scheme 34. Proposed Catalytic Cycle for Ru(II)-Mediated Azo Direct *ortho*-Arylation

Very recently, a major contribution in carboxylic acid-promoted ruthenium(II) catalysis was reported by Li and co-workers (Scheme 35).⁴⁶ To our knowledge, they described the first *meta/ortho*-selective arylation reactions of azoarenes using primary, secondary or tertiary alkyl bromides **45**. The optimal catalytic system required the combination of $[\text{Ru}(p\text{-cymene})\text{Cl}_2]_2$ catalyst, pivalic acid as additive and K_2CO_3 as base. Primary alkyl bromides selectively lead to *ortho*-functionalized products **46** whereas either secondary or tertiary alkyl bromides generate *meta*-functionalized products **47**. Both cyclic and acyclic reagents are well tolerated and the efficacy of the coupling was demonstrated on a gram-scale experiment. As already observed for rhodium-catalyzed direct $\text{C}_{\text{sp}}^2\text{-H}$ functionalization, both steric encumbrance and electronic nature of azoarene substituents influence the reaction rate and its regiocontrol: large steric hindrance or strong electronic deficiency inhibits the reaction.



Scheme 35. Regiocontrolled Ru(II)-Catalyzed Alkylation of Azobenzenes

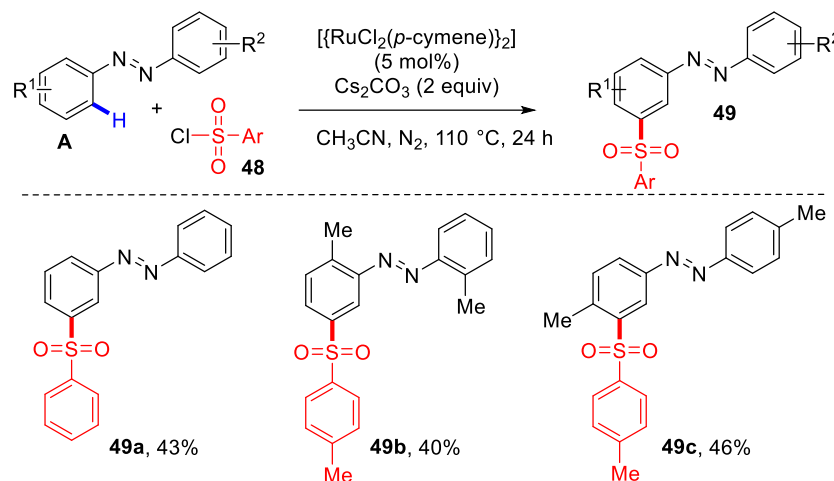
For these transformations, the authors proposed a mechanism involving the formation of a radical species since no desired product was formed in the presence of TEMPO. In addition, starting from a fully deuterated azobenzene, a significant *ortho* D/H exchange occurred while no *meta* D/H exchange was detected when the reaction was carried out under optimal conditions. This experiment clearly confirms that contrary to the *meta* position, the initial C-H metalation in *ortho* position is reversible. Finally, a cyclometalated complex was prepared by mixing azobenzene with $[\text{Ru}(p\text{-cymene})\text{Cl}_2]_2$ and characterized by X-ray diffraction. As it proved to efficiently catalyze the reaction, the latter may prefigure the crucial active catalyst in the *meta*-selective C-H functionalization. Based on these experimental data, a plausible mechanism was proposed for the reaction of *meta*-alkylation (Scheme 36). It begins by a reversible *ortho*-C-H ruthenation, affording the active cyclometalated complex **I'**. Subsequent electrophilic attack from the *para*-position of the Ru-C_{Ar} takes place due to the strong directing effect of the Ru-C_{Ar} σ-bond. Thereafter, a radical species **P** was generated through a Ru(II)-mediated SET and transformed into a more stable complex **I''** under the concomitant action of the base and the Ru(III) catalyst. Finally, proto-demetalation affords the *meta*-alkylated azo **47** and the active catalytic species.



Scheme 36. Proposed Catalytic Cycle for Ru(II)-Catalyzed *meta*-Selective C-H alkylation

Following their seminal report, the same group published a similar strategy for the synthesis of *meta*-selective sulfonation of azoarenes using aromatic and heteroaromatic sulfonyl chlorides **48** as electrophiles (Scheme 37).⁴⁷ The optimal conditions were reached in acetonitrile using $[\text{Ru}(p\text{-cymene})\text{Cl}_2]_2$ as catalyst and Cs_2CO_3 as base, in a sealed Schlenk tube under nitrogen atmosphere. Although the isolated yields remained moderate, this approach was proved very useful for the synthesis of a range of original *meta*-sulfonated azos **49**. As for the Ru(II)-catalyzed *meta*-alkylation, both electron-rich and weakly electron-poor azos can be accommodated and the reaction efficiency

is conditioned by the steric encumbrance of the substrate. The scope of arylsulfonyl chlorides **48** is quite broad tolerating alkyl, aryl, halogen, electron-donating and strong electron-withdrawing substituents. In opposite to their previous work, the reaction is still efficient in the presence of a radical scavenger such as TEMPO indicating that the mechanism should involve an electrophilic aromatic substitution process.

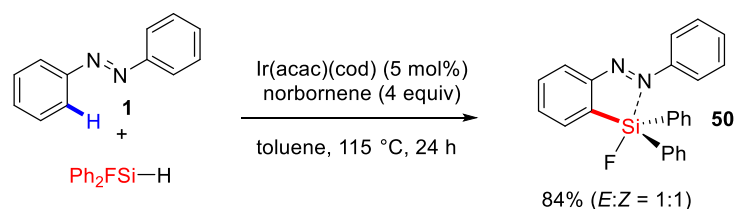


Scheme 37. Ru-Catalyzed Direct *Meta*-Selective Sulfonation of Azobenzenes

4. Miscellaneous Catalysis

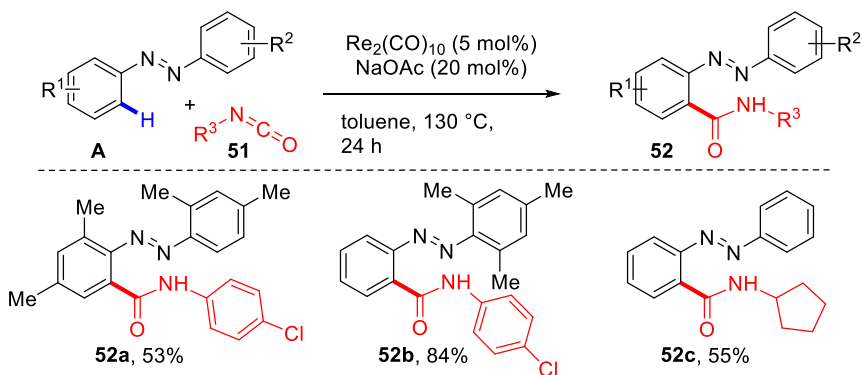
Besides palladium-, rhodium- and ruthenium-containing catalysts, iridium-, rhenium- and cobalt-based complexes have also been successfully applied to promote the *ortho*-selective C–H functionalization of azo-arenes.

In this way, the group of Kuninobu and Kani developed an efficient and gram-scale regioselective C_{sp^2} -H silylation of arenes using an iridium catalyst (Scheme 38).⁴⁸ After intensive transition metal catalysts screening, the authors found that the silylated product **50** is only produced in good yield in the presence of a combination of Ir(acac)(cod) and norbornene. The latter played a crucial role, presumably as a hydrogen acceptor and/or a ligand for the catalyst. The nature of the silylation agent was also essential for promoting the coupling reaction. Indeed, the fluorine atom of hydrosilanes was demonstrated to be indispensable while no desired product was detected by using of several hydrosilanes, such as HSiPh₃, HSiEt₃, and H₂SiPh₂, suggesting that Lewis acidity of the silicon atom is an important parameter. However, the reaction mechanism remains unclear. Interestingly, double *ortho*-silylation was never observed.



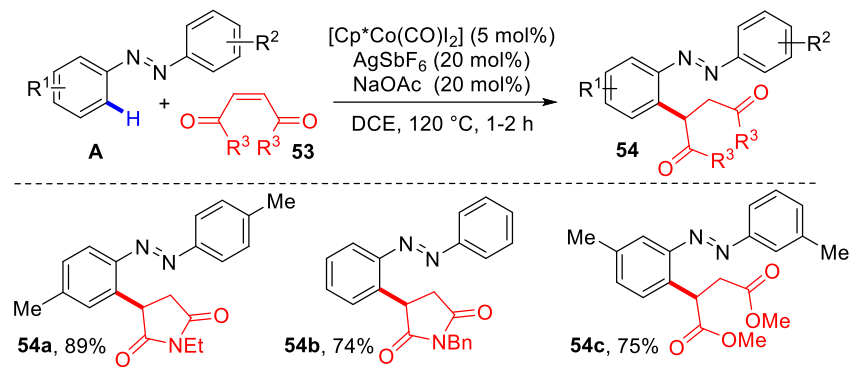
Scheme 38. Iridium-Catalyzed C–H Silylation of Azobenzene

Rhenium-catalysis is also an interesting manner to regioselectively activate C_{sp^2} -H bond for the C-C bond formation. The Wang's group demonstrated that $\text{Re}_2(\text{CO})_{10}$ can promote the aminocarbonylation of azobenzenes with isocyanates **51** without the formation of homocoupling or difunctionalized byproducts (Scheme 39).⁴⁹ Although the reaction required an excess of azo compounds and high reaction temperature, the coupling proceeds with a wide range of isocyanates **51** and azobenzenes **A**, showing wide functional group tolerance and allowing for an access of convertible tri-substituted scaffolds **52**. The presence of a catalytic amount of NaOAc resulted in an important increase of the reaction rate, probably due to the acceleration of the deprotonative C_{sp^2} -H activation step. From a mechanistic point of view, the authors isolated the supposed five-membered rhenacycle which was submitted to the reaction conditions. As the targeted product was obtained in a cleanly manner, it can be hypothesized that the reaction may follow a classical pathway *via* a five-membered rhenacycle formation, an isocyanate insertion to generate a seven-membered ring and a final protonation releasing the functionalized azo and the active Re species.



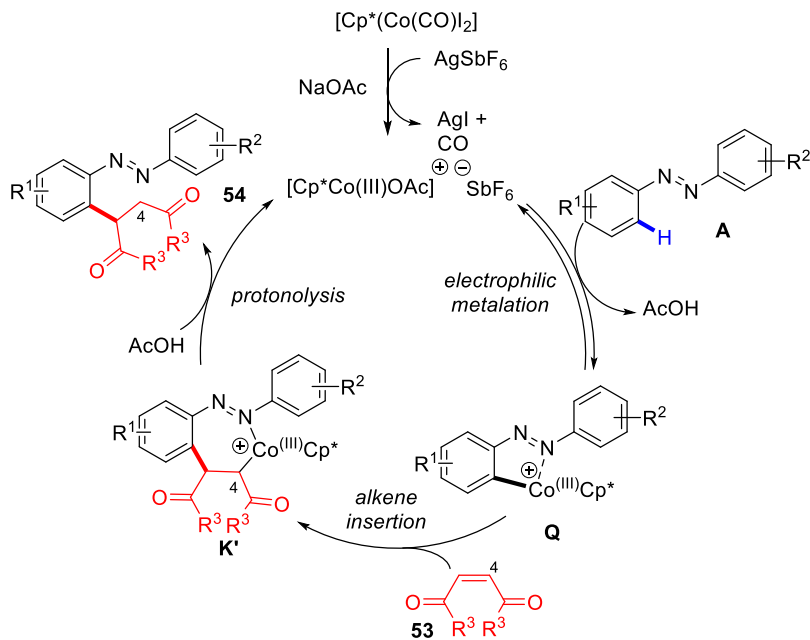
Scheme 39. Rhenium-Catalyzed C–H Aminocarbonylation of Azobenzenes

Earth-abundant and low-cost first-row transition metal catalysts recently attracted much attention in catalysis. Presenting the advantage to be air-stable and easily prepared, cobalt catalysts are recognized as a valuable alternative in activation of C_{sp^2} -H bond like rhodium complexes. In 2017, Prabhu and coworkers explored the cationic cobalt(III)-catalyzed functionalization of azobenzenes with *N*-alkyl maleimides (Scheme 40).⁵⁰ A catalytic amount of an acetate additive was found to be of prime importance both to reach good yields and to minimize the formation of the difunctionalized product. The optimal reaction conditions combining $[\text{Cp}^*\text{Co}(\text{CO})\text{I}_2]$ catalyst to AgSbF_6 and NaOAc additives in DCE at 120 °C have been successfully applied for regioselective alkylation of symmetrical and unsymmetrical azobenzenes by using various maleimides and maleate esters **53**. The substrate scope studies showed that the process is more efficient for electron-enriched or weakly deactivated azobenzenes. Steric hindrance induced by *ortho*-substitution had deleterious effect. Starting from unsymmetrical azobenzenes, the reaction occurred on the electron-rich aryl ring. The nature of the maleimide *N*-substituent had no influence on the reaction efficiency. The reaction also tolerated a variety of symmetrical dialkyl maleates.



Scheme 40. Cobalt-Catalyzed C–H Alkylation of Azobenzenes

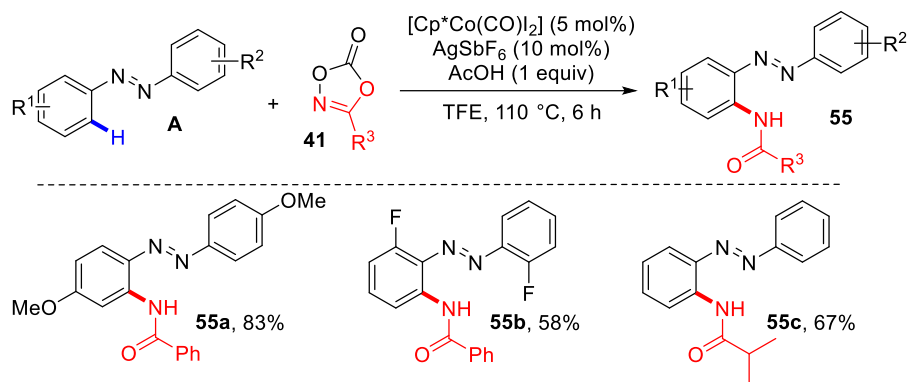
From a mechanistic point of view, the C_{sp^2} -H cleavage was proved to be reversible by H/D exchange experiments in D_2O . The authors also assumed that this step may not be involved in the rate-determining step of the reaction ($K_H/K_D = 1.44:1$). More interestingly, starting from a fully *ortho*-deuterated azobenzene, a 15% and 25% deuterium transfer was detected at the C-4 position of the succinimide ring, highlighting an *ortho*-proton transfer from the azo to the Michael acceptor *via* a cobaltacycle intermediate **K'** (Scheme 41). In this context, the proposed mechanism suggested the generation of an active cationic Co(III) species **Q** generated by anion exchange using NaOAc and AgSbF₆. The cationic complex would undergo C–H metalation and subsequent alkene insertion leading to the formation of a putative 7-membered intermediate **K'**. Protodemetalation of the latter afforded the alkylated azo compound **54** with concomitant regeneration of the active Co(III) catalyst.



Scheme 41. Proposed Catalytic Cycle for Direct Alkylation of Azobenzenes

At the same time, the $Cp^*\text{Co}(\text{III})$ -catalyzed direct *ortho*-amidation of azobenzenes was reported in the presence of dioxazolones **41** by the Patel's group (Scheme 42).⁵¹ Similarly to the Rh(III) version, both catalytic amounts of silver and acetate salts and the presence of acetic acid as an additive were

required to reach full conversion. Probably due to its moderate acidity and low coordinating ability, the solvent 2,2,2-trifluoroethanol (TFE) played a key role in the transformation by stabilizing the cationic active species. The efficiency of the *ortho*-amidation was not affected by the electronic nature of the azobenzene substituents when positioned in *para*. Owing to steric encumbrance, Co-catalyzed amidation of *ortho*-substituted azobenzenes provided the amidated compounds **55** in lower yield. The authors also demonstrated that dioxazolones **41** bearing aryl or alkyl substituents promoted the reaction in the presence of symmetrical azobenzenes. In addition, increasing the amounts of the dioxazolones **41** contributed to the formation of the deamidated compound. Interestingly, the second amidation occurred on the other phenyl ring, in opposite to those observed with Rh-catalytic system. If the reaction mechanism plausibly followed the usually accepted trends, the major difference lies in the irreversibility of the C_{sp^2} -H activation process.



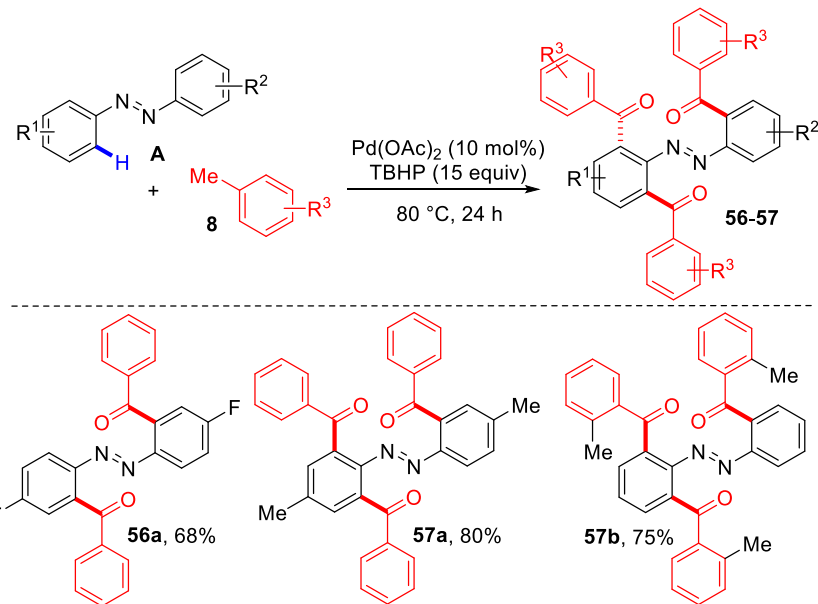
Scheme 42. Co-Catalyzed Direct Amidation of Azobenzenes

3. POLY-FUNCTIONALIZATION OF AZOBENZENES

As mentioned in the introduction part, the synthesis of poly-*ortho*-substituted azobenzenes is of prime importance and the activation of several C_{sp^2} -H bonds in a single one-step is a challenge for the organic chemist. At that time, only few efficient studies are reported.

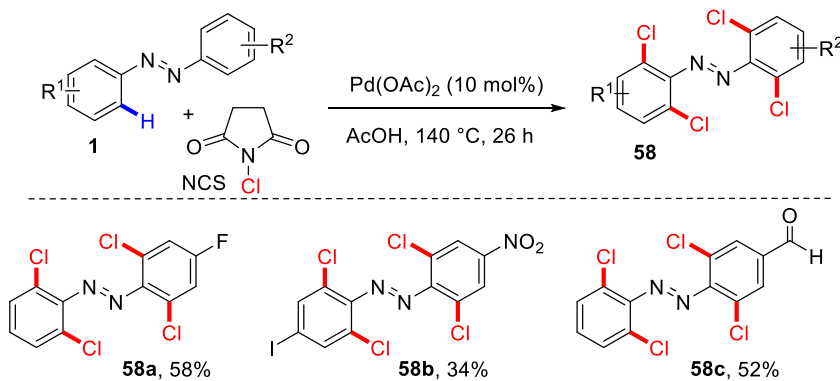
3.1. Palladium Catalysis

In 2014, Wu, Cui and co-workers accomplished the di- or triacylation of azobenzenes through Pd-catalyzed oxidative C-H bond activation in the presence of a large excess (15 equiv.) of *tert*-butyl hydroperoxide and toluene derivatives **8** used as both solvent and acylating agents (Scheme 43).^{14c} It was possible to perfectly control the di- or trifunctionalization of azo derivatives thanks to the electronic nature of the arene substituents. Performing the reaction with deactivating substituents favored the double acylation while activating substituents mainly afforded the triple acylated azo compounds **57**.



Scheme 43. Pd-Catalyzed Synthesis of Di- or Tri-*ortho*-Acylo Azobenzenes

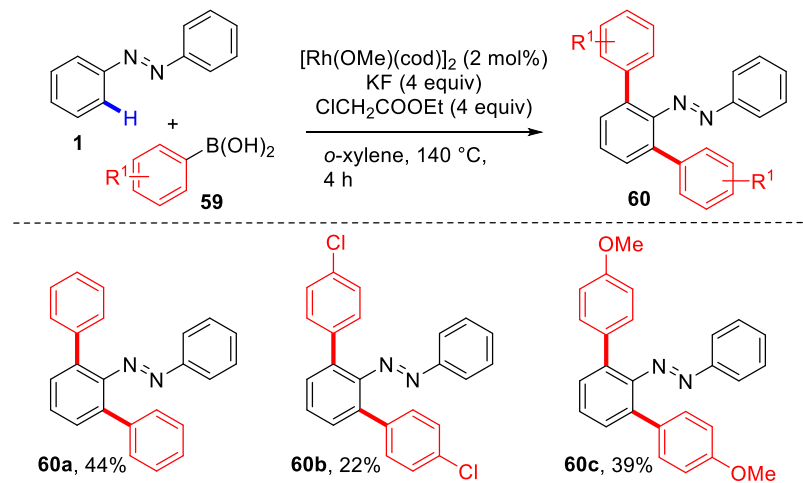
A milestone contribution was reported in 2016 by Trauner and coworkers who developed a general method for the synthesis of tetra-*ortho*-chloro-substituted azobenzenes **58** by direct Pd(II)-catalyzed C-H activation (Scheme 44).⁵² The optimal conditions were obtained with Pd(OAc)₂ in the presence of only 5 equivalents of *N*-chlorosuccinimide (NCS) in AcOH at 140 °C. Not only symmetrical but also unsymmetrical azobenzenes smoothly underwent the cross-coupling, leading to advanced synthons for the construction of photoswitches.



Scheme 44. Pd-Catalyzed Synthesis of Tetra-*ortho*-Chloro Azobenzenes

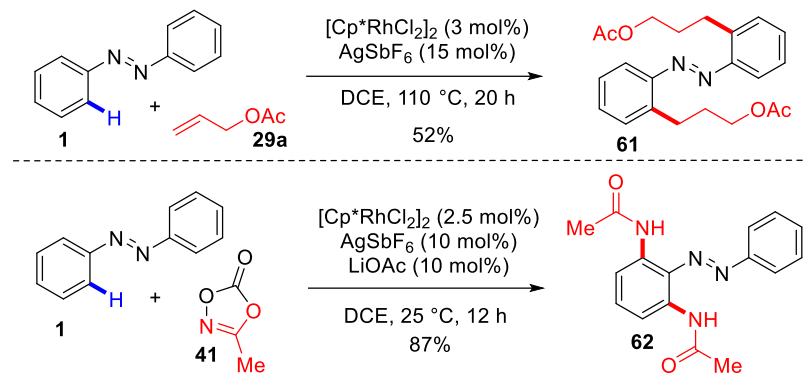
3.2. Rhodium Catalysis

The first example of polyfunctionalization using a Rhodium catalyst was described in 2008 by Miura, Satoh and co-workers (Scheme 45).⁵³ They showed that exposure of the azobenzene **1** to phenylboronic acids **59** in the presence of a catalytic amount of [Rh(OMe)(cod)]₂ and ethyl α -chloroacetate as hydrogen acceptor, generates double *ortho*-phenylated products **60**. A couple of pioneering examples were described, albeit in low yields. Note that the diarylation proceeds on the same aromatic ring despite the increasing steric encumbrance.



Scheme 45. Rh-Catalyzed Double *Ortho*-Arylation of Azobenzenes

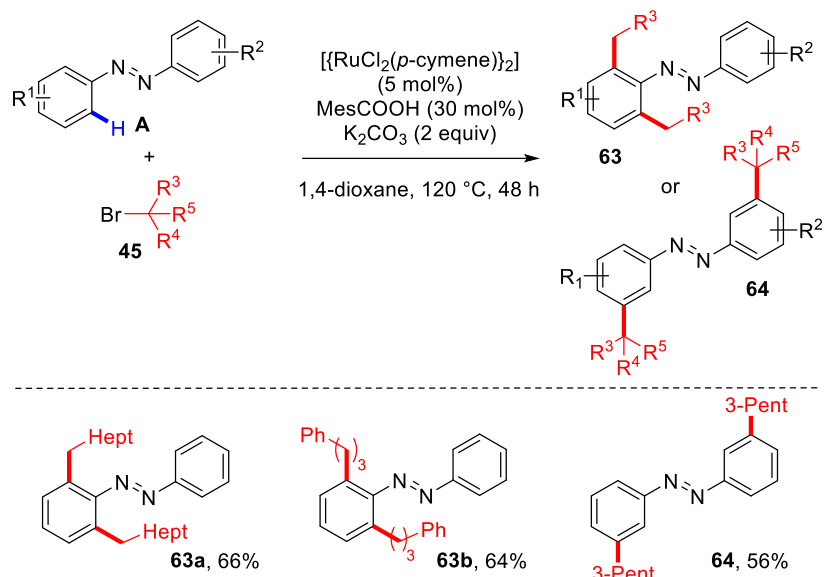
The following examples dealing with the synthesis of disubstituted scaffolds rely on some works previously depicted for azo mono-functionalization. Usually, the desired double C-H functionalization results from the use of the coupling partner in a higher excess. First, Wang and co-workers reported, in 2015, the synthesis of dialkylated scaffold **61** by employing 3 equivalents of allyl acetate **29a** (Scheme 46).³³ The double alkylation occurred symmetrically on each aromatic core. One year later, the Lee's group also extended its protocol of azobenzene amidation to the dual process allowing the selective formation of unsymmetrical diamidated azos **62**.⁴¹ If no explanation of the regiocontrol was proposed, it is important to notice that the site selectivity of the second coupling differs between these two examples.



Scheme 46. Rh-Catalyzed Double Functionalization of Azobenzenes

3.3. Ruthenium Catalysis

Interestingly, in conjunction with their work on Ru-catalyzed mono alkylation of azobenzenes, Li and co-workers showed that dialkylation was also feasible by doubling the stoichiometry of the electrophilic partner (Scheme 47).⁴⁶ Strikingly, a switch in the site selectivity was observed depending on the alkyl bromide nature: the *ortho*-dialkylation proceeds on the same aromatic core of the azoarene with primary and secondary bromides while the *meta*-dialkylation with a tertiary alkyl bromide takes place on each benzene ring affording the dialkylated azos **63** and **64**, respectively.



Scheme 47. Direct Ru-Catalyzed Site-Selective Double Alkylation of Azobenzenes

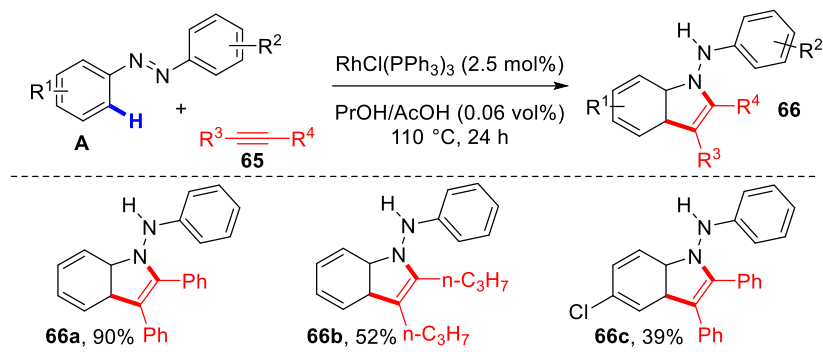
4. SYNTHESIS OF HETEROCYCLES VIA AZOBENZENES C-H FUNCTIONALIZATION

Heterocycles are ubiquitous in the large community of molecular chemists and the development of rapid and efficient synthetic methods is imperative. In this context, elegant transformations of azoarenes *via* cascade reactions including a C-H activation step have recently emerged for the synthesis of nitrogen-containing heterocycles. Methodologies discussed in this part will only cover one-pot processes.

4.1. Indoles

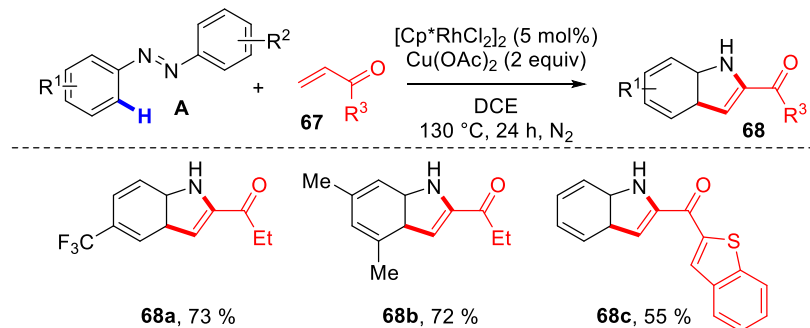
Indoles are widely distributed in nature and numerous indoles of natural or synthetic origin have found application as pharmaceuticals or agricultural chemicals. That's why, indole chemistry has been the object of intensive research especially in drug discovery.⁵⁴

In 1995, Kish and collaborators reported an early example of a rhodium-catalyzed transformation of azobenzenes into indole derivatives **66** involving aliphatic or aromatic internal alkynes **65** (Scheme 48).⁵⁵ A variety of 1,2-phenyldiazenes **A** and alkynes **65** were refluxed in a PrOH-AcOH solution in the presence of the Wilkinson's catalyst affording the targeted indoles **66** in low to excellent yields. Regarding the scope, the catalyst preferentially attacked the substituted phenyl ring when unsymmetrical azobenzenes were used. In addition, alkynes bearing electron-withdrawing substituents produced low yields. In this paper and based on the current literature in the C-H activation field, the authors concluded that the alkyne **65** is first metalated by exchange ligand prior to react with azobenzene, leading to an alkenated intermediate which underwent cyclisation by nucleophilic addition giving 2,3-dihydrocinnolines which rearranged into 1-aminoindoles under acidic catalysis.



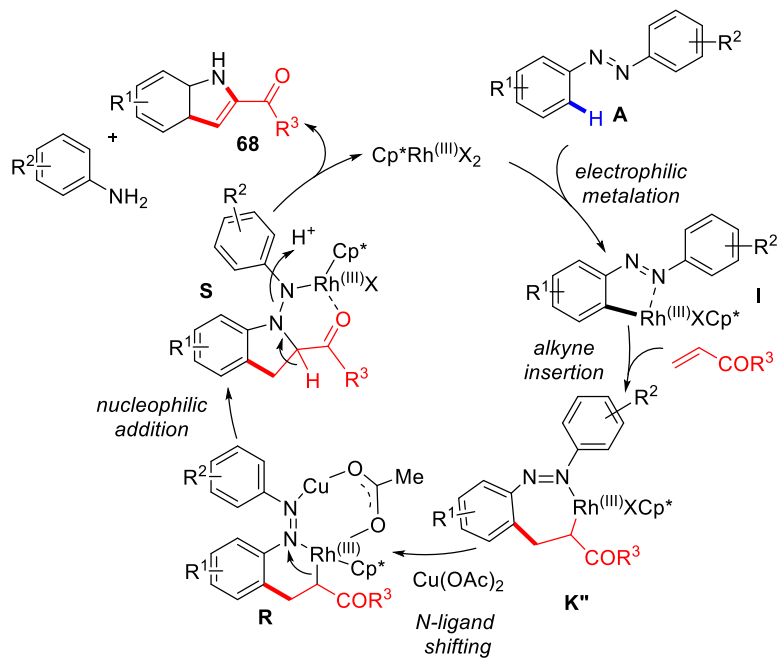
Scheme 48. Rh-Catalyzed Synthesis of Indoles

Very recently, Xi and co-workers have disclosed an elegant substrate-controlled transformation of azobenzenes into indoles through an oxidative Rh-catalyzed C-H activation using vinyl ketones or acrylamides **67** as electrophiles (Scheme 49).⁵⁶ Reaction conditions were compatible with a wide range of azobenzenes substituted by both electron-donating and electron-withdrawing groups, leading to 2-acyl (NH) indoles **68** in satisfying yields. Notably, the system gave excellent regioselectivity from unsymmetrical azobenzenes at the less sterically hindered ring. The generalization of this protocol with respect to the electrophilic partner was tested and either aliphatic and aromatic vinyl ketones or acrylamides **67** can be accommodated.



Scheme 49. Rh-Catalyzed Synthesis of Indoles with Vinyl Ketones

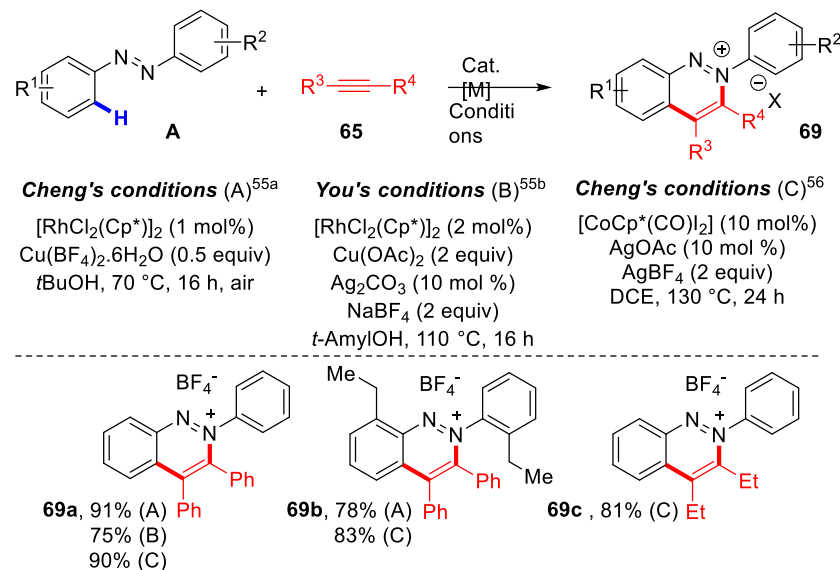
Based on a combination of mechanistic experiments and reported literature, the authors proposed the mechanism detailed in Scheme 50. A seven membered rhodacycle **K'** is first postulated by alkene coordination and insertion in the cyclorhodium(III) species **I**. The β -H elimination, which is usual in the Fujiwara-Moritani coupling, is here discarded to give a more stable six-membered Rh species **R** with the aid of Cu(OAc)₂. Nucleophilic addition of **R** gives **S**, which undergoes rearrangement with concomitant N-N bond cleavage affording the targeted indole **68** and the corresponding aniline as byproduct. The indole formation was attributed to the Lewis acid proprieties of copper acetate that activate the nucleophilic addition by coordinating with the azo group.



Scheme 50. Proposed Catalytic Cycle of Rh-Catalyzed Synthesis of Indoles with Vinyl Ketones

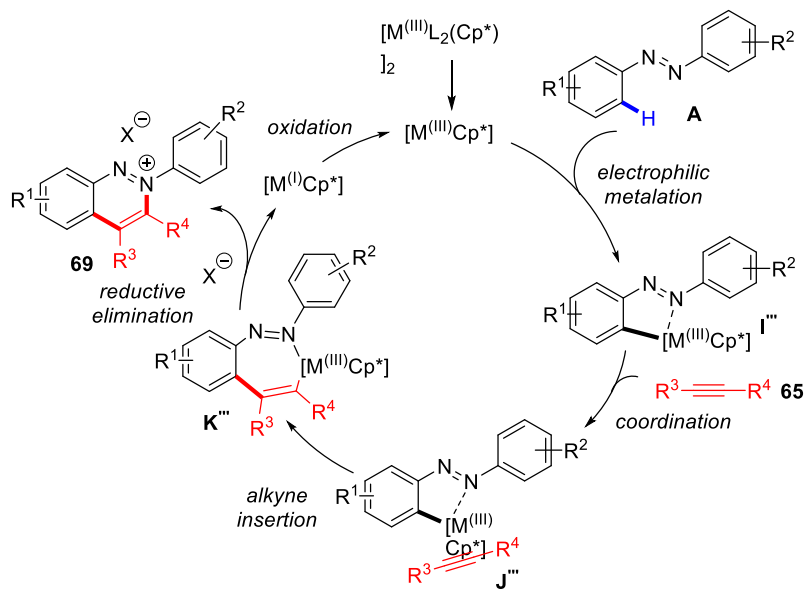
4. 2. Cinnolines and Cinnolinium Salts

Cinnolines and cinnolinium salts referred to pharmaceutically and biologically relevant structures in drug discovery or to structural motifs for their optical and luminescent properties.⁵⁷ In 2013, two consecutive papers reported the synthesis of cinnolinium salts **69** through a tandem oxidative C-H activation/cyclization by reacting azo compounds with internal alkynes **65** in the presence of the [RhCl₂(Cp*)]₂ catalyst and a combination of Cu(BF₄)₂ and air as oxidant (Scheme 51).⁵⁸ Since these works, the same cascade reaction using more abundant, less expensive, and less toxic metal through a high-valent cobalt catalyst, was reported by Cheng.⁵⁹ In general, the reactions worked well with a large scope of azoarenes as well as alkynes, and good to excellent yields can be provided. More in details, azobenzenes substituted at either *ortho* or *meta* positions were suitable for the reaction and starting from unsymmetrical derivatives, the reaction occurs more favorably at the most electron-rich phenyl ring. Specially, the reaction enjoys diverse counteranions by external addition of stoichiometric alkali metal salts.



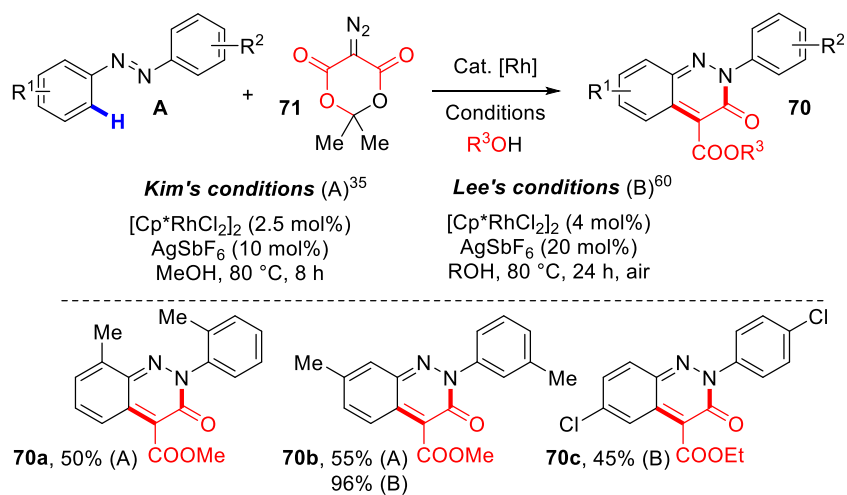
Scheme 51. Ru- and Co-Catalyzed Synthesis of Cinnolinium Salts

To get an insight in the cobalt-catalyzed reaction mechanism, deuterium-labeling experiments were conducted for competition and parallel reactions with a parent substrate, the 2-phenylpyridine. High intramolecular KIE values were observed (>2), suggesting that C-H bond cleavage at the arene *ortho*-position is credibly involved in the rate-limiting step. A general and possible reaction pathway is described in Scheme 52. After generation of the active metal species (Rh or Co), the catalytic cycle begins with the coordination of azobenzene to the metal to generate a five-membered metallacycle I''. Then, π coordination of the alkyne 65 to I'' gives a newly intermediate J'' and subsequent insertion provides the seven-membered metallacycle K''. Finally, K'' undergoes reductive elimination affording the targeted cinnolinium salt 69 accompanied by the reduced metal, which is oxidized to regenerate metal(III) species. BF_4^- salts play manifold roles: they serve to generate the active metal species, equilibrate the cationic cinnolinium as counterion and regenerate the metal under its active form.



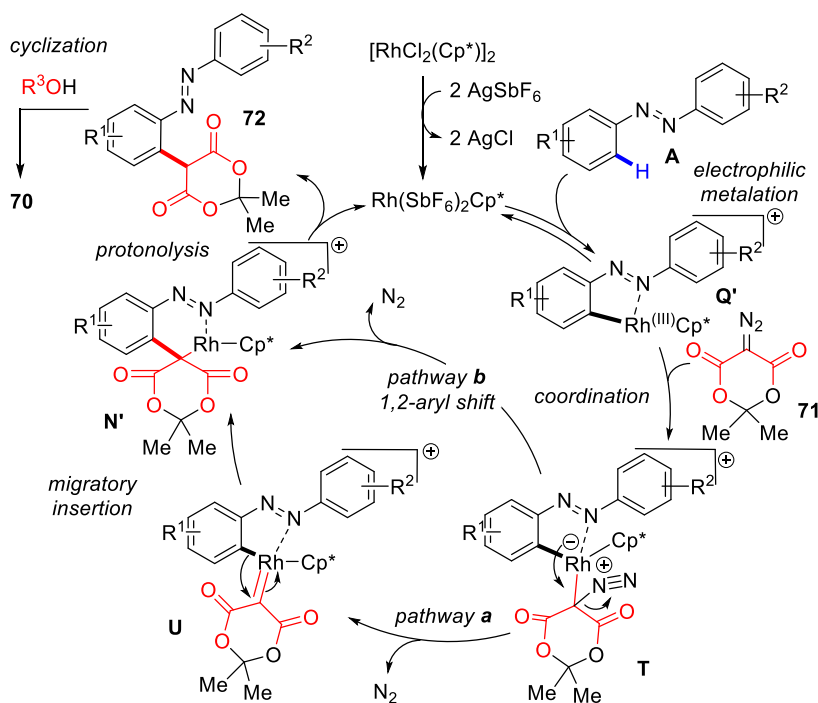
Scheme 52. Proposed Catalytic Cycle for Transition-Metal Catalyzed Synthesis of Cinnolinium Salts

An elegant access to cinnoline analogs was simultaneously considered by Kim and Lee in 2015 (Scheme 53).^{3,60} A synthetic method giving a wide range of highly functionalized cinnolin-3(2H)-ones **70** was developed from the reaction of azobenzenes with diazotized Meldrum's acid **71** *via* a tandem Rh(III)-catalyzed C-H alkylation/intramolecular cyclization. The reaction was efficiently applied to diversely *para*-substituted azobenzenes in the presence of the cationic rhodium complex generated *in situ* from $[Cp^*RhCl_2]_2$ and $AgSbF_6$. Cinnolin-3(2H)-ones **70** were obtained in moderate to good yields with modest regioselectivity in the case of unsymmetrical azos. The latter underwent C-H activation mostly on the electron-deficient phenyl ring. Interestingly, the method was proved to be efficient at a gram scale with the simple azobenzene **1**, affording under optimal conditions, the respective cinnolin-3(2H)-one in a reproducible 83 % isolated yield. Kim and colleagues also disclosed this procedure by employing acyclic α -diazo esters in order to isolate C8-alkylated cinnolin-3(2H)-ones.



Scheme 53. Rh-Catalyzed Synthesis of Cinnolin-3(2H)-ones

If the mechanism was thoroughly investigated, it remains unclear and the plausible catalytic route is depicted in Scheme 54. The catalytic cycle is initiated with the formation of five-membered rhodacycle **Q'** by C-H activation. Then the coordination of diazotized Meldrum's acid **71** to **Q'** led to the diazonium intermediate **T**. Two possible pathways are then proposed. In the first one, molecular nitrogen was liberated from **T**, providing Rh-carbene **U**. The latter then underwent migratory insertion to generate **N'**. Alternatively, the putative intermediate **T** could afford **N'** by intramolecular 1,2-aryl shift, affording alkylated product **72** and the regenerated catalyst after protonolysis. Subsequent elimination of acetone and esterification thanks to the solvent would take place to produce the desired product **70**.



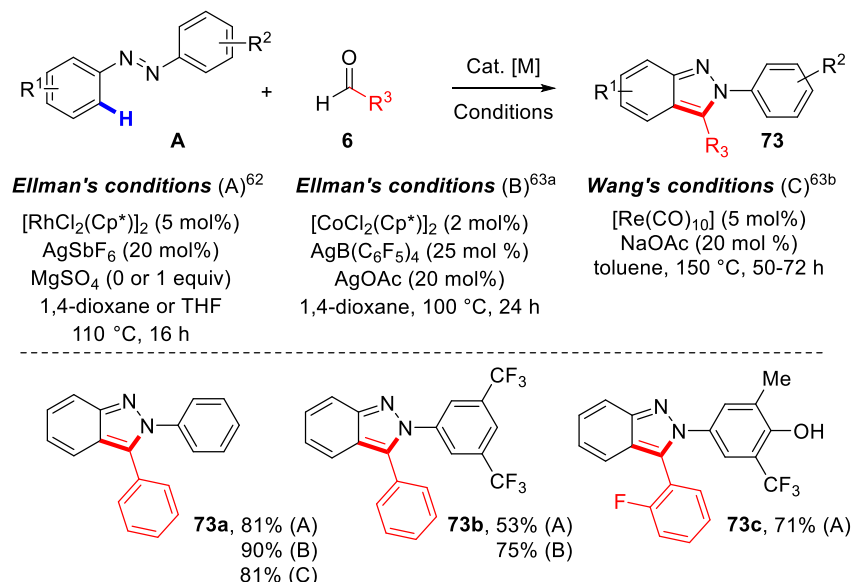
Scheme 54. Proposed Catalytic Cycle for Rh-Catalyzed Synthesis of Cinnolin-3(2*H*)-ones

4. 3. Indazoles

The indazole heterocycle is considered as a privileged pharmacophore which is largely widespread in natural products and pharmaceuticals.⁶¹ Consequently, chemist community has continuously deployed numerous efforts to develop new synthetic pathways of this biologically relevant skeleton. Noticeable progress in transition-metal catalysis has enabled the design of synthetic strategies more economical and oriented towards molecular and structural diversity.

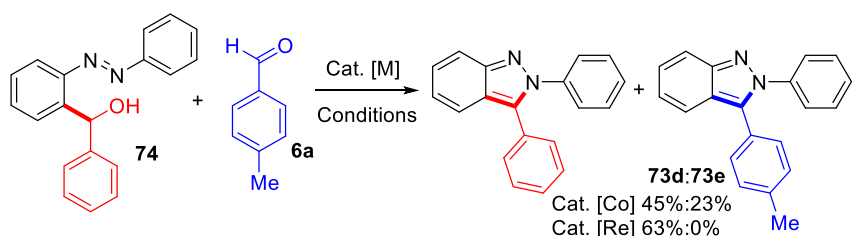
Knowing that the addition of C-H bonds to aldehydes is often reversible particularly with electron-deficient aldehydes, Ellman proposed on his first report a cyclative capture of the generated alcohol intermediate by an azo function to provide original indazoles **73**.⁶² After intensive screening, the robustness of the process was established for a combination of $[Cp^*RhCl_2]_2$ with $AgSbF_6$ in dioxane or THF as the most effective solvents (Scheme 55). During the investigation of substrates scope, the authors showed that the reaction regioselectivity can be controlled by playing on either electronic or

steric effects induced by azobenzene substituents: C-H functionalization occurred on the more electron-rich or the less hindered aromatic ring. Both electron-deficient and electron-rich aromatic aldehydes **6** as well as *ortho*-substituted ones furnished the indazole products **73**. In a general way, the cyclizing reaction is characterized by an excellent functional group compatibility. This report of indazoles synthesis was next remarkably expended by the same group *via* Co(III)-catalyzed reactions and by Wang *via* Re(I)-catalyzed reactions.⁶³



Scheme 55. Ru-, Co- and Re-Catalyzed Synthesis of Indazoles

The general mechanism is similar for the three catalytic systems: i) reversible metal insertion generates a five membered-metallacycle which undergoes the formation of a seven-membered-metallacycle through ii) the aldehyde coordination followed by iii) its migratory insertion; iv) protonation of the metallacycle liberates the alcohol and finally v) intramolecular nucleophilic substitution with concomitant dehydration followed by aromatization furnishes the expected indazole **73**. The major mechanistical difference lies in the reversibility of the aldehyde-insertion step: It was clearly established that, contrary to the case of Re(I)-based catalysis, the Rh(III)- or Co(III)-mediated insertion step is irreversible (Scheme 56). Indeed, when the upstream isolated alcohol **74** was subjected to 4-methyl benzaldehyde **6a** in the presence of Co(III)-catalyst, a mixture of crossover indazoles **73d** and **73e** was isolated whereas the Re(I)-catalysis only gave the alcohol-derived cyclized product **73d**.

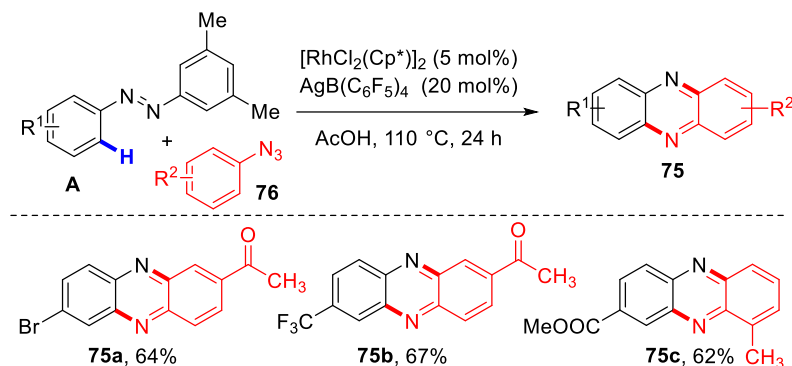


Scheme 56. Investigation of the Reversibility of Co(III)- or Re(I)-Catalyzed Aldehyde Insertion

In addition, the synthesis of diversely substituted indazoles according to a similar C-H activation/nucleophilic addition cascade has also been exemplified by using either acrylates⁵⁶ or glyoxals⁶⁴ as coupling partners.

4. 4. Phenazines

As part of its interest in functionalization of azo compounds, the Ellman's group established a very rapid access to phenazine derivatives **75** through a cascade process of Rh(III)-catalyzed amination followed by intramolecular electrophilic aromatic substitution and aromatization (Scheme 57).⁶⁵ This formal [3+3] annulation approach was carried out using diverse phenyl azides **76** as nitrogen source in the presence of the catalyst $[\text{Cp}^*\text{RhCl}_2]_2$ and the noncoordinating additive $\text{AgB}(\text{C}_6\text{F}_5)_4$. Glacial acetic acid used as solvent may also play a crucial role by facilitating the cyclization step and sequestering the released aniline by H-bonding or salt formation. During their investigations, the authors demonstrated that, with unsymmetrical azobenzenes, the reaction exclusively occurred on the unsubstituted ring. The scope of the reaction was evaluated with unsymmetrical bis-substituted derivatives. The outcomes indicated that a broad range of azides **76** are compatible, even *ortho*-substituted substrates as well as electron-deficient or -neutral derivatives were found to be good coupling partners. While azobenzenes bearing either electron-neutral or -attracting groups were found to be suitable for this transformation, electron-enriched azos afforded phenazines in lower yields.

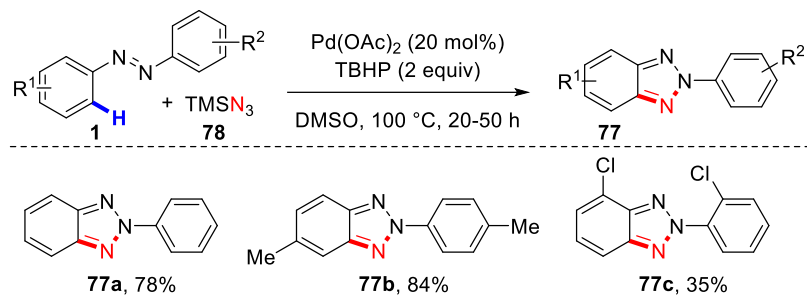


Scheme 57. Rh-Catalyzed Synthesis of Phenazines

4. 5. Benzotriazoles

In 2015, Patel and co-workers reported an interesting synthetic method of 2-aryl-2*H*-benzotriazoles **77** by direct C-H amination of azobenzenes using trimethylsilyl azide **78** as nitrogen source (Scheme 58).⁶⁶ The optimal coupling conditions were reached by combining the catalyst $\text{Pd}(\text{OAc})_2$ with two equivalents of TBHP as oxidant in DMSO at 100 °C under argon atmosphere. Starting from symmetrical azobenzenes substituted by weakly activating groups, a range of 2*H*-benzotriazoles **77** were smoothly prepared in moderate to good yields. Conversely, the presence of deactivating substituents on the aromatic ring inhibited the *ortho*-aminative heterocyclization providing the respective 2*H*-benzotriazoles **77** in moderate to low yields. In addition to these electronic effects, the reaction

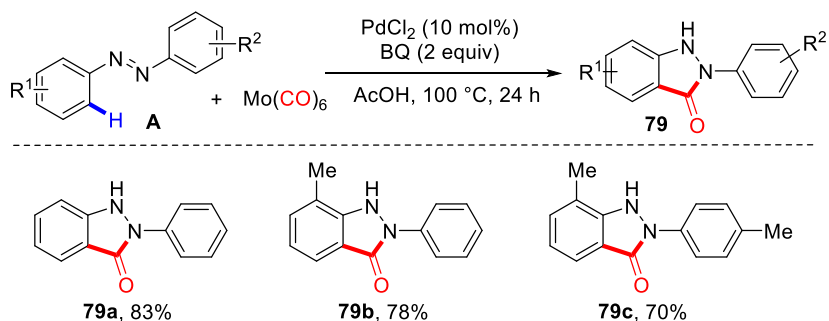
efficacy was also conditioned by steric factors and *meta* and *para* analogues were obtained in better yields than *ortho* ones. Noticeably, the use of dissymmetrical azoarenes induced the formation of a mixture of inseparable constitutional isomers. As usual, the *ortho*-aminative heterocyclization preferentially occurred at the electron-enriched aromatic ring. Mechanistic studies were in favor of the *in situ* generation of azide radical which reacts with the Pd(II)/azo complex to give the corresponding oxidized Pd(III)- and Pd(IV)-complexes. A reductive elimination furnished an *ortho*-azido azobenzene which cyclized through an intramolecular nucleophilic attack of the azo nitrogen onto the *ortho*-azide nitrogen accompanied by a concomitant expulsion of N₂.



Scheme 58. Pd-Catalyzed Synthesis of Benzotriazoles

4.6. Indazolones

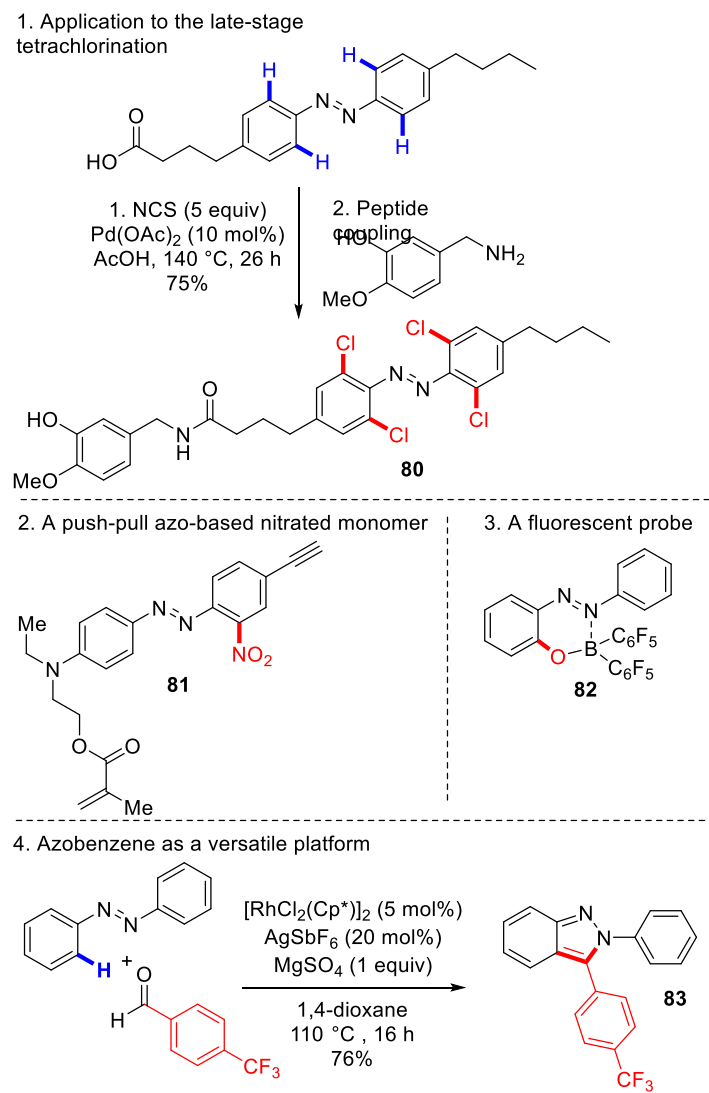
Driven by the wish to elaborate valuable scaffolds, Wu and coworkers investigated the Pd-catalyzed synthesis of indazolones **79** (Scheme 59).⁶⁷ They elegantly employed Mo(CO)₆ as a safe C1 building block, avoiding the use of toxic carbon monoxide. Several azo derivatives were found to be compatible with the procedure, leading to the targeted heterocycles **79** with high regioselectivity. We can notice that heterocyclic azo compounds were reluctant substrates. The authors assumed that the role of benzoquinone is dual, both acting as a Pd(II) ligand to prevent de generation of Pd black and as promoter for the generation of CO from Mo(CO)₆.



Scheme 59. Pd-Catalyzed Synthesis of Indazolones

5. APPLICATIONS OF ADVANCED AZO-CONTAINING SCAFFOLD

Beyond the achievement of all these catalytic reactions permitted the functionalization of azobenzenes, it is important to remind that the azo moiety is a powerful molecular switch. In this section, we would like to highlight the importance of introducing selected functional groups to get valuable azo-based molecular tools (Scheme 60). Among significant examples, redshifted azobenzene **80** was obtained by the Trauner's group *via* a simple late-stage tetra-chlorination followed by an amide bond formation.⁵² This compound enables optical control of the vanilloid receptor 1 (TRPV1). Introducing a nitro moiety in the *ortho* position of the arene is also an interesting process. If the 4-amino-4'-nitro push-pull structure is well-known, Barrett designed the monomer **81** by transferring the nitro group to an *ortho* position, making free the *para* position for "click chemistry".⁶⁸ The corresponding polymers undergo tailored macroscopic photo-induced motions with potential applications in optical nanopatterning. Traditionally obtained after a 3 or 4 steps sequence, azophenol **82** can be now synthesize *via* C-H hydroxylation followed by borylation.^{26,69} As previously described, the azo moiety can be also a versatile platform for the synthesis of relevant heterocycles. During its studies, the Ellman's group isolated several indazoles such as **83** bearing interesting fluorescence proprieties with high extinction coefficients and large Stokes shifts.⁶²



Scheme 60. Designed Azobenzenes Exhibiting Interesting Biophysical Properties

6. CONCLUSIONS AND PERSPECTIVES

Over the past few years, transition metal-catalyzed C-H reactions have emerged as a valuable tool for rapid functionalization of simple azobenzenes. Indeed, a wide range of coupling partners was efficiently engaged in these reactions, leading to original and new functionalized azo-arenes by creating C-C, C-S, C-P, C-O and C-N bonds among the most explored (Table 1).

Table 1. Principal Transition-Metal Catalyzed C_{sp^2} -H Functionalization of Azobenzenes

The diagram illustrates the general principle of transition-metal catalyzed C_{sp^2} -H functionalization. It shows an azobenzene molecule with substituents R^1 and R^2 reacting with a transition metal catalyst ($Pd(OAc)_2$) under $C-H$ bond functionalization conditions. The resulting product is an azobenzene derivative where one of the hydrogen atoms has been replaced by a functional group (FG), indicated by a green oval and red wavy line.

Table 1: Principal Transition-Metal Catalyzed C_{sp^2} -H Functionalization of Azobenzenes

Reaction	FG	Metal catalyst	Reference
Halogenation		$Pd(OAc)_2$	(10)
Acylation		$Pd(OAc)_2$	(14f)
Carbonylation		$Pd(OAc)_2$	(19)
Aminocarbonylation		$[Cp^*RhCl_2]_2$ $Re_2(CO)_{10}$ $[Cp^*Co(CO)I_2]$	(43) (49) (51)
Alkylation		$Pd(OAc)_2$ $[Cp^*RhCl_2]_2$ $\{RuCl_2(p\text{-cymene})\}_2$ $[Cp^*Co(CO)I_2]$	(16) (33) (46) (50)
Arylation		$Pd(OAc)_2$ $[Cp^*RhCl_2]_2$ $\{RuCl_2(p\text{-cymene})\}_2$	(18) (34) (45)
Cyanation		$[Cp^*RhCl_2]_2$	(36)
Acyloxylation		$Pd(OAc)_2$	(14b), (23)
Alkoxylation		$Pd(OAc)_2$	(24)
Aydroxylation		$Pd(OAc)_2$	(26)
Nitration		$Pd(CH_3CN)_2Cl_2$	(28b)
Sulfamidation and Amination		$[Cp^*RhCl_2]_2$	(40), (41)
Phosphonation		$Pd(OAc)_2$	(29)
Sulfonylation		$Pd(OAc)_2$	(30a)

Despite recent progresses in this area, several issues remain to be addressed in terms of selectivity, efficiency, and diversity in order to make these methods more useful to prepare advanced building blocks with dedicated applications. Among these challenges, we can cite: (a) one-pot multi-functionalization as underlined by the undersizing of the dedicated paragraph, (b) installation of fluorine atoms, (c) the use of first-row transition metals and (d) development of greener reaction conditions. Furthermore, identification of key parameters influencing the site selectivity combined with predictive approaches should open new advances in late stage functionalization of complex

azobenzenes bearing sensitive chemical moieties. The development of new catalytic systems in future studies will undoubtedly offer new opportunities for finely tuning photochromic properties of original azobenzenes.

AUTHOR INFORMATION

Corresponding Author

* E-mail: delphine.joseph@u-psud.fr

ACKNOWLEDGMENT

The Agence Nationale de la Recherche (ANR-13-BSV8-0020), the Université Paris-Sud, the French Ministry of Superior Education and Research, the CNRS, and the LabEx LERMIT are gratefully acknowledged for financial support.

ABBREVIATIONS

acac, acetylacetone; BQ, benzoquinone; COD, 1,5-cyclooctadiene; Cp*, pentamethylcyclopentadienyl; DEAD, diethyl azocarboxylate; HFIP, hexafluoroisopropanol ; KIE, kinetic isotope exchange; LG, leaving group; NHPI, *N*-hydroxyphthalimide; PIFA, [bis(trifluoroacetoxy)iodo]benzene; PIDA, [(diacetoxy)iodo]benzene; PINO, phthalimide *N*-oxyl radical; SDS, sodium dodecylsulfate; TBAB, tetrabutylammonium bromide; TBHP, tert-butyl hydroperoxide; TEMPO, 2,2,6,6-tetramethyl-1-piperidinyloxy.

REFERENCES

- (1) In *Molecular Switches*, 2nd ed.; Feringa, B. L., Browne, W. R., Eds; Wiley-VCH, Weinheim-VCH Verlag GmbH&Co: Weinheim, Germany, 2011.
- (2) Merino, E.; Ribagorda, M. *Beilstein J. Org. Chem.* **2012**, *8*, 1071-1090.
- (3) (a) Mart, R. J.; Allemann, R. K. *Chem. Commun.* **2016**, *52*, 12262-12277. (b) Broichhagen, J.; Frank, J. A.; Trauner, D. *Acc. Chem. Res.* **2015**, *48*, 1947-1960. (c) Bandara, H. M.; Burdette, S. C. *Chem. Soc. Rev.* **2012**, *41*, 1809-1825. (d) Beharry, A. A.; Woolley, G. A. *Chem. Soc. Rev.* **2011**, *40*, 4422-4437.
- (4) Merino, E. *Chem. Soc. Rev.* **2011**, *40*, 3835-3853.
- (5) (a) Hummel, J. R.; Boerth, J. A.; Ellman, J. A. *Chem. Rev.* **2017**, *117*, 9163-9227. (b) Yang, Y.; Lan, J.; You, J. *Chem. Rev.* **2017**, *117*, 8787-8863. (c) He, J.; Wasa, M.; Chan, K. S. L.; Shao, Q.; Yu, J.-Q. *Chem. Rev.* **2017**, *117*, 8754-8786. (d) Santoro, S.; Ferlin, F.; Luciani, L.; Ackermann, L.; Vaccaro, L. *Green Chem.* **2017**, *19*, 1601-1612. (e) Ping, Y.; Ding, Q.; Peng, Y. *ACS Catal.* **2016**, *6*, 5989-6005. (f) Gensch, T.; Hopkinson, M. N.; Glorius, F.; Wencel-Delord, J. *Chem. Soc. Rev.* **2016**, *45*, 2900-2936. (g) Jiao, J.; Murakami, K.; Itami, K. *ACS Catal.* **2016**, *6*, 610-633. (h) Daugulis, O.; Roane, J.; Tran, L. *Acc. Chem. Res.* **2015**, *48*, 1053-1064.
- (6) Kleiman, J. P.; Dubeck, M. *J. Am. Chem. Soc.* **1963**, *85*, 1544-1545.
- (7) Cope, A. C.; Siekman, R. W. *J. Am. Chem. Soc.* **1965**, *87*, 3272-3273.
- (8) (a) Fahey, D. R. *J. Organomet. Chem.* **1971**, *27*, 283-292; (b) Fahey, D. R. *J. Chem. Soc. D.* **1970**, 417a-417a.
- (9) Kalyani, D.; Dick, A. R.; Anani, W. Q.; Sanford, M. S. *Tetrahedron* **2006**, *62*, 11483-11498.
- (10) Ma, X.-T.; Tian, S.-K. *Adv. Synth. Catal.* **2013**, *355*, 337-340.
- (11) Li, H.; Li, P.; Wang, L. *Org. Lett.* **2013**, *15*, 620-623.
- (12) Xiao, F.; Chen, S.; Huang, H.; Deng, G.-J. *Eur. J. Org. Chem.* **2015**, *2015*, 7919-7925.
- (13) Liang, Y. F.; Wang, X.; Tang, C.; Shen, T.; Liu, J.; Jiao, N. *Chem. Commun.* **2016**, *52*, 1416-1419.
- (14) (a) Wang, L.; Wu, S.; Hong, G.; Aruma, A.; Zhu, X. *Synthesis* **2016**, *48*, 1147-1158. (b) Qian, C.; Lin, D.; Deng, Y.; Zhang, X. Q.; Jiang, H.; Miao, G.; Tang, X.; Zeng, W. *Org. Biomol. Chem.* **2014**, *12*, 5866-5875. (c) Song, H.; Chen, D.; Pi, C.; Cui, X.; Wu, Y. *J. Org. Chem.* **2014**, *79*, 2955-2962. (d) Li, H.; Li, P.; Tan, H.; Wang, L. *Chem.-Eur. J.* **2013**, *19*, 14432-14436. (e) Li, Z. Y.; Li, D. D.; Wang, G. W. *J. Org. Chem.* **2013**, *78*, 10414-10420. (f) Xiong, F.; Qian, C.; Lin, D.; Zeng, W.; Lu, X. *Org. Lett.* **2013**, *15*, 5444-5447.
- (15) Xu, N.; Li, P.; Xie, Z.; Wang, L. *Chem.-Eur. J.* **2016**, *22*, 2236-2242.
- (16) Premi, C.; Dixit, A.; Jain, N. *Org. Lett.* **2015**, *17*, 2598-2601.
- (17) Qian, C.; Lin, D.; Deng, Y.; Zhang, X.-Q.; Jiang, H.; Miao, G.; Tang, X.; Zeng, W. *Org. Biomol. Chem.* **2014**, *12*, 5866-5875.
- (18) Li, M.; Ye, Y. *ChemCatChem* **2015**, *7*, 4137-4142.
- (19) Xu, N.; Li, D.; Zhang, Y.; Wang, L. *Org. Biomol. Chem.* **2015**, *13*, 9083-9092.
- (20) Wang, Z.; Li, Y.; Zhu, F.; Wu, X.-F. *Adv. Synth. Catal.* **2016**, *358*, 2855-2859.

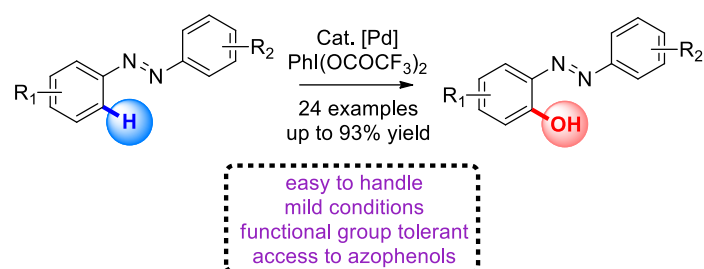
- (21)Dick, A. R.; Hull, K. L.; Sanford, M. S. *J. Am. Chem. Soc.* **2004**, *126*, 2300-2301.
- (22)Tato, F.; García-Domínguez, A.; Cárdenas, D. *J. Organometallics* **2013**, *32*, 7487-7494.
- (23)Fu, X.; Wei, Z.; Xia, C.; Shen, C.; Xu, J.; Yang, Y.; Wang, K.; Zang, P. *Catal. Lett.* **2017**, *147*, 400-406.
- (24)Yin, Z.; Jiang, X.; Sun, P. *J. Org. Chem.* **2013**, *78*, 10002-10007.
- (25)Seth, K.; Nautiyal, M.; Purohit, P.; Parikh, N.; Chakraborti, A. K. *Chem. Commun.* **2015**, *51*, 191-194.
- (26)Nguyen, T. H. L.; Gigant, N.; Delarue-Cochin, S.; Joseph, D. *J. Org. Chem.* **2016**, *81*, 1850-1857.
- (27) (a) Das, P.; Saha, D.; Saha, D.; Guin, J. *ACS Catal.* **2016**, *6*, 6050-6054. (b) Liang, Y.-F.; Wang, X.; Yuan, Y.; Liang, Y.; Li, X.; Jiao, N. *ACS Catal.* **2015**, *5*, 6148-6152.
- (28)(a) Dong, J.; Jin, B.; Sun, P. *Org. Lett.* **2014**, *16*, 4540-4542. (b) Majhi, B.; Kundu, D.; Ahammed, S.; Ranu, B. C. *Chem.-Eur. J.* **2014**, *20*, 9862-9866. (c) Liang, Y.-F.; Li, X.; Wang, X.; Yan, Y.; Feng, P.; Jiao, N. *ACS. Catal.* **2015**, *5*, 1956-1963.
- (29)Hong, G.; Mao, D.; Wu, S.; Wang, L. *J. Org. Chem.* **2014**, *79*, 10629-10635.
- (30) (a) Zhang, D.; Cui, X.; Zhang, Q.; Wu, Y. *J. Org. Chem.* **2015**, *80*, 1517-1522. (b) Xia, C.; Wei, Z.; Shen, C.; Xu, J.; Yang, Y.; Su, W.; Zhang, P. *RSC Adv.* **2015**, *5*, 52588-52594.
- (31)(a) Wangweerawong, A.; Hummel, J. R.; Bergman, R. G.; Ellman, J. A. *J. Org. Chem.* **2016**, *81*, 1547-1557. (b) Wangweerawong, A.; Bergman, R. G.; Ellman, J. A. *J. Am. Chem. Soc.* **2014**, *136*, 8520-8523.
- (32)(a) Ferreira, F.; Botuha, C.; Chemla, F.; Perez-Luna, A. *Chem. Soc. Rev.* **2009**, *38*, 1162-1186. (b) Morton, D.; Stockman, R. A. *Tetrahedron* **2006**, *62*, 8869-8905.
- (33)Deng, H.; Li, H.; Wang, L. *Org. Lett.* **2015**, *17*, 2450-2453.
- (34)Deng, H.; Li, H.; Wang, L. *Org. Lett.* **2016**, *18*, 3110-3113.
- (35)Sharma, S.; Han, S. H.; Han, S.; Ji, W.; Oh, J.; Lee, S. Y.; Oh, J. S.; Jung, Y. H.; Kim, I. S. *Org. Lett.* **2015**, *17*, 2852-2855.
- (36)Han, J.; Pan, C.; Jia, X.; Zhu, C. *Org. Biomol. Chem.* **2014**, *12*, 8603-8606.
- (37)Xie, F.; Qi, Z.; Yu, S.; Li, X. *J. Am. Chem. Soc.* **2014**, *136*, 4780-4787.
- (38)(a) Grohmann, C.; Wang, H.; Glorius, F. *Org. Lett.* **2012**, *14*, 656-659. (b) Ng, K.-H.; Zhou, Z.; Yu, W-Y. *Org. Lett.* **2012**, *14*, 272-275.
- (39)Yu, S.; Wan, B.; Li, X. *Org. Lett.* **2015**, *17*, 58-61.
- (40)(a) Ryu, T.; Min, J.; Choi, W.; Jeon, W. H.; Lee, P. H. *Org. Lett.* **2014**, *16*, 2810-2813. (b) Jia, X.; Han, J. *J. Org. Chem.* **2014**, *79*, 4180-4185. (c) Wang, H.; Yu, Y.; Hong, X.; Tan, Q.; Xu, B. *J. Org. Chem.* **2014**, *79*, 3279-3288.
- (41)Jeon, B.; Yeon, U.; Son, J. Y.; Lee, P. H. *Org. Lett.* **2016**, *18*, 4610-4613.
- (42)Mishra, N. K.; Oh, Y.; Jeon, M.; Han, S.; Sharma, S.; Han, S. H.; Um, S. H.; Kim, I. S. *Eur. J. Org. Chem.* **2016**, 4976-4980.
- (43)Han, S.; Mishra, N. K.; Sharma, S.; Park, J.; Choi, M.; Lee, S. Y.; Oh, J. S.; Jung, Y. H.; Kim, I. S. *J. Org. Chem.* **2015**, *80*, 8026-8035.
- (44)Kakiuchi, F.; Matsumoto, M.; Tsuchiya, K.; Igi, K.; Hayamizu, T.; Chatani, N.; Murai, S. *J. Organomet. Chem.* **2003**, *686*, 134-144.
- (45)Hubrich, J.; Himmeler, T.; Rodefeld, L.; Ackermann, L. *ACS Catal.* **2015**, *5*, 4089-4093.

- (46) Li, G.; Ma, X.; Jia, C.; Han, Q.; Wang, Y.; Wang, J.; Yu, L.; Yang, S. *Chem. Commun.* **2017**, *53*, 1261-1264.
- (47) Li, G.; Lv, X.; Guo, K.; Wang, Y.; Yang, S.; Yu, L.; Yu, Y.; Wang, J. *Org. Chem. Front.* **2017**, *4*, 1145-1148.
- (48) Wakaki, T.; Kanai, M.; Kuninobu, Y. *Org. Lett.* **2015**, *17*, 1758-1761.
- (49) Geng, X.; Wang, C. *Org. Biomol. Chem.* **2015**, *13*, 7619-7623.
- (50) Murinaj, N.; Prabhu, K. R. *J. Org. Chem.* **2017**, *82*, 6913-6921.
- (51) Borah, G.; Borah, P.; Patel, P. *Org. Biomol. Chem.* **2017**, *15*, 3854-3859.
- (52) Konrad, D. B.; Frank, J. A.; Trauner, D. *Chem.-Eur. J.* **2016**, *22*, 4364-4368.
- (53) Miyamura, S.; Tsurugi, H.; Satoh, T.; Miura, M. *J. Organomet. Chem.* **2008**, *693*, 2438-2442.
- (54) Taber, D. F.; Tirunahari, P. K. *Tetrahedron* **2011**, *67*, 7195-7210.
- (55) Aulwurm, U. R.; Melchinger, J. U.; Kisch, H. *Organometallics* **1995**, *14*, 3385-3395.
- (56) Cai, S.; Lin, S.; Yi, X.; Xi, C. *J. Org. Chem.* **2017**, *82*, 512-520.
- (57) Lewgowd, W.; Stanczak, A. *Arch. Pharm. Chem. Life Sci.* **2007**, *340*, 65-80.
- (58)(a) Muralirajan, K.; Cheng, C. H. *Chem.-Eur. J.* **2013**, *19*, 6198-6202. (b) Zhao, D.; Wu, Q.; Huang, X.; Song, F.; Lv, T.; You, J. *Chem.-Eur. J.* **2013**, *19*, 6239-6244.
- (59) Prakash, S.; Muralirajan, K.; Cheng, C. H. *Angew. Chem., Int. Ed.* **2016**, *55*, 1844-1848.
- (60) Son, J. Y.; Kim, S.; Jeon, W. H.; Lee, P. H. *Org. Lett.* **2015**, *17*, 2518-2521.
- (61) Gaikwad, D. D.; Chapolikar, A. D.; Devkate, C. G.; Warad, K. D.; Tayade, A. P.; Pawar, R. P.; Domb, A. *J. Eur. J. Med. Chem.* **2015**, *90*, 707-731.
- (62) Lian, Y.; Bergman, R. G.; Lavis, L. D.; Ellman, J. A. *J. Am. Chem. Soc.* **2013**, *135*, 7122-7125.
- (63)(a) Hummel, J. R.; Ellman, J. A. *J. Am. Chem. Soc.* **2015**, *137*, 490-498. (b) Geng, X.; Wang, C. *Org. Lett.* **2015**, *17*, 2434-2437.
- (64) Jeong, T.; Han, S. H.; Han, S.; Sharma, S.; Park, J.; Lee, J. S.; Kwak, J. H.; Jung, Y. H.; Kim, I. S. *Org. Lett.* **2016**, *18*, 232-235.
- (65) Lian, Y.; Hummel, J. R.; Bergman, R. G.; Ellman, J. A. *J. Am. Chem. Soc.* **2013**, *135*, 12548-12551.
- (66) Khatun, N.; Modi, A.; Ali, W.; Patel, B. K. *J. Org. Chem.* **2015**, *80*, 9662-9670.
- (67) Wang, Z.; Yin, Z.; Zhu, F.; Li, Y.; Wu, X.-F. *ChemCatChem* **2017**, *9*, 3637-3640.
- (68) Goulet-Hanssens, A.; Corkery, T. C.; Priimagi, A.; Barrett, C. J. *J. Mater. Chem. C.* **2014**, *2*, 7439-7696.
- (69) Yoshino, J.; Furuta, A.; Kambe, T.; Itoi, H.; Kano, N.; Kawashima, T.; Ito, Y.; Asashima, M. *Chem. Eur. J.* **2010**, *16*, 5026-5035.

Palladium-Catalyzed Direct Oxidative Synthesis of Unsymmetrical Azophenols

Thi Hong Long Nguyen,[†] Nicolas Gigant,[‡] Sandrine Delarue-Cochin, and Delphine Joseph*

Equipe de Chimie des Substances Naturelles, UMR BioCIS, CNRS, Univ. Paris-Sud, Université Paris-Saclay, 5 rue Jean-Baptiste Clément, F-92296 Châtenay-Malabry, France.



ABSTRACT: A straightforward palladium-catalyzed oxidative hydroxylation of azobenzenes is reported. The developed methodology tolerates various functional groups and allows the synthesis of diverse unsymmetrical azophenols under mild conditions in good to excellent yields. A complementary procedure was also investigated by *in situ* generation of PIFA. This study represents the first general method for the synthesis of *o*-hydroxy azobenzenes starting from simple azoarenes.

Aromatic azo compounds are important structures and find application in many fields due to their particular properties based on light-triggered switches.¹ They can be mainly involved as protein probes,² organic dyes,³ chemosensors,⁴ smart surface materials,⁵ polymers⁶ and molecular machines.⁷ Given this broad utility, azobenzene synthetic methods are keenly pursued.⁸ However, despite all these new methodologies for their preparation, no efficient synthesis of azophenol frameworks has been developed. As depicted in Figure 1, these privileged structures are very useful. For example, azophenol **A** has been approved as a food colorant in US, azophenol **B** has been used as coupling agent for peptide cyclization⁹ whereas the fluorescence of scaffold **C** has been recently explored.¹⁰ In addition, knowing that the incorporation of a hydroxyl group in compounds may significantly affect their original physical and chemical properties,¹¹ a general, mild and direct catalytic route to introduce this versatile functional group would be highly attractive.

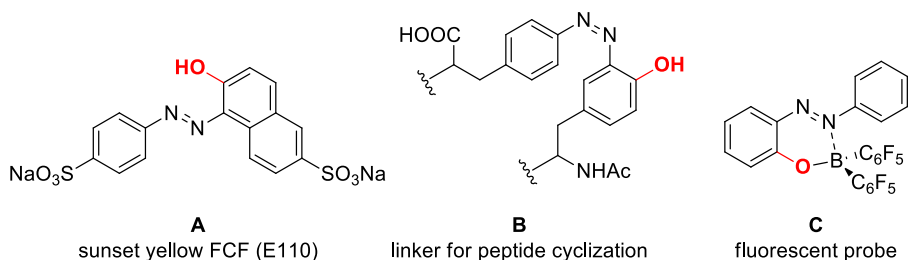
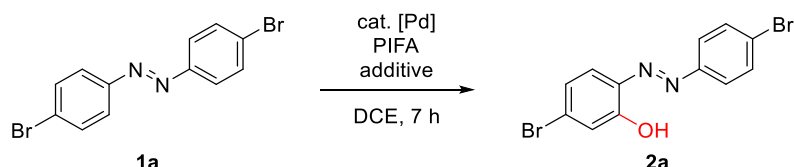


Figure 1. Representative *o*-Azophenol Derivatives

C-H bond transformations have attracted widespread attention as powerful and ideal reactions.¹² Indeed, the ability to directly oxidize carbon hydrogen bonds into carbon heteroatom bonds is highly important for the late-stage functionalization of complex molecules or to rapidly increase the molecular diversity.¹³ Over the past decade, there has been significant progress in the development metal-catalyzed C-H oxidation, and recently, several ruthenium- or palladium-catalyzed protocols have been established for hydroxylation in the presence of strong or weak coordinating directing groups.¹⁴ In addition, *ortho*-functionalizations of azobenzenes have been investigated toward various coupling partners.¹⁵ During our study, Chakraborti and co-workers have developed a practical palladium-catalyzed aryl hydroxylation by employing dioxane as a source of hydroxyl radicals.¹⁶ If the protocol was mainly very efficient with a range of benzoxazoles and benzothiazoles as directing groups, this latter was limited and unselective starting from simple azobenzenes due to the generation of the corresponding azoxybenzenes. Therefore, the need for methodology that can address this drawback remains a challenge. Inspired by a seminal work reported by Sanford and co-workers¹⁷ and other previous studies,¹⁸ we reasoned that hypervalent iodine reagents could be highly attractive for the synthesis of *ortho*-azophenols starting from simple azobenzenes. We focused particular attention in developing an operationally simple process involving mild reaction conditions. In this way, we shaped an easy and general route for the oxidative preparation of azophenol compounds. This synthetic method is far more direct and efficient than the rare and narrow previously reported procedures which are mainly based on the Wallach rearrangement.^{10,16,19}

The present study was initiated starting from the valuable dibromo azobenzene **1a**, which will allow chemical modulations for the introduction of designed molecular anchors.²⁰ First, **1a** was treated with 5 mol % of Pd(OAc)₂ and 1.5 equiv of oxidant, the [bis(trifluoroacetoxy)iodo]benzene (PIFA), in 1,2-dichloroethane (DCE) at 70 °C under air atmosphere (Table 1, entry 1). Fruitfully, the targeted azophenol **2a** was isolated in an encouraging 41% yield. A screening of the PIFA loading increases the yield of the reaction up to 67% by using 2 equiv of the hypervalent iodine reagent (Table 1, entries 2 and 3). The utilization of K₂S₂O₈ or oxone as alternative oxidant did not promote the reaction and the starting material **1a** was recovered. Importantly, a control experiment in the absence of metal yielded no product and resulted in the recovery of the starting material. Further optimization indicated that 5 mol % of Pd(OAc)₂ is the best loading to fully convert **1a** without significant degradation (Table 1, entries 4–7 vs 2). Surprisingly, although pyridine is known to increase the rate of the C-H oxygenation of arenes,²¹ this nitrogen-containing ligand totally inhibited the reaction (Table 1, entry 8). Moreover, considering the importance of influencing the electrophilicity of the palladium(II) catalyst,²² the

oxidative reaction was carried out in the presence of 1 equiv of AcOH or TFA, but none of them enhanced the yield of **2a** (Table 1, entries 9–11). Increasing or decreasing the temperature of the reaction did not lead to any additional improvements in the yield (Table 1, entries 12 and 13). Besides, the nature of solvent is also a critical factor in this reaction type. Although CH₃CN, dioxane or CH₃NO₂ have been commonly employed as efficient solvents in Pd^{II}/Pd^{IV} catalyzed C–H oxidation, they were absolutely not suitable in our case. Indeed, due to the lack of solubility of **1a** in CH₃CN and CH₃NO₂, and the absence of conversion in the presence of dioxane, the use of DCE was considered of prime importance to reach the reaction.



entry	Cat. [Pd] (mol%)	PIFA (equiv)	additive (mol%)	T (°C)	yield ^b (%)
1	Pd(OAc) ₂ (5)	1.5	-	70	41
2	Pd(OAc) ₂ (5)	2	-	70	67
3	Pd(OAc) ₂ (5)	2.5	-	70	56
4	Pd(OAc) ₂ (2.5)	2	-	70	46
5	Pd(OAc) ₂ (7.5)	2	-	70	39
6	PdCl ₂ (CH ₃ CN) ₂ (5)	2	-	70	50
7	Pd(TFA) ₂ (5)	2	-	70	45
8	Pd(OAc) ₂ (5)	2	pyridine (5)	70	0
9	Pd(OAc) ₂ (5)	2	AcOH (100)	70	8
10	Pd(OAc) ₂ (5)	2	TFA (100)	70	46
11	Pd(TFA) ₂ (5)	2	TFA (100)	70	56
12	Pd(OAc) ₂ (5)	2	-	60	49
13	Pd(OAc) ₂ (5)	2	-	80	41

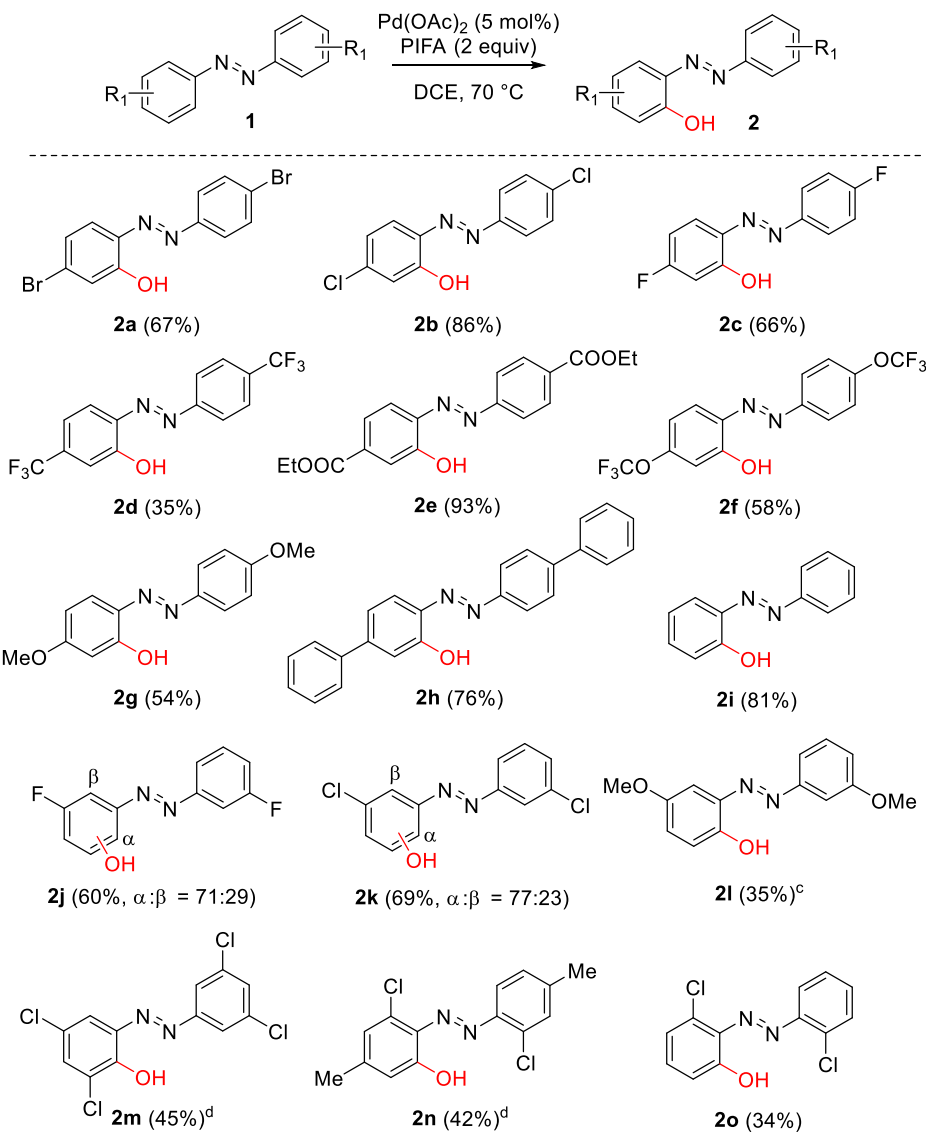
^aReaction conditions: **2a** (0.20 mmol) under the appropriate reaction conditions (*c* = 0.2 mol·L⁻¹).

^bIsolated yield.

Table 1. Optimization of the Reaction Conditions^a

We next explored the scope and limitations of this system under the optimized reaction conditions (Scheme 1). Gratifyingly, the reaction is tolerant toward a variety of *p*-substituted azobenzenes and showed good compatibility with a wide range of valuable functional groups such as halogen atoms

(2a-2c). Electron-withdrawing groups on the aromatic ring had different effects on the yield of the reaction **(2d-2f)**. Notably, the ester functionality proved to be the best substrate, leading scaffold **2e** in an excellent 93% yield. Substrates bearing a *p*-methoxy and a *p*-phenyl moieties underwent hydroxylation to give the corresponding unsymmetrical aromatic azo compounds **2g** and **2h** in good yields. Alternatively, the optimized conditions could be applied to a simple benzene ring substituent, providing the desired product **2i**. We next examined the reactivity of various *m*-monosubstituted azobenzenes. Starting from halo-substituted scaffolds **1j** and **1k**, the reaction mainly occurred at the sterically less hindered position and two regioisomers were formed with a moderate selectivity (**2j** and **2k**). At the opposite, it is important to highlight that the selectivity of the reaction was complete in the presence of the symmetrical *m*-methoxy azobenzene **1l**, only leading **2l**. In the example, 1.2 equiv of PIFA were employed even if roughly 20% of **1l** was recovered. Degradation was unexpected observed following our previous conditions or by attempting sequential additions of PIFA. We speculated that the low yield could result from the potential formation of cation radicals but this possibility was overcome by using degassed DCE under argon in dark conditions (30%). The versatility of the reaction was further demonstrated by the fact that azobenzenes equipped with sterically hindered atoms are also compatible (**2m-2o**). Although a slight increase of the catalyst loading was sometimes necessary for obtaining good conversions, **2m**, **2n** and **2o** were isolated in moderate yields. However, it's worth mentioning that the synthesis of densely substituted azoarenes is usually not an easy task.

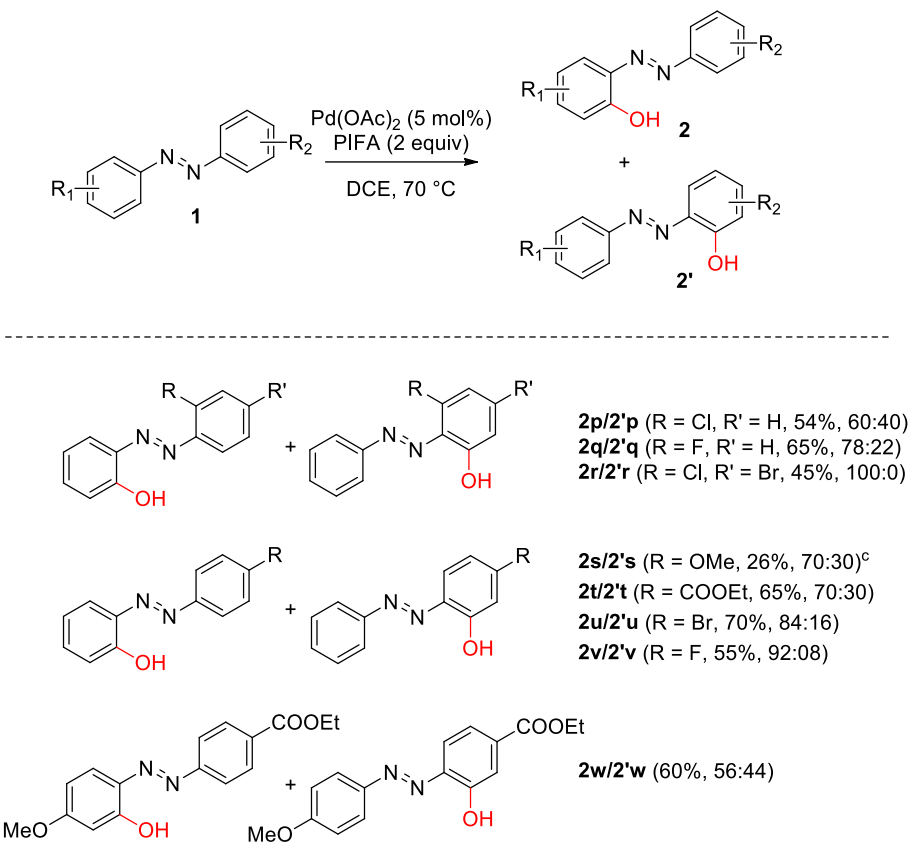


^aUnless otherwise noted, reaction conditions: **1** (1 equiv), PIFA (2 equiv), Pd(OAc)₂ (5 mol%) in DCE ($c = 0.2 \text{ mol.L}^{-1}$) at 70 °C. ^bIsolated yield. ^cPIFA (1.2 equiv). ^dPd(OAc)₂ (7.5 mol%).

Scheme 1. Substrate Scope of Symmetrical Azobenzenes^{a,b}

These results encouraged us to further survey the scope of this oxidative reaction with respect to unsymmetrical azo compounds (Scheme 2). When the reaction was carried out with *o*-monosubstituted unsymmetrical azos **1p** and **1q** bearing soft deactivating groups, two regiosomers were isolated with satisfying selectivities up to 78:22 (**2p** and **2q**). Each time, the aromatic ring was preferentially hydroxylated at the *ortho* position of the unsubstituted ring. Gratifyingly, starting from *o,p*-disubstituted unsymmetrical azo **1r**, the desired azophenol **2r** was formed as a single regiosomer. Other simple *p*-monosubstituted substrates such as **1s**, **1t** and **1u** reacted efficiently with moderate to good selectivities, furnishing products **2s**, **2t** and **2u**, respectively. Interestingly, we were pleased to find that the site selectivity of the hydroxylation was increased starting from fluorinated scaffold **1v**, leading **2v** in an excellent 92:08 ratio of regiosomers. To gauge the electronic properties effect of the substituent, the reaction was performed with **1w**. A low selectivity was observed, highlighting

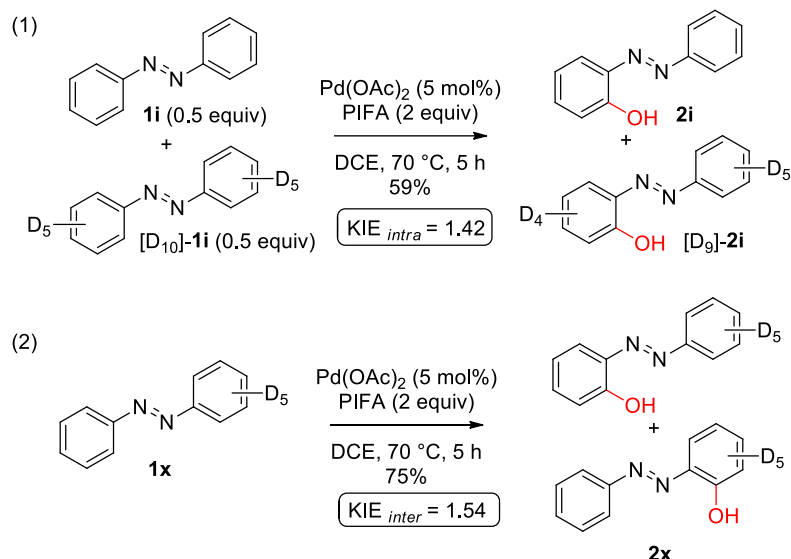
that the site selectivity of this example is mainly controlled by the steric hindrance of the starting material.



Unless otherwise noted, reaction conditions: **1** (1 equiv), PIFA (2 equiv), Pd(OAc)_2 (5 mol%) in DCE ($c = 0.2 \text{ mol.L}^{-1}$) at 70°C . ^bIsolated yield. ^cPIFA (1.2 equiv).

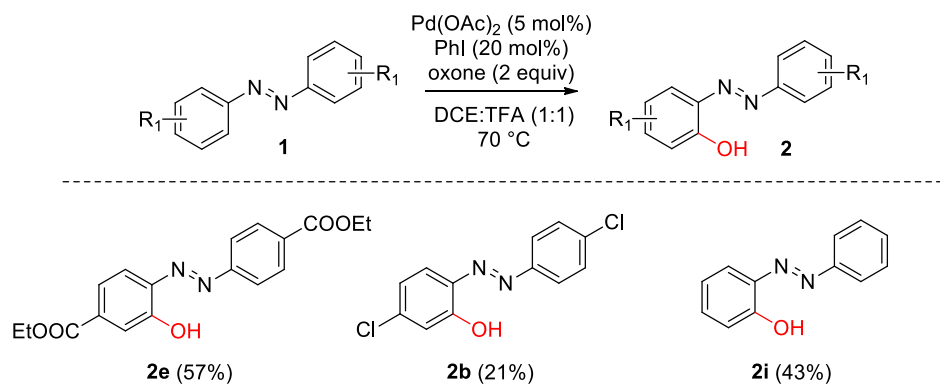
Scheme 2. Substrate Scope of Unsymmetrical Azobenzenes^{a,b}

Finally, to obtain mechanistic information, we evaluated the intramolecular isotope effect starting from an equimolar mixture of **1i** and $[\text{D}_{10}]$ -**1i** and moderate primary isotope effect ($k_{\text{H}}/k_{\text{D}} = 1.42$) was measured (Scheme 3, eq 1). A similar magnitude to the product ratio was confirmed with the intermolecular isotope effect starting from **1x** ($k_{\text{H}}/k_{\text{D}} = 1.54$) (Scheme 3, eq 2), indicating that the aromatic C-H bond cleavage by Pd may be involved in the rate determining step of the reaction.



Scheme 3. Evaluation of Deuterium Isotope Effect

Aware of the fact that PIFA produces equimolar amounts of iodobenzene as byproducts, we decided to explore the feasibility of a catalytic version of the hydroxylation of azobenzenes by *in situ* generation of PIFA (Scheme 4). A survey of various reaction conditions revealed after optimization that **2e** can be satisfactorily isolated by using 20 mol% of iodobenzene with oxone (2 equiv) in the presence of TFA as the cosolvent.²³ Following this modified oxidative procedure, azophenols **2b** and **2i** were then also obtained in moderate yields.

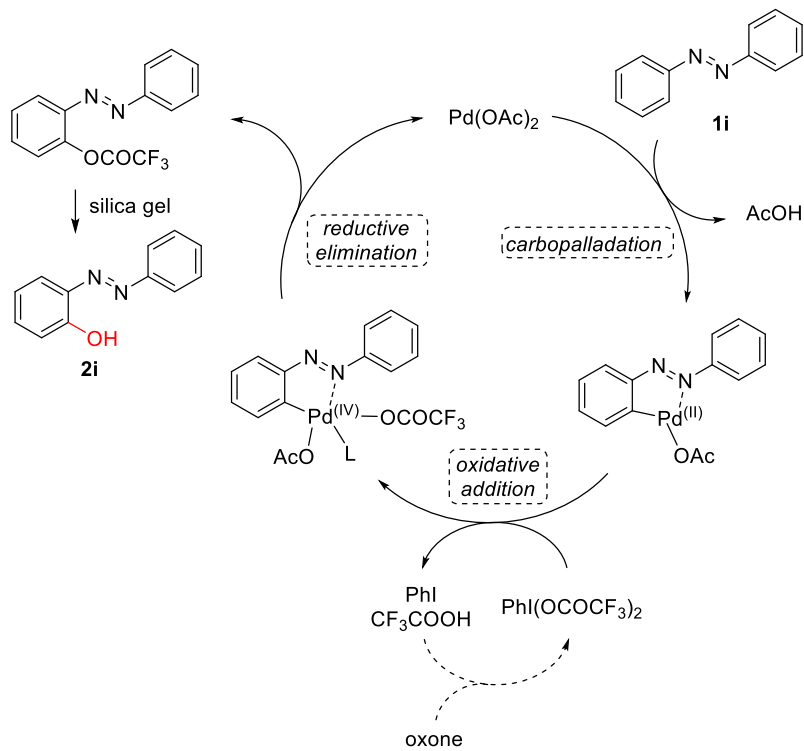


^aUnless otherwise noted, reaction conditions: **1** (1 equiv), PhI (20 mol%), oxone (2 equiv), Pd(OAc)₂ (5 mol%) in DCE ($c = 0.2 \text{ mol.L}^{-1}$) at 70 °C. ^bIsolated yield.

Scheme 4. Synthesis of azophenols by *in situ* generation of PIFA^{a,b}

The proposed catalytic cycle is depicted in Scheme 5 on the basis of the above observations and the previous literature.^{14,15} C-H activation of the arene substrate gives a five-membered palladacycle intermediate with concomitant loss of AcOH. Oxidative addition of PIFA to this arylpalladium(II) intermediate would then generate a Pd(IV) species, releasing iodobenzene and trifluoacetic acid.

Although a reaction mechanism involving a Pd^{II}/Pd^{IV} process for this system is proposed, an alternative Pd^{II}/Pd^{III} catalytic cycle through a bimetallic Pd(III) complex could be also envisaged.²⁴ Subsequent reductive elimination leads the targeted trifluoro-acylated azophenol with concomitant regeneration of the active catalyst. The final product is then obtained after simple hydrolysis on silica gel. In the iodobenzene catalytic version of the reaction, the PIFA is *in situ* generated in the presence of iodobenzene and Oxone in trifluoroacetic acid.



Scheme 5. Plausible Mechanism of the Reaction

In summary, we have developed a practical and efficient method for the direct hydroxylation of azobenzenes under mild conditions. The reaction showed very good functional groups compatibility, leading to a wide range of new and original azophenols in satisfying to high yields. In addition, our procedure was extended to the *in situ* generation of PIFA in the presence of catalytic amount of iodobenzene. Ongoing efforts are directed toward the application of this method to the synthesis of azophenols with potential photoswitchable and fluorescence proprieties.

REFERENCES

- (1) (a) Broichhagen, J.; Frank, J. A.; Trauner, D. *Acc. Chem. Res.* **2015**, *48*, 1947-1960. (b) Bandara, H. M. D.; Burdette, S. C. *Chem. Soc. Rev.* **2012**, *41*, 1809-1825. (c) Samanta, S.; Babalhavaeji, A.; Dong, M.-X.; Wooley, G. A. *Angew. Chem. Int. Ed.* **2013**, *52*, 14127-14130.
- (2) Among significant examples, see: (a) Lim, S.-Y.; Hong, K.-H.; Kim, D. I.; Kwon, H.; Kim, H.-J. *J. Am. Chem. Soc.* **2014**, *136*, 7018-7025. (b) Kienzler, M. A.; Reiner, A.; Trautman, E.; Yoo, S.; Trauner, D.; Isacoff, E. Y. *J. Am. Chem. Soc.* **2013**, *135*, 17683-17686.
- (3) Bafana, A.; Devi, S. S.; Chakrabarti, T. *Environ. Rev.* **2011**, *19*, 350-370.
- (4) Isaad, J.; Perwuelz, A. *Tetrahedron Lett.* **2010**, *51*, 5810-5814.
- (5) Lim, H. S.; Han, J. T.; Kwak, D.; Jin, M.; Cho, K. *J. Am. Chem. Soc.* **2006**, *128*, 14458-14459.
- (6) Lee, K. M.; Wang, D. H.; Koerner, H.; Vaia, R. A.; Tan, L.-S.; White, T. J. *Angew. Chem. Int. Ed.* **2012**, *51*, 4117-4121.
- (7) Baroncini, M.; Bergamini, G. Azobenzene in Molecular and Supramolecular Devices and Machines, in Discovering the Future of Molecular Sciences; Wiley-VCH: Weinheim, **2014**, 379-397.
- (8) (a) For a review, see: Merino, E. *Chem. Soc. Rev.* **2011**, *40*, 3835-3853. For recent selected examples, see: (b) Wang, J.; He, J.; Zhi, C.; Luo, B.; Li, X.; Pan, Y.; Cao, X.; Gu, H. *RSC Adv.* **2014**, *4*, 16607-16611. (c) Cai, S.; Rong, H.; Yu, X.; Liu, X.; Wang, D.; He, W.; Li, W. *ACS Catal.* **2013**, *3*, 478-486. (d) Okumura, S.; Lin, C.-H.; Takeda, Y.; Minakata, S. *J. Org. Chem.* **2013**, *78*, 12090-12105. (e) Zhu, Y.; Shi, Y. *Org. Lett.* **2013**, *15*, 1942-1945. (f) Takeda, Y.; Okumura, S.; Minakata, S. *Angew. Chem. Int. Ed.* **2012**, *51*, 7804-7808. (g) Zhang, C.; Jiao, N. *Angew. Chem. Int. Ed.* **2010**, *49*, 6174-6177.
- (9) Huang, F.; Nie, Y.; Ye, F.; Zhang, M.; Xia, J. *Bioconjugate Chem.* **2015**, *26*, 1613-1622.
- (10) Yoshino, J.; Furuta, A.; Kambe, T.; Itoi, H.; Kano, N.; Kawashima, T.; Ito, Y.; Asashima, M. *Chem. Eur. J.* **2010**, *16*, 5026-5035.
- (11) (a) Rappoport, Z. *The Chemistry of Phenols*; Wiley-VCH: Weinheim, **2003**. (b) Tyman, J. H. P. *Synthetic and Natural Phenols*; Elsevier: New York, **1996**.
- (12) (a) Ackermann, L. *Acc. Chem. Res.* **2014**, *47*, 281-295. (b) Li, B.; Dixneuf, P. H. *Chem. Soc. Rev.* **2013**, *42*, 5744-5767. (c) (e) Kuhl, N.; Hopkinson, M. N.; Wencel-Delord, J.; Glorius, F. *Angew. Chem. Int. Ed.* **2012**, *51*, 10236-10254. (d) Yamaguchi, J.; Yamaguchi, A. D.; Itami, K. *Angew. Chem. Int. Ed.* **2012**, *51*, 8960-9009. (e) Chen, D. Y.-K.; Youn S. W. *Chem. Eur. J.* **2012**, *18*, 9452-9474. (h) Neufeldt, S. R.; Sanford, M. S. *Acc. Chem. Res.* **2012**, *45*, 936-946. (f) Engle, K. M.; Mei, T.-S.; Wasa, M.; Yu J.-Q. *Acc. Chem. Res.* **2012**, *45*, 788-802. (g) Lyons, T. W.; Sanford, M. S. *Chem. Rev.* **2010**, *110*, 1147-1169.
- (13) Wencel-Delord, J.; Glorius, F. *Nature Chem.* **2013**, *5*, 369-375.
- (14) For recent reviews, see: (a) Thirunavukkarasu, V. S.; Kozhushkov, S. I.; Ackermann, L. *Chem. Commun.* **2014**, *50*, 29-39. (b) Enthaler, S.; Company, A. *Chem. Soc. Rev.* **2011**, *40*, 4912-4924. (c) Alonso, D. A.; Nájera, C.; Pastor, I. M.; Yus, M. *Chem. Eur. J.* **2010**, *16*, 5274-5284.
- (15) For selected Pd catalyzed examples, see: (a) Premi, C.; Dixit, A.; Jain, N. *Org. Lett.* **2015**, *17*, 2598-2601. (b) Dong, J.; Jin, B.; Sun, P. *Org. Lett.* **2014**, *16*, 4540-4542. (c) Majhi, B.; Kundu, D.; Ahmmed, S.; Ranu, B. C. *Chem. Eur. J.* **2014**, *20*, 9862-9866. (d) Song, H.; Chen, D.; Pi, C.; Cui, X.; Wu, Y. *J. Org. Chem.* **2014**, *79*, 2955-2962. (e) Xiong, F.; Qian, C.; Lin, D.; Zeng, W.; Lu, X. *Org. Lett.* **2013**, *15*, 5444-

5447. (f) Li, H.; Li, P.; Wang, L. *Org. Lett.* **2013**, *15*, 620-623. (g) Yin, Z.; Jiang, X.; Sun, P. *J. Org. Chem.* **2013**, *78*, 10002-10007. (h) Ma, X.-T.; Tian, S.-K *Adv. Synth. Catal.* **2013**, *355*, 337-340. For selected Rh catalyzed examples, see: (i) Deng, H.; Li, H.; Wang, L. *Org. Lett.* **2015**, *17*, 2450-2453. (j) Yu, S.; Wan, B.; Li, X. *Org. Lett.* **2015**, *17*, 58-61. (k) Jia, X.; Han, J. *J. Org. Chem.* **2014**, *79*, 4180-4185. (l) Han, J.; Pan, C.; Jia, X.; Zhu, C. *Org. Biomol. Chem.* **2014**, *12*, 8603-8606. For a Re catalyzed example, see: (m) Geng, X.; Wang, C. *Org. Biomol. Chem.* **2015**, *13*, 7619-7623. For a Ru catalyzed example, see: Hubrich, J.; Himmler, T.; Rodefeld, L.; Ackermann, L. *ACS Catal.* **2015**, *5*, 4089-4093.
- (16) Seth, K.; Nautiyal, M.; Purohit, P.; Parikh, N.; Chakraborti, A. K. *Chem. Commun.* **2015**, *51*, 191-194.
- (17) Dick, A. R.; Hull, K. L.; Sanford, M. S. *J. Am. Chem. Soc.* **2004**, *126*, 2300-2301.
- (18) (a) Kim, K.; Choe, H.; Jeong, Y.; Lee, J. H.; Hong, S. *Org. Lett.* **2015**, *17*, 2550-2553. (b) Yang, F.; Rauch, K.; Kettelhoit, K.; Ackermann, L. *Angew. Chem. Int. Ed.* **2014**, *53*, 11285-11288. (c) Zhang, H.-Y.; Yi, H.-M.; Wang, G.-W.; Yang, B.; Yang, S.-D. *Org. Lett.* **2013**, *15*, 6186-6189. (d) Liu, W.; Ackermann, L. *Org. Lett.* **2013**, *15*, 3484-3486. (e) Mo, F. ; Trzepkowski, L. J.; Dong, G. *Angew. Chem. Int. Ed.* **2012**, *51*, 13075-13079.
- (19) Oae, S.; Kukumoto, T.; Yamagami, M. *Bull. Chem. Soc. Jap.* **1963**, *36*, 601-605.
- (20) For a selected examples, see: Yamamura, M.; Okazakia, Y.; Nabeshima, T. *Chem. Commun.* **2012**, *48*, 5724-5726.
- (21) Emmert, M. H.; Cook, A. K.; Xie, Y. J.; Sanford, M. S. *Angew. Chem. Int. Ed.* **2011**, *50*, 9409-9412.
- (22) Ackermann, L. *Chem. Rev.* **2011**, *111*, 1315-1345.
- (23) See the Supporting Information for more details.
- (24) Powers, D. C.; Ritter, T. *Nat. Chem.* **2009**, *1*, 302-309.

Pour plus d'informations sur la partie expérimentale, veuillez contacter delphine.joseph@u-psud.fr

3. Article 3 : Azophenol *via* C-H activation: regioselectivity, mechanistic understanding and potential ion sensor

Azophenol *via* C-H activation: regioselectivity, mechanistic understanding and potential ion sensor

Abstract: A novel series of azophenols as chemosensor has been reported. The detection process of several anions and cations was determined using visual color change, UV-Vis and NMR experiments. Azophenols exhibited highly selective recognition for Ni^{2+} , Cu^{2+} , Ag^+ , Na^+ , K^+ . These azophenols were obtained by a straightforward *ortho*-hydroxylation of azobenzenes. We also evaluated the influence of aromatic substituents on the site-selectivity of the reaction by synthetizing various series of azophenols diversely substituted in *para* or *ortho* positions and by using Jaffé equation and its extension. Both studies demonstrated that electron-withdrawing substituents on the arene are favorable for the *ortho*-hydroxylation, as well as for the ion detection process.

Introduction

Synthesis of anion and cation sensors via organic synthesis has been a significantly important research field over the past years.^{70,71,72,73,74} Indeed, due to their essential and crucial roles for the selective recognition in a wide range of applications such as biology, environmental chemistry⁷⁵, biomedicines^{76,77} as well as industry, the development of new sensors is of primary importance. Among key anions, an excess of fluoride, cyanide or phosphate is harmful to environment likewise to human health. In fact, these toxic contaminants can be wasted by the degradation of chemical agents like sarin, soman, taban, by gold extraction, by synthetic fibers, resins and herbicides processes.⁷⁸ More in details, although fluoride is safe and benefit for dental health at low concentrations⁷⁹, large amounts of fluoride can dangerously cause fluorosis⁸⁰, bones weakening⁸¹, increase in hip, wrist fractures, kidney injury⁸² and thyroid effects.⁸³ Besides, cyanide is extremely

⁷⁰ Gale, P. A.; Busschaert, N.; Haynes, C. J.; Karagiannidis, L. E.; Kirby, I. L., Anion receptor chemistry: highlights from 2011 and 2012, *Chem. Soc. Rev.* **2014**, 43, 205-241.

⁷¹ Kaur, K.; Saini, R.; Kumar, A.; Luxami, V.; Kaur, N.; Singh, P.; Kumar, S., Chemodosimeters: an approach for detection and estimation of biologically and medically relevant metal ions, anions and thiols, *Coord. Chem. Rev.* **2012**, 256, 1992-2028.

⁷² Cho, D.-G.; Sessler, J. L., Modern reaction-based indicator systems, *Chem. Soc. Rev.* **2009**, 38, 1647-1662.

⁷³ Sessler, J. L.; Gale, P. A.; Cho, W.-S., *Anion receptor chemistry*, Royal Society of Chemistry, **2006**.

⁷⁴ Martinez-Manez, R.; Sancenón, F., Fluorogenic and chromogenic chemosensors and reagents for anions, *Chem. Rev.* **2003**, 103, 4419-4476.

⁷⁵ Beer, P. D.; Gale, P. A., Anion recognition and sensing: the state of the art and future perspectives, *Angew. Chem. Int. Ed.* **2001**, 40, 486-516.

⁷⁶ Calnan, B. J.; Tidor, B., Arginine-mediated RNA recognition: the arginine fork, *science* **1991**, 252, 1167-1168.

⁷⁷ Kavallieratos, K.; Bertao, C. M.; Crabtree, R. H., Hydrogen bonding in anion recognition: A family of versatile, nonpreorganized neutral and acyclic receptors, *J. Org. Chem.* **1999**, 64, 1675-1683.

⁷⁸ Yang, Y. C.; Baker, J. A.; Ward, J. R., Decontamination of chemical warfare agents, *Chem. Rev.* **1992**, 92, 1729-1743.

⁷⁹ Kirk, K. L., The Halogens: Discovery, Occurrence, and Biochemistry of the Free Elements, *Biochemistry of the Elemental Halogens and Inorganic Halides*, Plenum Press, Springer, **1991**.

⁸⁰ Shivarajashankara, Y.; Shivasankara, A.; Rao, S. H.; Bhat, P. G., Oxidative stress in children with endemic skeletal fluorosis, *FLUORIDE* **2001**, 34, 103-107.

⁸¹ Wiseman, A., *Handbook of Experimental Pharmacology XX/2*, Springer-Verlag, Berlin **1970**, 48-97.

⁸² Cousins, M.; Skowronski, G.; Plummer, J., Anaesthesia and the kidney, *Anaesthet. Intens. Care* **1983**, 11, 292-320.

hazardous to wildlife, producing massive fish kill or aquatic biota.⁸⁴ In addition, it may also cause a variety of urgent environmental problems and for human health; depending on the dose and the way of exposure, it may induce from airway irritation to cardiovascular collapse and death to humans.⁸⁵ On the other side, metals such as K⁺, Ag⁺, Cu²⁺, Ni²⁺ are also extremely toxic for human and environment. For instance, it is proved that high concentration of Cu²⁺ can cause irritation of nose and throat, nausea, vomiting, diarrhea or even liver damage.⁸⁶ Nickel is a metal commonly used to make coins, magnets, jewelry, stainless steel, electronics, and components of industrial machines. However, nickel exposure, can present significant health hazards: high blood pressure, cardiovascular disease, lung cancer, neurological deficits, developmental deficits in childhood.⁸⁷ Nickel is also one of many carcinogenic metals known to be an environmental and occupational pollutant. Silver can produce discoloration of the skin (argyria) or eyes (argyrosis) or other toxic effects, including irritation of the eyes, skin, respiratory and intestinal tract, liver and kidney damage and changes in blood cells.⁸⁸ Potassium is one of the most abundant ions in the human body. Potassium can be beneficial, but excess potassium in the body leads to hyperkalaemia, manifesting in significant cardiovascular changes, in muscular weakness or in gastrointestinal symptoms.⁸⁹ Thus, the detection of anions and cations with inexpensive and efficient sensors has highly acquired considerable research interests.

Compared to electrochemical sensors, colorimetric sensors are more appealing and more practical due to the simplicity, low costs, no instrument requirements and visual color change for the detection responses.^{74,75} A variety of sensors has been reported, containing efficient subunits coordinating anions or cations such as urea^{90,91}, thiourea^{92,93}, imidazole⁹⁴, benzimidazole⁹⁵,

⁸³ Struneka, A.; Struneky, O.; Patocka, J., Fluoride plus aluminum: useful tools in laboratory investigations, but messengers of false information, *Physiol. Res.* **2002**, 51, 557-564.

⁸⁴ Eisler, R.; Wiemeyer, S. N., Cyanide hazards to plants and animals from gold mining and related water issues, *Rev. Environ. Contam. Toxicol.*, Springer, **2004**.

⁸⁵ Brennan, R. J.; Waeckerle, J. F.; Sharp, T. W.; Lillbridge, S. R., Chemical warfare agents: emergency medical and emergency public health issues, *Ann. Emerg. Med.* **1999**, 34, 191-204.

⁸⁶ Basa, P. N.; Sykes, A. G., Differential sensing of Zn (II) and Cu (II) via two independent mechanisms, *J. Org. Chem.* **2012**, 77, 8428-8434.

⁸⁷ Chervona, Y.; Arita, A.; Costa, M., Carcinogenic metals and the epigenome: understanding the effect of nickel, arsenic, and chromium, *Metalomics* **2012**, 4, 619-627.

⁸⁸ Drake, P. L.; Hazelwood, K. J., Exposure-related health effects of silver and silver compounds: a review, *Ann. Occup. Hyg.* **2005**, 49, 575-585.

⁸⁹ Saxena, K., Clinical features and management of poisoning due to potassium chloride, *Med. Toxicol. Adverse. Drug. Exp.* **1989**, 4, 429-443.

⁹⁰ Amendola, V.; Fabbrizzi, L.; Mosca, L., Anion recognition by hydrogen bonding: urea-based receptors, *Chem. Soc. Rev.* **2010**, 39, 3889-3915.

⁹¹ Boiocchi, M.; Del Boca, L.; Gómez, D. E.; Fabbrizzi, L.; Licchelli, M.; Monzani, E., Nature of urea- fluoride interaction: incipient and definitive proton transfer, *J. Am. Chem. Soc.* **2004**, 126, 16507-16514.

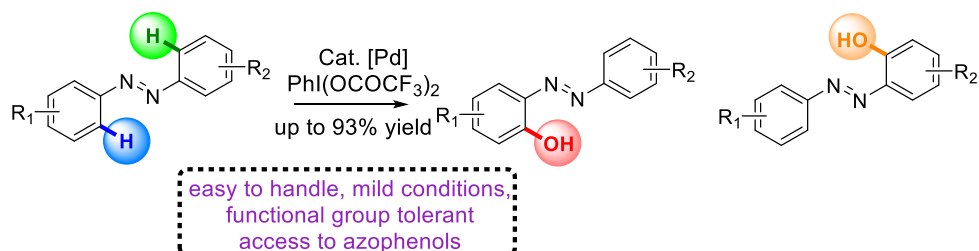
⁹² Berry, S. N.; Soto-Cerrato, V.; Howe, E. N.; Clarke, H. J.; Mistry, I.; Tavassoli, A.; Chang, Y.-T.; Pérez-Tomás, R.; Gale, P. A., Fluorescent transmembrane anion transporters: shedding light on anionophoric activity in cells, *Chem. Sci.* **2016**, 7, 5069-5077, Murali, M.; Vishnumurthy, K.; Seethamraju, S.; Ramamurthy, P. C., Colorimetric anion sensor based on receptor having indole- and thiourea-binding sites, *RSC Adv.* **2014**, 4, 20592-20598.

⁹³ Evans, L. S.; Gale, P. A.; Light, M. E.; Quesada, R., Anion binding vs. deprotonation in colorimetric pyrrolylanidothiourea based anion sensors, *Chem. Commun.* **2006**, 965-967.

⁹⁴ Toure, M.; Charles, L.; Chendo, C.; Viel, S.; Chuzel, O.; Parrain, J. L., Straightforward and Controlled Shape Access to Efficient Macrocyclic Imidazolylboronium Anion Receptors, *Chem. Eur. J.* **2016**, 22, 8937-8942.

⁹⁵ Kaur, N.; Dhaka, G.; Singh, J., Simple naked-eye ratiometric and colorimetric receptor for anions based on azo dye featuring with benzimidazole unit, *Tetrahedron Lett.* **2015**, 56, 1162-1165.

anthraquinone⁹⁶, pyrrole^{97,98}, thiosemicarbazide^{99,100}, azobenzene¹⁰¹, naphthalen¹⁰²... Crowded azophenols have also been used for the sensitive colorimetric determination of alkali, and alkaline earth metal ions.^{103,104,105} Recently, simple azophenols or complexe azophenol-thioureas, azophenol-thiacalix[4]arenes have also been developed as effective classes of sensor tools which showed a coloration with F⁻, H₂PO₄⁻ and AcO⁻.^{106,107,108,109,110} However, the hydroxy function has always been introduced on the *para* position of the arene, giving a limited color change to purple or light pink. Based on our previous work for the synthesis of *ortho*-azophenols by direct *ortho*-hydroxylation on azobenzenes via Pd catalyzed C-H activation¹¹¹ (Scheme 1), we expected that this new class of original compounds would give highly attractive colorimetric sensors.



Scheme 1. Synthesis of azophenol from azobenzene

Using unsymmetric azobenzenes as starting materials gave a large panel of regioselectivities. This seminal work encouraged us to elucidate the relationship between the substituents on the

⁹⁶ Ghosh, A.; Jose, D. A.; Kaushik, R., Anthraquinones as versatile colorimetric reagent for anions, *Sens. Actua. B: Chem.* **2016**, 229, 545-560.

⁹⁷ Ghorpade, T. K.; Patri, M.; Mishra, S. P., Highly sensitive colorimetric and fluorometric anion sensors based on mono and di-calix [4] pyrrole substituted diketopyrrolopyrroles, *Sens. Actua. B: Chem.* **2016**, 225, 428-435.

⁹⁸ Wang, Y.; Mao, P.-D.; Wu, W.-N.; Mao, X.-J.; Fan, Y.-C.; Zhao, X.-L.; Xu, Z.-Q.; Xu, Z.-H., New pyrrole-based single-molecule multianalyte sensor for Cu²⁺, Zn²⁺, and Hg²⁺ and its AIE activity, *Sens. Actuator B Chem.* **2017**,

⁹⁹ Farrugia, K. N.; Makuc, D.; Podborska, A.; Szaciłowski, K.; Plavec, J.; Magri, D. C., Colorimetric Naphthalene-Based Thiosemicarbazide Anion Chemosensors with an Internal Charge Transfer Mechanism, *Eur. J. Org. Chem.* **2016**, 2016, 4415-4422.

¹⁰⁰ Farrugia, K. N.; Makuc, D.; Podborska, A.; Szaciłowski, K.; Plavec, J.; Magri, D. C., UV-visible and ¹H-¹³C NMR spectroscopic studies of colorimetric thiosemicarbazide anion sensors, *Org. Biomol. Chem.* **2015**, 13, 1662-1672.

¹⁰¹ Arslan, Ö.; Aydiner, B.; Yalçın, E.; Babür, B.; Seferoğlu, N.; Seferoğlu, Z., 8-Hydroxyquinoline based push-pull azo dye: Novel colorimetric chemosensor for anion detection, *J. Mol. Struct.* **2017**, 1149, 499-509.

¹⁰² Paul, B. K.; Kar, S.; Guchhait, N., A Schiff base-derived new model compound for selective fluorescence sensing of Cu(II) and Zn(II) with ratiometric sensing potential: synthesis, photophysics and mechanism of sensory action, *J. Photochem. Photobiol. A* **2011**, 220, 153-163.

¹⁰³ Loehr, H. G.; Vögtle, F., Chromo-and fluoroionophores. A new class of dye reagents, *Acc. Chem. Res.* **1985**, 18, 65-72.

¹⁰⁴ Kaneda, T.; Umeda, S.; Tanigawa, H.; Misumi, S.; Kai, Y.; Morii, H.; Miki, K.; Kasai, N., A spherand azophenol dye: lithium ion specific coloration with "perfect" selectivity, *J. Am. Chem. Soc.* **1985**, 107, 4802-4803.

¹⁰⁵ Nakashima, K.; Yamawaki, Y.; Nakatsui, S. i.; Akiyama, S.; Kaneda, T.; Misumi, S., Complexation of "crowned" dinitrophenylazophenol with alkali and alkaline earth metal ions and its application to the colorimetric determination of Rb (I) and Cs (I), *Chem. Lett.* **1983**, 12, 1415-1418.

¹⁰⁶ Kumar, M.; Babu, J. N.; Bhalla, V., Azophenol appended (thia)calix[4]arenes for colorimetric sensing of anions: A complexation induced extended conjugation, *Talanta* **2010**, 81, 9-14.

¹⁰⁷ Choi, M. K.; Kim, H. N.; Choi, H. J.; Yoon, J.; Hyun, M. H., Chiral anion recognition by color change utilizing thiourea, azophenol, and glucopyranosyl groups, *Tetrahedron Lett.* **2008**, 49, 4522-4525.

¹⁰⁸ Lee, D. H.; Im, J. H.; Son, S. U.; Chung, Y. K.; Hong, J.-I., An azophenol-based chromogenic pyrophosphate sensor in water, *J. Am. Chem. Soc.* **2003**, 125, 7752-7753.

¹⁰⁹ Lee, D. H.; Lee, K. H.; Hong, J.-I., An azophenol-based chromogenic anion sensor, *Org. Lett.* **2001**, 3, 5-8.

¹¹⁰ Lee, K. H.; Lee, H.-Y.; Lee, D. H.; Hong, J.-I., Fluoride-selective chromogenic sensors based on azophenol, *Tetrahedron Lett.* **2001**, 42, 5447-5449.

¹¹¹ Nguyen, T. H. L.; Gigant, N.; Delarue-Cochin, S.; Joseph, D., Palladium-Catalyzed Oxidative Synthesis of Unsymmetrical Azophenols, *J. Org. Chem.* **2016**, 81, 1850-1857.

azobenzenes and the side selectivity of our reaction. In the litterature, Hammett equation and its extension (Brown, Jaffé, Taft, Beson...) have been the most widely used method to correlate chemical reactivity to the substrate structure in organic chemistry.^{112,113,114} Apart from this classical application, Hammett equation was evolved in various other fields such as mechanistic studies^{115,116}, mass spectrometry¹¹⁷, chromatography¹¹⁸, drug metabolism¹¹⁹, environmental toxicology...

Herein, through Hammett-Jaffé analyses, we will report a study that explores both electronic and steric perturbations induced by the substituent nature to the regioselectivity of the reaction. This relationship and the ρ value of the equation will also demonstrate the intimate mechanism of C-H activation Pd-catalyzed hydroxylation.

We will also observe different visual color changes depending on the sensibility of our sensors with the anions. Anion sensing characteristics will also be determined using UV-Vis titrations and NMR spectroscopy.

Results and discussions

Hammett-Jaffé relationships

Azobenzenes were synthetized following the general procedure described in our previous work. First, a series of various *para*-substituted azobenzenes was evaluated and results on the side selectivity were shown in Table 1. Generally, the reaction mainly occurred at the more electron-rich arene moiety. Standard Hammett equation did not result linear relationship with a poor correlation coefficient $r^2 = 0.70$ (Figure 1). This could be explained by the fact that the Hammett equation gave satisfying result only if one position on the molecule had a much more powerful effect than the others.¹²⁰ In our case, the reaction rate may be influenced by substituents on both two reactive sites (Scheme 2). Fortunately, the Jaffé equation, an extension of the Hammett equation, could correlate data of this reaction as well as other reactions in which two positions (*meta* and *para*) were affected.^{112,121} These two centers were in *para* and *meta* positions relative to the substituent X (Scheme 2b). In our case, Jaffé correlation study revealed a magnificent linear free energy

¹¹² Edwards, D. R.; Neverov, A. A.; Brown, R. S., Dissociative Solvolytic Cleavage of Methyl (ortho-Carboxymethyl) Aryl Phosphate Diesters Mediated by Yb³⁺ in Methanol Gives a 1012-Fold Rate Acceleration Attributable to Leaving Group Assistance, *J. Am. Chem. Soc.* **2009**, *131*, 368-377.

¹¹³ Kumar, M. S.; Rajanna, K.; Venkateswarlu, M.; Rao, K. L., Tertiary Butyl Nitrite Triggered Nitration of Phenols: Solvent-and Structure-Dependent Kinetic Study, *Int. J. Chem. Kinet.* **2016**, *48*, 171-196.

¹¹⁴ Abou-Hatab, S.; Spata, V. A.; Matsika, S., Substituent Effects on the Absorption and Fluorescence Properties of Anthracene, *J. Phys. Chem. A.* **2017**, *121*, 1213-1222.

¹¹⁵ Rangappa, K.; Anitha, N.; Made Gowda, N., Mechanistic investigations of the oxidation of substituted phenethyl alcohols by manganese (III) sulfate catalyzed by ruthenium (III) in acid solution, *Synth. React. Inorg., Met-Org. Chem.* **2001**, *31*, 1499-1518.

¹¹⁶ Stowers, K. J.; Sanford, M. S., Mechanistic Comparison between Pd-Catalyzed Ligand-Directed C–H Chlorination and C–H Acetoxylation, *Org. Lett.* **2009**, *11*, 4584-4587.

¹¹⁷ Harrison, A. G., Linear free energy correlations in mass spectrometry, *J. Mass. Spectrom.* **1999**, *34*, 577-589.

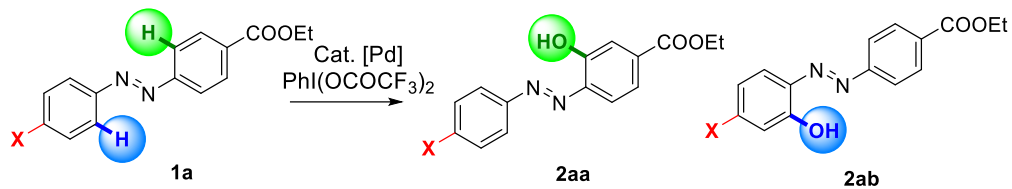
¹¹⁸ Mokrosz, J.; Ekiert, L., Linear free energy relationship in thin layer chromatography of 5-arylidenebarbiturates, *Chromatographia* **1984**, *18*, 401-405.

¹¹⁹ Huang, J.; Dunford, H. B., Oxidation of substituted anilines by horseradish peroxidase compound II, *Can. J. Chem.* **1990**, *68*, 2159-2163.

¹²⁰ Jaffé, H., Application of the Hammett equation to fused ring systems, *J. Am. Chem. Soc.* **1954**, *76*, 4261-4264.

¹²¹ Jensen, K. H.; Webb, J. D.; Sigman, M. S., Advancing the mechanistic understanding of an enantioselective palladium-catalyzed alkene difunctionalization reaction, *J. Am. Chem. Soc.* **2010**, *132*, 17471-17482.

relationship with $\rho_m \approx +2.11$, $\rho_p \approx -0.34$ and an excellent correlation coefficient $r^2 = 0.9979$ (Figure 1b).



Entry	X	2aa	2ab	Yield	
1	OCH ₃	0.78	:	1	60 %
2	CH ₃	0.36	:	1	60 %
3	H	0.43	:	1	65 %
4	F	1	:	0.47	83 %
5	Br	1	:	0.40	73 %
6	NO ₂	1	:	0.25	62 %

Table 1. Results of the *ortho*-hydroxylation of azobenzene **1a**

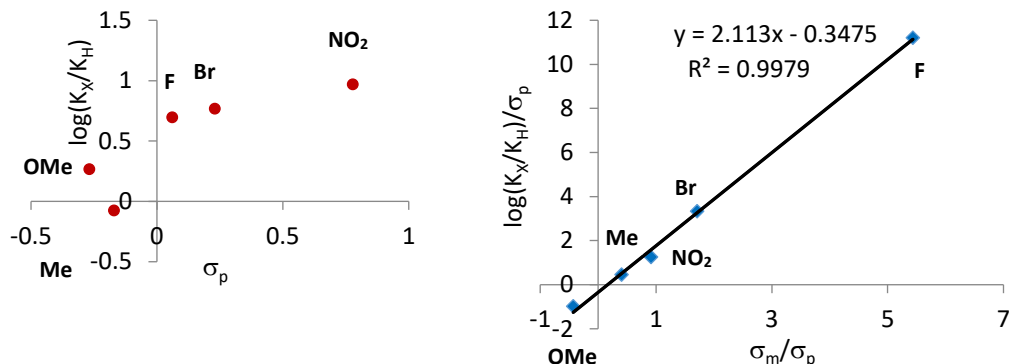


Figure 1. (a) Hammett and (b) Jaffé plots of **1a** substrate on ratio

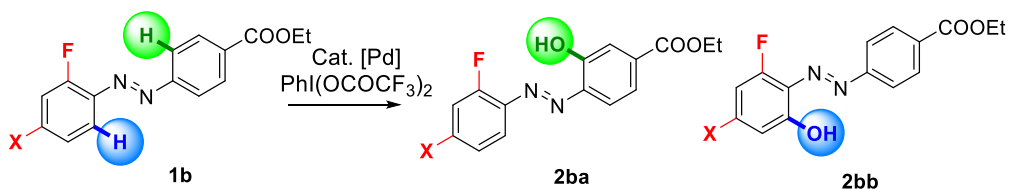
Hammett equation	Jaffé equation
$\log \frac{k_X}{k_H} = \rho \sigma$	$\log \frac{k_X}{k_H} = \rho_m \sigma_m + \rho_p \sigma_p$
$\Rightarrow \frac{\log \frac{k_X}{k_H}}{\sigma_p} = \frac{\rho_m \sigma_m}{\sigma_p} + \rho_p$	

Scheme 2. (a) Hammett and Jaffé equations, (b) *meta* and *para* positions influenced in Jaffé plots.

We then investigated several *para*-functionalized azobenzenes bearing either a fluorine atom or a chlorine atom at the *ortho* position. By using these substrates, yields could be generally improved

from 20 % to 50 % by increasing the reaction temperature up to 90 °C. With *ortho*-fluoro substituent, the less hindered arene, with no substituent in *ortho* position was preferentially hydroxylated, whatever the nature of *para* substituents. Indeed, azobenzene **1b** bearing either OCH₃ or NO₂ moieties at *para* position on one aromatic ring afforded only one regioisomer with the hydroxyl group on the less crowded ring (entries 1 and 7 of Table 2). When the reaction was carried out with *ortho*-chloro **1c** azobenzene, the reaction mainly occurred at the more electron-rich arene moiety. The electron-donating groups X afforded major product **2cb** with hydroxy group on the more substituted at the same time the more electron-rich moiety (entry 1 of Table 3). On the contrary, substrates with electron-withdrawing groups X reacted in the less hindered but more electron-rich aromatic ring, furnishing **2ca** as major product (entries 3-7 of Table 3).

Evaluations with Jaffé equation also gave good correlations for the Pd catalyzed *ortho*-hydroxylation, providing large positive slopes of 5.89 ($r^2 = 0.9895$) and of 3.47 ($r^2 = 0.9867$) for the *ortho*-F and the *ortho*-Cl series respectively (Figure 2). Taken together with the $r^2 = 0.9979$ determined above with no-*ortho*-substituted azobenzenes, these values demonstrated that there is evidently an effect of the fluoro or chloro substituent in the *ortho* position, producing a slight decrease of r^2 .¹²² Indeed, this result was fully consistent with the literature data, since the Hammett equation and its extension reported that *ortho*-substituents may influence the reactivity due to their electronic or/and steric effects.¹²³ The σ_{ortho} constants are not included in the Hammett equation, because they were represented by a lot of factors and varied from a substrate to another and from a reaction to another. Thus, only the experiments can show whether the equation is suitable for the reaction and for the substrate.

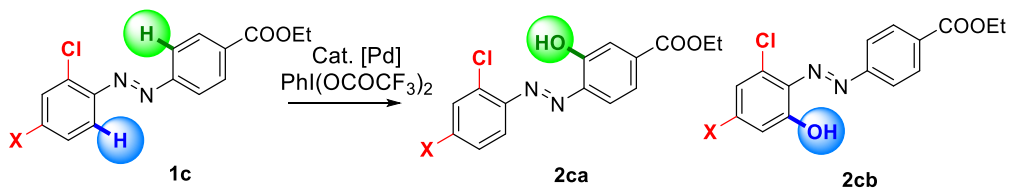


Entry	X	2ba	2bb	Yield
1	OCH ₃	1	:	0
2	CH ₃	1	:	0.7
3	H	0.9	:	1
4	F	1	:	0.02
5	Br	1	:	0.12
6	CF ₃	1	:	0.1
7	NO ₂	1	:	0

Table 2. Results of the *ortho*-hydroxylation of azobenzene **1b**

¹²² Szostak, M.; Spain, M.; Eberhart, A. J.; Procter, D. J., Mechanism of SmI₂/Amine/H₂O-Promoted Chemoselective Reductions of Carboxylic Acid Derivatives (Esters, Acids, and Amides) to Alcohols, *J. Org. Chem.* **2014**, 79, 11988-12003.

¹²³ Jaffé, H. H., A reexamination of the Hammett equation, *Chem. Rev.* **1953**, 53, 191-261.



Entry	X	2ca	2cb	Yield
1	CH ₃	0.08	:	1 47 %
2	H	0.22	:	1 52 %
3	F	1	:	0.3 33 %
4	Br	1	:	0.2 52 %
5	OCF ₃	1	:	0.14 55 %
6	COOMe	1	:	0.85 37 %
7	NO ₂	1	:	0.02 52 %

Table 3. Results of the *ortho*-hydroxylation of azobenzene **1c**

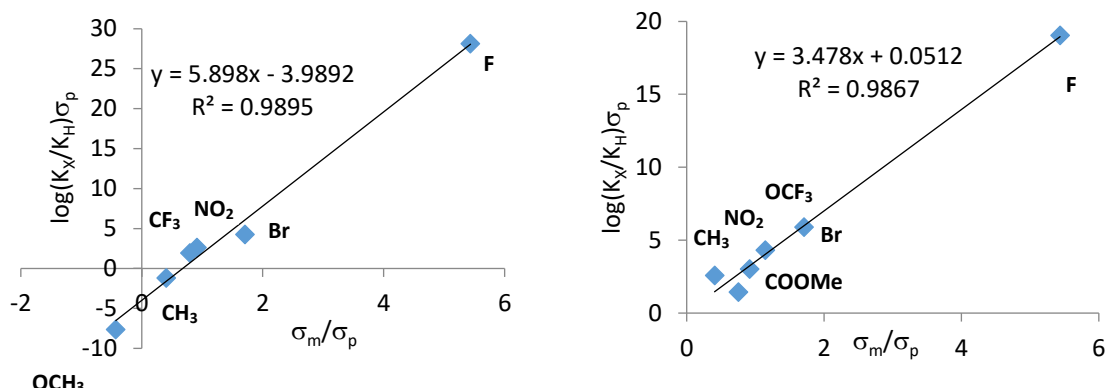
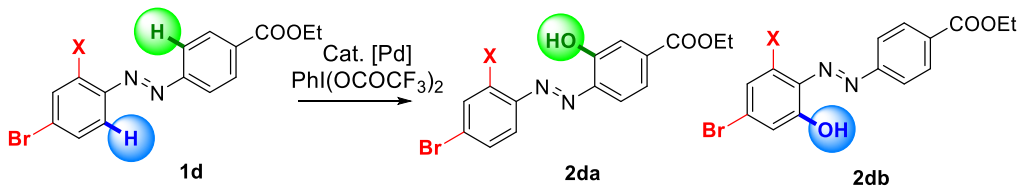


Figure 2. Jaffé plots of (a) **1b** and (b) **1c** on ratio

These results encouraged us to further survey the relationship of this reaction with respect to unsymmetrical azobenzenes **1d** bearing a bromine atom fixed at *para* position and several substituents at *ortho* position. Our results were revealed in Table 4. We noticed the same effect as with azobenzene **1c** even in this case the varied substituent was in *ortho* position. Substrates with electron-withdrawing groups X in *ortho* position produced the major regioisomer **2da** in the less substituted benzene ring while substrates with electron-donating groups reversed the side selectivity of the hydroxylation. In all case, the reaction preferentially happened at the more electron-rich arene moiety. Notably, an excellent selectivity giving only one regioisomer was obtained when the substrate bearing an *ortho* nitro group was employed (entry 7 of Table 4).



Entry	X	Ratio		Yield
		2da	2db	
1	CH ₃	0.3	:	39 %
2	H	1	:	73 %
3	F	1	:	54 %
4	OCF ₃	1	:	51 %
5	Cl	1	:	52 %
6	Br	1	:	48 %
7	NO ₂	1	:	68 %

Table 4. Results of the *ortho*-hydroxylation of azobenzene **1d**

Much later following Jaffé extension, Benson and others authors reported that the effect of multiple substituents on the benzene ring could be expressed by the sum of all substituent constants.^{124,125} Additive effect was inspected not only in classical Hammett system of substituted benzoic acid¹²⁶ but also in polyfluorinated tryptophans¹²⁷ or in the electrostatic potential of substitution.¹²⁸ Brought together with Jaffé equation, we could state the assumption of these two equations, knowing that X was a *meta* substituent relative to the hydroxylation position and bromine could be considered as a *meta* and *para* substituent like discussed above (Scheme 3). A reasonable correlation line was also obtained with a positive $\rho_m \approx +0.34$, $\rho_p \approx -0.97$ and $r^2 = 0.9069$ (Figure 3). This erosion in the r^2 value was due to the absence of the *ortho* effect of X regarding to azo N=N group. Obviously, knowing that *ortho* substituent constants varied extremely from one reaction to another¹²⁹, we hence decided to skip these values.

¹²⁴ Taha, A. A., Solvolysis of 2-chloro-2 (3,4-disubstituted) phenylpropanes: Validity of Hammett–Brown $\sigma+$ constants in assessing additive effects of substituents, *Int. J. Chem. Kinet.* **2012**, *44*, 514-523.

¹²⁵ Stone, R.; Pearson, D., Notes. Are Organic Group Influences Additive in All Reactions of Aromatic Compounds?, *J. Org. Chem.* **1961**, *26*, 257-259.

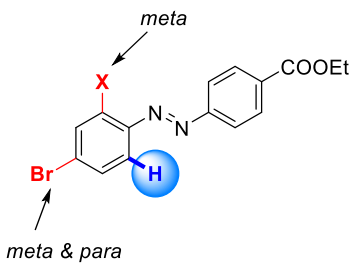
¹²⁶ Pytela, O.; Kulhánek, J.; Ludwig, M.; Říha, V., Chemometrical Analysis of Substituent Effects. III. Additivity of Substituent Effects in Dissociation of 3, 4-Disubstituted Benzoic Acids in Organic Solvents, *Czech. Chem. Commun.* **1994**, *59*, 627-638.

¹²⁷ Zhong, W.; Gallivan, J. P.; Zhang, Y.; Li, L.; Lester, H. A.; Dougherty, D. A., From ab initio quantum mechanics to molecular neurobiology: a cation–π binding site in the nicotinic receptor, *Proc. Natl. Acad. Sci. USA* **1998**, *95*, 12088-12093.

¹²⁸ Sayyed, F. B.; Suresh, C. H., Quantification of substituent effects using molecular electrostatic potentials: additive nature and proximity effects, *New J. Chem.* **2009**, *33*, 2465-2471.

¹²⁹ Charton, M., Nature of the *ortho* effect. V. *ortho*-substituent constants, *J. Am. Chem. Soc.* **1969**, *91*, 6649-6654.

Benson equation	Jaffé equation
$\log \frac{k_X}{k_H} = \rho \sum \sigma$	$\log \frac{k_X}{k_H} = \rho_m \sigma_m + \rho_p \sigma_p$
$\Rightarrow \log \frac{k_X}{k_H} = \rho_m (\sigma_{m-X} + \sigma_{m-Br}) + \rho_p \sigma_{p-Br}$	
$\frac{\log \frac{k_X}{k_H}}{\sigma_{p-Br}} = \frac{\rho_m (\sigma_{m-X} + \sigma_{m-Br})}{\sigma_{p-Br}} + \rho_p$	



Scheme 3. The assumption of Jaffé equation and total effect equation

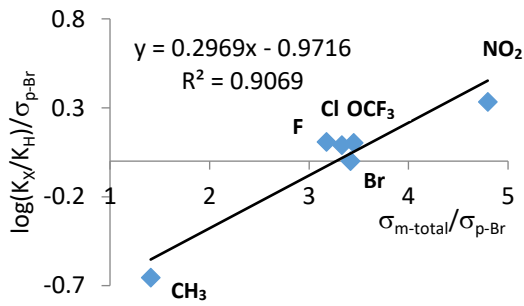
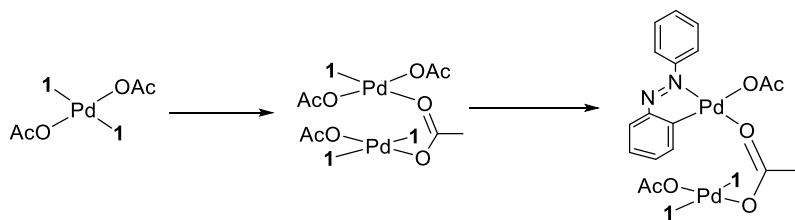


Figure 3. Correlation of **1d** with the ratio

Our previous work on the mechanism of this reaction indicated that the rate-determining step may be the C-H bond cleavage.¹¹¹ On the basis of the proposed catalytic cycle, the precious work of Sanford and the positive ρ_m values in all cases demonstrated above, the mechanism for the turnover-limiting step was clarified in Scheme 4.^{116,130,131} An acetate-bridged dimer $Pd_2(OAc)_4(1)_3$ could be generated, affording the cyclometallation intermediate. The relative positive ρ_m also expressed that electron-withdrawing substituents increased the K constant value of the reaction and rendered the system more reactive.



Scheme 4. Turnover-limiting intermediate

¹³⁰ Kurzeev, S. A.; Kazankov, G. M.; Ryabov, A. D., Second-and inverse order pathways in the mechanism of orthopalladation of primary amines, *Inorg. Chim. Acta* **2002**, *340*, 192-196.

¹³¹ Vicente, J.; Saura-Llamas, I., *ortho*-Palladation of primary amines: the myth dispelled, *Comments Inorg. Chem.* **2007**, *28*, 39-72.

Anion and cation detection

Choice of substrates

Hydroxylated azobenzenes in hand, we would like to investigate the nature of the substituents affecting anion selectivity by examining different azophenol substrates. We first chose two compounds **2ba7** and **2da7** which were obtained with excellent regioselectivity (Figure 4). In order to compare and understand the importance of the substituents on the anion detection property, we selected azophenols **3-6**, which bore different substituents in *para* position. In addition, we also tested electron-deficient compound **7** with Cl and NO₂ groups in the same ring and no substituent in the other ring.

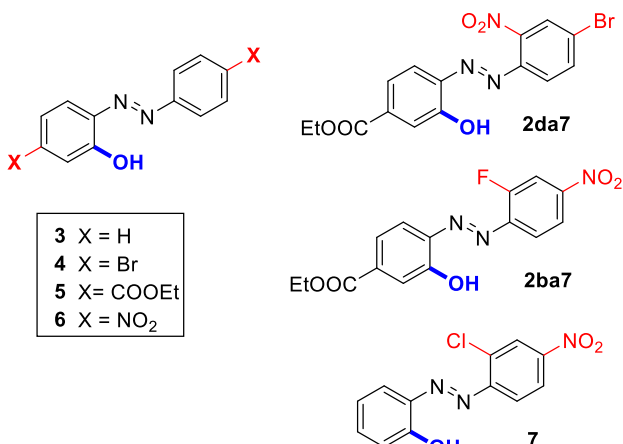


Figure 4. Azophenol substrates for the anion detection studies

Anion detection

Colorimetric signaling

The colorimetric properties were firstly examined by a naked-eye color change observation in the presence of various anions (with *n*-tetrabutylammonium as counter anion) (Figure 5). Compound **3** with no substituent did not conduct to a clearly naked-eye color change, only showing an evolution of colorless to a slight red color with F⁻ and OH⁻ ions (Figure 5a). At the opposite, compounds **4-7**, **2ba7** and **2da7** marked their potential affinity to anions by causing visual color changes to red, purple and blue (Figure 5b-g), due to different substituents borne on their aromatic rings. More precisely, compound **4** gave a red color, compounds **5** and **2da7** gave a violet color, while compounds **6**, **7** and **2bad** gave a blue color. Ions such as CN⁻, F⁻, OH⁻ reacted with all azophenols while H₂PO₄⁻ ion was detected by compounds **5**, **6**, **7**, **2ba7**, **2da7**. Importantly, HSO₄⁻, OAc⁻ ions were only recognized by compound **6**. It is important to note that **4** was the most selective, detecting only 3 ions. **5**, **7** and **2da7**, detecting four anions, were also highly selective. However, ions such as NO₃⁻, I⁻, ClO₄⁻, Br⁻, Cl⁻ ion did not produce any obvious color change, even when a huge excess of 100 equivalents of ions was added, mainly related to insufficient strong hydrogen-bonding interactions with the sensor. In order to gauge anion effects, pKa values were measured in CH₃CN solutions by using a pH meter (Table 5 and 6). The basicity order of anions was then established, and we found that the most basic ions such as HSO₄⁻, OAc⁻, H₂PO₄⁻, CN⁻, F⁻, OH⁻ gave the most powerful complexes with azophenol

compounds. We also remarked that the worst acid azophenol sensors **3**, **4** were the most selective for the anions detection, providing only color change with three anions. Moreover, the color change was correlated to the acidity of the azophenol substrate and effectively to the substituents on aromatic rings. Strong electron withdrawing group NO_2 in *para* position rendered the substrates **6**, **7**, **2ba7** more acid, probably causing the blue color. Less acid substrates such as **5** with COOEt groups in *para* position or **2da7** with NO_2 group in *ortho* position performed the purple color. The worst acid substrates **4** with bromine atoms in *para* and **3** with no substituent yield the red color change. Nonetheless, it was impossible to discriminate an anion to another with the same azophenol solution since only one color was detected.

Anion	NO_3^-	I^-	ClO_4^-	Br^-	Cl^-	HSO_4^-	OAc^-	H_2PO_4^-	CN^-	F^-	OH^-
pKa	4.1	6.6	6.7	7.3	8.1	8.5	10.9	11.3	15.3	16.6	20.2

Table 5. Measured pKa values of anion solutions in MeCN

Azophenol	3	4	5	2da7	7	2ba7	6
pKa	7.1	6.9	6.3	6.2	6.1	6.1	5.9

Table 6. Measured pKa values of azophenol **3-6**, **2ba7**, **2da7** in MeCN

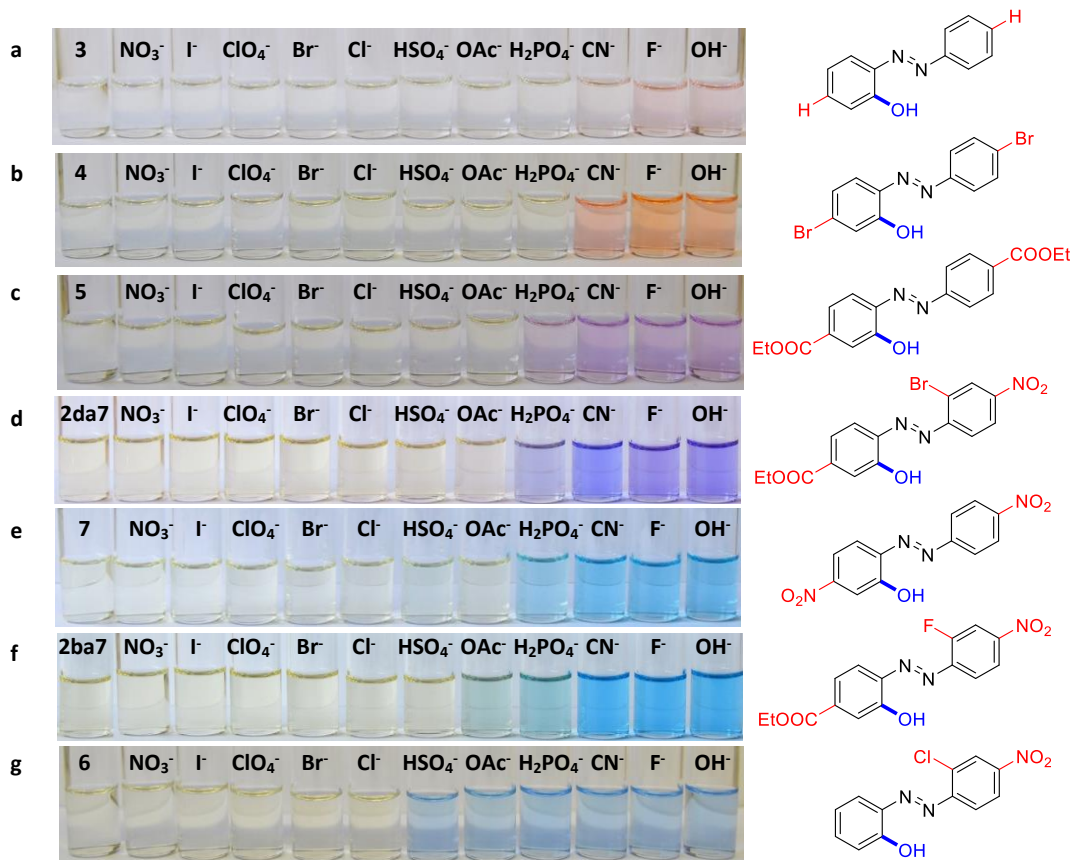


Figure 5. Visual color change of azophenol substrates with the addition of anions in CH_3CN

UV-Vis absorption studies

The anion recognition properties of **3-7**, **2ba7**, **2da7** were next studied by UV-Vis spectroscopy in the absence and in the presence of anions. Solutions of azophenol without anions were characterized by an absorption maximum band at 330-380 nm (Figure 6). A decrease of this band was observed upon the addition of anions such as OAc^- , H_2PO_4^- , CN^- , F^- , OH^- accompanied by a significant increase of an absorption band in visible range (Table 7). Remarkably, the weak interaction of **3** with anions resulted in a slight pic appearance at 492 nm (Figure 6a), while other compounds allowed intense red-shifted pics when anions were added (Figure 6b-d). All anions which did not give visual color change did not also proceed any change in UV-Vis absorption.

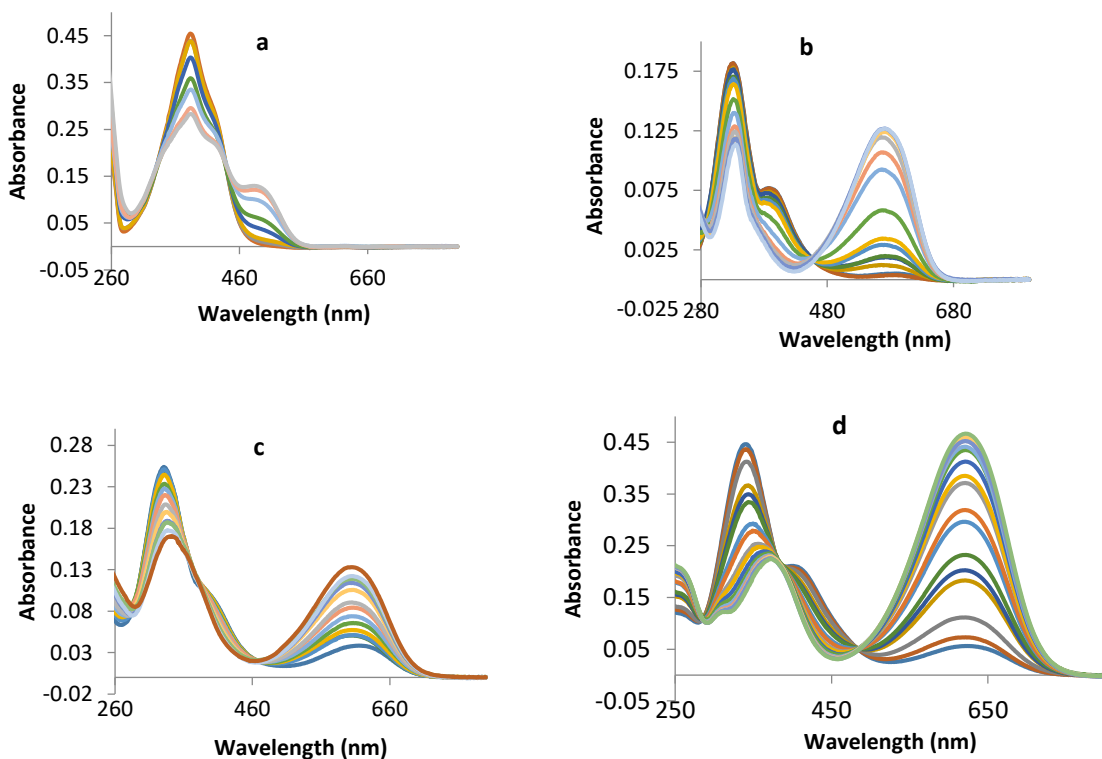


Figure 6. UV-Vis absorption spectra evolution of the solution of 10 μM in MeCN upon the addition of anions (a) **3** with OH^- , (b) **5** with F^- , (c) **6** with H_2PO_4^- , (d) **2ba7** with CN^-

Compound	λ_{\max} (no anion)	λ_{\max} (with anion)	$\Delta\lambda_{\max}$	Iisosbestic point
3	383	492	109	442
4	334	505	176	436
5	329	572	243	460
6	328	617	289	474
2ba7	339	621	280	487
2da7	336	581	245	474
7	343	612	269	464

Table 7. UV-Vis absorption data for **3-7**, **2ba7**, **2da7** without anions and in the presence of anions

Strong basic anions such as CN^- , F^- , OH^- started to react with azophenol sensors from 0.1 equiv and the complexe solution became saturated when the addition of these anions reached 1 equiv (Figure 7). By contrast, an anion such as H_2PO_4^- that formed a weaker complexe with azophenol could only initiate UV-Vis data change from 1 equiv and achieve the saturation level at 5 equiv (compounds **6**, **7**, **2ba7**) or even at 500 equiv (coumpounds **5**), respectively.

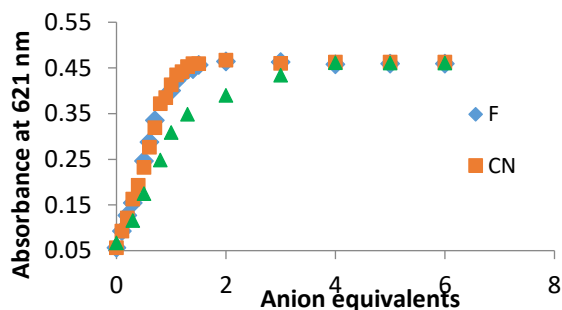


Figure 7. Titration profiles of 10 μM of **2ba7** with F^- (blue), CN^- (orange), H_2PO_4^- (green)

The generation of different colors after the addition of anions into receptor solutions could be logically demonstrated by the theory of color absorption and reflexion. For example, the complex anion-substrate **6** solution, absorbing the orange frequency of light ($\lambda_{\text{max}} = 617 \text{ nm}$), reflected and appeared as its complementary colour, which was blue (Figure 8a). The chromatic circle is helpful to find the complementary colours that are opposite to each other (Figure 8b).

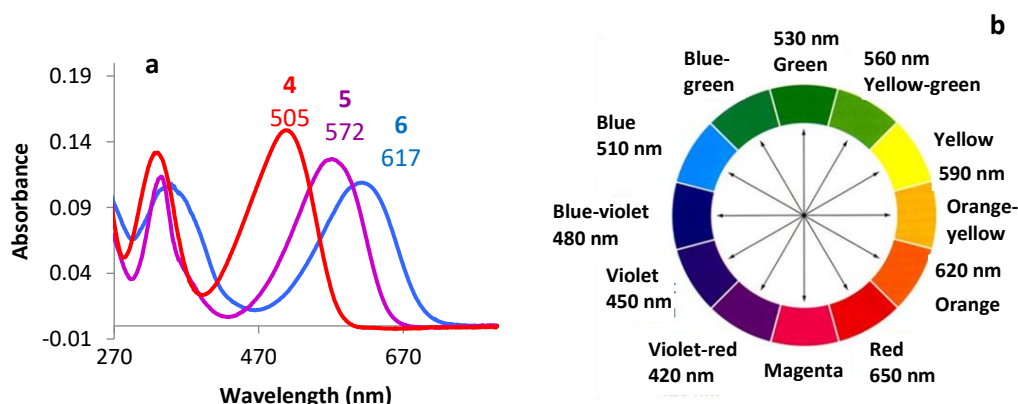


Figure 8. (a) Bathochromic shift upon addition of anions with **4** (red), **5** (violet), **6** (blue);
(b) Chromatic circle

Cations sensors measurements

In order to investigate whether azophenols can be used for colorimetric sensors of cations, **2ba7** was evaluated with different counter-ions. Among azophenols tested, we decided to choose compound **2ba7** for cations detection due to the clearest color change and the most powerful absorbance intensity of a new pic in visible range.

The first series of cations is based on the use of fluoride salts. Visual color change and UV-Vis are shown in Figure 9. After the addition of cation into the azophenol solution, the color changed immediately from colorless to violet, light-green and blue with Ag^+ , K^+ and TBA^+ . UV-Vis spectral experiments were also evaluated. In the presence of Ag^+ , K^+ and TBA^+ the absorbance maxima of **2ba7** at 339 nm decreased slowly with an increase of a absorption band at 586 nm, 614 nm and 621 nm, respectively. Other cations, such as Na^+ , Ca^{2+} , Cs^+ and NH_4^+ , did not significantly change color as well as UV-Vis spectra.

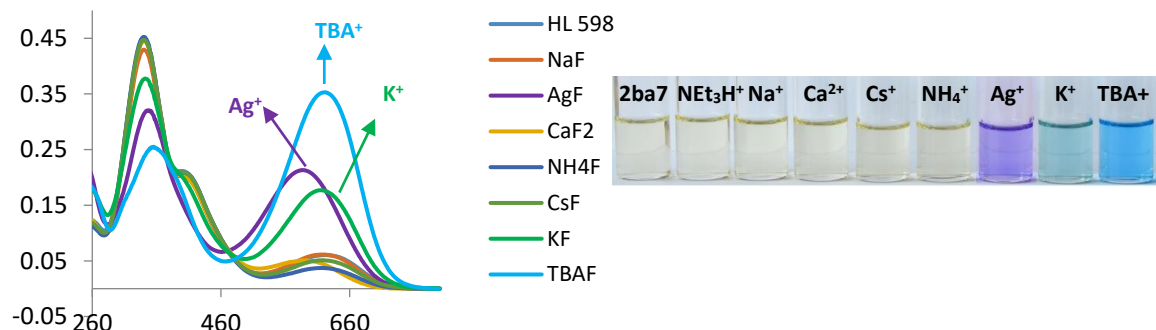


Figure 9. Color change and absorbance spectra change of 10 μM of **2ba7** upon addition of various cations (with fluoride as counter cation)

The same responses were observed when the sensing ability of **2ba7** against Mn^{3+} , NH_4^+ , Hg^{2+} , Cu^+ , Pd^{2+} , Ni^{2+} , Cu^{2+} , Ag^+ , Na^+ , K^+ , TBA^+ with acetate as the counter cation was performed (Figure 10). Cations Ni^{2+} and Cu^{2+} gave a slight red color, corresponding to a new absorption band in visible range at 504 nm and 491 nm respectively. Cations such as Ag^+ and Na^+ caused a green color and a new absorption band centered at 602 nm and 616 nm. Cations K^+ , TBA^+ induced a blue color and a broad band at 621 nm. However, no response was monitored when cations such as Mn^{3+} , NH_4^+ , Hg^{2+} , Cu^+ , Pd^2 were added into **2ba7** solution. Therefore **2ba7** can be used as a colorimetric probe for the discrimination of Ni^{2+} , Cu^{2+} , Ag^+ , Na^+ , K^+ .

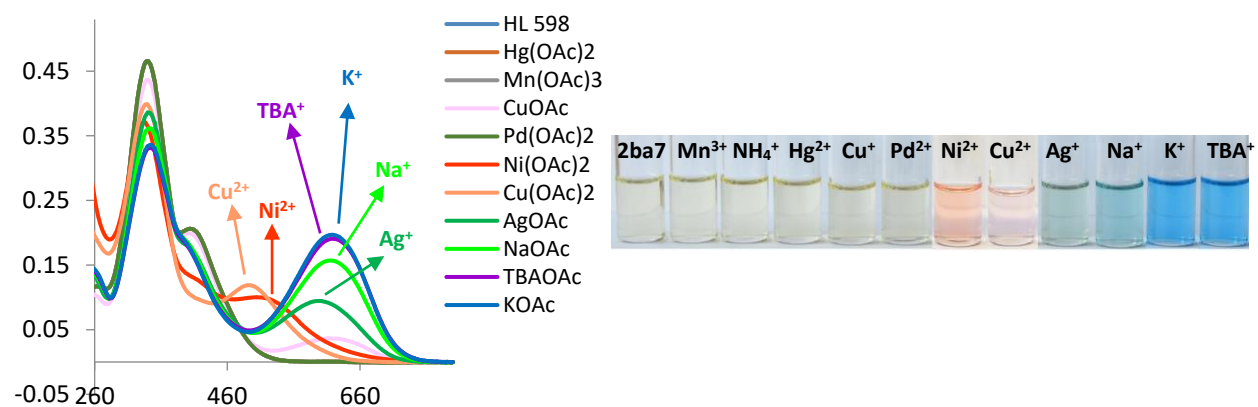


Figure 10. Color change and absorbance spectra change of 10 μM of **2ba7** upon addition of various cations (with acetate as counter cation)

Both the stoichiometry and the association constant K between azophenol compounds and anions/cations were determined by using the Benesi-Hildebrand relation, which is based on UV-Vis titration data at absorption maxima of each complexe.^{132,133}

$$\frac{1}{A - A_0} = \frac{1}{A_{max} - A_0} + \frac{1}{(A_{max} - A_0)K[Anion/cation]^n}$$

In the equation, A_0 , A , A_{max} are the absorbance in the absence of anion/cation, after adding an anion/cation at every step and at concentration of saturation respectively. [Anion/cation] indicates concentration af anion or cation, n is the stoichiometric of anion or cation, and K is binding constant. Shown in Figure 11a, the titration study of **2** with TBACN gave a good linear correction, indicating a 1:1 (1 ligand : 1 anion/cation) stoichiometry and an association constant of $2.0 \cdot 10^2 \text{ M}^{-2}$. The respective binding constant of **2ba7** with various anions are shown in Table 8. The constant values reported the strength of the interaction, which was in adequation with the basicity order of anions: the more important the constant was, the more basic the anion was.^{33,134} On the other hand, the 1:1 stoichiometry was also demonstrated by the Job's method of continuous variations (Figure 11b).¹³⁵ In all cases with the Benesi-Hildebrand as well as the Job plots, the 1:1 complex was approved (see Supporting information).

Anion	H_2PO_4^-	CN^-	F^-
K	$0.1 \cdot 10^2$	$2.0 \cdot 10^2$	$2.9 \cdot 10^2$

Table 8. Association constants of **2ba7** with various anions

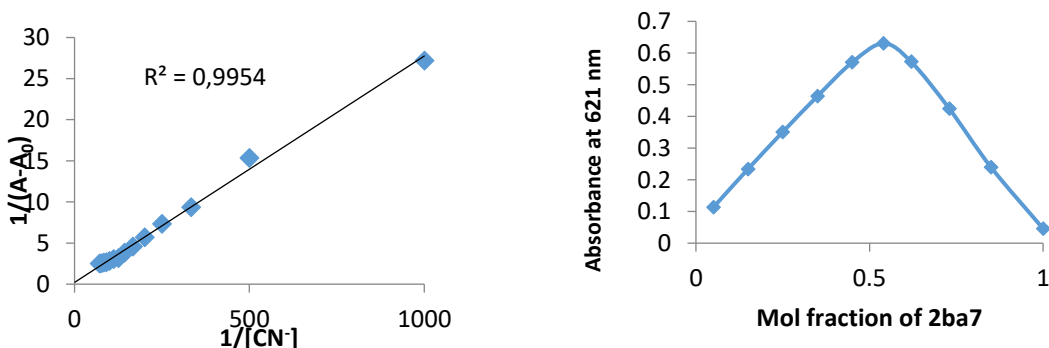


Figure 11. (a) Benesi-Hildebrand plot and (b) Job's plot of **2ba7** with TBACN with absorbance change at 621 nm

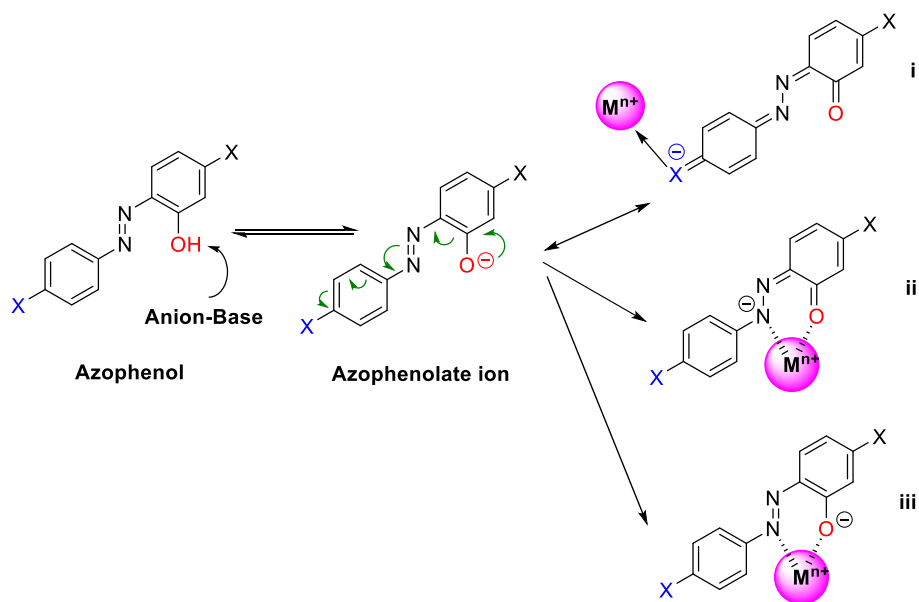
¹³² Benesi, H. A.; Hildebrand, J., A spectrophotometric investigation of the interaction of iodine with aromatic hydrocarbons, *J. Am. Chem. Soc.* **1949**, *71*, 2703-2707.

¹³³ Kuntz Jr, I.; Gasparro, F.; Johnston Jr, M.; Taylor, R., Molecular interactions and the Benesi-Hildebrand equation, *J. Am. Chem. Soc.* **1968**, *90*, 4778-4781.

¹³⁴ Kigga, M.; Trivedi, D. R., "Naked-eye" detection of inorganic fluoride ion in aqueous media using base labile proton: A different approach, *J. F. Chem.* **2014**, *160*, 1-7.

¹³⁵ MacCarthy, P., Simplified experimental route for obtaining Job's curves, *Anal. Chem.* **1978**, *50*, 2165-2165.

The bathochromic shift, or the red shift of the UV-VIs spectra could be presumably explained by the interaction between azophenol and anion/cation. Anion deprotonated the -OH function which generated a resonance of the rising electron density on the "O" atom with the X group through π -conjugated benzene ring system, realizing the color change, as well as the appearance of a ref-shifted band.^{107,110} (Scheme 5). The presence of an electron-withdrawing group in *para* position in the second aromatic ring with respect to the -OH group increased the acidity of the phenol moiety, thereby enhancing the hydrogen donor properties of azophenols. Thus, it merged that hydrogen binding affinity/acidity of chemosensors as well as the basicity of the anions were key factors in selectivity trends. The more *para* substituents electron-withdrawing ($\text{NO}_2 > \text{COOEt} > \text{Br} > \text{H} > \text{OMe}$) and the more basic anions ($\text{OH}^- > \text{F}^- > \text{CN}^- > \text{H}_2\text{PO}_4^- > \text{OAc}^- > \text{HSO}_4^- > \text{Cl}^- > \text{Br}^- > \text{ClO}_4^- > \text{I}^- > \text{NO}_3^-$) were, the more effective association between the sensor and the guest was.¹³⁶ Here we propose three mechanisms for cation binding (Scheme 5): (i) intramolecular charge transfer transition in the azophenol sensor and cation is linked to X in *para* position, (ii) charge transfer transition in one aromatic cycle and cation is bound to nitrogen atom,¹³⁷ (iii) cation is chelated by nitrogen and oxygen atoms.¹³⁸ Selective recognition for several cations such as Ni^{2+} , Cu^{2+} , Ag^+ , Na^+ , K^+ can be explained by the satisfactory coordination geometry conformation of the sensor, the ion radius and sufficient binding energy of cations.¹³⁹



Scheme 5. Proposed mechanism interaction of azophenol and anion/cation

¹³⁶ Dalapati, S.; Alam, M. A.; Jana, S.; Guchhait, N., Naked-eye detection of F^- and AcO^- ions by Schiff base receptor, *J. Fluor. Chem.* **2011**, 132, 536-540.

¹³⁷ Yıldız, M.; Demir, N.; Ünver, H.; Sahiner, N., Synthesis, Characterization, and Application of a Novel Water-soluble Polyethyleneimine-based Schiff base Colorimetric Chemosensor for Metal Cations and Biological Activity, *Sens. Actuator B Chem.* **2017**,

¹³⁸ Orojloo, M.; Amani, S., Synthesis and studies of selective chemosensor for naked-eye detection of anions and cations based on a new Schiff-base derivative, *Talanta* **2016**, 159, 292-299.

¹³⁹ Yang, L.; Zhu, W.; Fang, M.; Zhang, Q.; Li, C., A new carbazole-based Schiff-base as fluorescent chemosensor for selective detection of Fe^{3+} and Cu^{2+} , *Spectrochim. Acta Mol. Biomol. Spectrosc.* **2013**, 109, 186-192.

¹H NMR titration studies

To further get an inside in the mechanism of intermolecular interactions between azophenol sensors and anions, ¹H-NMR spectral experiments were carried out in DMSO-*d*₆. Azophenol **4** was chosen due to its selectivity on the detection of only three anions as well as its clear and simple ¹H-NMR spectrum. Upon the addition of 0.25 equiv of tetrabutylammonium cyanide (TBACN) in the presence of **4**, the band at δ 11.09 ppm, which has been assigned to the -OH group, disappeared due to the deprotonation of -OH upon interaction with CN⁻ (Figure 12). All other aromatic protons H1-H5 were drastically upshifted, indicating an increase in the electron density of the benzene ring owing to the charge transfer after the deprotonation. Interestingly, a new broad band at δ 3.69 ppm after the addition of 0.75 equiv of TBACN was observed, which was attributed to the formation of HCN and confirmed the deprotonation of -OH group in compound **4**. Hence, both the result of the UV-Vis experiments and the ¹H-NMR titration were assembled to highlight the interaction mechanism during the anion/cation recognition process of azophenol receptor as shown in Scheme 5. The anion was initially binded through hydrogen bonding to the -OH group of the azophenol, inducing deprotonation of this latter. Subsequently, charge transfer transition within the host compound, between the electron withdrawing group at *para* position and electron rich O⁻, called tautomeric equilibrium, occurred and thus led to the electron density increase. This resulted in a new red-shifted absorption band allowing significant colorimetric change.

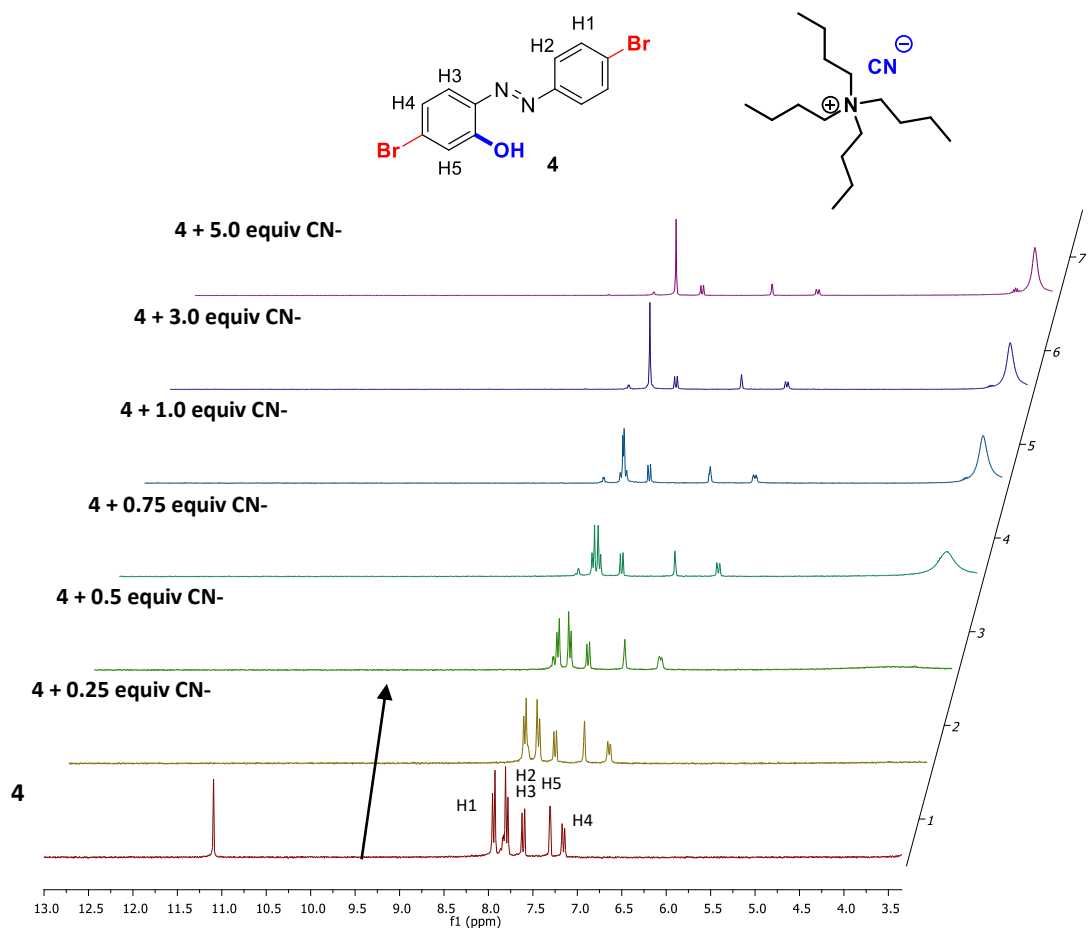


Figure 12. ¹H-NMR experiment of **4** in DMSO-*d*₆ with TBACN

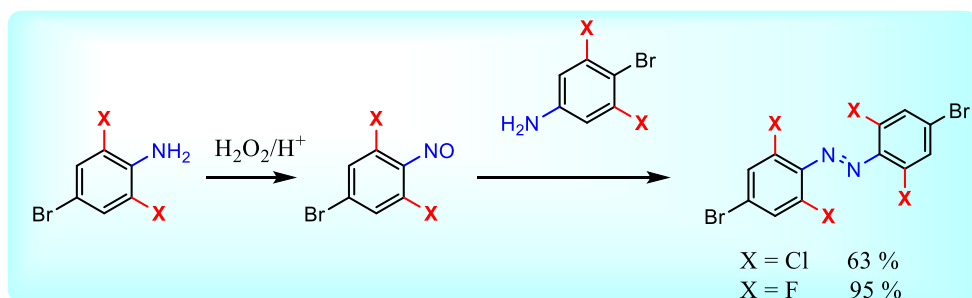
Conclusion

In summary, pursuing our previous work on the straightforward *ortho*-hydroxylation of azobenzenes, we have synthetized various series of azophenols diversely substituted in *para* or *ortho* positions in order to evaluate the influence of aromatic substituents on the site-selectivity of the reaction and on the anion sensor ability. The Jaffé equation and its extension delivered a linear free energy relationship, providing further evidence for a turnover-limiting cyclopalladation in the mechanism. Finally, azophenols showed a highly selective naked-eye colorimetric sensors for discrimination cations such as Ni^{2+} , Cu^{2+} , Ag^+ , Na^+ , K^+ . UV-Vis spectral titrations and NMR experiments were carried out in order to characterize them and to elucidate the binding mechanism. All these studies demonstrated that electron-withdrawing substituents on the arene are favourable for the *ortho*-hydroxylation, as well as for the ion detection process.

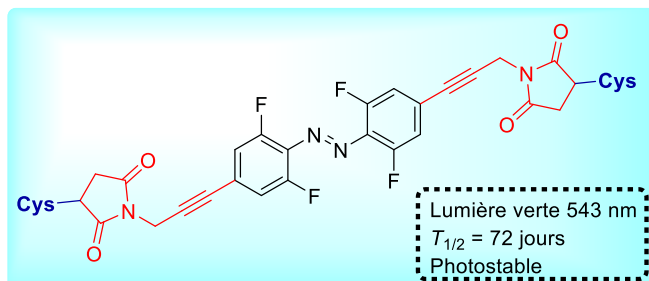
Pour plus d'informations sur la partie expérimentale, veuillez contacter delphine.joseph@u-psud.fr

Conclusions et Perspectives

Au cours de ce travail, nous avons effectué une étude méthodologique concernant la synthèse d'azobenzènes tétrasubstitués en position *ortho* pour mieux comprendre les éléments affectant leurs synthèses, généralement inefficaces, et afin d'en améliorer les rendements. En passant du dérivé non-substitué à un dérivé mono-substitué puis di-substitué, nous notons un abaissement de l'efficacité de la synthèse, causé par des effets stéréoélectroniques : l'effet stérique du substituant en position *ortho*, qui s'ajoute à l'effet électronique du groupement en position *para*. Après plusieurs optimisations, nous avons réussi à synthétiser un azobenzène tétrachloré et un azobenzène tétrafluoré en passant par un intermédiaire nitrosobenzène avec de bons rendements.



Le dérivé tétrafluoro azobenzène a été ensuite fonctionnalisé en introduisant une chaîne alcyne terminée par un groupement maléimide afin permettre sa fixation sur un résidu cystéine. Les propriétés physicochimiques très intéressantes de cette pince ont été évaluées. Ce composé peut s'isomériser avec de la lumière, a une demi-vie très longue de 72 jours et est photostable. Par ailleur, il est possible d'obtenir presque 100 % de l'isomère *E* ou 90 % de *Z* avec le jeu d'irradiation.



Comme la synthèse directe des azobenzènes multi-substitués est très compliquée, une voie alternative d'introduction de substituants en position *ortho* sur les azobenzènes simples a été étudiée. Une synthèse efficace et pratique pour générer directement la fonction hydroxyle en *ortho* de l'azobenzène dans des conditions douces a été développée. La méthode montre une très bonne tolérance pour différents groupements fonctionnels, donnant accès à une large gamme d'azophénols originaux avec des bons rendements.



Nous avons synthétisé plusieurs séries en faisant varier les substituants en positions *para* ou/et en *ortho* afin d'étudier l'influence de ces substituants sur la régiosélectivité de cette *ortho*-hydroxylation. L'équation de Jaffé et ses extensions ont donné une relation linéaire avec d'excellents coefficients de détermination R². Nous avons également obtenu deux azophénols avec d'excellentes régiosélectivités possédant des groupements différents permettant d'envisager une bio conjugaison orthogonale.



Enfin, les azophénols ont été évalués comme des détecteurs colorimétriques d'anions et de cations. Leurs caractéristiques ainsi que le mécanisme d'interaction ont été déterminés par une inspection visuelle, des mesures UV-Visible et des expériences de RMN.

Les travaux devront être poursuivis en

- développant des méthodologies basées sur d'autres fonctionnalisations efficaces
- concevant des structures de pinces innovantes à la fois potentiellement fixables sur GLIC (pinces dissymétriques permettant une bio conjugaison orthogonale) et possédant des propriétés physicochimiques particulières (pinces fluorescantes).

Au niveau des azophénols, le champ d'application devrait être poursuivi en pH méttrie ou en détection sélective des cations.

Titre : Pinces moléculaires photo-isomérisables pour l'étude des changements allostériques des récepteurs pentamériques canaux

Mots clés : azobenzène, photoisomérisable, C-H activation, Hammett, Jaffé, détection d'ions

Résumé : Au cours de ce travail, nous avons effectué une étude méthodologique concernant la synthèse d'azobenzènes tétrasubstitués en position *ortho* pour mieux comprendre les éléments affectant leurs synthèses, généralement inefficaces, et afin d'en améliorer les rendements. Nous avons conclu que l'inefficacité de cette synthèse est causée par des effets stéréoélectroniques : l'effet stérique du substituant en position *ortho*, qui s'ajoute à l'effet électronique du groupement en position *para*. Après différentes optimisations, nous avons réussi à synthétiser un azobenzène tétrachloré et un azobenzène tétrafluoré *via* un intermédiaire nitrosobenzène avec de bons rendements.

Le dérivé tétrafluoro azobenzène a été ensuite fonctionnalisé en introduisant une chaîne alcyne terminée par un groupement maléimide afin de permettre sa fixation sur un résidu cystéine. Les

propriétés physicochimiques très intéressantes (lumière verte d'irradiation, $\tau_{1/2} = 72$ jours, photostable) de cette pince ont été évaluées. Parallèlement, une synthèse efficace et pratique pour générer directement la fonction hydroxyle en *ortho* de l'azobenzène dans des conditions douces a été développée. Nous avons synthétisé plusieurs séries en faisant varier les substituants en positions *para* ou/et en *ortho* afin d'étudier l'influence de ces substituants sur la régiosélectivité de cette *ortho*-hydroxylation. L'équation de Jaffé et ses extensions ont donné une relation linéaire avec d'excellents coefficients de détermination R^2 .

Enfin, les azophénols ont été évalués comme des détecteurs colorimétriques d'anions et de cations. Leurs caractéristiques ainsi que le mécanisme d'interaction ont été déterminés par une inspection visuelle, des mesures UV-Visible et des expériences de RMN.

Title : Molecular photoswitches for studying of allosteric transitions of pentameric ligand-gated ion channels

Keywords : azobenzene, photoswitch, C-H activation, Hammett, Jaffé, ion sensor

Abstract : A methodological study on the synthesis of tetrasubstituted azobenzenes has been realized. We concluded that synthesis of multisubstituted azobenzene is hardly affected by the steric hindrance in *ortho* position and the electronic effect of *para* substituents.

A tetrachloro and a tetrafluoro azobenzene have been synthesized in good yields, *via* nitrosobenzene intermediate. The tetrafluoro derivative was then functionalized with an alkyne chain containing a maleimide group for bioconjugation to cysteine residue. Its interesting photoisomerisation properties (green light of irradiation, $\tau_{1/2} = 72$ days, photostable) were evaluated.

We also developed a practical and effective method for direct *ortho*-hydroxylation of azobenzenes under mild conditions. The reaction showed a very good functional groups tolerance, leading to a wide range of original azophenols in satisfying to high yields.

Through Hammett-Jaffé analyses, we presented a study that correlated electronic and steric perturbations induced by substituents nature to the regioselectivity of this direct hydroxylation process.

Azophenols were finally evaluated as ion sensors. Anion sensing characteristics as well as interaction mechanism were determined using visual inspection, UV-Vis and NMR spectroscopy.

